ROS and mitochondrial genetic abnormalities as novel indicators to predict anticancer drug efficacy

By

Tarek Zaidieh

School of Pharmacy and Biomedical Sciences

University of Portsmouth

White Swan Road

Portsmouth, United Kingdom

April 2020

The thesis is submitted in partial fulfilment of the requirement for the award of the degree of Doctor of Philosophy of the University of Portsmouth

Abstract

Mitochondria are considered a primary intracellular site of reactive oxygen species (ROS) generation. Mitochondrial genetic abnormalities (mutations and copy number change) have been reported in various cancer types that might be associated with elevated ROS levels in cancer cells compared to normal cells. Since high levels of ROS can trigger apoptosis, treating cancer cells with ROS-stimulating agents may enhance cell death. This study aimed to investigate: 1) how baseline ROS levels might influence cancer cells' response to ROS-stimulating therapy; 2) the link between mitochondrial genetic abnormalities and baseline ROS levels; 3) how specific mitochondrial DNA mutations might be utilised to predict cancer cells' response to ROS-stimulating therapy.

Sanger sequencing was used to screen for mitochondrial DNA (mtDNA) mutations and qPCR to measure mtDNA copy number (mtDNAcn) in four cancer and one non-cancerous cell lines. Three-dimensional structural mapping and analysis of all the non-synonymous mutations were then performed to assess their functional importance. The overall baseline intracellular ROS levels and mitochondrial superoxide were measured using the 2',7'-dichlorofluorescin diacetate assay and MitoSOX indicator, respectively. Cells were treated with a conventional drug (cisplatin) and a mitochondria-targeting agent (dequalinium chloride hydrate) separately and jointly. Cell viability was assessed using MTS assays and drug combination synergisms were analysed using the Combination Index method. Apoptosis events were detected and the relative expression levels of the genes and proteins involved in ROS-mediated apoptosis pathways were also investigated.

Greater numbers of non-synonymous mutations in the mitochondrial complexes I/III coding regions were detected in cancer cells with higher ROS levels. Our data showed a positive correlation between the baseline ROS levels, number of non-synonymous mutations, mtDNAcn and drug resistance levels in the tested cells. Synergistic effect of both drugs was also observed with ROS being the key contributor in cell death.

Our findings assert that cancer cells with low levels of ROS are more sensitive to ROS-stimulating agents, while cells with high levels of ROS are more resistant. Moreover, specific mutations in the complexes I/III coding regions, A10398G, T11120C, C12084T, A13681G, G13708A, C13802T, A13966G and T14798C, could be used to indicate elevated intracellular ROS and therefore to predict drug resistance. Patient-derived

primary cell cultures and tissues, and in vivo experiments will be required to validate the present findings.

Contents list

Declaration

Whilst registered as a candidate for the above degree, I have not been registered for any other research award. The results and conclusions embodied in this thesis are the work of the named candidate and have not been submitted for any other academic award.

Word count

43320

List of tables

Chapter 1

Chapter 2

Chapter 3

Chapter 6

Appendices

List of figures

Chapter 1

Chapter 2

Chapter 3

Chapter 4

Chapter 5

Chapter 6

Appendices

Abbreviations

2-DG: 2-deoxyglucose

3D: Three-dimensional

Acetyl-CoA: Acetyl coenzyme A

ADP: Adenosine diphosphate

AIF: Apoptosis-inducing factor

AKT: Protein Kinase B

ANT: Adenine Nucleotide Translocator

AP: Apurinic/apyrimidinic site

AP-1: Activator protein 1

APAF-1: Apoptosis protease-activating factor

APE1: AP endonuclease

APS: Ammonium persulfate

ARE: Antioxidant responsive element

ASK1: Apoptosis signal regulated kinase 1

ATM: Ataxia telangiectasia mutated

ATP: Adenosine triphosphate

ATR: Ataxia telangiectasia and Rad3-related

BAD: BCL2 associated agonist of cell death

BAX: Bcl-2-associated X protein

BCA: Bicinchoninic acid

BER: Base excision repair

BNIP3: BCL2 Interacting Protein 3

BSA: Bovine serum albumin

CAT: Catalase

CDC25C: Cell division cycle

CDDP: Cisplatin or Cisdiamminedichloroplatinum (II)

CDK1: Cyclin-dependent kinase 1

cDNA: Complementary DNA

CER I: Cytoplasmic Extraction Reagent I

CER II: Cytoplasmic Extraction Reagent II

c-FLIP: Cellular FLICE-like inhibitory protein

CHK1: Checkpoint kinase 1

CHK2: Checkpoint kinase 2

CI: Combination Index

c-IAP1: Cellular inhibitor of apoptosis protein 1

c-IAP2: Cellular inhibitor of apoptosis protein 2

CLL: Chronic lymphocytic leukemia

CO: Cytochrome *c* oxidase

COOT: Crystallographic Object-Oriented Toolkit

CTR: Copper transport

CYB: Cytochrome *b*

Cybrid: cytoplasmic hybrid

CypD: Cyclophilin D

Cyt *c*: Cytochrome *c*

DAPIT: Diabetes-associated protein in insulin-sensitive tissues

DCF: Dichlorofluorescein

DCFDA: 2',7'-dichlorofluorescin

DIABLO: Direct inhibitor of apoptosis-binding protein with low pI

DLCs: Delocalised lipophilic cations

D-loop: Displacement-loop region

Dlx-2: Distal-less homobox-2

dNTPs: Deoxyribonucleoside triphosphates

DQA: Dequalinium chloride

DRP1: Dynamin-related protein 1

DTT: Dithiothreitol

EGF: Epidermal growth factor

EGFR: Epidermal growth factor receptor

EMT: Epithelial mesenchymal transition

Endo G: Endonuclease G

ER: Estrogen receptor

ERK: Extracellular signal-regulated kinase

ETC: Electron transport chain

FADH2: Flavin adenine dinucleotide

FANCE: Fanconi anemia, complementation group E protein.

FAO: Fatty acid oxidation

FBS: Fetal bovine serum

FDA: Food and Drug Administration

FIS1: Fission protein homolog 1

FLICE: FADD-like IL-1β-converting enzyme

FMN: Flavin mononucleotide

FUNDC1: FUN14 domain containing 1

GBM: Glioblastoma multiforme

GPxs: glutathione peroxidases

GR: Glutathione reductase

Grx: Glutaredoxin

GSH: Glutathione

GSK3β: Glycogen synthase kinase 3β

GSSG: Glutathione disulphide

GTPases: Guanosine triphosphatases

HCC: Hepatocellular carcinoma

HDACi: Histone deacetylases inhibitor

HER2: Human epidermal growth factor receptor 2

HIF-1: Hypoxia-inducible factor 1

HIF-1α: Hypoxia-inducible factor 1-alpha

HIF-1β: Hypoxia-inducible factor 1-beta

HK-II: Hexokinase II

HmtDB: Human Mitochondrial DataBase

HNE: 4-hydroxynonenal

HSP: Heavy strand promotor

H-strand: Heavy strand

IAPs: Inhibitor of apoptosis proteins

IC50: Half maximal inhibitory concentration

IL-1β: Interleukins 1 beta

IL-6: Interleukins 6

IL-8: Interleukins 8

IMM: Inner mitochondrial membrane

IMS: Intermembrane Space

IR: Ionizing radiation

ISP: Iron-sulfur protein

JNK: c-Jun N-terminal kinase

Keap1: Kelch-like ECH-associated protein 1

LDH: Lactate dehydrogenase

LHON: Leber's Hereditary Optic Neuropathy

LIG3: DNA ligase 3

LND: Lonidamine

LOO·: Lipoperoxyl radical

LOOH: Lipid hydroperoxide

LSP: Light strand promotor

L-strand: Light strand

Maf: Musculoaponeurotic fibrosarcoma

MAPKs: Mitogen-activated protein kinase family

MDDS: Mitochondrial DNA depletion syndrome

MDM2: Murine double minute 2

MDR1: Multidrug resistance protein 1

MFN-1: Mitofusin-1

MFN-2: Mitofusin-2

Mitophagy: Mitochondria-specific autophagy

MKT-077: Rhodacyanine

MMPs: Matrix metalloproteinases

MMR: Mismatch repair

MOMP: Mitochondrial outer membrane permeabilisation

MPT: Mitochondrial permeability transition

MPTP: Mitochondrial permeability transition pore

MRC: Mitochondrial respiratory chain

mROS: Mitochondrial ROS

mtDNA: Mitochondrial DNA

mtDNAcn: Mitochondrial DNA copy number

MTERF1: Mitochondrial termination factor 1

mtSSB: Mitochondrial single strand DNA binding protein

NAC: N-acetyl cysteine

NADH: Nicotinamide adenine dinucleotide

NADPH oxidase (NOX): Nicotinamide adenine dinucleotide phosphate oxidase

NCR: Non-coding region

ND: NADH dehydrogenase

nDNA: Nuclear DNA

NEIL1/ NEIL2: Nei endonuclease VIII-like 1 and 2

NER: Nucleotide excision repair

NGS: Next Generation Sequencing

NF-κB: Nuclear factor kappa-light-chain-enhancer of activated B cells

NIX: BNIP3-like

NPC: Nasopharyngeal carcinoma

Nrf2: Nuclear factor erythroid 2-related factor 2

NSCLC: Non-small cell lung carcinoma

NTHL1: Endonuclease III-like protein 1

OGG1: 8-oxoguanine DNA glycosylase

O_H: Origin for the heavy strand DNA replication

O_L: Origin of the light strand DNA replication

OMM: Outer mitochondrial membrane

OPA1: Optic Atrophy type 1

OSCP: Oligomycin sensitivity conferral protein

OXPHOS: Oxidative phosphorylation

PBR: Peripheral benzodiazepine receptor

PBS: Phosphate buffered saline

PCNA: Proliferating cell nuclear antigen

PDGFR: Platelet-derived growth factor

PDH: Pyruvate dehydrogenase

PDK1: Pyruvate dehydrogenase kinase 1

PDT: photodynamic therapy

PHD2: Prolyl hydroxylase domain-containing protein 2

PI: Propidium iodide

PI3K: Phosphoinositide 3-kinase

PINK1: PTEN-induced kinase 1

PMS: Phenazine methosulfate

POLG: Polymerase gamma

POLRMT: Mitochondrial RNA polymerase

POLγ: DNA polymerase γ

PP2: Protein phosphatase 2

PPP: Pentose phosphate pathway

Prxs: Peroxiredoxins

PS: Phosphatidylserine

PS: Photosensitizing drugs

PTEN: Phosphatase and tensin homolog

PTP1B: Protein tyrosine phosphatase 1B

PTPC: Permeability transition pore complex

PVDF: Polyvinylidene fluoride membrane

Q: Ubiquinone

QH_2: Ubiquinol

RCSB PDB: Research Collaboratory for Structural Bioinformatics Protein Data Bank

Rh123: Rhodamine 123

ROS: Reactive oxygen species

RRM2B: Ribonucleotide reductase regulatory TP53 inducible subunit M2B

rRNA: Ribosomal RNA

RT-qPCR: Real-time quantitative polymerase chain reaction

SCC: Squamous cell carcinoma

SDH: Succinate dehydrogenase

SDS: Sodium dodecyl sulfate

SDS-PAGE: Sodium dodecyl sulfate polyacrylamide gel electrophoresis

Smac: Second mitochondria-derived activator of caspases

Snail: Zinc finger protein SNAI1

SOD: Superoxide dismutase

ssDNA: Single strand DNA

STAT3: Signal transducer and activator of transcription 3

STR: Short tandem repeat

TAS: Termination associated sequences

TBHP: Tert-Butyl hydrogen peroxide

TBST: Tris-buffered saline and Tween 20

TCA: Tricarboxylic acid cycle

TEFM: Transcription elongation factor TEFM

TEMED: Tetramethylethylenediamine

TFAM: Mitochondrial transcriptional factor A

TFB2M: Mitochondrial transcription factor B2

TGF-β: Transforming growth factor beta

TIGAR: TP53-inducible glycolysis and apoptosis regulator

TNF: Tumour necrosis factor

TR: Thioredoxin reductase

TRAIL: TNF-related apoptosis inducing ligand

tRNA: Transfer RNA

Trxs: Thioredoxins

UNG1: Uracil DNA glycosylase

VDAC: Voltage Dependent Anion Channel

VEGF: Vascular endothelial growth factor

VEGFR: Vascular endothelial growth factor receptor

WBC: White blood cell

WST: Water-soluble tetrazolium salts probe

XIAP: X-linked inhibitor of apoptosis protein

$\Delta\Psi m$/MMP: Mitochondrial transmembrane potential

Acknowledgements

Prima facie, I am grateful to the God for the good health and wellbeing that were necessary to complete this thesis.

Firstly, I would like to express my sincere gratitude to my supervisor Dr Qian An for the continuous support of my PhD study and related research, for her patience, motivation, and immense knowledge. Her guidance helped me in all the time of research and writing of this thesis. I could not have imagined having a better advisor and mentor for my PhD study. Besides my supervisor, I would like to thank Dr James Smith my second supervisor and Dr Karen Ball my third supervisor for their advice, guidance and encouragement.

My sincere thanks also go to Prof. Darek Gorecki, Dr Jerome Swinny, Dr Rhiannon McGeehan and Dr Sassan Hafizi who all provided me with their help and support, who gave me access to the laboratory and research facilities. Without their precious support it would not be possible to conduct this research.

I must express my very profound gratitude to the University of Portsmouth and the School of Pharmacy and Biomedical Sciences. I am extremely thankful and indebted to the Council for At-Risk Academics (Cara) for helping and providing the funding for this project and for supporting my work and development as a PhD student. I am grateful to each member of Cara for their patience and support in overcoming numerous obstacles I have been facing through my research life. This accomplishment would not have been possible without them. Thank you.

I thank my fellow lab/office mates for the stimulating discussions, for the sleepless nights we were working together before deadlines, and for all the fun we have had. I would also like to thank my best friends Mohsen, Diana, Adina, Fadhael and Nadide for accepting nothing less than excellence from me. My life in Portsmouth would have been much more difficult without their support and help.

Last but not least, my family has given me everything a family can give; I am forever grateful to my wife, my dad, my mum, my sister and my brother for their love and emotional support along the way and for always being there for me in happy and difficult times, despite of the geographical distance.

I also place on record, my sense of gratitude to one and all, who directly or indirectly, have lent their hand in this venture.

Dedication

إلى قدوتي و ملهمي، إلى من نذر حياته من أجلي، إلى من منحني الثقة ببريق عينيه، إلى من علمني حب الحياة، إلى من حلم طويلاً و طويلاً كي يراني في هذا المكان، إلى من كان صديقي و أخي قبل أي شيئ

أستاذي و معلمي ..... أبي

إلى من يرتجف صوتي الأن إجلالاً لدموعها، إلى من ضحت بكل ما تملك من أجلي، إلى من غمرتني بعطفها و حنانها، إلى من كانت ابتسامتها مصدر قوتي و نجاحي، إلى من زرعت في الطموح و الأمل

أغلى ما في الوجود ..... أمي

إلى هديتي من السماء، إلى النور الذي أضاء حياتي بالحب و الحنان، إلى من شاركتني الطموح و الأحلم، إلى من أستمد من بريق عينيها التفاؤل و الأمل، إلى من كانت السبب الأول و الأخير لوقوفي هنا، إلى فرحي و جنوني

رفيقيتي و حبيبتي و زوجتي ..... نور

إلى من شاركوني أجمل لحظات حياتي حلوّها و مرّها، إلى من تقاسمت معهم البتسامات و الدموع، إلى من كانو لي السند في أصعب الأوقات، إلى من كانو لي الفرح في أجمل الأيام، إلى من غيبتهم عني قساوة الغربة

إخوتي..... رزان و غياث

إننا السوريون

نحيا نفكر ..... و نبدع

نطوي جراحنا و نبتسم للمستقبل

هكذا نحن ..... و هذا هو قدرنا

خُلقنا لنكون

أبناء الحياة

سوريا ..... لك السلام

Dissemination

EACR, February 2020, Italy. Poster: Mitochondrial genetic abnormalities as novel biomarkers to predict drug efficacy.

BACR, November 2018, UK. Poster: ROS and mitochondrial genetic abnormalities as novel indicators for anti-cancer drug sensitivity.

NCRI, November 2018, UK. Poster: ROS and mitochondrial genetic abnormalities as novel indicators for anti-cancer drug sensitivity.

IBBS, September 2018, UK. Poster: ROS and mitochondrial genetic abnormalities as novel indicators for anti-cancer drug sensitivity.

University of Portsmouth Science Faculty Poster Presentation Day, June 2017, UK. Poster: Evaluation of anti-tumour compounds in the treatment of hormone-dependent cancer.

Full publications

Zaidieh T, McGeehan RE, Smith JR, Ball KE, An Q. Mitochondrial DNA abnormalities provide mechanistic insight and predict reactive oxygen species-stimulating drug efficacy. (Under revision, *BMC Cancer*).

Zaidieh T, Smith JR, Ball KE, An Q. ROS as a novel indicator to predict anticancer drug efficacy. *BMC Cancer*. **2019**;19(1):1-14.

.

Chapter 1

General introduction

1.1 Mitochondria

1.1.1 Mitochondria structure and functions

Mitochondria are semiautonomous organelles that are present in almost all eukaryotic cells. Each mitochondrion is enclosed by double lipid membrane: the outer membrane (OMM) that covers the organelle and the inner membrane (IMM) that markedly folds and creates layered structures called cristae which extend into the matrix; the space between the outer membrane and the inner membrane is called the intermembrane space (IMS) (reviewed in Ref. [1]). One unique feature of mitochondria is that they contain their own genome, mitochondrial DNA (mtDNA; a small circular DNA of 16569 bp), independent of nuclear DNA (nDNA) (reviewed in Ref. [2]) (Figure 1.1).

Each human cell can contain hundreds to thousands mitochondria, and each mitochondrion contains 2–10 mtDNA copies [3]. The synthesis and degradation of mtDNA is rapid and independent of the cell cycle so the dynamic equilibrium between them determines the mitochondrial DNA copy number (mtDNAcn) (reviewed in Ref. [4]).

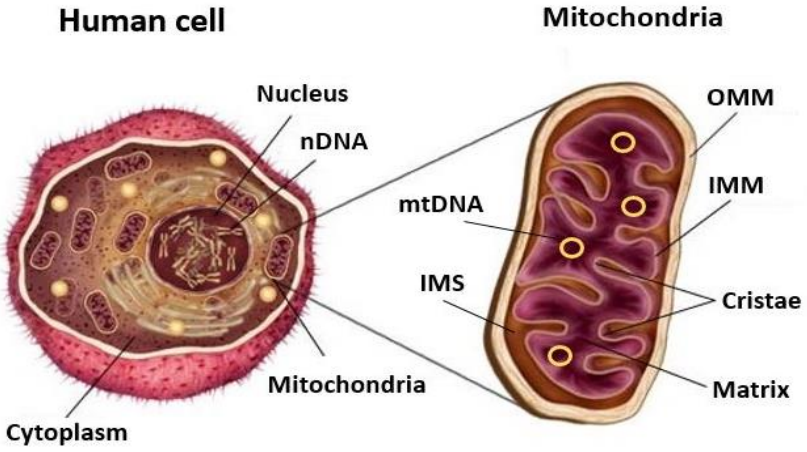

Figure 1.1. Structure of human mitochondria [2].

Mitochondria are considered the energy powerhouse of the cells since the majority of the adenosine triphosphate (ATP) is generated by the mitochondria via fatty acid oxidation (FAO), tricarboxylic acid cycle (TCA) also known as the Krebs cycle and oxidative phosphorylation (OXPHOS). The amount of produced ATP is influenced by the abundance of mitochondria and number of mtDNA copies according to the cell types and the physiological conditions. Furthermore, mitochondrial double lipid membrane contains various types of ion channels responsible for the maintenance of the homeostatic levels of Ca^{2+}, Na^{+}, and K^{+} ions, which regulate the cellular homeostasis, TCA cycle

activity and ATP production, mitochondrial transmembrane potential (ΔΨm), mitochondrial permeability transition pore (MPTP) opening and cross-talk between the inside and outside of the mitochondria. Moreover, mitochondria are implicated in multiple cellular processes such as cell communication, cell differentiation, cell apoptosis and they have anabolic functions in the biosynthesis of lipids, amino acids and nucleotides.

Mitochondria are dynamic organelles that can rapidly sense stress signals and subsequently coordinate several biochemical pathways required to adapt to environmental changes (reviewed in Ref. [5]).

Communication between mitochondria and nucleus is essential for maintaining mitochondrial function and cellular homeostasis. In response to environmental stressful conditions, the nucleus regulates the transcription and translation of genes responsible for mitochondrial biogenesis and OXPHOS functions directly via the anterograde pathway. On the other hand, dysfunctional mitochondria interact with the nucleus via the retrograde signalling pathway to activate various nuclear responses, consequently promoting multiple pathways that regulate energy homeostasis, oxidative stress, mitophagy and other functions to facilitate cellular-adaptation strategies (reviewed in Ref. [6]).

1.1.2 Mitochondrial dynamics

To survive from external and internal stressors, cells are required to preserve a balance of the main intracellular parameters to regain homeostasis. Mitochondria are the key players in this process as their responses to stress are essential to cell maintenance and fate. The mitochondrial adaptation mechanisms involve a reshape provided by mitochondrial motility, fusion and fission processes and other homotypic/heterotypic interactions (such as tethering with the endoplasmic reticulum) [7,8].

Mitochondria fusion is characterised by the union of two mitochondria forming one mitochondrion. This process helps cells to moderate stress by sharing multiple elements which sustain mitochondrial biology [9]. It is regulated by large Guanosine triphosphatases (GTPases) of the dynamin family. Membrane-anchored dynamin family members called Mitofusin 1 and 2 (MFN1 and MFN2) mediate the fusion of the outer membrane whereas a single dynamin family member called Optic Atrophy type 1 (OPA1) mediates the fusion of the inner membrane [10–12].

On the contrary, mitochondrial fission is the division of one mitochondrion in two mitochondria. It is regulated by dynamin-related protein 1 (DRP1) and fission protein homolog 1 (FIS1), which are located at the OMM during the fission process [13]. This process is required for mitochondrial genome replication and redistribution and motility of mitochondria during cell division (reviewed in Ref. [14]).

Several studies have evidenced that mitochondrial fission is also essential for the separation of damaged mitochondria via mitochondria-specific autophagy (mitophagy) triggered by DRP1. Mitophagy is well known as a substantial process for the maintenance of mitochondria and cellular physiology. It also appears to act as a pro-survival mechanism in cell metabolism. Various mitophagy effectors have been identified in mammalian cells, including proteins involved in the PINK1/Parkin pathway and the mitophagy receptors NIX, BNIP3, and FUDNC1 [15,16]. The balance between mitochondrial fusion and fission controls mitochondrial abundance, size, and distribution within the cytoplasm, and allows remodelling when cells are stressed (reviewed in Ref. [17]).

Given the critical role of mitochondria in cellular bioenergetic and in many other important physiological processes such as cell communication, differentiation and apoptosis, mitochondrial dysfunction can be involved in the development of various human disease, including cancers [18].

1.1.3 Mitochondrial genome

1.1.3.1 Mitochondrial DNA structure

Mitochondrial DNA (mtDNA) is a small circular and double-stranded DNA of 16569 bp and characterised by high gene density and absence of intron. The two strands of mitochondrial DNA are named the heavy strand (H-strand) and the light strand (L-strand), the former being guanine rich and the latter cytosine rich (reviewed in Ref. [19]). MtDNA contains 38 regions that encodes for 13 protein subunits for four of the five complexes of the oxidative phosphorylation system (OXPHOS) namely (ND1, ND2, ND3, ND4, ND4L, ND5, ND6, CYB, COI, COII, COIII, ATP6 and ATP8), which generates the majority of cellular ATP. Of these genes, 12 are located on the heavy strand and one on the light strand. MtDNA also encodes 2 rRNAs (12S and 16S) and 22 tRNAs which are involved in the translation of the mitochondrial encoded subunits within the mitoribosomes.

The displacement-loop region (D-loop) is a long non-coding region (NCR) of approximately 1.1k bp long and plays a fundamental role in controlling the initiation of mtDNA transcription and replication via the interaction of its regulatory elements with several nuclear DNA-encoded factors that are imported into the mitochondria [20,21]. In the D-loop region, there are polycistronic transcription promoters for each mitochondrial genome strand; the heavy strand promotor (HSP) and the light strand promotor (LSP). It also contains the origin for the heavy strand DNA replication (O_H), whereas the origin of the light strand DNA replication (O_L) is harboured outside the D-loop region approximately 11,000 bp downstream of O_H within a tRNA cluster [22] (Figure 1.2).

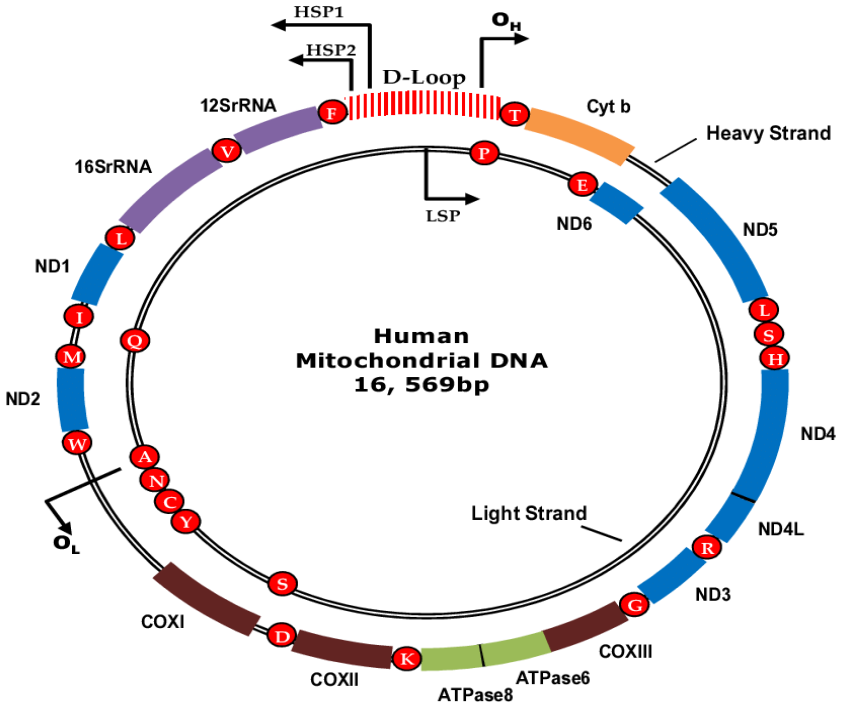

Figure 1.2. Structure of the human mitochondrial genome; a double-stranded DNA that encodes 13 essential OXPHOS subunits. The diagram also shows the two ribosomal RNA (12S rRNA and 16S rRNA) genes and the 22 transfer RNA genes (red spheres depicted by single-letter amino acid code abbreviations) required for mitochondrial protein synthesis. F = Phenylalanine; V = Valine; L = Leucine; I = Isoleucine; Q = Glutamine; M = Methionine; W = Tryptophan; A = Alanine; N = Asparagine; C = Cysteine; Y = Tyrosine; S = Serine; D = Aspartic acid; K = Lysine; G = Glycine; R = Arginine; H = Histidine; E = Glutamic acid; T = Threonine; P = Proline. HSP 1, 2: heavy strand promoter 1 and 2, LSP: light strand promoter, O_H: origin of replication of heavy strand; O_L: origin of replication of light strand [23].

Several proteins are involved in mtDNA replication or transcription, and mitochondrial transcriptional factor A (TFAM) plays dual roles in mtDNA replication and transcription through binding to D-loop [24]. Notably, mtDNA was initially thought to be naked, unprotected, and vulnerable to damage, but a recent report (reviewed in Ref. [25]) has suggested that the mitochondrial genome is protein-coated and packaged into nucleoids by TFAM due to its ability to bind, wrap, bend and unwind DNA without sequence

specificity. Mice with overexpression of TFAM showed a higher mtDNAcn while a decrease of mtDNAcn was observed with the knockdown of TFAM expression. Moreover, phosphorylation of TFAM evidenced to define its activity therefore, might be involved in the regulation of mtDNAcn [26,27].

Another nuclear DNA encoded protein, Ribonucleotide reductase regulatory TP53 inducible subunit M2B (RRM2B), has also been implicated in mtDNA replication and maintenance of mitochondrial DNA content by supplying deoxyribonucleoside triphosphates (dNTPs) for DNA damage repair [28,29]. It has been shown that abnormalities in its gene are one of the causes of the Mitochondrial DNA Depletion Syndrome (MDDS) [30].

Generally, cellular mtDNA content ranges from 10^3 copies to 10^4 copies per cell and is strictly regulated during differentiation. The actual mtDNA copy number (mtDNAcn) is determined by the demand for ATP generated through OXPHOS, and this is associated with other internal and external factors. Cells with higher requirement for ATP have larger mtDNAcn, whereas those with lower requirement have fewer mtDNA copies. Moreover, the synthesis and degradation of mtDNA are rapid and independent of the cell cycle so the dynamic equilibrium between them also influences the overall mitochondrial content [18,20,26].

1.1.3.2 Mitochondrial DNA replication and transcription

Mitochondrial DNA is replicated by proteins different from the ones used by the nuclear genome (reviewed in Ref. [31]). DNA polymerase γ (POLγ) is the replicative polymerase in mitochondria. In human, POLγ is a heterotrimer with one catalytic subunit (POLγA) that acts to proofread the newly synthesised DNA strand and two accessory subunits (POLγB), which promote the interactions with the DNA template and increase the activity of POLγA. Additional polymerases have also been reported to be involved in mitochondrial DNA replication such as PrimPol, DNA polymerase β, DNA polymerase θ, and DNA polymerase ζ [22]. Since POLγA is not able to use double-stranded DNA as a template, the DNA helicase TWINKLE moves in front of the POLγ to unwind the mtDNA and form the required single-stranded DNA (ssDNA). The exposed ssDNA will be protected against nucleases by its binding to mitochondrial single strand DNA binding protein (mtSSB), which also plays a role in preventing secondary structure formation and stimulating activities of TWINKLE and POLγA [22,32].

Mitochondrial DNA replication is initiated at O_H and a new H-strand will be synthesised while the parental H-strand is covered by mtSSB (Figure 1.3). Once the replication passes the O_L, parental H-strand forms a stem-loop structure at O_L to block the binding to mtSSB and a short singlestranded DNA in the loop region will be presented where mitochondrial RNA polymerase (POLRMT) can initiate primer synthesis [22,32]. Directly after 25 nucleotides, POLRMT will be replaced by POLγA at the 3′-end of the primer and L-strand will be initiated. Synthesis of the two strands proceeds continuously until they both reach the full circle. When the synthesis of the two strands is complete, the new strands will be ligated by DNA ligase III after the removal of the RNA primers used for the initiation of mtDNA synthesis by RNASEH1 [22,32].

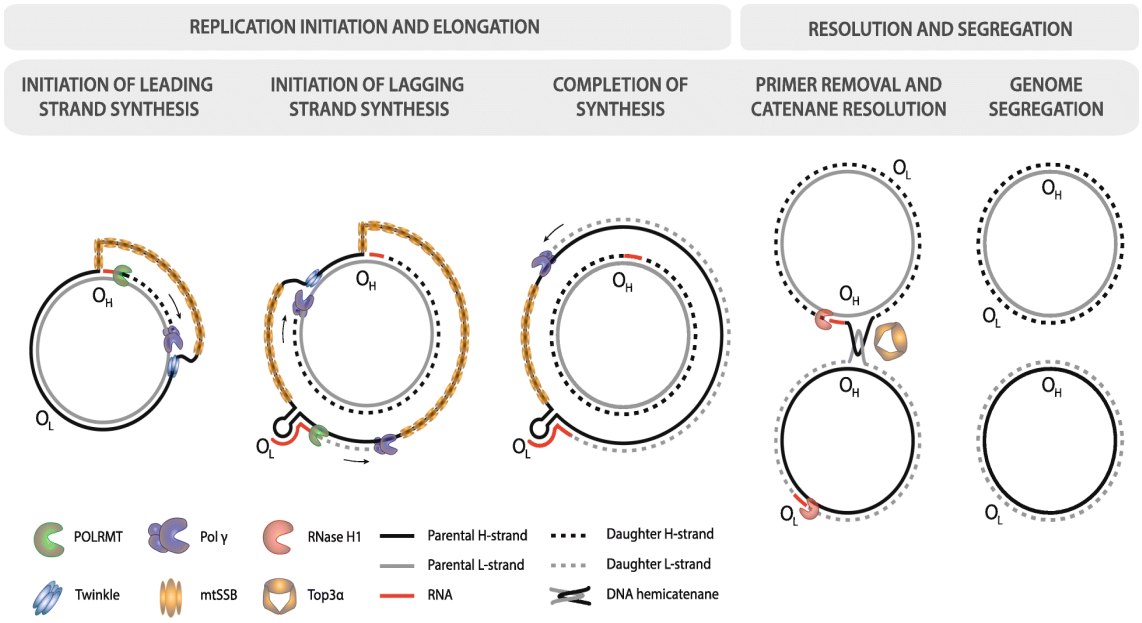

Figure 1.3. Replication of the human mitochondrial DNA [33].

Generally, 95% of the replication events initiated at O_H do not reach the full circle, and they usually terminate after 650 nucleotides at the termination associated sequences (TAS). This newly formed short DNA fragment (called 7S DNA) remains attached to the parental L-strand while the parental H-strand is displaced (Figure 1.4). As a result, a triple-stranded displacement loop structure, a D-loop, is formed [22].

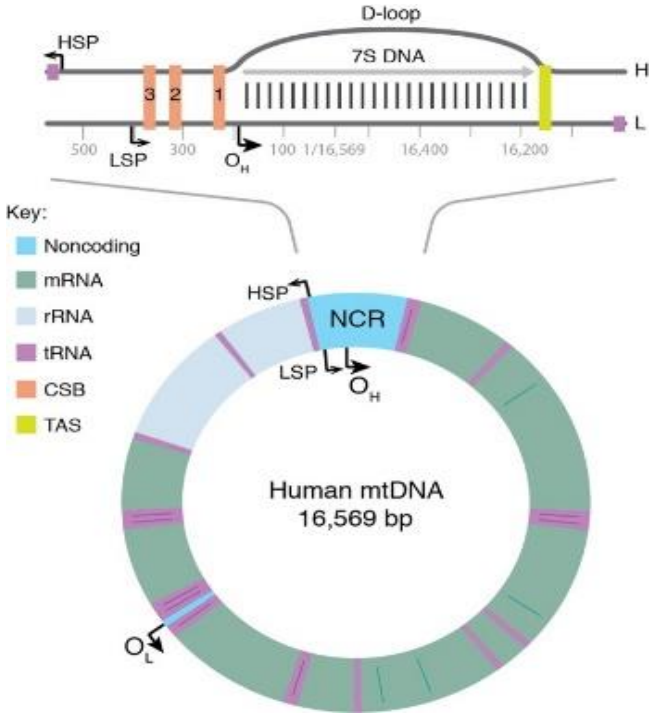

Figure 1.4. Structure of the triple-stranded displacement-loop (D-loop) region. The major noncoding region, which is shown enlarged at the top, contains the heavy and light strand promoters (HSP & LSP), three conserved sequence boxes (CSB1-3, orange), the H-strand origin of replication (O_H), and the termination-associated sequence (TAS, yellow). The triple-stranded DNA (D-loop) is formed by an early termination of nascent H-strand DNA synthesis at TAS. The short H-strand replication product formed in this manner is termed 7S DNA. Another minor NCR (non-coding region), located approximately 11,000 bp downstream of O_H, contains the L-strand origin of replication (O_L) [22].

Transcription of the mitochondrial DNA initiates in the D-loop region which contains the L-strand promotor (LSP) and the H-strand promotor (HSP). The transcription of eight of the tRNAs and the MT-ND6 gene are controlled by light strand promoter. Whereas the transcription of the two rRNAs (12S and 16S), the remaining 14 tRNAs and almost the entire OXPHOS subunits are produced by HSP transcription. The machinery needed for transcription initiation requires the association of three proteins: mitochondrial RNA polymerase (POLRMT), mitochondrial transcription factor A (TFAM) and mitochondrial transcription factor B2 (TFB2M). Recent studies [32,34] have shown that in the transcription initiation complex, TFAM bounds to DNA and facilitates the recruitment of POLRMT to the promoter via its large N-terminal extension, then TFB2M modifies the structure of POLRMT to induce opening of the promoter. The elongation stage requires an additional transcription elongation factor (TEFM) which significantly enhances POLRMT activity and promotes the formation of longer transcripts. Mitochondrial termination factor 1 (MTERF1) is responsible for transcription termination through DNA binding, which prevent the transcription from progressing [32,34].

1.1.4 ATP generation

ATP is the energy currency of cells and mainly produced by the oxidation of glucose which is a two-stage process: glycolysis at the cytosol and oxidative phosphorylation (OXPHOS) at the mitochondria. Since most of the ATP is produced inside the mitochondria, they are considered as the primary source of ATP production in human cells (reviewed in Ref. [35]).

Generally, glycolysis is an anaerobic process (does not require O_2) and triggered by a sequence of multiple reactions that metabolises one molecule of glucose to two molecules of pyruvate with the net production of two molecules of ATP. Produced pyruvate can be later processed anaerobically to lactate (lactic acid fermentation) or ethanol (ethanol fermentation). However, pyruvate under aerobic condition is transported to mitochondria and can be fully oxidised into carbon dioxide and water resulting in much more ATP generation through TCA cycle and electron transport chain (reviewed in Ref. [19]).

The starting point of this oxidative pathway is acetyl coenzyme A (acetyl-CoA) that is produced inside the mitochondrial matrix by the oxidative decarboxylation of pyruvate. Subsequently, citric acid cycle removes electrons from acetyl-CoA and uses these electrons to form NADH and FADH2. During the OXPHOS process, electrons released from acetyl-CoA flow through a series of membrane proteins (known as electron transport chain, ETC) which consists of approximately 100 protein subunits clustered in four specific ‘complexes’ housed within the mitochondrial inner membrane to produce a proton gradient across the mitochondrial membrane. These protons flow through ATP synthase to generate the ATP from ADP (reviewed in Ref. [19]) (Figure 1.5).

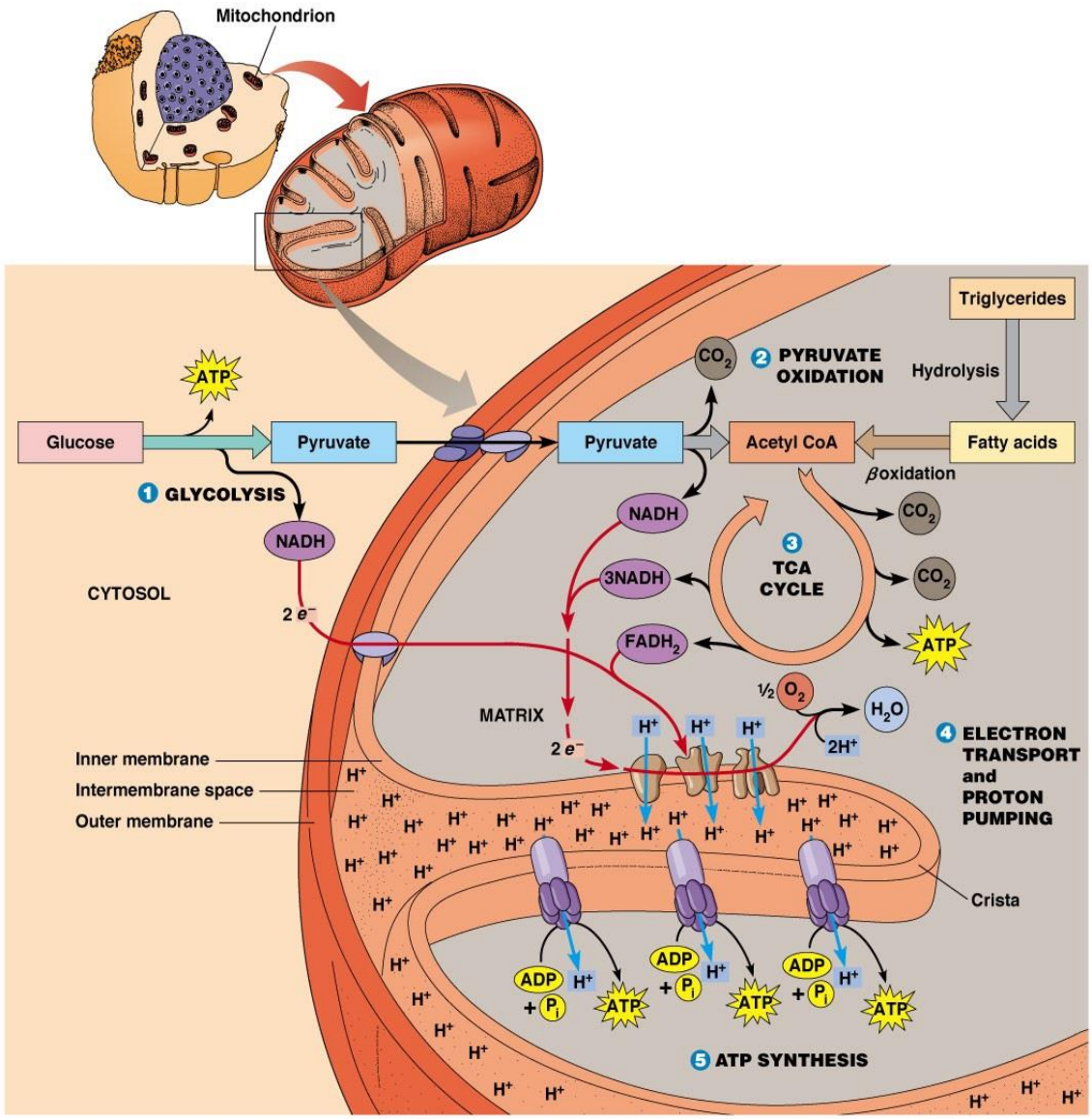

Figure 1.5. Overview of ATP generation [35].

1.1.5 Mitochondrial respiratory chain

Electron transport chain (ETC) is also known as mitochondrial respiratory chain (MRC). There are 13 protein subunits for four of the five MRC complexes encoded by the mitochondrial genome, namely seven subunits of NADH dehydrogenase (complex I), one of cytochrome *c* oxidoreductase (complex III), three of cytochrome *c* oxidase (complex IV) and two of ATP synthase (complex V). The four subunits of respiratory enzyme complex II are totally encoded by nuclear DNA (nDNA), transcribed and translated in the cytoplasm and then transported into the mitochondria. Over 70 nuclear subunits complete this elegant molecular machine, and the interaction between these complexes enables the production of the majority of ATP through OXPHOS [21,36].

As mentioned earlier, the process of OXPHOS initiates when electrons are received from electron donors produced from the glycolysis and citric acid cycle (e.g. nicotinamide adenine dinucleotide (NADH) and flavin adenine dinucleotide (FADH2)). These molecules donate electrons to complexes I and II in the respiratory chain, and the electrons flow on to complexes III and IV. A small amount of energy is released at each of these steps that is used to pump protons (H^+) across the inner mitochondrial membrane creating an excess of hydrogen ions in the intermembrane space and an electrochemical proton gradient (Figure 1.6). The energy stored in this electrochemical potential is then able to flow down this gradient, through complex V (ATP synthase) resulting in the production of ATP in a phosphorylation reaction utilising ADP and inorganic phosphate (Pi). The electrons reaching the end of this chain at complex IV are accepted by oxygen and eventually form water (H_2O) (reviewed in Ref. [19]).

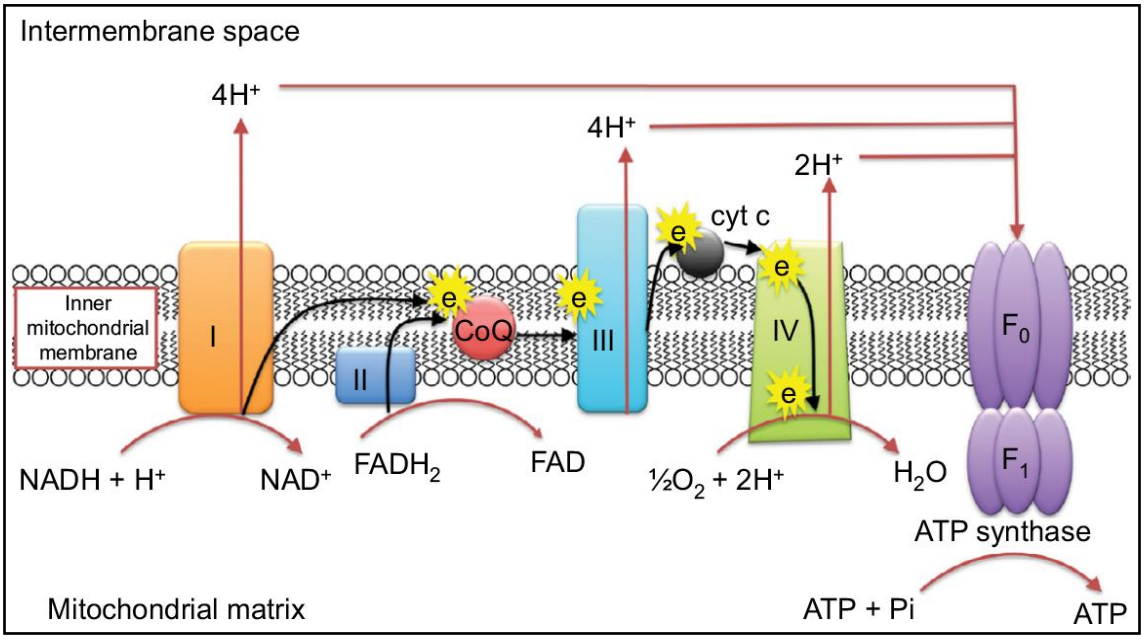

Figure 1.6. Mitochondrial respiratory chain. NADH and FADH2 donate electrons (e^-) to complex I and complex II. They then pass through co-enzyme Q (CoQ) onto complexes III, IV and cytochrome *c* oxidase. These stages allow hydrogen ions (H^+) to be pumped into the IMS which then flow back through complex V into the mitochondrial matrix generating ATP [37].

1.1.5.1 Complex I

Complex I (NADH dehydrogenase; ND), also known as NADH: ubiquinone oxidoreductase, is one of the largest membrane-bound enzymes in the cell. It contains 45 subunits resolved in the L-shaped molecule, comprising 14 core subunits that house the catalytic machinery with their nine cofactors (a flavin mononucleotide (FMN) and eight iron sulfur (FeS) clusters) and 31 supernumerary subunits that are central to the structure stability and assembly of the complex, and some of which also have regulatory or independent metabolic roles [38]. Seven subunits of the core subunits are totally encoded by the mitochondrial genome (ND1, ND2, ND3, ND4, ND4L, ND5 and ND6) and harboured in the hydrophobic membrane domain whereas the hydrophilic matrix arm harbours the nuclear DNA-encoded core subunits and the FMN and FeS clusters [39] (Figure 1.7).

Complex I powers the ATP synthesis in mitochondria via the oxidation of NADH into NAD^+ by the FMN, and two electrons released from NADH are transferred along a chain of FeS to the highly hydrophobic exogenous ubiquinone (Q). The latter lies at the interface of the hydrophilic nuclear subunits (49 KDa/PSST) and the membrane ND1/ND3 subunits which will be reduced to ubiquinol (QH_2) (Figure 1.7). Coupled with the electron transport during this step of OXPHOS, four protons are translocated across the inner mitochondrial membrane through four different routes structured inside ND2, ND4, ND5 individually and ND1+ND4L+ND6 jointly [38–40].

This step of reaction can be presented in the following formulation:

$$NADH + H^+ + Q + 4H^+_{in} \longrightarrow NAD^+ + QH_2 + 4H^+_{out}.$$

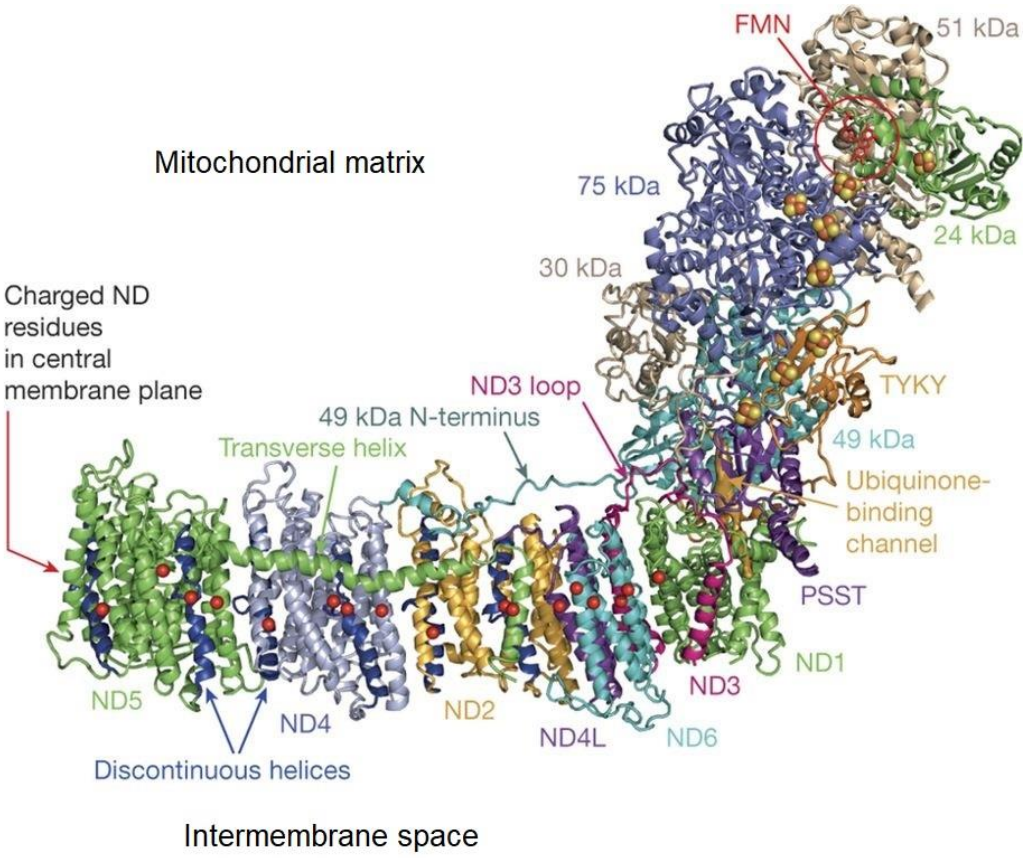

Figure 1.7. Crystal structure of the core subunits and ubiquinone-binding site of mammalian complex I [38].

1.1.5.2 Complex II

Complex II (Succinate dehydrogenase; SDH) comprises four subunits (SDHA, SDHB, SDHC and SDHD) which are totally encoded by the nuclear DNA (Figure 1.8). In addition to its role in OXPHOS, SDH is a component of the TCA cycle, making a functional link between these two essential processes. In the TCA cycle, complex II oxidises succinate to fumarate. As part of OXPHOS, SDH transfers electrons from succinate via FAD and its FeS clusters to ubiquinone (reviewed in Ref. [41]).

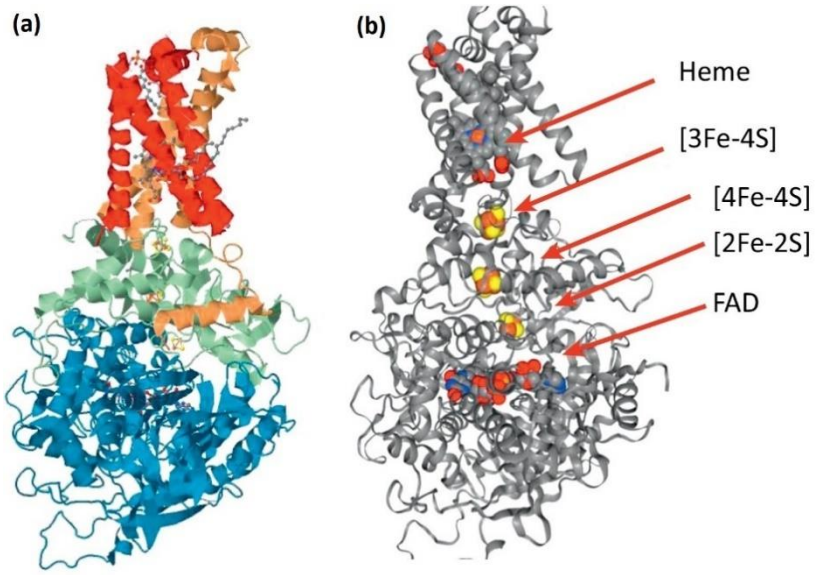

Figure 1.8. Crystal Structure of complex II. (**a**) shows subunits of SDH: SDHA (blue), SDHB (green), SDHC (brown) and SDHD (red). (**b**) highlights three iron sulfur (FeS) clusters of SDH [41].

1.1.5.3 Complex III

Complex III (ubiquinol-cytochrome *c* oxidoreductase), also known as the cytochrome *bc1* complex, occupies the middle position of the OXPHOS system. It catalyses the transfer of electrons to cytochrome *c* (Cyt *c*) from ubiquinol which is coupled with protons translocation across the mitochondrial inner membrane [42]. Complex III exists as a functional dimer where each monomer is composed of 11 different subunits. All subunits are encoded by the nuclear genome except cytochrome *b* (Cyt *b*), a predominantly hydrophobic protein which is encoded by the mitochondrial gene, MT-CYB [43]. At least three redox active subunits are existing in each half of complex III: iron-sulfur protein (ISP) containing 2Fe-2S cluster, cytochrome c_1 and cytochrome *b* with two hemes (b_H and b_L) and two separate quinone binding sites called Q_o site for ubiquinol oxidation and Q_i site for ubiquinone reduction (Figure 1.9) [44].

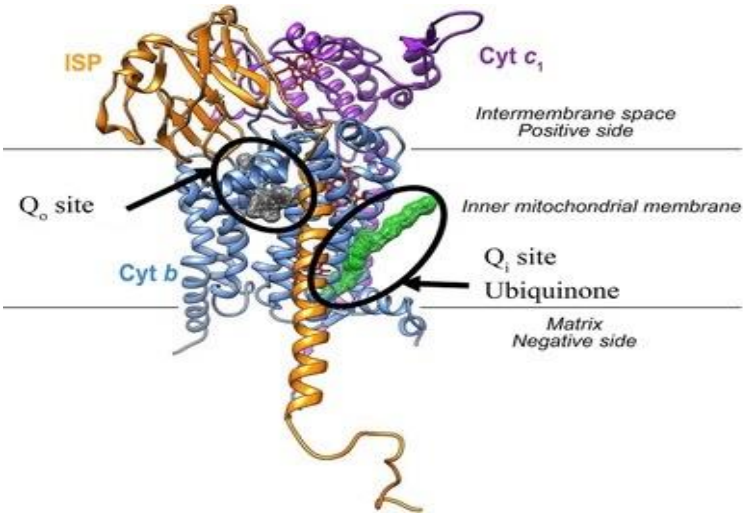

Figure 1.9. The catalytic core complex III. Redox active groups are located within three subunits that form the catalytic core: cytochrome c_1 (purple), ISP (yellow) and cytochrome *b* (blue) which contains two hemes (b_H and b_L) and forms the two quinol binding sites: Q_o and Qi [43].

There is a bifurcated electron flow at the Q_o site where two electrons are transferred from ubiquinol to two different chains. The first electron is transferred to the ISP, then to cytochrome c_1 and finally to Cyt *c*. The second electron is transferred sequentially to heme b_L then b_H, and later to the ubiquinone at Q_i site. In the full catalytic cycle, two cyt *c* molecules are reduced, and two ubiquinol molecules are oxidised at the Q_o into ubiquinone and one molecule of ubiquinone is reduced to ubiquinol at the Q_i site. A total of four protons are translocated across the inner mitochondrial membrane from the matrix to the intermembrane space during this cycle [43,45]

Finally, both reduced Cyt *c* molecules are released from complex III and diffuse to complex IV to transfer their electrons to complex IV where the O_2 is reduced to H_2O accompanied with the translocation of two protons [46].

1.1.5.4 Complex IV

Complex IV (cytochrome *c* oxidase; CO) is the terminal oxidase of the electron transport chain. It is composed of 13 subunits: three subunits (COI, COII and COIII) are encoded by the mitochondrial DNA and form the central core, and 10 subunits are encoded by the nuclear genome and form a structural scaffold around the core [45]. Complex IV also contains two iron sites (heme a and a_3), two copper sites (Cu_A and Cu_B), one zinc ion, one magnesium ion and several phospholipid molecules [47]. There are three main parts of complex IV: an inner region that faces the matrix side, an outer area that faces the inter membrane space and a large transmembrane region which contains the three mitochondrial subunits [45].

Among the three mitochondrial subunits, COIII forms a homodimer at the centre of complex IV. Although COIII does not have any binding pocket or active site, it plays an important role in the formation and stabilisation of the complex IV dimer [42]. On the other hand, COI is the major subunit of complex IV and along with COII, responsible for electron and proton transfer. COI and COII create the channels for O_2 to reach the dioxygen reduction site and for the produced water to be removed from the same site [45,48].

In a complete catalytic cycle, complex IV accepts 4 electrons from 4 reduced Cyt *c* produced by complex III to reduce oxygen (O_2) and form 2 molecules of water. This process is coupled with 6 protons being removed from the matrix of which two are translocated across the inner mitochondrial membrane [45,47,49] (Figure 1.10).

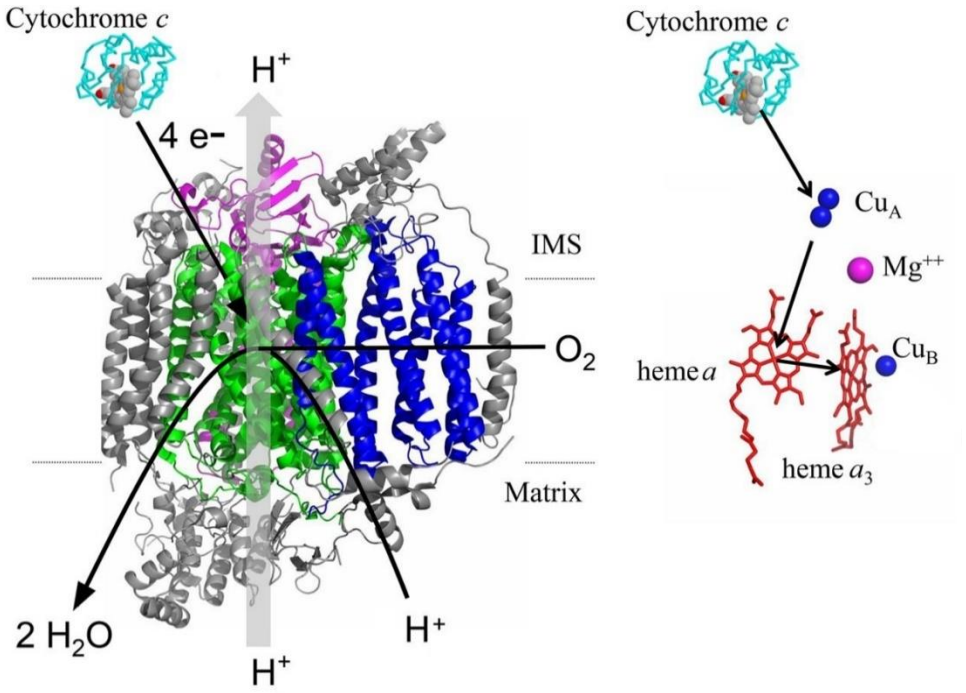

Figure 1.10. Overall structure and cofactors of mammalian cytochrome *c* oxidase. The three mitochondrial subunits (COI, COII and COIII) are shown in green, purple and blue respectively. Cytochrome *c* in the IMS sequentially donates four electrons which are accepted initially by Cu_A and later transferred via the low spin heme a into the haem a_3/Cu_B. Molecular oxygen enters complex IV from the membrane phase to be reduced to two water molecules with the uptake of four protons [50].

Complex I, complexes III and IV preserve the cross-membrane proton gradient that is the driving force behind ATP generation in the mitochondrial respiratory chain via the F_OF_1 ATP synthase [45].

1.1.5.5 Complex V

Complex V (ATP synthase) is the primary producer of adenosine triphosphate (ATP). It is composed of a hydrophobic membrane inserted region F_O that traverses the inner mitochondrial membrane and a soluble hydrophilic catalytic F_1-ATPase region that protrudes into the matrix. Two mitochondrial encoded subunits, ATP6 and ATP8 (also known as subunit a and A6L respectively), form the F_O region with the presence of several nuclear encoded subunits (e, f, g, DAPIT and the two hydrophobic alpha-helices of subunit b), a proteolipid and the c_8-ring (known as the rotor), whereas the F_1-ATPase region is formed by the α, β, γ, δ, ε subunits. The F_O and F_1-ATPase regions are linked via subunits OSCP, F_6, d and the hydrophilic portion of subunit b (Figure 1.11) [42,51].

Complex V drives the protons from the IMS to the matrix through two half channels formed by ATP6 and the rotor. The first half channel allows protons to move half way from the IMS across the lipid bilayer and protonate the Glu85 residue in one of the c subunits and consequently induce c-ring to rotate. Once the protonated Glu residues have moved full circle around the rotor, the other half channel provides an exit for the proton into the matrix [42,51].

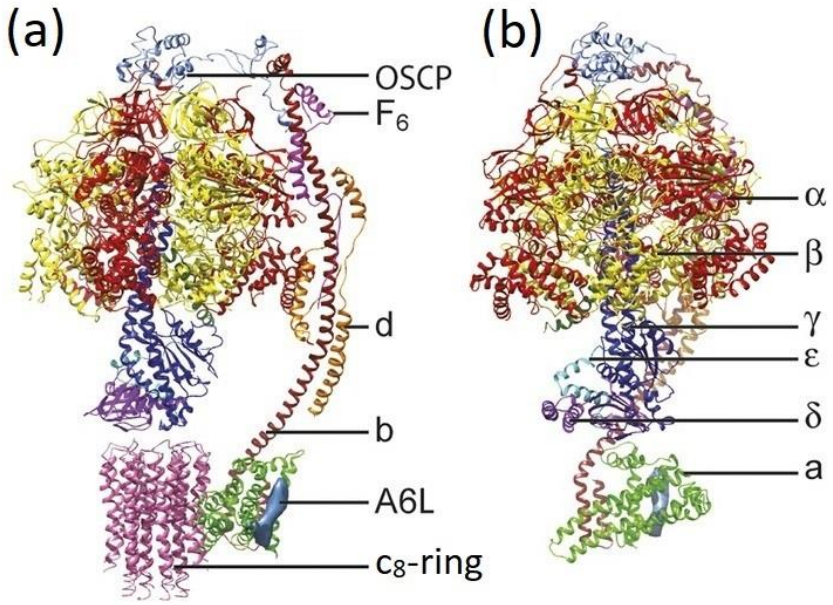

Figure 1.11. Crystal structure of complex V shown in different orientations with the c_8-ring removed for better clarity in panel (**b**) [51].

Oxidative phosphorylation (OXPHOS) is a pivotal system for the production of cellular energy in the form of ATP. Various other processes coupled to the electron transfer and proton translocation of the MRC include the regulation of nucleotide pools, tricarboxylic acid-cycle (TCA) flux, reactive oxygen species (ROS) production and signalling, calcium homeostasis, mitochondrial transmembrane potential and apoptosis. Due to the importance of OXPHOS, genetic mutations (germ-line or somatic) in both the mtDNA and nDNA sequences that result in aberrant protein subunits of the OXPHOS system may not only affect the mitochondrial function but also contribute to numerous human diseases [21].

1.1.6 Mitochondrial role in apoptosis

Mitochondria are essential for life due to their vital role in biosynthetic processes such as ATP generation. Paradoxically, mitochondria play a central role in apoptotic cell death (reviewed in Ref. [52]). They contain a number of proteins implicated in cell death initiation following their release from IMS to the cytosol. Specific pro-apoptotic proteins have been confirmed to be converged at mitochondrial level such as cytochrome *c*, second mitochondria-derived activator of caspases/direct inhibitor of apoptosis-binding protein with low pI (Smac/DIABLO), apoptosis-inducing factor (AIF) and endonuclease G (Endo G) [53,54].

Apoptosis is a programmed cell death characterised by controlled auto digestion of the cell. It differs from necrosis by specific morphological features including chromatin condensation, DNA fragmentation and the breakdown of the cell into a series of membrane-bound fragments called apoptotic bodies [55]. Moreover, apoptosis is also sub-classified into two pathways, namely the extrinsic pathway and the intrinsic mitochondria-mediated pathway (Figure 1.12). The extrinsic pathway requires effective engagement between the death receptors such as tumour necrosis factor receptor (TNFR), CD95 (also known as first apoptosis signal/Fas) and TNF-related apoptosis inducing ligand (TRAIL) receptors found on the surface of the cell membranes and their respective ligands. Activation of CD95 or TNF receptors leads to the activation of initiator caspase, procaspase 8. Subsequently, activated caspase 8 triggers the execution phase of apoptosis by activating the downstream effector caspase, caspase 3 (reviewed in Ref. [35]). Caspases are family of cysteine proteases that play a major role in the regulation of cell survival and the execution of apoptotic events [56].

On the contrary, the intrinsic pathway (illustrated in Figure 1.12) is activated by several receptor-independent stimuli such as radiation, free radicals and viral infections. In this process, the defining event is mitochondrial outer membrane permeabilisation (MOMP). This event results in the release of pro-apoptotic proteins that facilitate the activation of caspase 9, an initiator caspase to the apoptotic pathway [26].

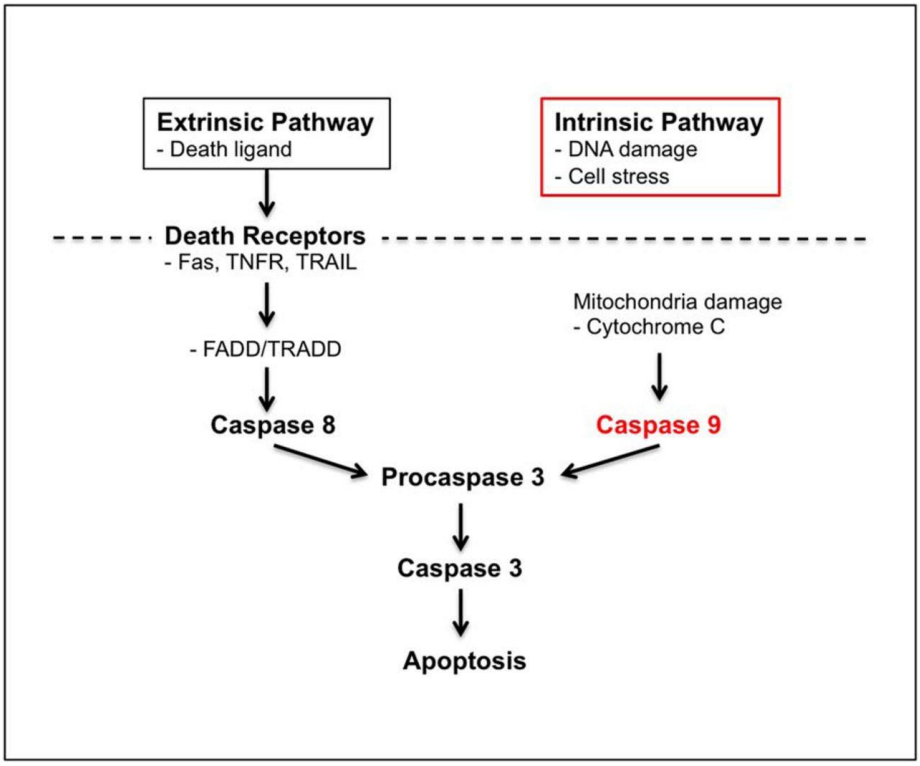

Figure 1.12. Overview of apoptosis pathways. FADD: Fas-associated protein with death domain, TRADD: Tumour necrosis factor receptor type 1-associated death domain.

Cytochrome *c* binds to the apoptosis protease-activating factor (APAF-1) and causes its oligomerisation with pro-caspase 9. This active Cyt *c*/APAF-1/pro-caspase 9 activates caspase 9 that in turn cleaves and activates executioner caspases 3 (Figure 1.13).

A proteolytic cascade is then initiated with the cleavage of procaspases 6 and 7 leading to the dismantling of the cell with distinctive biochemical and morphological hallmark (reviewed in ref [54]). On the other hand, Smac/DIABLO binds to IAPs (inhibitor of apoptosis proteins) and deactivates them, thus preventing IAPs from binding to the activated forms of caspase 3 and caspase 9, as well as preventing their block of the apoptosome-mediated caspase activation, and consequently permitting apoptotic progression. In some models, the release of AIF and Endo G is a late event in apoptosis, which occurs once the cells are committed to apoptosis. Both AIF and Endo G provoke caspase independent DNA degradation and execute cell death. Alterations in this natural death mechanism can lead to diseases such as cancer (reviewed in Ref. [35]).

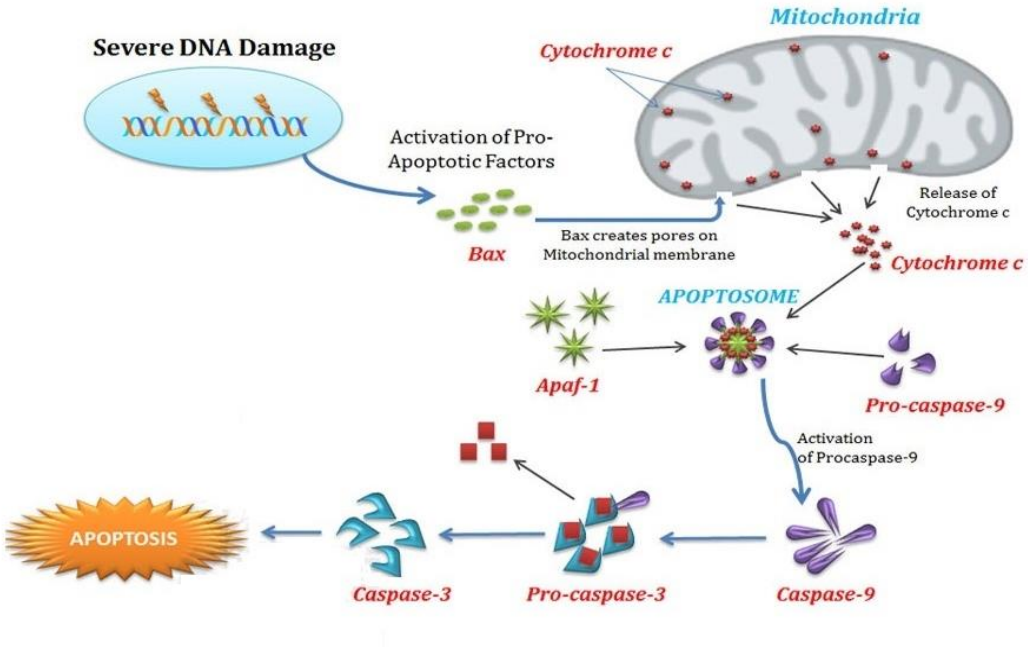

Figure 1.13. Intrinsic pathway of apoptosis [57].

MOMP effectively represents a point of no return, and it is highly regulated by members of the BCL-2 protein family. This family is subdivided into anti-apoptotic BCL-2 proteins (BCL-2, BCL-XL, MCL-1, A1, BCL-B, BCL-w), pro-apoptotic proteins (BAK and BAX) and pro-apoptotic BH3-only proteins (BID, BIM, PUMA, Noxa, HRK, BIK, BMF, BAD) which can be further subdivided into activators that are able to directly activate BAX/BAK or sensitisers that neutralise the apoptotic brake regulated by anti-apoptotic BCL-2 proteins (reviewed in Ref. [52]). Activation and oligomerisation of BAX or BAK require direct interaction with a member of the BH3-only protein family (e.g. BID). Such conformational changes lead to the formation of the mitochondrial permeability transition pore (MPTP) [35,54].

The MPTP consists of ANT (adenine nucleotide translocator), CypD (cyclophilin D), PBR (peripheral benzodiazepine receptor) and VDAC (voltage-dependent anion channel) (reviewed in Ref. [35]). VDAC1, the most abundantly expressed protein of the three isoforms of the mammalian VDAC, has been reported to be a target for both pro-apoptotic (BAX and BAK) and anti-apoptotic (BCL-XL) proteins [58,59]. Interaction of VDAC1 with the pro-apoptotic BCL-2 members is thought to result in OMM permeabilisation that is potentially linked with the release of cytochrome *c* from the IMS, whereas interaction with the anti-apoptotic BCL-2 proteins supresses VDAC1 oligomerisation and prevents OMM permeabilisation (reviewed in Ref. [60]).

It has been demonstrated that once BAX binds to VDAC1, this assembly facilitates the formation of a channel complex with sufficient pore size capable of releasing cytochrome *c* from the IMS to the cytosol and consequently triggers caspase-initiated apoptosis [61]. The formation of the MPTP has also been linked to the interaction of BAX with ANT, as well as the BID-induced channel closure of VDAC (reviewed in ref [54]).

Anti-apoptotic BCL-2 proteins counteract the activity of BAK/BAX and prevent the formation of the MPTP by either binding to the activated BAK/BAX directly or binding to BID and consequently blocking its interaction with BAK/BAX (reviewed in Ref. [52]). It has also been shown that BCL-XL can protect the cells from apoptosis by maintaining mitochondrial membrane integrity and therefore avoiding the release of apoptogenic factors such as Cyt *c*. This is through the interaction of BCL-XL with ANT/VDAC which prevents the latter from forming the mitochondrial pores (reviewed in Ref. [35]).

The inner membrane transmembrane potential is often used as an indicator for cellular viability, as the proton gradient across the IMM is essential for the ATP synthase activity in the OXPHOS process, as well as for the import of mitochondrial proteins and the regulation of metabolite transport. Thus, disruptions to this transmembrane potential have severe consequences in mitochondrial respiration, energy production, and consequently, cell survival (reviewed in Ref. [54]).

Apoptosis is an energy-dependent phenomenon as the complete apoptotic program involves the formation of apoptosome (when Cyt *c* and ATP bind to APAF-1 and activates pro-caspase-9) and hydrolysis of macromolecules. However, the inhibition of ATP production occurs relatively late in apoptosis compared to other types of cell death where necrosis is characterised by an early loss of ATP synthesise [54]. Leist *et al.* [62] reported that depletion of cellular ATP using oligomycin, an ATP synthase inhibitor, resulted in the switch from apoptosis to necrosis in leukemic cells. Similar results were observed when rat fibroblastic cells were treated with antimycin, inhibitors of complex III [63]. Thus, ATP demonstrates a key role in determining the cell death pathway engaged under various metabolic conditions (reviewed in Ref. [54]).

Given the important role of mitochondria in apoptosis, it is not surprising that downregulated, suppressed or mutated pro-apoptotic proteins as well as overexpressed anti-apoptotic proteins have the propensity to allow cells to acquire resistance to apoptosis, and develop diseases as cancer (reviewed in Ref. [35]).

1.1.7 MtDNA Mutations

MtDNA is protein-coated and packaged into nucleoids by mitochondrial transcription factor A (TFAM) due to its ability to bind, wrap, bend and unwind DNA without sequence specificity. Unlike nuclear DNA, mtDNA lacks introns and protective histones due to the poor fidelity of DNA polymerase, hence the mutation rate of mtDNA is substantially greater than that of nuclear DNA [64]. In addition, because mtDNA is close to mitochondrial respiratory chain that continuously generates oxidizing products known as reactive oxygen species (ROS), mtDNA is more susceptible to ROS-induced mutations. As a result, the incidence of mtDNA mutation can be 10 times higher than that of nDNA mutation (reviewed in Ref. [65]). However, beside its dual roles in mtDNA replication and transcription through binding to D-loop, TFAM is believed to exert the histone-like protection and provide proper architecture to mtDNA, so downregulation of TFAM may promote mtDNA mutations [18,25].

Both point mutations and deletions in mtDNA can occur either due to mtDNA replication aberrations or induced by chemical and physical mutagenic agents such as UV or X radiation, ROS and RNS (reactive nitrogen species) [19,66].

In most animals, as in humans, the mitochondrial genome does not follow the Mendelian rules of inheritance. It is maternally inherited, and therefore a mother carrying a germline mtDNA mutation can transmit it to her children, and only her daughters can further transfer it to the next generation (reviewed in Ref. [25]).

Somatic mutations in human mtDNA have been proposed to accumulate during the life span. Accordingly, it has been observed that the mitochondrial genome in the heart, brain and skeletal muscle of ageing humans harbour higher numbers of mutations compared to the corresponding tissues of young subjects. The age-correlated accumulation of mtDNA mutations has been suggested to be the progressive result of a mitochondrial vicious circle [53,67,68]. According to this theory, mutations in either mitochondrial or nuclear genes encoding subunits of the ETC will impair electron transfer leading to increased ROS production. Eventual oxidative damage to mtDNA induces further impairments of the mitochondrial subunits of the ETC, which in turn results in higher ROS production and further mtDNA damage, thus establishing a vicious circle rendering an accumulation of mtDNA mutations (reviewed in Ref. [69]).

Five different types of DNA repair mechanisms are present in the cell to avoid the accumulation of DNA defects: base excision repair (BER), nucleotide excision repair (NER), DNA double-strand break repair, direct reversal and mismatch repair (MMR).

BER is the most documented mechanism in mitochondria, and it has been recently suggested that it is modulated by TFAM (reviewed in Ref. [25]). It is a fundamental weapon in correcting alkylated, hydrolytic and oxidative lesions as well as ROS induced DNA breaks. BER repairs a wide range of base modifications, fixes abasic sites (also known as apurinic/apyrimidinic site; AP site) and single-strand breaks in DNA. The mitochondrial BER machinery includes DNA glycosylases (OGG1, MUTYH, UNG1, NTHL1, NEILI1/2, MTH1) that recognise and remove mutated base [70].

OGG1, also known as 8-oxoguanine DNA glycosylase, mainly removes 8oxoG adducts, the most remarkable mutagenic lesions generated by ROS resulting in mismatch pairing with adenine or thymine during replication thus generating the G:C → T:A transversions [71]. Since OGG1 does not recognise adenines mispaired with 8oxoG bases, MUTYH are required to firstly remove the adenine and allow subsequent BER [72] (Figure 1.14).

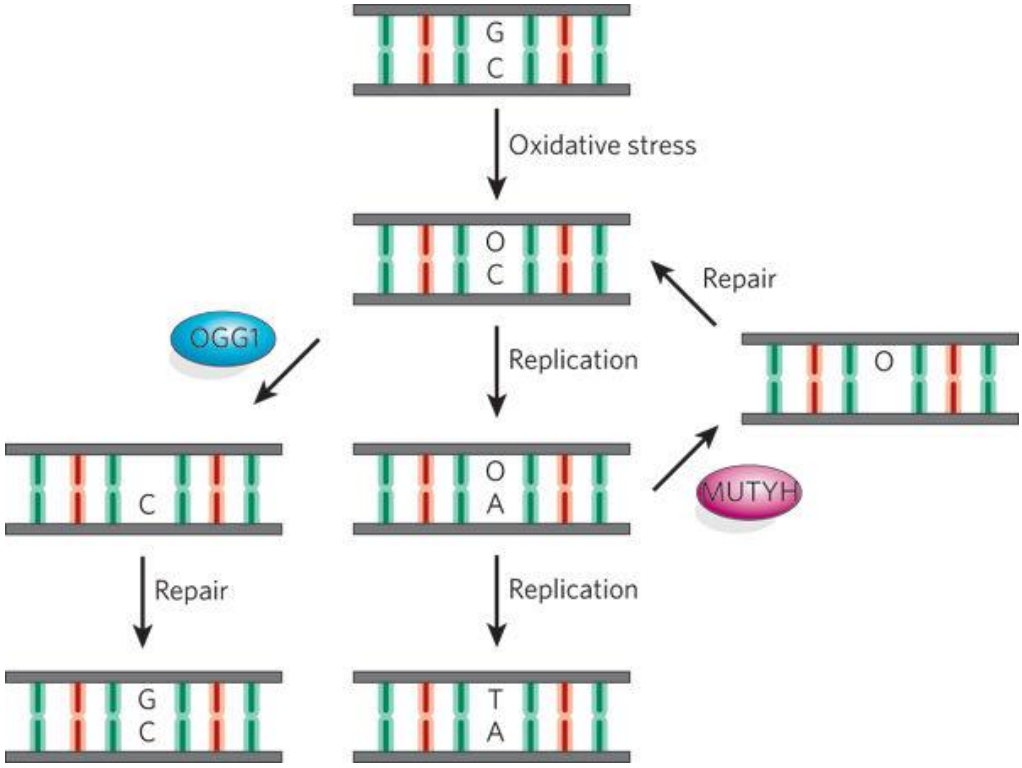

Figure 1.14. The 8oxoG base excision repair. The presence of 8oxoG in DNA results in G:C to T:A transversion mutations during DNA replication or inaccurate DNA repair. Human DNA glycosylases OGG1 and MUTYH are involved in the excision of bases (O and A) from the DNA [73].

Moreover, MTH1, an 8-oxoGTPase, primarily prevents oxidised purine dGTP from being incorporated into DNA and consequently eliminates A:T to C:G and G:C to T:A transversions caused by oxidised purines (reviewed in Ref. [25]). UNG1, uracil DNA glycosylase, removes uracil bases that appear in DNA strands as a result of misincorporation of dUMP instead of dTMP during replication or due to spontaneous deamination of cytosine [74].

On the other hand, NEIL1 and NEIL2 (Nei endonuclease VIII-like 1 and 2) are DNA glycosylases that recognise oxidised pyrimidine, formamidopyrimidine and 5-hydroxyuracil. Both proteins have associated DNA glycosylase/lyase activity towards mismatched thymine and uracil favouring removal of T:C and U:C mismatches. In addition, NTHL1 (endonuclease III-like protein 1) also recognises the oxidised ring pyrimidine residues and initiates the BER repair to remove the lesion that results in an AP site [75].

BER also includes AP endonuclease (APE1) that processes the abasic site. In addition, BER repairs single-strand breaks in DNA employing polymerase gamma (POLG) and DNA ligase (LIG3). POLG re-synthesises missing DNA fragments whereas LIG3 seals the gaps between newly synthesised DNA fragments (reviewed in Ref. [25]).

MtDNA exists in a large number of copies, and it may be all of the same type (homoplasmy) being *wild type* or mutant, or different genotypes may coexist (heteroplasmy) in the cell or tissue (reviewed in Ref. [36]). Threshold effect represents the minimal critical level of a mutation in mtDNA to manifest a pathogenic phenotype when *wild type* molecules cannot compensate for mutant mtDNA molecules within the cell (reviewed in Ref. [19]). The thresholds of various types of mtDNA mutations range from 60% for large mtDNA deletions to 90% for certain tRNA mutations (reviewed in Ref. [25]) (Figure 1.15).

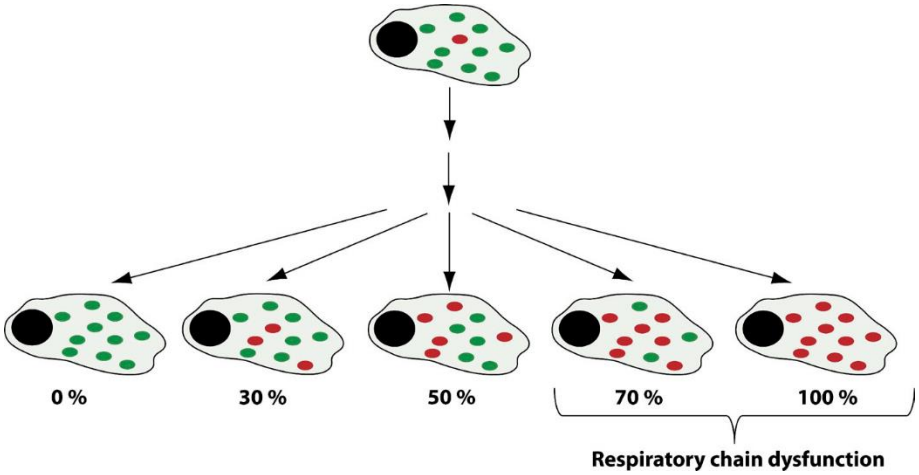

Figure 1.15. Mitotic segregation of mtDNA. Heteroplasmy in a cell is created by a single mutation. Red dots represent the level of mutated mtDNA. Green dots represent the level of wild type mtDNA. The accumulation of mutated mtDNA during cell division above a certain threshold will lead to impaired respiratory chain function [34].

Mitochondrial dysfunction resulted from mtDNA mutations has been implicated in over production of ROS which induces genomic instability (reviewed in Ref. [76]). Moreover, mtDNA mutations have been strongly linked to oxidative stress and associated with increased cancer susceptibility and resistance to apoptosis [53,65,77,78]. To date, mitochondrial genetic abnormalities such as point mutations and large deletions within the displacement loop and coding regions as well as mtDNA copy number changes have been reported in several human cancers including breast, colon, stomach, kidney, thyroid, head and neck and ovarian cancers [18,79–81].

1.2 Mitochondria and cancer

1.2.1 The hallmarks of cancer

Cancer is a devastating disease. It starts when abnormal cells begin to grow and reproduce uncontrollably. Usually the human body has just the right number of each type of cells because they produce signals which control how much cells should divide [82]. Evidently, cancer is considered as a group of multi-process and multifactorial genetic diseases since it is caused by accumulation of mutations in a number of genes in both nDNA and mtDNA that drives normal cells to become progressively malignant (reviewed in Ref. [83]). Hanahan and Weinberg [19,84] firstly suggested a series of common characteristics of cancer called 'hallmarks of cancer' which included: sustained proliferative signals, activation of metastasis and invasion, induction of angiogenesis, evasion of growth suppression, replicative immortality and evasion of programmed cell death (apoptosis). Recently, new cancer hallmarks were proposed including tumour-promoting inflammation, reprogramming of energy metabolism, evading immune destruction and genome instability (summarised in Figure 1.16).

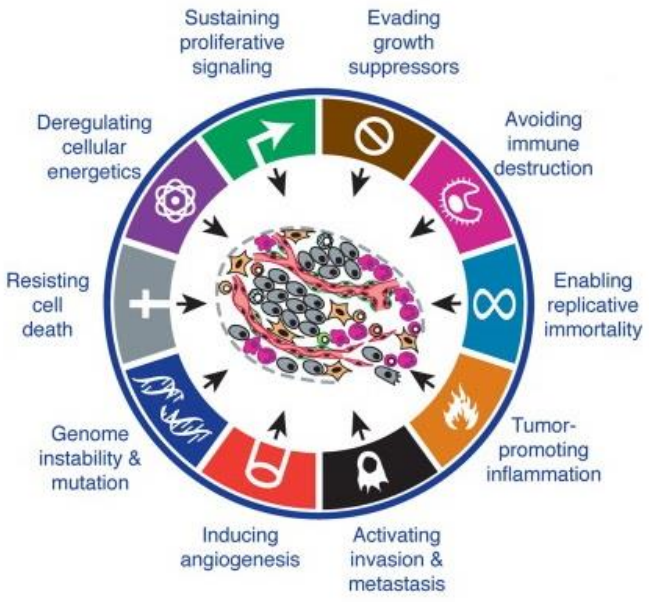

Figure 1.16. A graphic representation of the 'Hallmarks of Cancer' from Hanahan and Wienberg [84].

Furthermore, cancers have the ability to develop resistance through different mechanisms such as drug inactivation, drug target alteration, drug efflux, DNA damage repair, cell death inhibition and the epithelial-mesenchymal transition (EMT). The increasing prevalence of these drug resistant cancers necessitates further research and novel treatment development (reviewed in Ref. [85]).

Mitochondria are fundamental intracellular organelles that regulate energy production, cell death and vital signalling pathways that are essential for cell differentiation and proliferation. Thus, mitochondria are fundamentally involved in cancer biology and a set of orchestrated mitochondria functional modifications are implicated in cancer initiation, growth, metastasis, relapse and acquired drug resistance. Those modifications include a shift of energy production mechanisms, increased ROS production and equivalently increased antioxidant activity, disruption of apoptotic signalling and increased mtDNA mutation (reviewed in Ref. [19]). Indeed, mitochondria of cancer cells are structurally and functionally different from their non-cancerous counterparts, and their dysfunctions result in many defects and grant key roles in the development and progression of cancer (reviewed in Ref. [86]).

1.2.2 Cancer as a mitochondrial metabolic disease

The somatic mutation theory, the most accepted view of the origin of cancer, states that cancer is a genetic disease, as it is caused by changes in genes that control cell functions especially how they grow and divide. However, emerging evidence suggests that cancer is primarily a mitochondrial metabolic disease and the origin of cancer is due to damages to the mitochondria in the cytoplasm rather than damages to the genome in the nucleus. This is supported by observations that although the imbalance between oncogenes and tumour suppressor genes is predominantly the result of nuclear DNA damage in tumour cells, such genomic abnormalities follows, rather than precedes, the disturbance in cellular respiration [87].

Several nuclear-cytoplasmic transfer experiments examined the influence of cytoplasm on the expression of tumorigenicity in cytoplasmic hybrids (cybrids). For example, Koura and co-authors [88] fused intact B16 mouse melanoma cells with cytoplasts (absent nucleus) from non-tumorigenic rat myoblasts, and their finding showed that normal cytoplasm containing mitochondria from non-tumorigenic cells could suppress the malignant phenotype of tumour cells. Israel and Schaeffer [89] also demonstrated 100% suppression of malignancy in cybrids containing tumorigenic nucleus and normal cytoplasm, whereas normal cell nucleus was unable to supress the tumorigenesis when fused in tumour cell cytoplasm. These observations are in agreement with the view of Darlington [87] who showed that the cytoplasm, rather than the nucleus, determined the tumorigenic state of the cells.

Moreover, Singh and co-authors [90] provided evidence for the role of mitochondria in suppressing tumorigenic phenotype when *wild type* mitochondria were transferred into cells with their own mitochondria DNA depleted (i.e. the rho0 cells). Wallace and co-authors [91] also provided evidence for the role of mitochondrial respiration in the origin of prostate cancer by introducing specific pathogenic mtDNA mutation into PC-3 prostate cancer cells through cybrid transfer. More recent experiments from the Wallace and Cruz-Bermudez groups [91,92] showed that introduction of mtDNA mutations could alter the anti-tumorigenic effect of normal mitochondria in cybrids. These findings indicate that mitochondrial respiration is fundamental in cancer prevention and specific mtDNA mutations can play an important role in cancer aetiology [87]. Similar findings were also obtained from *in vivo* experiments. Morgan *et al.* [93] observed no malignancies or abnormal cell growth in any of the recipient mice when nuclei from mouse brain tumour cells were transplanted into enucleated non-cancerous somatic cells. All previous experiments showed that somatic nuclear mutations alone could not account for the origin of cancer, and cytoplasm containing normal mitochondria could suppress tumorigenicity (Figure 1.17). It is now well known that the Ras oncogene induces tumorigenesis through an inhibitory effect on mitochondrial oxidative phosphorylation [94].

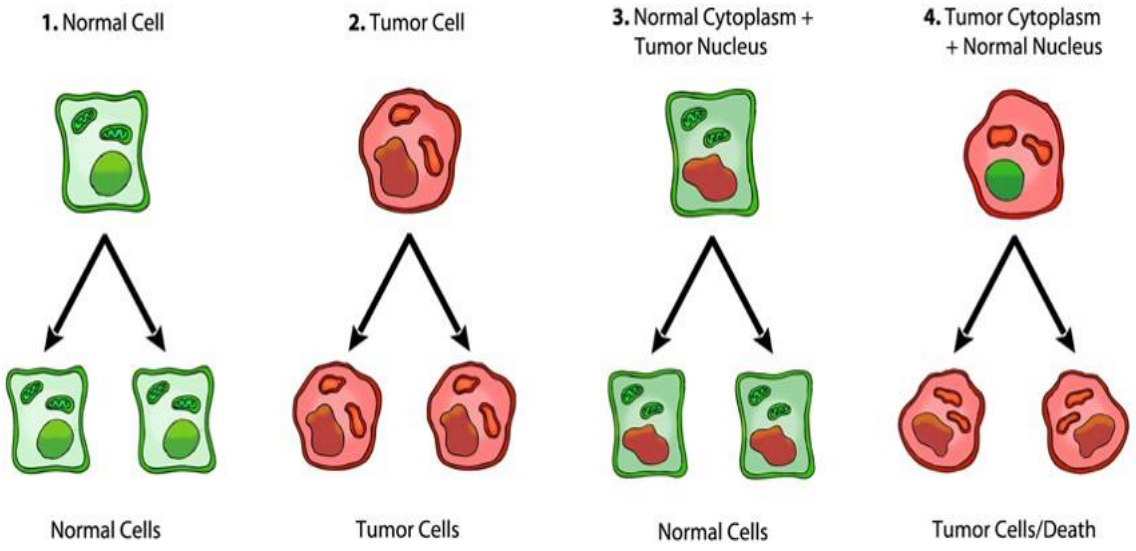

Figure 1.17. Summary of the role of mitochondria in the origin of tumorigenesis. Normal cells with normal nuclear and mitochondrial morphology indicative of normal gene expression and respiration are shown in green. Tumour cells with abnormal nuclear and mitochondrial morphology indicative of genomic instability and abnormal respiration are shown in red. (1) Normal cells beget normal cells. (2) Tumour cells beget tumour cells. (3) Transfer of a tumour cell nucleus into a normal cytoplasm begets normal cells, despite the presence of the tumour-associated genomic abnormalities. (4) Transfer of a normal cell nucleus into a tumour cell cytoplasm begets dead cells or tumour cells, but not normal cells. The results suggest that nuclear genomic defects alone cannot account for the origin of tumours, and that normal mitochondria can suppress tumorigenesis [87].

However, the role of mitochondrial DNA abnormalities in the origin and progression of cancer is still controversial. Various studies have failed to evidence the initiator role of mitochondria, and rather suggest that nDNA, not mtDNA, is responsible for carcinogen-induced malignant transformation [87]. Further studies are still needed to reconcile variations in results gained from some *in vitro* and *in vivo* transfer experiments, and also to identify specific pathogenic mtDNA mutations responsible for the origin of cancer.

Although the aforementioned nuclear-cytoplasmic transfer experiments do not support the somatic mutation theory, they strongly favour the Warburg theory of cancer, i.e. cancer is primarily a mitochondrial metabolic disease [87]. It would be expected that the existence of normal mitochondria in cancer cells would retrieve the redox state, downregulate the mitochondrial stress response, and ultimately reduce or eliminate the need for fermentation to preserve viability [87]. In conclusion, normal mitochondria would maintain the differentiated state by enhancing respiration and thereby suppressing oncogene expression and tumorigenicity, whereas dysfunctional mitochondria lead to glycolysis and enhance cellular dedifferentiation thereby facilitating carcinogenesis [87].

1.2.3 Mitochondrial metabolic reprograming in cancers

The first characterisation of tumour metabolism is attributed to Warburg who was the first to elucidate that cancer cells exhibit an altered energy metabolism by depending more on glycolysis with regard to OXPHOS even with enough oxygen supply (i.e. aerobic glycolysis). Warburg hypothesised that cancer cells rely more on glycolysis for ATP production due to mitochondrial dysfunction [95]. Currently, this “Warburg effect” is referred to as “metabolic reprogramming in cancer” [96,97].

Cancer cells are well characterised with their fast proliferation and high growth rate, however tumour tissue readily becomes hypoxic due to the lack of oxygen supply by local vasculature. These conditions are usually lethal to non-cancerous cells because of the hypoxia-induced p53-mediated apoptosis [98], but cancer cells can avoid hypoxia-mediated death due to down regulation or mutation of p53 [99]. The insufficiency of mitochondria under hypoxic conditions to generate adequate ATP for cell survival leads to the upregulation of glycolytic pathway. This pathway takes place by the induction of hypoxia-inducible factor 1 (HIF-1) that catalyses key steps of glycolysis and regulates genes that control angiogenesis, invasion and cell survival [100].

Normally, transformation between OXPHOS and glycolysis is controlled by the relative activities of pyruvate dehydrogenase (PDH) and lactate dehydrogenase (LDH). HIF-1 has been reported to induce pyruvate dehydrogenase kinase 1 (PDK1) that inactivates PDH and consequently supresses the Krebs cycle and mitochondrial respiration. It has been shown that HIF-1 also facilitates the conversion of pyruvate to lactate by catalysing the expression of LDH. As a result, the contribution of mitochondria in ATP production declines, although the mitochondrial function might remain intact [99]. On the other hand, the activities of Krebs cycle proteins and OXPHOS in cancer are significantly altered due to mutations in nuclear and mitochondrial DNA that encode for Krebs cycle proteins and mitochondrial respiratory complexes. TCA cycle dysfunction and the resultant oxidative stress activate HIF-1 signalling pathway leading to tumour growth and vascularisation, even in the absence of hypoxic conditions (Figure 1.18) [101].

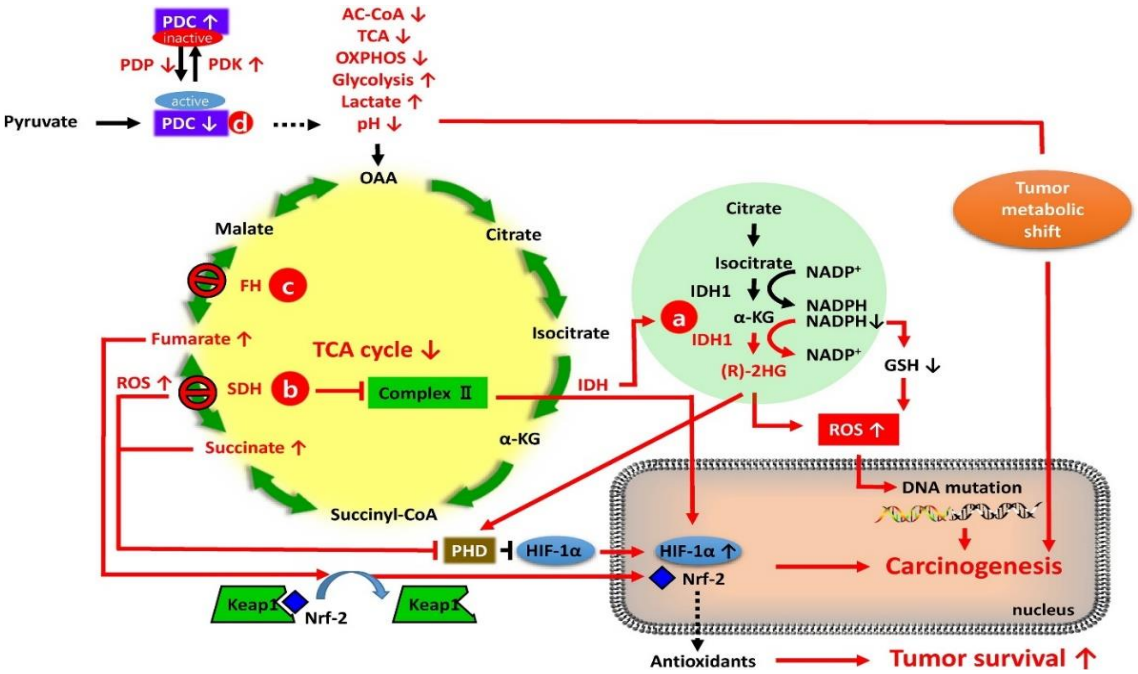

Figure 1.18. TCA cycle modifications in cancers. Metabolic alteration by mutations in TCA cycle enzymes (a, b, and c) and inhibition of pyruvate dehydrogenase complex (PDC) activity (d) are shown. (a) Isocitrate dehydrogenase (IDH) mutations can catalyse the NADPH-dependent reduction of α-ketoglutarate to (R)-2-hydroxyglutarate (2HG), which decreases NADPH and GSH but increases (R)-2HG and ROS accumulation. (R)-2HG also regulates the activity of prolyl hydroxylase (PHD), a negative regulator of oncogenic HIF-1α [102]. (b) Succinate dehydrogenase (SDH) mutations supress complex II activity, subsequently activating HIF-1α and ROS generation. SDH mutations also increase the accumulation of succinate which suppresses the PHD activity, triggering HIF-1α-mediated carcinogenesis. (c) Mutations of fumarate hydratase enhance Nrf2 nuclear translocation causing the transcription of oncogenic genes and antioxidants which increases both tumorigenesis and tumour cell survival. (d) PDC activity is suppressed via downregulation of pyruvate dehydrogenase phosphatase (PDP) and upregulation of pyruvate dehydrogenase kinase (PDK) in various cancer cells. Inhibition of PDC reduces acetyl-CoA level, TCA cycle activity and oxidative phosphorylation but increases glycolysis, lactate production and acidification in cancer cells. These metabolic shifts facilitate carcinogenesis and tumour survival [101].

Several oncogenes have also been involved in the induction of glycolysis in human cancer including v-akt murine thymoma viral oncogene homolog 1 gene (*AKT*) and v-myc myelocytomatosis viral oncogene homolog gene (*MYC*)-encoded MYC. AKT and MYC can activate various genes coding for glycolytic enzymes including hexokinase II (HK-II), LDH and enolase to enhance glycolysis [103–105]. Aerobic glycolysis not only produces ATP for cells but also provides glycolytic intermediates required for the biosynthesis of nucleotides and proteins to support fast cell proliferation. This shift in cellular metabolism can also protect cancer cells from oxidative damage caused by ROS, side products of OXPHOS [106]

Since cancer cells depend on different metabolic pathways for energy production for their survival, these metabolic alterations can affect the capacity of cancer cells to engage in catabolic processes including apoptosis (reviewed in Ref. [86]).

1.2.4 Apoptosis in cancer

As mentioned earlier, mitochondria control the intrinsic pathway of apoptosis. They regulate the translocation and release of pro-apoptotic proteins from the IMS to the cytosol (reviewed in Ref. [107]). Several studies have shown that cancer cells over express anti-apoptotic BCL-2 proteins through different mechanisms including gene amplification, transcriptional upregulation (driven by oncogenic signalling) or downregulation of microRNAs that suppress anti-apoptotic BCL-2 protein expression. Besides inhibiting the function of key apoptotic effectors such as BAX or BAK by anti-apoptotic proteins, expression of the BAX, BAK and other pro-apoptotic BH3-only genes such as PUMA, NOXA and BIM can be downregulated in a variety of cancer types through either DNA deletion or promoter hypermethylation leading to transcriptional silencing [52,108].

It has also been shown that anti-apoptotic proteins BCL-2 and BCL-XL can protect cells from apoptosis by interacting with mitochondrial proteins such as ANT or VDAC thus preventing them from forming mitochondrial pores [109].

Maintaining genetic integrity is one of the functions of the tumour suppressor gene p53 [55]. It also contributes to other cellular processes such as differentiation, DNA repair and angiogenesis, which also appear to be vital for tumour suppression (reviewed in Ref. [110]).

The p53 protein is activated by internal and external stress signals that induce its nuclear accumulation in an active form. Consequently, activated p53 induces either cell cycle arrest or apoptosis by downregulating anti-apoptotic protein BCL-2 and upregulating pro-apoptotic proteins including BAX, APAF-1, the BH3-only proteins, and notably PUMA [55,110].

However, the tumour suppressor gene p53 is inactivated in the majority of human cancers; 50% of human cancers carry mutated p53 gene and the majority of the remaining cancer cases have a compromised p53 activity due to overexpression of p53 inhibitors. Murine double minute 2 (MDM2), a negative regulator of the p53 protein, inhibits the transcription factor activity of p53 and triggers its degradation by proteolysis (reviewed in Ref. [110]).

Moreover, cancer cells incur significant alterations in the components of the permeability transition pore complex (PTPC). PTPC mediates the mitochondrial permeability transition (MPT) to trigger the release of cytochrome *c*, a key step in the intrinsic apoptosis pathway [111]. Alterations in PTPC can interfere with apoptosis regulation and therefore promote cancer cell survival.

Cancer cells also inhibit caspase function following MOMP allowing them to survive under these conditions. They inhibit caspase activity via downregulation of apoptosome activity through epigenetic silencing or inhibitory phosphorylation of APAF-1. Cancer cells can also abolish the pro-apoptotic activity of cytochrome *c* by its ubiquitination and proteasome-dependent degradation following MOMP [112]. Caspase function can be directly inhibited by the X-linked inhibitor of apoptosis protein (XIAP) or indirectly by c-IAP1 and c-IAP2 (cellular inhibitor of apoptosis protein 1 and 2) through their ability to bind and neutralise the XIAP inhibitor, Smac (Figure 1.19) (reviewed in Ref. [52]).

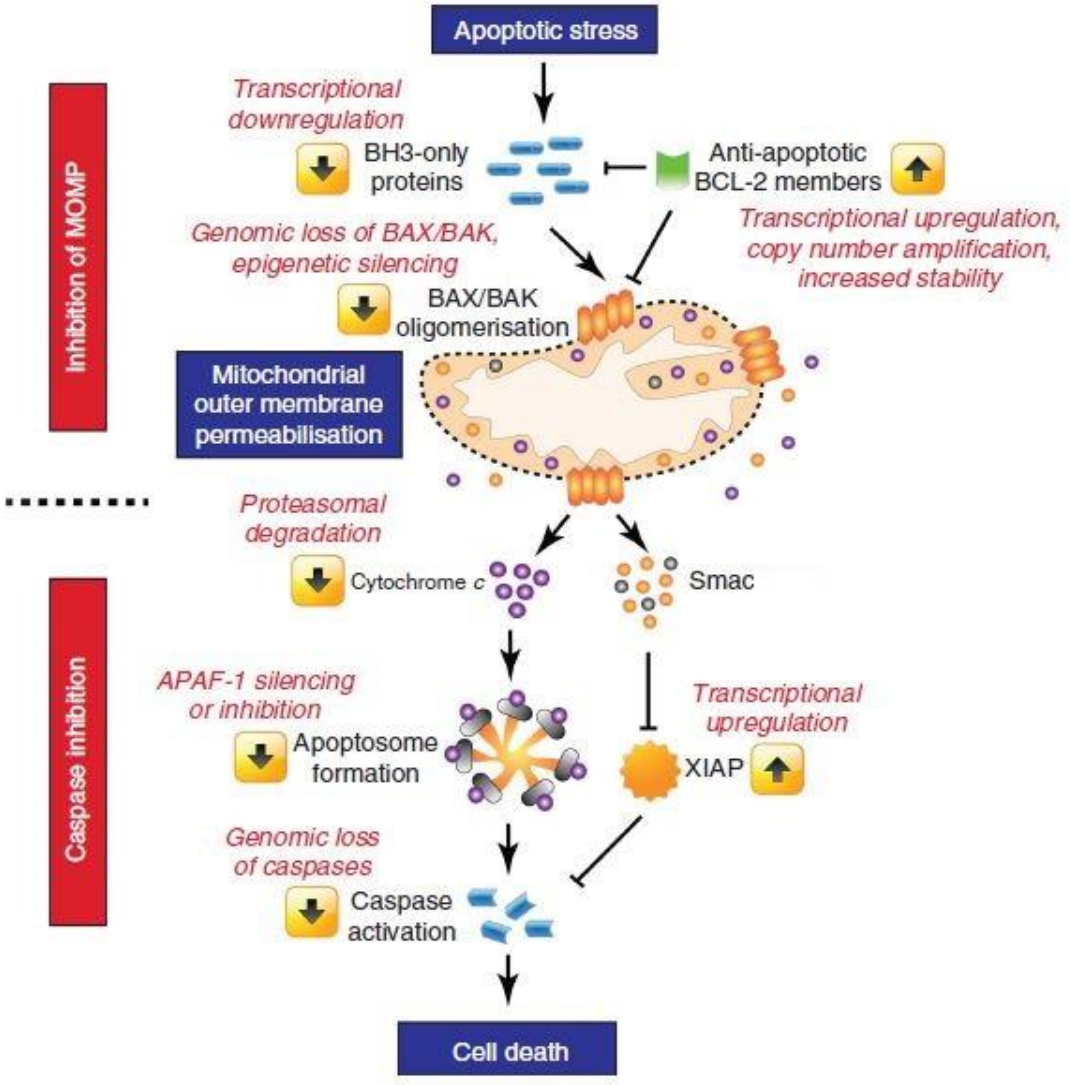

Figure 1.19. Execution of mitochondrial apoptosis pathway and escape mechanisms in cancer cells. Apoptotic stresses trigger the accumulation of the BH3-only proteins resulting in BAX/BAK oligomerisation, MOMP and release of pro-apoptotic proteins. Release of cytochrome c results in apoptosome formation, which leads to caspase activation and apoptosis. Smac neutralises the activity of caspase inhibitor XIAP. Various strategies to escape apoptosis by inhibiting either MOMP or caspase activity are presented in red [52].

Due to various mitochondrial dysfunctions that have been linked to multiple aspects of tumorigenesis and tumour progression, mitochondria represent a promising target for cancer-specific therapies (reviewed in Ref. [86]).

1.2.5 Mitochondrial DNA mutation and epigenetics in tumorigenesis

Somatic mutation within the mitochondrial genome is a common phenomenon in the process of cell transformation. Indeed, point mutations or deletions within the displacement loop and coding regions have been observed in various types of cancer such as colon, breast, kidney, thyroid, and head and neck [81,113,114] (Figure 1.20). Mutations within the protein-coding region have been proved to affect the stability, assembly and function of the complexes in the respiratory chain causing OXPHOS deficiency. Hence, the frequency of mutations observed in the mitochondrial genome of various types of cancer is thought to be correlated to the extent of respiratory dysfunction (reviewed in Ref. [66]).

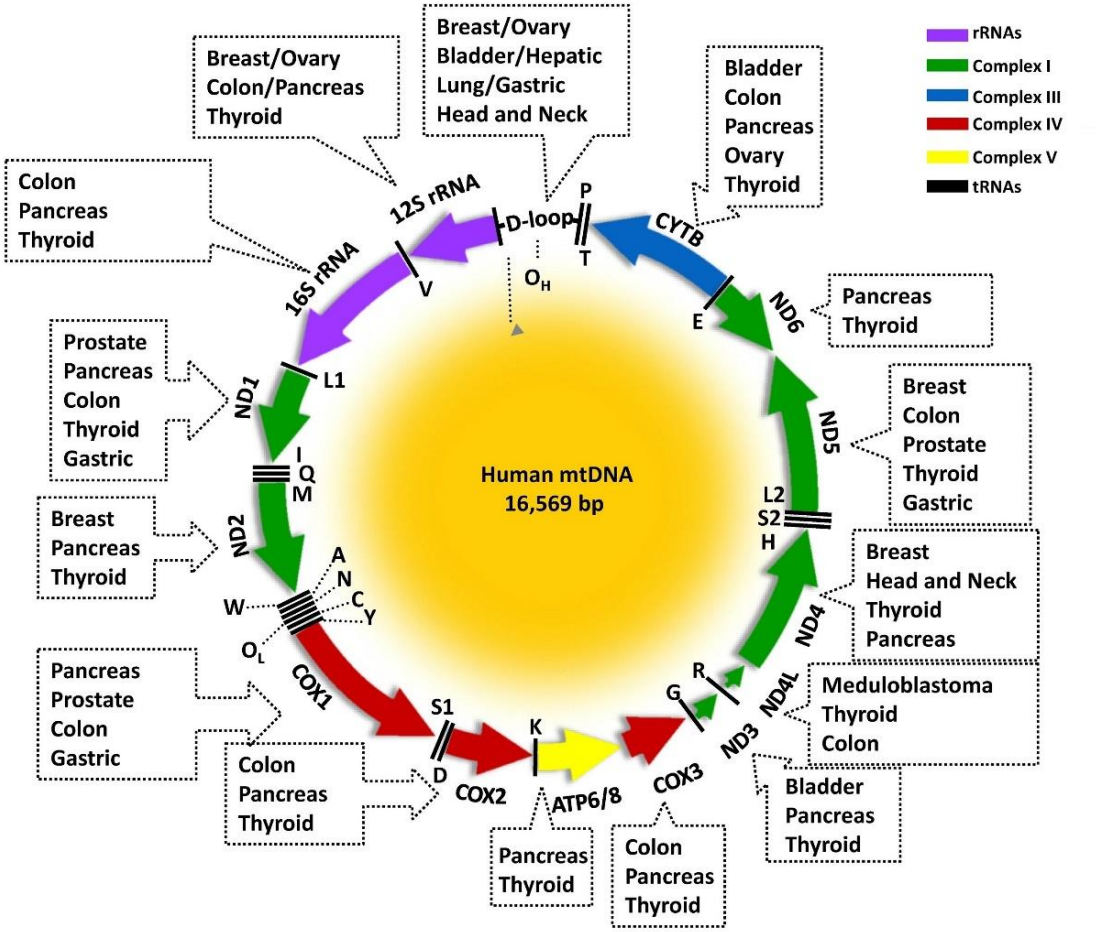

Figure 1.20. Regions of mitochondrial DNA mutations and related cancers [101].

A previous study on colorectal cancer showed that certain mtDNA mutations in the ND5 subunit in complex I demonstrated not only gradual decreases in OXPHOS but also increased glucose-dependent lactate production and progression in tumour growth [80]. Moreover, the ND5 mutation-induced complex I dysfunction activates the AKT signalling pathway to enhance tumorigenesis [115]. These results suggest that mutated mtDNA genes are not just innocent victims to the oxidative stress, but in fact they are major initiation factors in tumorigenesis [101].

A total of 635 mutations have been reported in the D-loop region, including 510 point mutations, 56 deletions and 69 insertions, which cause alterations in mtDNAcn and mtDNA gene expression. More mutations have been identified in the coding region: 593 mutations in complex I subunits, 343 mutations in complex III, IV and V subunits, and 165 mutations in tRNA and rRNA genes [116].

1.2.5.1 D-loop mutations in human cancer

The D-loop region is well known to be a hotspot for mtDNA mutation in tumour cells with the majority of somatic mutations occurring in the hypervariable regions (HV1 and HV2) [117]. Mutations in this region have been identified in several types of cancer: breast cancer, ovarian carcinomas, prostate cancer, hepatocellular carcinoma, endometrial cancer and bladder cancer (reviewed in Ref. [66]). It has been reported that D-loop mutations have consequences on cell physiology. For example, mtDNA copy number was significantly reduced in patients with hepatocellular carcinoma (HCC) due to the occurrence of point mutations near the replication origin of the heavy strand [118]. Moreover, HCC tissues containing D-loop mutations had higher ROS levels than their adjacent tissues with the *wild type* D-loop region [119]. On the other hand, clinical implications were contributed to D-loop mutations. Correlation between mitochondrial D-loop mutations and cancer characteristics has been observed in HCC, lung and colorectal cancers, and the frequency of mutations was higher in later tumour stage than early stage [120]. Mutations in this region were also associated with the response to chemotherapy. Stage III colon cancer with mutations in the D-loop region showed resistance to fluoruracil-based adjuvant therapy [121]. Most importantly, D-loop mutations have been suggested as biomarkers for early detection strategy of cancer. Sequence variants within the D-loop region have been implicated in the development of familial breast cancer as specific polymorphisms that occur more frequently in patients with family history could be responsible for inherited cancer susceptibility [122].

1.2.5.2 tRNA and rRNA mutations in human cancers

A few somatic mutations localised in the tRNA genes have been reported in cancer cases such as A3243G in colon cancer [123]; G4450A in splenic lymphoma [124]; G3244A in lung tumour and gastric carcinoma [123] and C4312T, C5633T, G7521A and G12236A in thyroid tumours [125]. Several mutations in 12S and 16S ribosomal RNA have also been reported in various types of cancer including T2664C and C2998CT in lung cancer [123,126]; T2445C and G3054A in bladder cancer [90]; A1811G in head and neck cancer [126]; G2923A in prostate cancer [127]; G687A, T1243C, T1406C, A1676G, G2015A, T2222C, A2805T and A2905G in pancreatic cancer [128]. It has been suggested that mutations in the tRNA and rRNA genes can impact on cell physiology because such mutations impair mitochondrial protein synthesis and therefore result in defective activities of respiratory chain enzymes (reviewed in Ref. [66]).

1.2.5.3 OXPHOS complex I mutations in human cancer

Colon cancer was the first type of cancer to be reported with mutations in the ND genes among known human cancers (reviewed in Ref. [66]). Missense T10563C and frameshift A12418AA (located in ND4L and ND5, respectively) in colorectal cancer were reported by Polyak *et al*. in 1998 [113]. Since then, a number of complex I mutations have been identified in other cancer types: G3421A, A3505G, G3670A, T10970C, T11703C, T11781C, A14552G, G14603A and G10176A in pancreatic cancer [128]; A4986C, A10398G and A5026G in head and neck cancer [129]. The ND2 gene was believed to be a hotspot for mutation in squamous cell carcinoma (SCC) [130] whereas ND1, 4 and 5 mutations were found in early stage of prostate cancer [127].

Mutations in complex I have been indicated to be correlated with loss of complex I activity and assembly, and also involved in overproduction of ROS [131,132]. Moreover, complex I mutations have been suggested to be metastasis promoting factors. Ishikawa and co-authors [77] proposed that G13997A and 13885insC (mutations located in ND6) were responsible for promoting metastasis, based on their cytoplasmic hybrid data using mouse tumour cell lines with different metastatic potentials. Those mutations cause downregulation of complex I activity and overproduction of ROS, accompanied with upregulation of the HIF-1, MCL-1 and vascular endothelial growth factor (VEGF) genes [77].

Since several subunits within complex I are necessary for the assembly of the complex, lack of individual subunits or an assemble factor will lead to the degradation of the remaining subunits [133]. Recently, NDUFS1, a nuclear DNA subunit and part of the iron sulfur clusters of complex I, was shown to be proteolytically cleaved by caspase-3. This indicates that complex I may have a dual function: creating the proton gradient across the membrane and participating in apoptosis after caspase cleavage. Hence, any loss of this step during apoptosis caused by complex I deficiency might lead to an advantage for cancer cells [134].

1.2.5.4 OXPHOS complex III mutations in human cancer

Mutated cytochrome *b* (MT-CYB) has been reported in various types of cancer such as C14866T, C15646T and G15884C in pancreatic cancer [128]; G14869A in breast cancer [135]; G14985A, G14963A and T15572C in colon cancer [136]; G15179A, T15312G and A15182G in thyroid tumour [137]; G15761A in ovarian cancer [138].

A study on human model of bladder cancer showed that overexpression of mutated MT-CYB was correlated with overproduction of ROS, increased oxygen consumption and lactate production [139].

Moreover, the NF-κB (nuclear factor kappa-light-chain-enhancer of activated B cells) signalling pathway was upregulated in cells with mutated MT-CYB, promoting rapid tumour growth and progression both *in vitro* and *in vivo*, which supported the conclusion that mitochondrial gene mutations play critical roles in cancer progression [139].

1.2.5.5 OXPHOS complex IV mutations in human cancer

Somatic mutations within mitochondrial DNA encoded cytochrome *c* oxidase subunit I, II and III are frequent in various human cancers [140] such as A8701G, A8716G and T9137C in thyroid cancer [66]; G8557A in colon cancer [136]; T9070G and T8696C in pancreatic cancer [128]. COI mutations were identified in 12 % of prostate cancer patients in a study reported by Petros *et al*. [91].

Notably, an investigation conducted by Vives-Bauza and colleagues employing cybrids revealed that cells with mutated complex IV did not demonstrate any increase in ROS production and oxidative stress, nor any elevation of antioxidants [141]. This may not be surprising since complexes I and III are considered the main sites of ROS production in the OXPHOS system.

1.2.5.6 OXPHOS complex V mutations in human cancer

Mutations in the mitochondrial genome encoding for complex V have also been reported in human cancers such as A8701G, A8716G and T9137C in thyroid cancer [125]; T8696C and T9070G in pancreatic cancer [128]. Complex V is vital not only for ATP production but also for other processes such as apoptosis, and therefore it is not unexpected that complex V mutations have been identified in cancer cells [66].

A study on cybrids with a T8993G or T9176G mutation derived from patients with mitochondrial encephalomyopathy showed that when transplanted into nude mice, those cybrids containing the above complex V mutations granted an advantage in the early stage of tumour growth by their contributing to the prevention of apoptosis and hence resulting in tumour development [142]. Moreover, complex V activity is important to the maintenance of mitochondrial transmembrane potential (MMP) that is required for the normal mitochondrial matrix activity, so although complex V-mutant cells can switch to glycolysis for ATP generation, those cells may still maintain the MMP required for the mitochondrial matrix activity [143].

1.2.5.7 Large mitochondrial deletions in human cancers

Large deletions within mtDNA have also been associated with cancer. For instance, deletion of a 4977-bp fragment within mtDNA was observed in HCC which removed all or part of the genes encoding four complex I subunits, one complex IV subunit and two complex V subunits, as well as five tRNA genes [144]. HCC patients carrying this deletion showed a marked increase in ROS level and elevated mtDNAcn compared with the healthy controls, which indicates that this deletion may play an important role in the carcinogenesis of HCC [144]. Another deletion of a 4981-bp fragment was observed in nasopharyngeal carcinoma (NPC) and proposed to be involved in the development and progression of NPC (reviewed in Ref. [66]).

1.2.6 MtDNA copy number in human cancers

The mtDNAcn per cell is preserved within a stable range to achieve the required energy of the cell and hence ensure normal physiological functions. It ranges among the population from 10^3 to 10^4 per cell type [145]. Such variations also reflect the imbalance between ROS production and antioxidant capacity, so mtDNAcn has been considered as a potential diagnostic and prognostic biomarker for several cancer types [146]. Several factors in cancer possibly alter mtDNAcn such as mutations in the D-loop region (highly

susceptible site for oxidative damage compared with other regions of mtDNA), methylation profile of D-loop and the expression level of mitochondrial transcription factor A (TFAM) [147].

MtDNAcn is strictly regulated during differentiation, and cells with a high demand for ATP by OXPHOS have higher mtDNAcn than cells with a low ATP requirement [20]. An increased mtDNAcn was observed in endometrial [148], untreated head and neck [149], prostate [149], pancreatic [150] and colorectal [151] cancers. Such an increase is assumed to compensate for the damaged mtDNA and maintain adequate ATP supply by mitochondrial respiration [105]. On the contrary, a decrease of mtDNAcn was noticed in renal [152], thyroid [153], breast [154], previously treated head and neck [81], hepatic [155] and ovarian cancers [156]. Such a decrease would result in the reduction of mitochondrial function [105].

Generally, decline in mitochondrial activity appears to be an adaptation to hypoxic conditions during tumour development since low oxygen initiates lower oxidative stress [146]. The preservation of low mtDNAcn promotes aerobic glycolysis for ATP generation, and a combination of glycolysis with a small contribution from OXPHOS promotes cell proliferation, invasion, metastasis whereas prevents differentiation [20]. Alterations of mtDNAcn were also shown to be associated with tumour development.
A recent study by Dang and co-authors [18] on laryngeal cancer patients showed that tumours with low mtDNA content were more aggressive compared with those with high mtDNA content. In addition, patients with late-stage tumours had a remarkably lower mtDNA content than those with early-stage tumours.

On the other hand, increased mtDNAcn could be a defensive mechanism to avoid apoptosis [26]. Studies on transgenic mice with mtDNA depletions showed that mice could not survive the embryonic period accompanied with high numbers of apoptotic cells in these embryos [157,158]. Another study by Wang *et al.* [158] on tissue-specific mtDNA knockout mice showed a large number of apoptotic cells in the myocardium. In addition, increased mtDNAcn can also protect cells from ROS-induced apoptosis. Mei and co-authors [26] found that mtDNAcn increased in apoptotic tumour cells. They also observed that reduced mtDNAcn inhibited antioxidant gene expression and resulted in elevated intracellular ROS levels, which made tumour cells more sensitive to chemotherapeutic agents.

1.3 Reactive oxygen species (ROS)

ROS are described as chemically reactive molecules containing oxygen and by-products of normal cellular metabolism. The three major types of ROS are superoxide anion ($O_2^{\bullet -}$), hydroxyl radicals ($OH^{\bullet}$) and hydrogen peroxide (H_2O_2) (reviewed in Ref. [159]) (Figure 1.21). They can be also classified into two groups of compounds, namely radicals and non-radicals. Radicals such as hydroxyl radical ($OH^{\bullet}$) and superoxide anion ($O_2^{\bullet -}$) contain one unpaired electron in the shell or outer orbit, making them unstable and highly reactive. These radicals tend to donate or obtain another electron to attain stability. The none-radical species such as hydrogen peroxide (H_2O_2) are not free radicals but can easily lead to free radical reaction in the living organism [159,160].

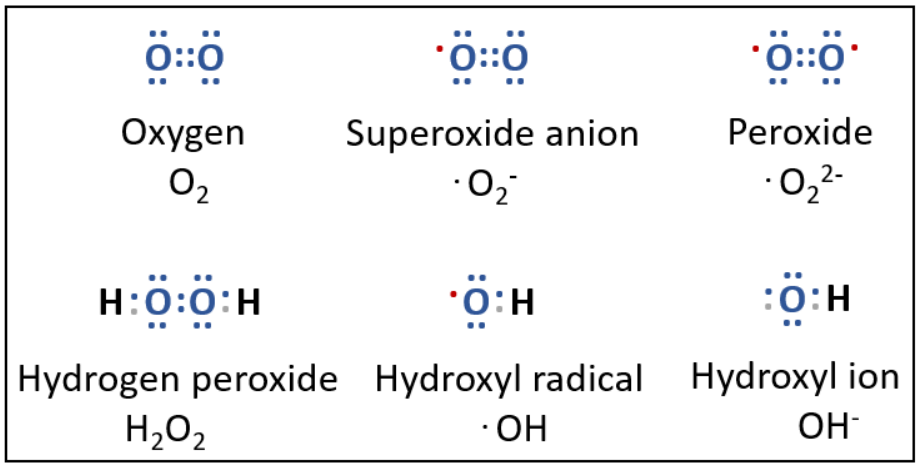

Figure 1.21. Electron structures of common reactive oxygen species. The red • designates an unpaired electron [161].

1.3.1 Source of ROS

ROS can be generated from both endogenous sources (mitochondria, peroxisomes, endoplasmic reticulum where the oxygen consumption is high) and exogenous sources (pollution, alcohol, tobacco smoke, heavy metals such as iron and copper, certain drugs and radiation) [159,162]. However, mitochondria are considered a primary intracellular site of ROS generation. Some electrons in the mitochondrial electron transport chain escape from the mitochondrial respiratory complexes I/III and react with oxygen to generate superoxide radicals. This generation of superoxide is non-enzymatic and therefore higher metabolic rate results in greater production of ROS (reviewed in Ref. [163]).

Superoxide anion has a low reactivity with biomolecules but later can be converted to hydrogen peroxide via dismutation reaction catalysed by the superoxide dismutase enzymes (SOD). Hydrogen peroxide can easily penetrate the biological membranes with no direct effect on biomolecules. However, it can damage DNA by producing hydroxyl radical via Fenton reaction in the presence of metal ions (Fe^{2+} or Cu^{+}). Hydroxyl radical is a highly reactive radical and can react with biomolecules including DNA, lipids and proteins causing severe damages to the cell more than any other ROS (reviewed in Ref. [159]) (Figure 1.22).

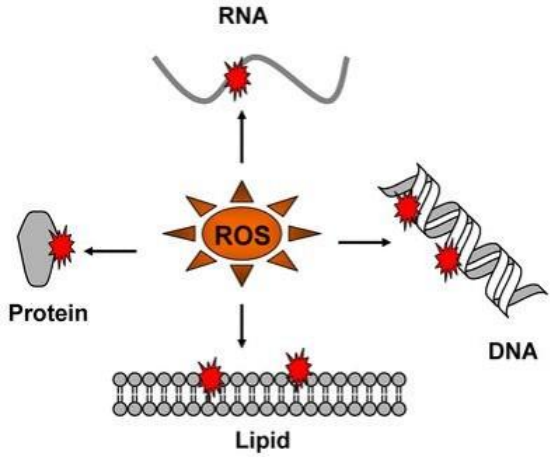

Figure 1.22. Interaction between ROS and biomacromolecules [160].

Peroxisome is also a major site of ROS production due to xanthine oxidase activity in the peroxisomal matrix and membranes. Endoplasmic reticulum also contribute to the production of ROS via the activity of cytochrome p-450 [164].

Membrane-bound enzymes such as NADPH oxidases (nicotinamide adenine dinucleotide phosphate oxidase; also known as NOXs) are also important contributors to the generation of ROS. The NOX genes produce the transmembrane proteins responsible for transporting electrons across biological membranes, which leads to the reduction of oxygen into superoxide [165].

Mammalian NOXs primarily localise on the cytoplasmic membrane, but they can also be found on other membranes, including those of mitochondria, nucleus, and endoplasmic reticulum [166].

1.3.2 Oxidative stress

In an organism, the redox balance depends on the production of ROS and their elimination via endogenous and exogenous antioxidants which act as "free radical scavengers" to prevent the damages caused by ROS (reviewed in Ref. [167]). In healthy tissues, intracellular ROS are preserved at a steady low level by the equilibrium between ROS generation and neutralisation via the activity of enzymatic antioxidants. The balance between ROS production and their elimination by endogenous mechanism is vital for preserving normal cell homeostasis since some types of ROS such as hydrogen peroxide and superoxide serve as important cell signalling molecules (reviewed in Ref. [168]). The shift in the balance between oxidant/antioxidant in favour of oxidants is termed "oxidative stress" [162].

Generally, low levels of ROS act as mitogens and promotes cell survival and proliferation, whereas moderate levels cause a transient or permeant cell cycle arrest and induces cell differentiation. At higher levels, ROS can lead to oxidative damage to cell components such as proteins, lipids and mainly to DNA resulting in mutations that consequently lead to the development of various pathological conditions including cancer [169]. However, excessive production of ROS causes severe oxidative damage to biomacromolecules which consequently induces cell death [164] (Figure 1.23).

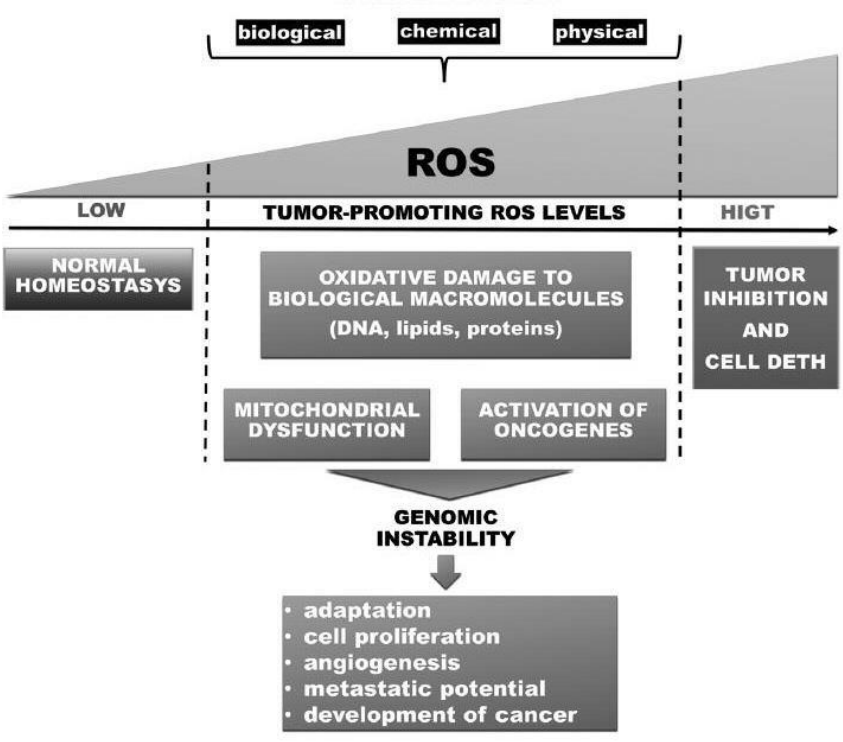

Figure 1.23. Role of low and high levels of ROS on cell response: survival or cell death [168].

1.3.2.1 Effects of oxidative stress on DNA

ROS can cause DNA alterations in various ways including bases degradation, single- or double-strand breaks, pyrimidine and purine modifications, deletions and cross-linking with proteins [170]. The majority of these alterations are highly associated with several diseases including cancer [162]. 8-Oxoguanine (8-oxoG) is the most remarkable mutagenic lesion generated by ROS and considered a potential biomarker for carcinogenesis [25,162] (Figure 1.24).

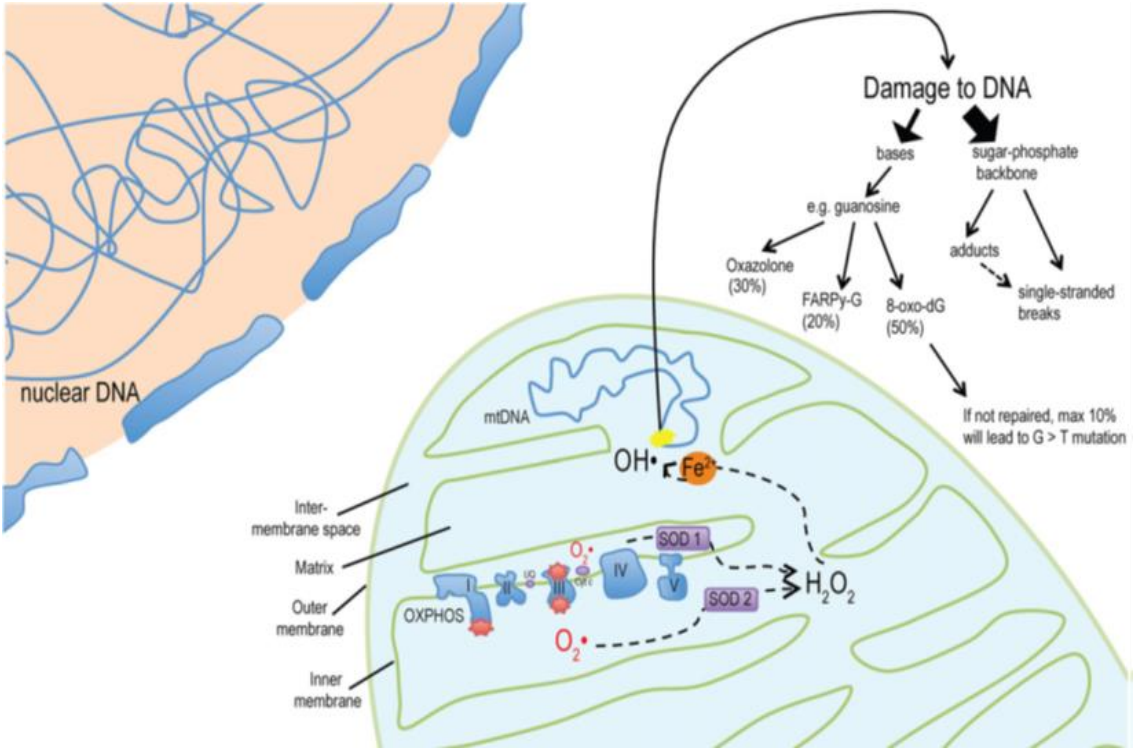

Figure 1.24. A schematic representation of oxidative damage to mtDNA and its consequences. OH• can react with either bases or the sugar-phosphate backbone leading to DNA single-strand breaks, abasic sites, DNA–DNA intrastrand adducts, DNA–protein crosslinks and base damage. For example, the main products of guanosine base damage are oxazolone, FAPy-G and 8-oxo-dG, with the highest measured mutagenic potential for 8-oxo-dG being 10% [69].

Promoter regions of genes harbour the binding sites for transcription factors. These binding sites contain GC-rich sequences that are susceptible to oxidant attacks. Formation of 8-oxoG in these sites can alter the binding of transcription factors, subsequently change the expression of the related genes [162].

1.3.2.2 Effects of oxidative stress on lipids

ROS can induce lipid peroxidation and alter the cell membrane lipid bilayer arrangement that may inactivate membrane-bound receptors and enzymes and increase tissue permeability [162]. Lipid peroxidation causes the production of lipoperoxyl radical (LOO·) which in turn reacts with a lipid to produce a lipid hydroperoxide (LOOH). These LOOHs are unstable products and can generate new peroxyl and alkoxy radicals. Free radicals generated during lipid peroxidation have a very local effect due to their short life cycles. However, 4-hydroxynonenal (HNE), aldehydes, hexanal and malondialdehyde, breakdown products of lipid peroxides, serve as "oxidative stress secondary messengers" due to their longer half-life and their ability to diffuse to other sites and hence interact with proteins and DNA resulting in covalent modifications on macromolecules [164].

1.3.2.3 Effects of oxidative stress on proteins

ROS can result in peptide chain fragmentation, protein electrical charge alteration, protein-protein cross-links and oxidation of specific amino acids (reviewed in Ref. [171]). These modifications lead to increased susceptibility to proteolysis and degradation by specific proteases. Methionine and cysteine residues are predominantly more susceptible to oxidation. Oxidation of methionine or sulfhydryl group residues of proteins causes conformational changes, protein unfolding and degradation. In addition, oxidative modification of enzymes has been shown to inhibit their activities [162].

Oxidative stress on protein can result in either reversible or irreversible oxidative modifications. One example of reversible oxidative modifications is the mechanism of redox signalling which involves the oxidation of cysteine residues in proteins. During redox signalling, ROS oxidises cysteine residues that exist as thiolate anions ($Cys\text{-}S^-$) into the sulfenic form (Cys-SOH) causing allosteric changes within the protein that alter its function. The sulfenic form can be reduced to thiolate anions by antioxidant enzymes such as disulfide reductases, thioredoxin (Trx) and glutaredoxin (Grx) to restore the original state and function of the proteins. At higher levels of ROS, oxidised thiolate anions are oxidised into sulfinic (SO_2H) or sulfonic (SO_3H) species which, unlike sulfenic modifications, are irreversible and result in permanent oxidative damage of the protein [164] (Figure 1.25).

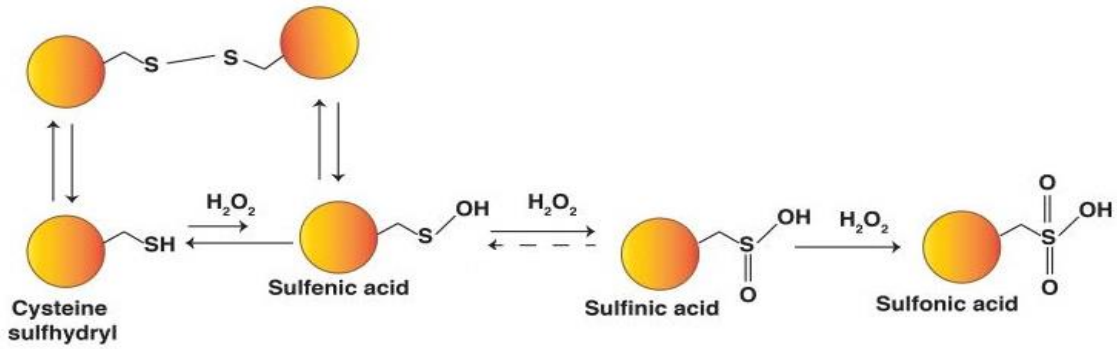

Figure 1.25. Oxidative modifications of the amino acid Cysteine. Reactive cysteine thiols (R-SH) can be oxidised by hydrogen peroxide to form sulfenic acids which can go on to form reversible disulfides (R-SS-R') or irreversible oxidation products such as sulfinic acids or sulfonic acids [166].

1.3.2.4 Effects of oxidative stress on signal transduction

ROS can promote the expression of several genes implicated in signal transduction. Disruption of the redox balance causes the activation of redox sensitive transcription factors, such as NF-$_k$B and activator protein 1 (AP-1) and HIF-1 that are involved in the inflammatory response [162].

Activation of transcription factors via ROS is achieved by signal transduction cascades that transfer the information from the outside to the inside of the cell. Receptor tyrosine kinases such as epidermal growth factor receptor (EGFR) and vascular endothelial growth factor receptor (VEGFR) and platelet-derived growth factor receptor (PDGFR) are targets of ROS. Members of mitogen-activated protein kinase family (MAPKs) such as c-Jun N-terminal kinases (JNKs) and p38 are implicated in various processes including proliferation, differentiation and apoptosis. They are also responsive to stress stimuli and can be regulated by oxidants [162].

Under oxidative stress conditions, such as ROS, NF-$_k$B can be activated allowing it to enter the nucleus to activate gene transcription [172]. NF-$_k$B regulates the expression of several genes that participate in immune response such as interleukins 1 beta, 6 and 8 (IL-1β, IL-6, IL-8) and several adhesion molecules such as Cadherins and Integrins.
NF-$_k$B also regulates cell proliferation and differentiation as well as angiogenesis [162].

AP-1 is also regulated by redox state. It has been shown that hydrogen peroxide can enhance the activation of AP-1 and increase the binding to DNA by the reduction of a single conserved cysteine residue in the DNA-binding domain of each of protein of the heterodimer AP-1 [173]. The AP-1 transcription factor is involved in the regulation of a wide range of cellular processes including differentiation, proliferation and apoptosis via its gene expression modulation function (reviewed in Ref. [174]).

Therefore, it is not surprising that aberrant function and regulation of p38, NF-$_k$B, MAPK and other ROS-related molecules have been correlated with both dysregulation of apoptosis and tumour initiation [53]. HIF-1 will be further discussed in section 1.3.5.

1.3.3 Antioxidant defence mechanisms

In order to protect biomolecules from oxidative damage by ROS, cells orchestrate a complex network of enzymatic and non-enzymatic endogenous antioxidants to preserve proper cellular functions. Enzymatically, superoxide dismutase (SOD) activity converts superoxide to hydrogen peroxide that will be converted later into water by catalase (CAT), peroxiredoxin (Prx) and glutathione peroxidase (GPx). On the other hand, free radical activity can be eliminated non-enzymatically through the interaction with substrates such as glutathione (GSH) [166,175]. Antioxidant mechanisms are summarised in Figure 1.26.

1.3.3.1 Superoxide dismutase

SOD is the first line of defence against free radicals and responsible for rapid conversion of superoxide anion into hydrogen peroxide to prevent $O_2^{\bullet-}$ -induced damage to proteins and other biomolecules. This enzyme has three isoforms, SOD1, SOD2 and SOD3, and is expressed in several cellular compartments: cytosolic Cu,Zn-SOD (SOD1), mitochondrial Mn-SOD (SOD2) and extracellular EC-SOD (SOD3) [166,175].

1.3.3.2 Catalase

CAT exists as a tetramer composed of 4 identical monomers, each of which contains a heme group at the active site. It can be found abundantly in peroxisomes [162]. Catalase binds NADPH and functions as a reducing equivalent by decomposing hydrogen peroxide (H_2O_2) into water and oxygen. This process prevents H_2O_2 from entering the Fenton reaction if ions are available, and thus avoids the formation of highly toxic hydroxyl radicals that can damage various biomolecules [162,166].

1.3.3.3 Peroxiredoxins

Prxs are ideal scavengers for H_2O_2 due to their abundant expression and wide distribution of their six isoforms across the cell inside mitochondria, cytosol, peroxisome and endoplasmic reticulum. Oxidised Prxs are reduced by thioredoxins (Trxs) which can be restored to their reduced state by thioredoxin reductase (TR) and the reducing equivalent, NADPH [162,166].

1.3.3.4 Glutathione peroxidase

GPx is one of the antioxidant enzymes that have several isoforms (GPx1-8). GPx can convert H_2O_2 to water and lipid peroxides to their corresponding alcohols in mitochondria and cytoplasm. During this process, GPxs eliminate H_2O_2 by using it to oxidise reduced glutathione (GSH) to oxidised glutathione (GSSG); glutathione reductase (GR) will regenerate GSH by reducing GSSG using NADPH as an electron donor [166,167].

1.3.3.5 Glutathione

GSH is a non-enzymatic antioxidant that prevents the oxidative damage of protein, lipids and DNA. GSH is highly abundant in all cellular compartments and the major soluble antioxidant. It exists in two forms: the thiol reduced form (GSH) or the oxidised glutathione disulfide (GSSG) form. In healthy cells, the predominant form is the reduced form accounting for 99% of total GSH. GSH/GSSG ratio is a major determinant of oxidative stress. GSH functions as an antioxidant through scavenging hydrogen peroxide, with the help of glutathione peroxidase as mentioned earlier [162].

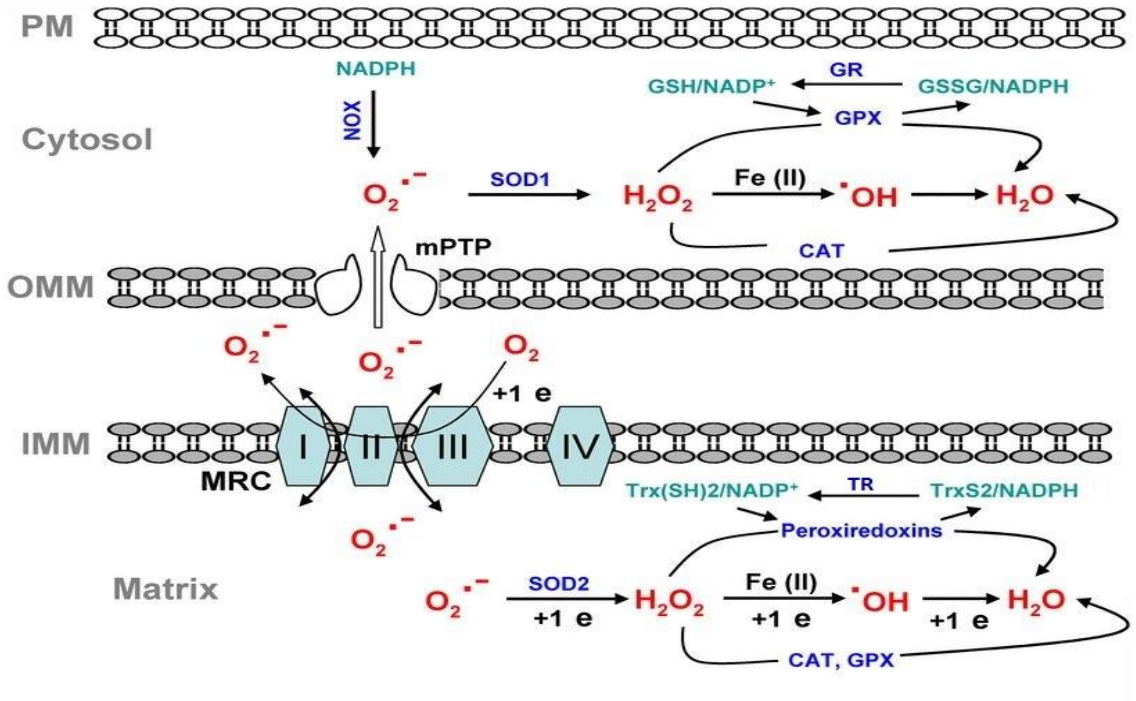

Figure 1.26. Antioxidant defence mechanisms. Superoxide generated during OXPHOS is converted to hydrogen peroxide by the activity of SOD1 and SOD2 in cytosol and mitochondria, respectively. Hydrogen peroxide is then converted to water by the activity of CAT and GPx, which prevents hydrogen peroxide from entering the Fenton reaction in the presence of iron and thus avoids the formation of hydroxyl radicals [160].

N-Acetyl-L-cysteine (NAC) is a remarkable antioxidant drug due to its role in enhancing the synthesis of glutathione (GSH), one of the substrates that eliminate free radical activity non-enzymatically [166,175]. It easily enters the cells and then is converted within the cytosol to L-cysteine which is a precursor to GSH. NAC is also a source of sulfhydryl groups inside the cell, and therefore a ROS scavenger in its own right because sulfhydryl groups can interact with hydroxyl radicals (OH•) and hydrogen peroxide (H_2O_2) [166].

1.3.4 Antioxidative role of transcriptional factors

The production and activity of the enzymatic antioxidants and their reducing equivalents are regulated by different key transcription factors. Nuclear factor erythroid 2-related factor 2 (Nrf2) is a prime regulator of redox homeostasis in response to oxidative stress, and it is activated to upregulate the expression of genes implicated in protective activities. In normal conditions, Nrf2 remains in the cytoplasm bounded to its endogenous inhibitor Kelch-like ECH-associated protein 1 (Keap1). Keap1 supresses Nrf2 signalling by inducing Nrf2 degradation through proteasomal pathway. Once ROS react with redox reactive cysteines in Keap1, Nrf2 is released from Keap1 followed by its translocation to the nucleus [176].

In the nucleus, Nrf2 forms a heterodimer with small musculoaponeurotic fibrosarcoma (Maf) protein and binds to the antioxidant responsive element (ARE) located in the promoter of the antioxidative genes. Nrf2-ARE binding regulates the expression of genes involved in the cellular antioxidant system (Figure 1.27) [164,166].

The transcription factor p53 has also been presented to repress the accumulation of ROS by either upregulating the expression of several antioxidant genes or via the induction of the metabolic gene, TP53-inducible glycolysis and apoptosis regulator (TIGAR). TIGAR redirects glucose to the pentose phosphate pathway (PPP) resulting in increased generation of cytosolic NADPH and suppression of ROS accumulation within the cell [166].

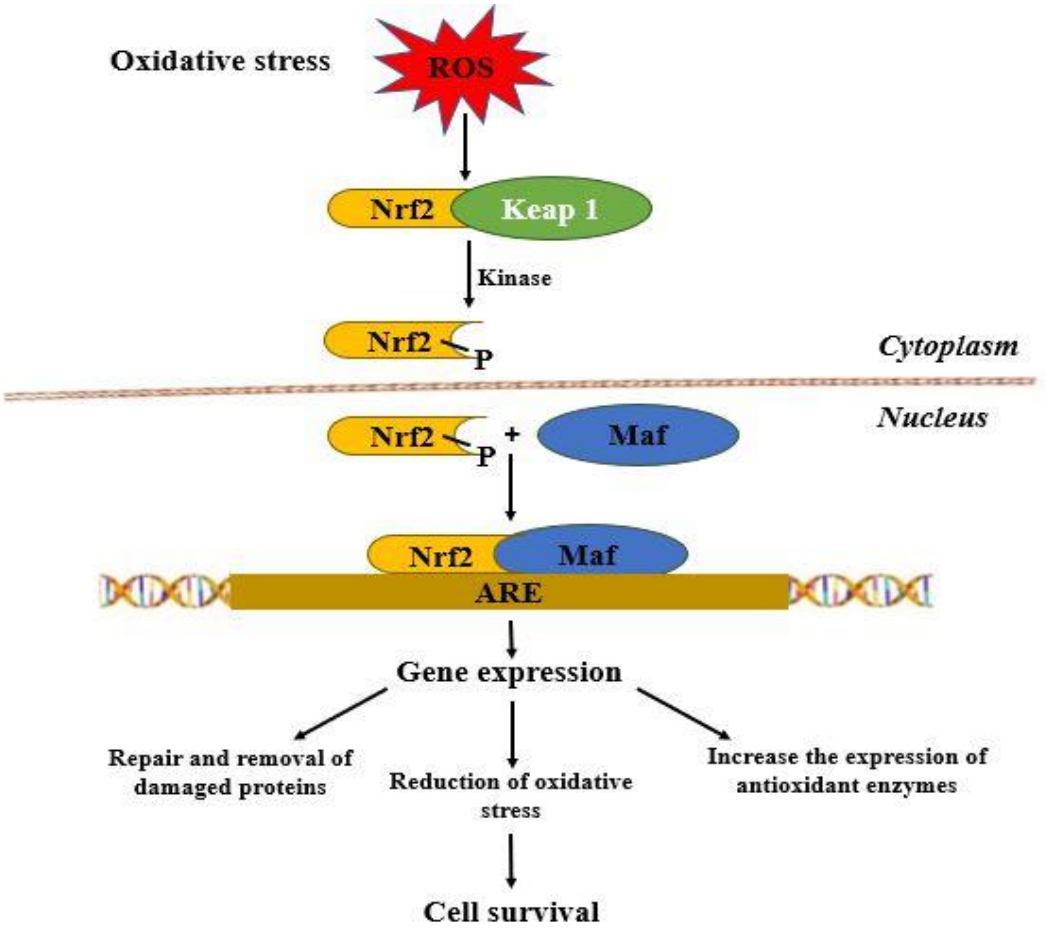

Figure 1.27. Nrf2-ARE activation pathway. In the cytoplasm, Nrf2 is bound to Keap1 in the form of dimer Nrf2-Keap1. During oxidative stress, Nrf2 is released from Keap1, which allows Nrf2 to translocate to the nucleus. Nrf2 forms a heterodimer with Maf which then binds to the ARE-regulated genes. This in turn upregulates the expression of antioxidant and therefore promotes cell survival [164].

1.3.5 Mitochondrial ROS functions as second messenger molecules

Although ROS have been described as by-products of oxidative phosphorylation for decades, it has been established that they function as second messenger under normal concentrations. ROS have been evidenced to regulate gene expression by controlling transcription factors; they also appear to influence protein activity by controlling phosphatases and kinases [177]. This regulatory function is exerted through ROS's redox potential. For example, ROS-induced oxidation of cysteine-rich proteins will result in the formation of disulfide bonds in the same molecule or between two cysteine-rich molecules. This modification can therefore result in conformational changes of one molecule or dimerisation of two or more molecules, hence modulating the activity of those molecules (reviewed in Ref. [178]). More importantly, ROS-regulated molecules have been implicated in cell survival, cell cycle control, apoptosis, differentiation and several stress responses [53].

Hypoxia-inducible factor 1 (HIF-1) activity has been demonstrated to be regulated by ROS. ROS stabilise HIF-1α allowing it to dimerise with HIF-1β and forming an active nuclear transcription factor. Active HIF-1 is well known to regulate the expression of glycolytic enzymes and VEGF, and to interfere with pro-apoptotic pathways [53].

Mitogen-activated protein kinases (MAPK) are a superfamily of protein kinases that regulate several cell functions including gene expression, proliferation, cycle progression and apoptosis. Oxidative stress has been demonstrated to activate apoptosis signal regulated kinase 1 (ASK1) that regulates the c-Jun N-terminal kinase (JNK) and p38/MAPK pathways leading to apoptosis through phosphorylation of members of the MAPK cascades (reviewed in Ref. [167]). On the other hand, the ROS-activated MAPK/ERK (extracellular signal-regulated kinase) pathway can also lead to non-apoptotic outcomes such as differentiation, proliferation and cell division, thus reinforcing the role of ROS signalling in cellular homeostasis [53,167].

Phosphoinositide 3-kinase (PI3K) and AKT pathway is another signalling pathway subjected to reversible redox regulation by ROS. It is regulated by ROS in a similar manner as the MAPK pathways at the oxidative interface where phosphatase and tensin homolog (PTEN), a natural inhibitor of the PI3K/AKT pathway, is directly oxidised by ROS. This renders inactivation of PTEN and consequently results in sustained activation of the PI3K/AKT and MAPK pathways that play critical roles in cell proliferation and survival [53,167].

1.3.6 ROS regulating apoptosis and cell cycle

In the mitochondrial apoptotic process, initial damage induced by stress does not kill the cell immediately. Instead, it induces an apoptotic signalling program that cause cell death. At high levels, ROS appear to act as substantial regulatory signals in the apoptotic process through their interactions with essential signalling molecules [55].

ASK1 is an upstream MAPKKK that regulates the JNK pathways leading to apoptosis through phosphorylation of JNK. ASK1 kinase activity is shown to be directly inhibited by thioredoxin (Trx). However, ROS can oxidise Trx and cause the formation of a disulfide bond between Cys-32 and Cys-35 in Trx, leading to the release of ASK1 from Trx. This separation allows ASK1 to undergo complete homo-oligomerisation and subsequent autophosphorylation, resulting in its activation. Subsequently, ASK1-

acitvated JNK can phosphorylate pro-apoptotic BH3-only proteins (BID and BMF). The phosphorylated BID and BMF further activate BAX and BAK to initiate apoptosis respectively [160].

ROS formation is also a key factor that facilitates MPTP opening and release of apoptosis-inducing proteins [99]. In fact, it has been proposed that oxidation of adenine nucleotide translocase (ANT) by ROS is also linked to the regulation of the MPTP opening [160]. Moreover, ROS have been confirmed to regulate the activity of the BCL-2 family proteins, the dominant regulators of the mitochondrial apoptotic pathway. Elevated ROS have been shown to abate the anti-apoptotic activity of BCL-2 by directly oxidise it at Cys158 and Cys229. On the other hand, ROS can abrogate the ubiquination of BAX, whereas promote ubiquitination of BCL-2, thus allowing the activation and oligomerisation of BAX/BAK, resulting in the formation of a VDAC-containing pore and permeabilisation of mitochondrial membranes to facilitate cyt *c* release [160].

ROS were also proposed to mediate the death receptor dependent apoptosis (i.e. extrinsic apoptosis) [160]. Although ROS do not directly act via death receptors, it can influence the extrinsic pathway by modifying the intracellular milieu, hence allowing the environment to facilitate effective binding between death ligands and their receptors and the execution of the downstream cascades leading to apoptosis [179]. Moreover, ROS have been shown to supress the expression of cellular FLICE (FADD-like IL-1β-converting enzyme)-inhibitory protein (c-FLIP), the endogenous inhibitor of TRAIL, and therefore promote extrinsic apoptosis [180]. In addition, several studies have suggested that ROS have a critical role in regulating the expression of functional FasL, a major death ligand in the extrinsic pathway [181] (Figure 1.28).

Furthermore, ROS play an essential role in cell cycle blockade, which can result in cell cycle G2/M arrest [182] (Figure 1.28). The CDK1/Cyclin B1 complex is a fundamental regulator in cell cycle progression from G2 phase into M phase. During G2 phase, CDK1 is activated by cell division cycle (CDC25C) through dephosphorylation and triggers the initiation of mitosis. However, activation of the ataxia telangiectasia mutated (ATM) protein triggered by ROS-induced DNA damage mediates activation of checkpoint kinase 1 and 2 (CHK1, CHK2), which subsequently results in CDC25C inhibition and degradation. Deactivated CDC25C can no longer dephosphorylate CDK1, resulting in cell cycle arrest at G2/M phase [182,183].

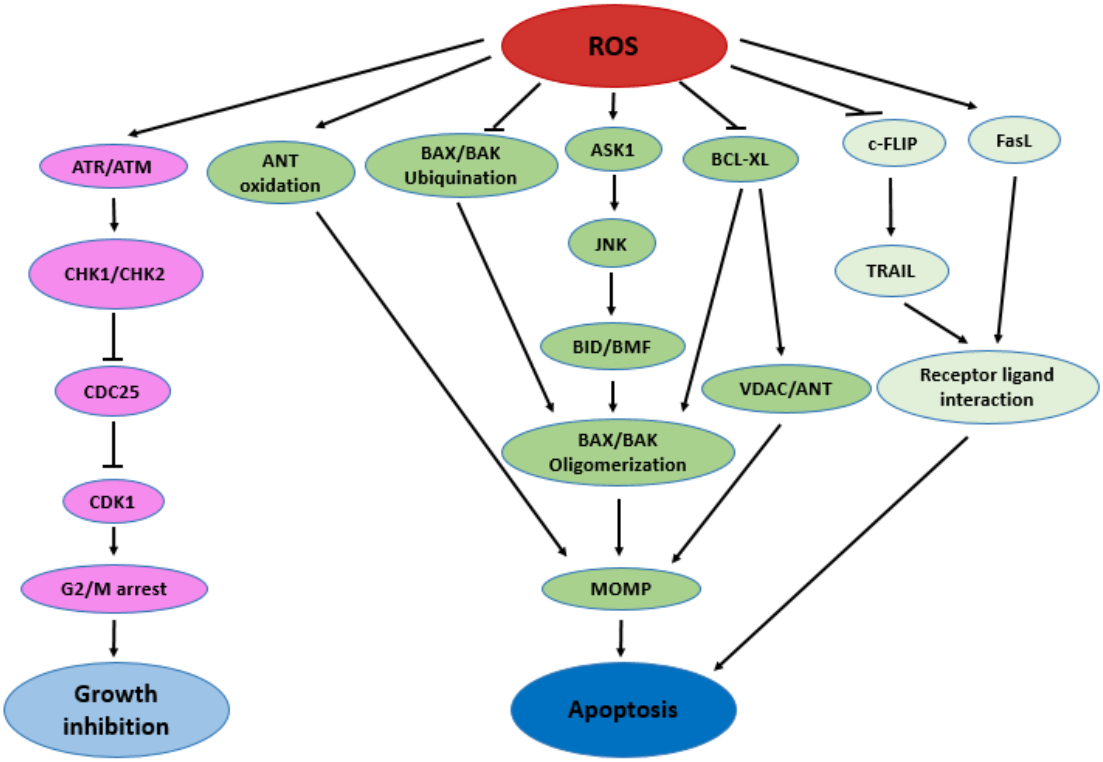

Figure 1.28. Summary of the roles of ROS in apoptosis and cell cycle.

Oxidative stress mainly induces programmed cell death. However, ROS can also trigger necrosis. As mentioned earlier, ROS modify lipids and result in lipid oxidation. This can lead to the loss of integrity of both plasma membrane and intracellular membranes, rendering the release of proteases and consequently necrosis. Another target of ROS is amino acid residues. ROS-mediated protein modification contributes to necrosis through the modification of Ca^{2+} channels. The resulting influx of Ca^{2+} into the cytoplasm from the extracellular environment and from the endoplasmic reticulum can trigger necrosis (reviewed in Ref. [184]).

1.3.7 Mitochondrial ROS (mROS) in cancer development

Oxidative stress or overproduction of ROS has been associated with various disease processes including cancer, and unlimited growth of cancer cells in response to ROS accumulation has been the focus of interest in recent studies [175].

Generally, cancer cells have a constant metabolic oxidative stress compared to normal cells, and the elevated levels of ROS during cancer transformation are due to high mitochondrial metabolic rate that results in increased electron leakage and ROS generation [164]. However, it has also been established that beside their mitogenic effect in tumours, excessive levels of ROS can induce damage in cancer cells and trigger apoptosis if not counteracted by antioxidant systems. Therefore, cancer cells are required to achieve a delicate redox balance to ensure survival, growth and metastasis (Figure 1.29). Mutations in mitochondrial DNA, deactivation of tumour suppressor genes and upregulation of oncogene expression are some mechanisms that are ROS-regulated and can in turn ensure an adequate tumorigenic ROS production [175].

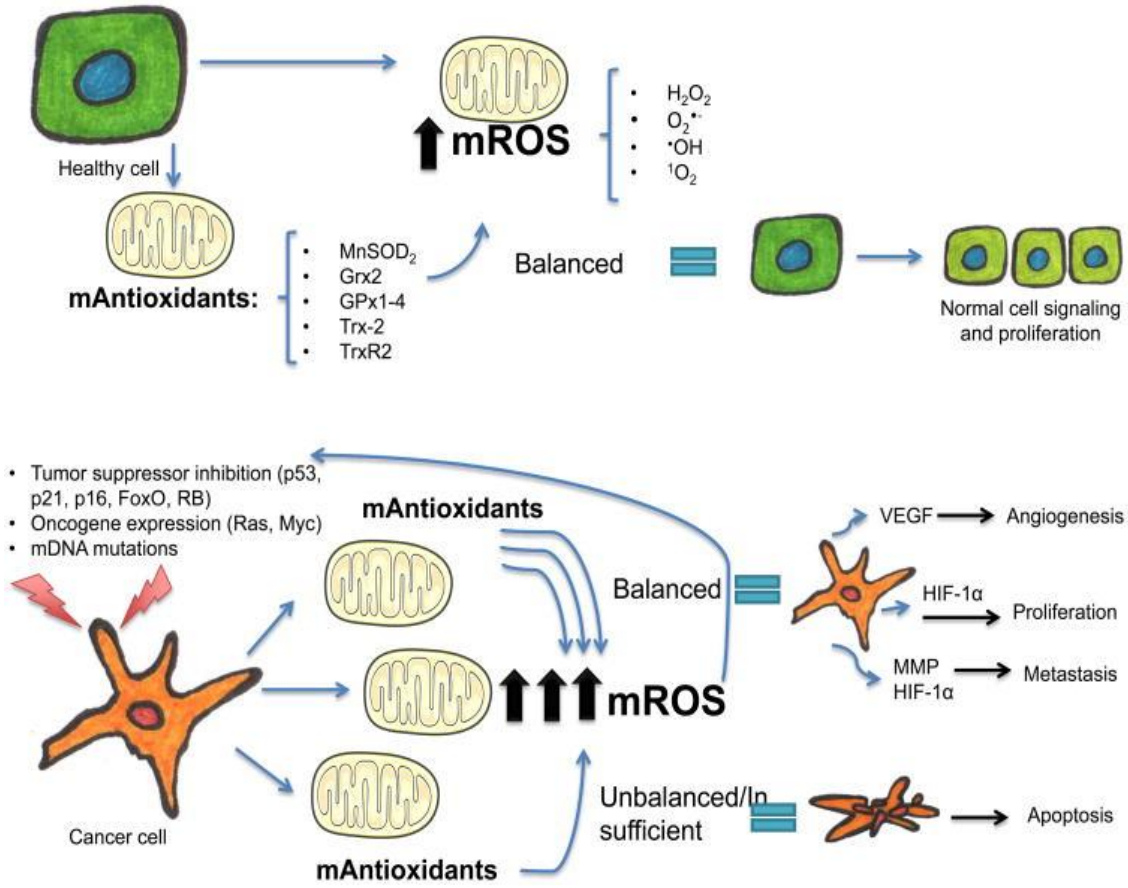

Figure 1.29. Mitochondrial redox control in healthy and cancer cells. Balanced production and scavenging of mROS grant cell survival and induce more altered gene expression, and enhance cellular mitosis, angiogenesis and metastasis through mROS-mediated mechanisms. In contrast, when the oxidant scavenging system is overpowered by mROS production in cancer cells, an oxidative stress-induced apoptosis occurs [175].

Tumour suppressor genes that regulate vital cellular activities such as cell proliferation, differentiation and apoptosis respond to oxidative stress by regulating both antioxidant and pro-oxidant responses. For example, mROS-mediated upregulation of the P53 protein can enhance the expression of its downstream target genes, which subsequently limit or promote further ROS production to either restrict DNA damage or induce apoptosis through excessive DNA damage [185,186]. Oncogene expression can also promote the generation of mROS and tumour proliferation. For example, the Ras and Myc oncogenes can induce ROS production in mitochondria and modulate tumorigenic and migratory signalling. On the other hand, oncogene-driven ROS generation induces mutation within the mitochondrial genome leading to mitochondrial dysfunction and further production of ROS and eventually apoptosis [175].

Mitochondrial DNA instability is a main mechanism associated with tumorigenesis that involves increased mROS production and oxidative stress-induced mtDNA damage. Both mitochondrial superoxide and hydrogen peroxide have been shown to induce mutations in the ND6 subunit in the HepG2 cells (human liver carcinoma) [187]. This is consistent with the findings reported by Ishikawa and co-authors [77] that mutations in ND6 enhanced the metastatic potential of tumour cell lines which was reversed by ROS scavengers. Moreover, another study on osteosarcoma cell lines by Sharma *et al*. [115] showed that inhibition of complex I resulted in overproduction of mROS and increased activation of AKT that promoted cell survival.

Other ROS-mediated pathways are shared between cancer and healthy cells in terms of cellular proliferation. For instance, the mechanism of mROS-modulated angiogenesis under hypoxic conditions via mROS-induced HIF-1α stabilisation is also utilised by cancer cells to promote growth and proliferation. Indeed, HIF-1α has been associated with invasiveness of various types of cancer [188]. Matrix metalloproteinases (MMPs), a large family of proteases capable of degrading all kinds of extracellular matrix proteins, have also been associated with tumour progression [189]. ROS can indirectly modulate MMP gene expression by activating the MAPK family members ERK 1/2 which leads to the subsequent transcription of MMP genes such as MMP-1 [190].

Since both HIF-1α and MMPs are highly regulated by mROS and play pivotal roles in metastatic disease progression, it is possible that their association with tumorigenesis is mediated by mitochondria through redox dependent programming [175].

1.3.8 ROS as signalling molecules in cancer survival and metastasis

ROS play a pivotal role at every stage of cancer development including initiation, progression and survival. Hydrogen peroxide reversibly causes the oxidation of cysteine thiol groups of phosphatases such as protein phosphatase 2 (PP2), protein tyrosine phosphatase 1B (PTP1B) and phosphatase and tensin homolog (PTEN). This modification results in the loss of their activity and activation of the PI3K/Akt/mTOR survival pathway (Figure 1.30). Several studies have shown that hydrogen peroxide can enhance growth factor signalling and Ras activation that result in promoting PI3K/Akt/mTOR and MAPK/ERK signalling cascades. In addition, oxidisation of prolyl hydroxylase domain-containing protein 2 (PHD2) by H_2O_2 results in stabilising HIF-1 during hypoxia, hence promoting angiogenesis and metastasis by inducing the expression of pro-angiogenic genes [164].

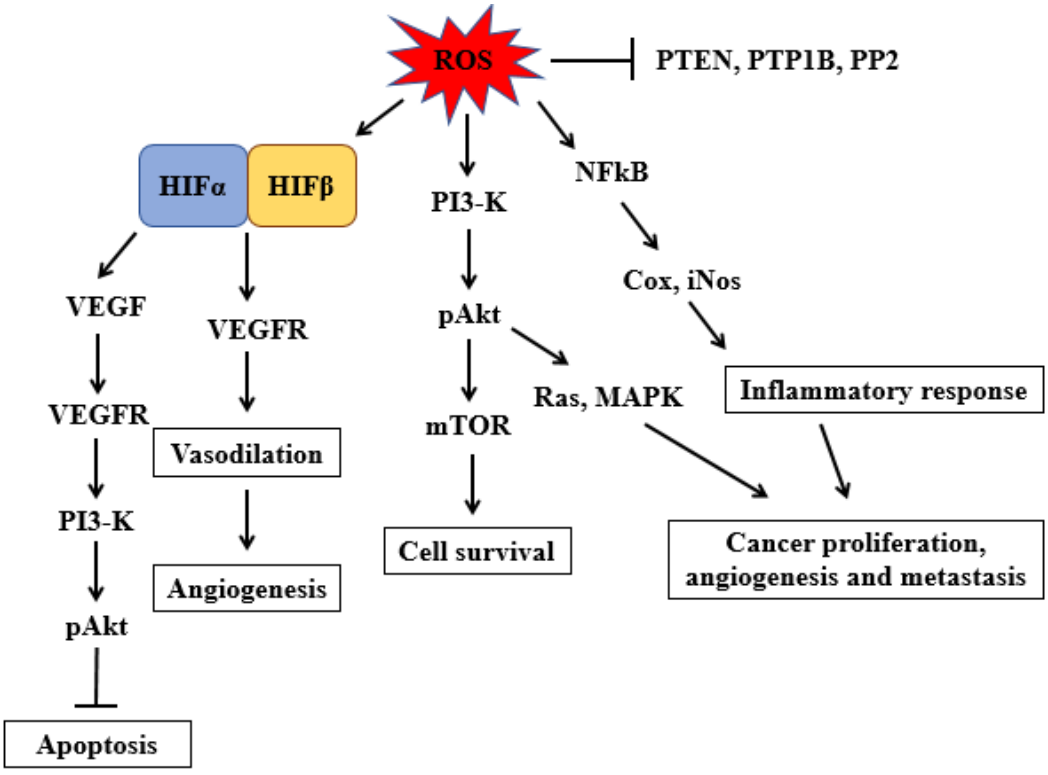

Figure 1.30. Role of ROS in signal transduction. High level of ROS in cancer cells activates survival pathway and inactivates PTEN pathway, which initiates apoptosis. ROS trigger activation of the PI3K/AKT/mTOR survival signalling resulting in metabolic modulation, cell survival and activation of Ras-MAPK pathway, leading to cell proliferation. Hypoxia causes activation of HIFα and HIFβ, which further activates VEGF, an angiogenic growth factor [164].

It is well established now that metastasis requires a series of stages that leads to the formation of secondary tumours in distant organs, and ROS have been shown to regulate several signalling pathways (e.g. PI3K/AKT/mTOR and MAPK/ERK) and

transcriptional activities (e.g. HIF and Snail) that facilitate cancer cell migration and invasion. More importantly, elevated levels of ROS due to mutations in the mitochondrial genome have been shown to promote cancer metastasis [164].

ROS also seem to induce epithelial mesenchymal transition (EMT), a critical initial step of metastasis that allows cancer cells to avoid hostile environments. EMT is controlled by a network of signalling pathways involving growth factors (e.g. EGF, TGF-β) and their associated signalling proteins (e.g. NF-κB, ERK, PI3K/AKT) in response to stresses implicated in tumorigenesis, including oxidative stress. These signals promote transcription factors such as zinc finger protein SNAI1 (Snail) which regulates the expression of proteins engaged in cell-cell contact, cytoskeletal maintenance and extracellular matrix degradation. They also trigger loss of E-cadherin, an epithelium-specific protein, which is considered as a key feature of EMT [191].

ROS have been shown to upregulate Snail expression by activating EGFR, ERK, and p38/MAPK cascades and subsequently deactivating the endogenous inhibitor of Snail, glycogen synthase kinase 3β (GSK3β) [192]. ROS also contribute to activation of the AP-1 transcription factor that directly induces Snail expression [191]. In addition, it has been reported that ROS increase the expression of distal-less homobox-2 (Dlx-2), an upstream regulator of Snail, thereby activating Snail [191]. Moreover, ROS have been shown to activate NF-κB signalling which is known to stabilise Snail by preventing its ubiquitination and degradation [193].

When EGFR/PI3K/AKT pathway is activated by ROS, it subsequently inactivates GSK3β to increase the expression of activated Snail [194]. EGFR/PI3K/AKT pathway also activates signal transducer and activator of transcription 3 (STAT3) which is known to facilitate invasion by upregulating MMPs [191]. Recently, increased expression of MMP-2, MMP-3 and MMP-9 has been considered to be a significant factor in triggering EMT and predicative of tumour aggressiveness, invasion, metastasis and poor patient survival [164]. A recent study by Mori *et al*. [195] has shown that NOX4-mediated mitochondrial ROS signalling increases MMP9 mRNA stability and affects cancer invasiveness. The ROS-quenching agent N-acetyl cysteine (NAC) was shown to inhibit MMP-induced EMT, suggesting that ROS scavenging could be useful in the reversal of EMT leading to decreased tumour aggressiveness [164].

1.3.9 Role of ROS in cancer therapies

Emerging evidences have revealed that ROS act as a double-edged sword in cancer cells as they have quite opposite impacts on the cells according to their levels. Low to moderate levels of ROS play critical roles in promoting cell survival/proliferation and cancer progression. On the other hand, an excessive level of ROS is able to cause irreversible damage to DNA, lipids and proteins leading to cell death [196].

Generally, cancer cells exhibit elevated levels of ROS due to their genetic abnormalities, active energy metabolism and microenvironment associated instability. However, cancer cells can compensate for excessive levels of ROS and overcome oxidative stress in order to enhance survival and growth. This is achieved by increasing cellular antioxidant capacity and reprograming metabolic pathways [164]. Therefore, further increase of ROS levels using ROS-stimulating agents in cancer therapy has attracted more attention in the past decades, and various therapeutic strategies to utilise ROS have been developed [160].

1.3.9.1 Role of ROS in targeted molecular therapy

Monoclonal antibodies and small-molecule inhibitors are the main biological agents targeting tyrosine kinases in cancer treatments. Several studies evidenced ROS-mediated anti-tumour effects of these drugs. Yang *et al*. [197] showed that Trastuzumab, a monoclonal antibody targeting human epidermal growth factor receptor 2 (HER2), promoted ROS generation which contributed to death of HER2-positive breast cancer cells. Other studies showed that Cetuximab, a monoclonal antibody which binds to and inhibits EGFR, increased intracellular ROS levels in laryngeal carcinoma cells by reducing the amount of glutathione, resulting in ROS-mediated apoptosis [198,199]. EGFR inhibitors (Erlotinib and Gefitinib), in combination with Vorinostat, a histone deacetylases inhibitor (HDACi), increased ROS levels in non-small cell lung carcinoma (NSCLC) cells and promoted caspase-dependent apoptosis [200]. Inhibition of EGFR by Echinatin has also been shown to induce the G2/M cell cycle arrest, and apoptosis via the intrinsic pathway of caspase-dependent activation due to ROS overproduction [201]. Bortezomib, a proteasome inhibitor and an approved drug for treating myelanoma, in combination with SAHA (an HDACi), was found to induce ROS generation to further promote mitochondria-dependent apoptosis in nasopharyngeal carcinoma cells [202]. Moreover, STAT3 inhibitors have been shown to promote ROS-dependent apoptosis in pancreatic cancer cells [203].

1.3.9.2 Role of ROS in photodynamic therapy and radiotherapy

Photodynamic therapy PDT is a method that requires a photosensitising agent, oxygen and light of a specific wavelength for the treatment of neoplastic diseases [204]. Once the agent enters cancer cells and the tumour is exposed to light, the agent changes from its ground state (i.e. the lowest energy state) to an excited state by absorbing the light. As it returns to the ground state, released energy is transferred to oxygen to generate ROS that destroy cancer cells via ROS-mediated apoptosis or necrosis [205].

Ionising radiation (IR) is a common therapeutic tool for the treatment of solid tumour. ROS have been evidenced to play a critical role in promoting the biological effect of IR [160]. IR can generate excessive ROS by water radiolysis during radiotherapy mainly hydroxyl radicals. High level of hydroxyl radicals induces cancer cell death by damaging the cellular DNA (reviewed in Ref. [206]).

1.3.9.3 Role of ROS in cancer chemotherapy

Regardless their strong side effects, chemotherapeutic drugs are still the most common treatment for cancer. Many of those drugs cause DNA damage leading to cell death. However, a large number of chemotherapeutic agents cause intracellular ROS accumulation either by accelerating ROS production or by supressing ROS clearance in tumour cells. Several studies evidenced the accumulation of ROS upon treatment with chemotherapeutic drugs. For example, cisplatin was reported to cause excessive accumulation resulting in cytotoxic effect in various types of cancer such as breast cancer [207], prostate cancer [208,209] and ovarian cancer [196]. However, drug resistance is still the main obstacle for efficient cancer treatment with chemotherapeutic drugs. Multidrug resistance protein 1 (MDR1) plays a critical role in drug efflux, hence decreasing the cytotoxicity of the drug [210]. Accumulating evidences have shown that ROS can downregulate MDR1 expression whereas other reports have suggested that ROS promote MDR1 expression in cancer cells instead [160,211]. This debate raises the possibility that ROS are involved in the regulation of MDR1. Indeed, Terada *et al.* [212] showed that low concentrations of ROS increase the expression of MDR1 whereas high concentrations of ROS decrease its expression in Caco-2, a human colon cancer cell line. Therefore, ROS not only induce chemo-resistance but also enhance chemo-sensitivity in tumour cells [160].

1.4 Mitochondria as anticancer target

The fact that mitochondria contribute to key cellular processes including ATP production, ROS generation for cell signalling, maintenance of intracellular homeostasis and regulation of apoptosis makes them an attractive target for cancer therapy [99]. Understanding different features of mitochondria in cancer cells compared to normal cells could help researchers exploit mitochondrial Vulnerabilities to Trigger Apoptosis Selectively in Cancer Cells [213]. Indeed, several therapeutic approaches have been proposed to target mitochondria as a tool for tumour elimination, as discussed below.

1.4.1 Targeting the transition of cell metabolism

Since cancer cells mostly rely on glycolysis for ATP generation compared to non-malignant cells, drugs that disturb cellular metabolism mainly at the level of glycolysis can display effective anticancer effects. Indeed, inhibition of glycolysis in a variety of cancer cells by a non-metabolisable glucose analogue, 2-deoxyglucose (2-DG), resulted in significant ATP reduction. This ATP depletion also triggered dephosphorylation of BAD, translocation of BAX from cytosol to mitochondria and permeabilisation of OMM, leading to massive cell death [214]. However, one clinical trial for 2-DG as a glycolytic inhibitor for prostate cancer has been suspended, mainly due to the lack of cancer-specific targeting of the drug which caused severe damage to the normal tissue [215]. Lonidamine (LND), a derivative of indazole-3-carboxilic acid, is known for its ability to inhibit aerobic glycolysis in cancer cells. LND has shown synergistic effects when used in combination with chemotherapeutic agents such as cisplatin and doxorubicin [216]. Several phase III clinical trials of lonidamine have been carried out in breast cancer and NCLC (reviewed in Ref. [86]).

1.4.2 Targeting the disabled apoptosis pathway

Another approach to targeting mitochondria is the activation of the pro-apoptotic potential. The anti-apoptotic BCL-2 family proteins are well known to be overexpressed in many cancers and associated with cancer initiation and resistance to therapy by their attenuating the release of cytochrome *c* and inactivating other pro-apoptotic proteins. Therefore, researchers have focused on developing drugs that can neutralise the binding of anti-apoptotic proteins to BAK and BAX, hence allowing pore formation in the OMM.

ABT-199 (trade name Venetoclax), a selective small-molecular inhibitor of the anti-apoptotic protein BCL-2, was found to disrupt the interaction between anti- and pro-apoptotic proteins. ABT-199 was approved by Food and Drug Administration (FDA) in 2016 for its use in patients with chronic lymphocytic leukemia (CLL) [217])

1.4.3 Targeting cellular damage caused by abnormal ROS production

Modulation of mitochondrial respiratory chain activity has been under investigation to stimulate cancer cell death. Indeed, inhibitors of mitochondrial respiratory chain including rotenone (complex I-specific inhibitor), antimycin (complex III-specific inhibitor) and oligomycin (inhibitor of mitochondrial ATP synthase) were shown to induce apoptosis in cultured human lymphoblastoid cells [218]. Cell death resulted from mitochondrial respiratory chain inhibition is predominantly mediated by overproduction of ROS [99]. Arsenic trioxide, a clinically used drug for treating acute myeloid leukaemia, can cause increased leakage of electrons by interfering with OXPHOS, hence promoting ROS generation and the subsequent apoptosis [219]. Other agents have been evidenced to exert their anticancer effects by supressing antioxidant enzymes leading to over-accumulation of ROS [220]. For example, 2-methoxyoestradiol, an estrogen derivative, can selectively kill leukaemia cells (but not normal lymphocytes) by supressing superoxide dismutase. Phase I/II clinical studies have showed that 2-methoxyoestradiol causes disease stabilisation in patients with solid malignancies or multiple myeloma [221,222]. A recent study by Kim *et al*. [223] showed that oxalomalate, a well-known competitive inhibitor of isocitrate dehydrogenase (IDH) isoenzymes which serve as the major antioxidants and redox regulators in the mitochondria and cytosol, resulted in induction of ROS stress response, ultimately leading to apoptotic cell death and antiangiogenic effects in melanoma cells.

1.4.4 Induction of mitochondrial permeability transition pore

Induction of MPTP is another approach to overcoming the resistance to OMM permeabilisation as a result of overexpression of anti-apoptotic BCL-2 family proteins. Multiple conventional anticancer treatments (e.g ionising radiation) are exerting their anticancer effects by stimulating excessive ROS production that is a key factor in facilitating the induction of MPT. Anticancer drug-induced MPT may result from oxidative modification of the components of the MPT pore. For instance, due to its

mechanism of action as described above, arsenic trioxide was found to cause ROS-mediated modification to thiol group in ANT thus resulting in cytochrome *c* release through MPT induction [99].

VDAC is another component of MPT. The interaction of VDAC with hexokinase II, a glycolytic enzyme usually over expressed in cancer cells, holds VDAC in the open state, which counteracts OMM permeabilisation to prevent apoptosis. Moreover, this interaction obstructs the binding of pro-apoptotic proteins to VDAC and subsequently supresses the induction of apoptosis (reviewed in Ref. [224]). Several compounds trigger cell death through interacting with VDAC. For example, Avicins, a group of anti-inflammatory-molecules with pro-apoptotic effects, target and close VDAC. Closure of VDAC leads to permeabilisation of the OMM and release of cytochrome *c* [225].

1.4.5 Targeting mutated mtDNA

Several compounds that target the mitochondrial genome or the enzymes related to its replication process have potential clinical applications. For example, cisplatin, one of the most commonly used chemotherapeutic agents, is found to preferentially bind to the mitochondrial genome more than to nuclear DNA, which results in the formation of cisplatin–mtDNA adducts and subsequently inhibits OXPHOS and decreases ATP generation [226]. Ditercalinium, a bis-intercalating agent that accumulates specifically in mitochondria, can cause depletion of the mitochondrial genome and inhibit its replication. This agent exhibits *in vivo* anticancer effect in animal models, and several studies have shown a complete elimination of mtDNA upon treatment with ditercalinium [227].

1.5 Cisplatin

Cisplatin [cisplatinum or cisdiamminedichloroplatinum (II)] (CDDP; Figure 1.31) is one of the most commonly used chemotherapeutic agents to treat various cancers in both adults and children, including ovarian, cervical, testicular, bladder, head and neck, lung and colorectal cancers, either as a solo therapy or in combination with other anticancer drugs such as doxorubicin and paclitaxel [228,229]. Cisplatin was approved by FDA in 1978 for the treatment of bladder and testicular cancers.

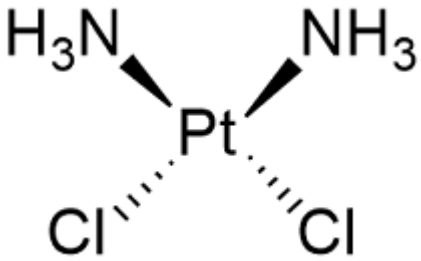

Figure 1.31. Chemical structure of cisplatin. Cisplatin loses chloride moieties in an aqueous medium and enters the cell. Once inside the cell, the positively charged platinum (Pt) reacts with DNA and forms cross-links and adducts.

CDDP can enter cells through passive diffusion, and recent studies have suggested an active uptake of CDDP facilitated by the copper transport proteins (CTR1 and CTR2) as another major mechanism for cisplatin uptake (reviewed in Ref. [230]).

Previous studies have shown that once inside the cells, cisplatin is a highly reactive molecule which forms various types of adducts by binding to DNA, RNA and sulfudryl groups of proteins, and the cytotoxic effect of cisplatin is mainly due to the lesions formed within the nuclear DNA [231,232]. The platinum atom of cisplatin forms hydrogen and covalent bonds with purine bases producing intrastrand and interstrand crosslinks [233]. These CDDP-nDNA adducts interfere with DNA transcription and/or replication and subsequently trigger apoptosis [234–237].

However, more recent studies from the last decade have challenged the previous observations by stating that very low percentage of cisplatin interacts with the nuclear genome. Those studies have found that the largest amount of cisplatin accumulates inside mitochondria and interacts with mitochondrial DNA and proteins causing significant changes in mitochondrial structure and metabolic function. This leads to significant modifications in metabolites levels associated with the TCA cycle and glycolysis pathway [238,239].

Recent reports evinced that cisplatin-induced apoptosis could be inhibited by compounds that interfere with ROS generation (Figure 1.32). These observations elucidate that the killing effect is correlated to activation of oxidative stress pathways [240].

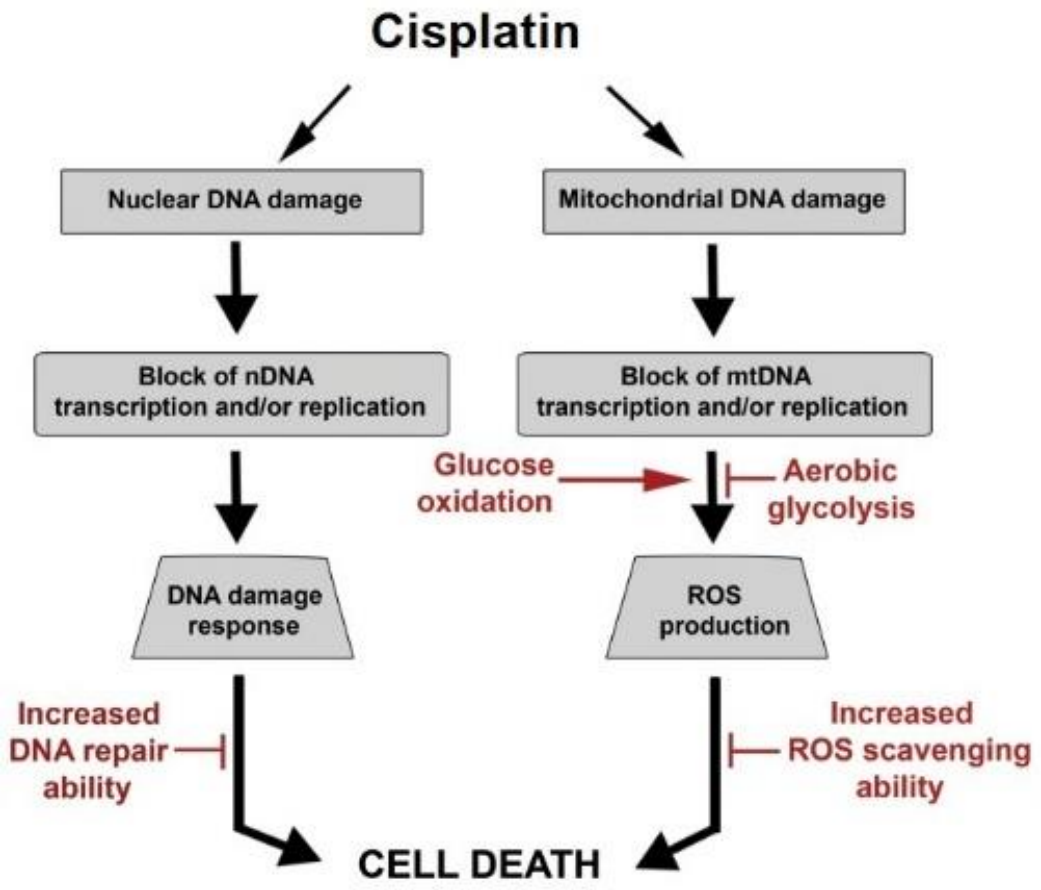

Figure 1.32. Model for major components of cisplatin-induced cytotoxicity. Cisplatin causes direct damage to mtDNA leading to reduction of mitochondrial protein synthesis, impairment of electron transport chain function, hence increasing intracellular ROS levels. ROS ultimately promote cell death and therefore significantly enhance the cytotoxic effect exerted by cisplatin-induced nDNA damage. Mitochondrial dysfunction, increased mROS scavenging and glycolytic metabolism can reduce cellular sensitivity to the mROS-mediated component of cisplatin toxicity. Cells can also become more resistant to cisplatin through increased DNA repair capacity [209].

Despite its effectiveness, cisplatin is non cancer specific and the clinical use of cisplatin is limited because of its severe irreversible side effects including neurotoxicity, ototoxicity and nephrotoxicity which has been reported as the main limitation of cisplatin [241–243]. In addition, many cancer patients exhibit an intrinsic resistance to cisplatin or develop resistance during the treatment course resulting in therapy failure (reviewed in Ref. [244]). More specifically, colorectal and prostate cancers are intrinsically resistant to cisplatin whereas acquired resistance is commonly observed in ovarian cancer patients [245–247].

Researches [248–251] have proposed reasons for cisplatin resistance such as decreased drug uptake, increased drug efflux, elevated detoxification system achieved by high levels of scavengers, enhanced tolerance to DNA damage and highly efficient DNA repair mechanisms. These mechanisms are specific to individual cancer cases where each single cancer cell may possess one or more or even the whole resistance mechanisms.

In addition, a number of studies have highlighted the potential involvement of the mitochondrial genome in cisplatin resistance. Qian *et al.* [252] showed that the Rho0 cells (i.e. cells depleted of mtDNA) generated from a normal intestinal epithelial cell line, IEC-6, demonstrated a significantly increased resistance to cisplatin compared to their parental counterparts. Similar results were observed by Park and co-authors in hepatocarcinoma cells [253]. This suggests that the mitochondrial genome is a target of cisplatin and mitochondria are pivotal in the apoptotic process. On the other hand, several studies have indicated that mtDNA copy number reduction, unlike complete mtDNA depletion, may contribute to enhanced cisplatin sensitivity. Mei *et al.* [174] showed that decreasing mtDNA copy number sensitised tumour cells to cisplatin. In their study, they observed that reducing mtDNAcn by treatment with ethidium bromide or transfection with shRNA-TFAM significantly elevated ROS levels and subsequently enhanced tumour cells' sensitivity to cisplatin. Therefore they proposed that altering mDNAcn could be a new approach to improved cancer treatment [26].

According to the aforementioned results, the mitochondrial genome appears to have a significant impact on drug efficacy in terms of cisplatin. Therefore, mtDNA could be a promising target for treating otherwise cisplatin-resistant cancers, and selective delivery of cisplatin to cancer cells can further enhance the efficacy.

In a study conducted by Marrache *et al*., an engineered hydrophobic cisplatin prodrug, Platin-M, was efficiently delivered inside the mitochondria of neuroblastoma cells, facilitated by a positively charged mitochondria-targeting nanoparticle. The authors observed a much greater activity level of Platin-M compared to unmodified cisplatin (17 times more active) [254].

1.6 Delocalised lipophilic cations

Traditional chemotherapeutic drugs have achieved limited success in cancer treatment due to their marked side effects as a result of their lacking specificity for cells of tumorigenic origin. Therefore, developing new strategies to provide selective cancer cell killing which depends on novel cellular targets sufficiently different between cancer and normal cells is crucial [255]. Delocalised lipophilic cations (DLCs) comprise a potential new class of anticancer agents that accumulate in mitochondria, driven by the negative electric potential across the mitochondrial membrane. It has been reported that DLCs are selectively more toxic to cancer cells than to normal ones [255,256].

1.6.1 Accumulation of delocalised lipophilic cations in mitochondria

Translocation of protons across the inner mitochondrial membrane from the matrix to the intermembrane space by the mitochondrial proton pumps (complexes I, III and IV) during the oxidative phosphorylation results in the generation of mitochondrial transmembrane potential ($\Delta\Psi m$). In response to the negative inside transmembrane potential, lipophilic cations possessing a delocalised positive charge can penetrate the lipid membranes and accumulate in the mitochondrial matrix. It has been reported that $\Delta\Psi m$ is approximately 60 mV higher in carcinoma cells than that of normal epithelial cells [257]. According to the Nernst equation ($\Delta\Psi$ (mV) = 61.5 $\log_{10}\{[cation]_{in}/[cation]_{out}\}$), a 61.5 mV difference in mitochondrial transmembrane potential between normal and cancer cells results in a ten-fold increase in DLC accumulation in carcinoma mitochondria (reviewed in Ref. [258]), making the selective accumulation of DLCs in the mitochondria of cancer cells an attractive approach to cancer-specific therapy. The difference in $\Delta\Psi m$ between carcinoma and normal epithelial cells may be attributed to differences in the structure and function of the mitochondrial components that serve to create and maintain the electrical gradient such as mitochondrial complexes, electron carriers, ATP syntheses and membrane lipid structure (reviewed in Ref. [255]).

1.6.2 Selective mitochondrial toxicity of delocalised lipophilic cations

All DLCs share a common mechanism for mitochondrial accumulation due to their lipophilic nature and response to the negative inside transmembrane potential. However, their mechanisms of toxicity to mitochondria at high concentrations are very different. For example, rhodamine 123 (Rh123) inhibits F_0F_1-ATPase resulting in compromised

mitochondrial bioenergetic function [259]. In contrast, dequalinium chloride (DQA) damages mtDNA and inhibits NADH ubiquinone reductase activity in complex I resulting in disruption in mitochondrial respiration [260]. Another DCL, rhodacyanine (MKT-077), causes a general disturbance of mitochondrial membrane leading to nonspecific inhibition of mitochondrial respiratory enzymes [261]. In addition, MKT-077 was also shown to have a degradative effect on mtDNA [262].

1.6.3 Delocalised lipophilic cations as chemotherapeutic agents

The selective accumulation of DLCs in cancer cells due to the increased ΔΨm and their mitochondrial toxicity suggest a rationale for utilising DLCs to achieve cancer-specific therapy. Different DLCs have already demonstrated various degrees of cancer cell killing *in vitro* and/or *in vivo* [255]. Rh123 was the first DLC to show anticancer activity. In a study published in 1982 by Bernal *et al*., Rh123 noticeably supressed the clonal growth of carcinoma cells *in vitro* [263]. In a follow-on study conducted by the same research group, Rh123 was also found to prolong the survival of mice implanted with the MB49 cells (mouse bladder cancer) [264]. DQA showed a 100-fold greater level of clonal growth suppression of carcinoma cells *in vitro* compared to control epithelial cells [265]. The same study also demonstrated DQA's anticancer efficacy in nude mice implanted with human colon adenocarcinoma cells [265]. Several studies showed that MKT-077 significantly inhibited growth in various human cancer cell lines *in vitro* [266], and it had marked anticancer efficacy in nude mice implanted with human melanoma (LOX) and prostate carcinoma (DU-145) cells [255]. MKT-077 was the first DLC to be approved for clinical trial by FDA for the treatment of cancer. However, the trials were stopped in phase II since the efficacy in cancer cell killing was not observed at the approved dose and drug regimen [255]. Recently, D112, a photosensitiser developed by Eastman Kodak Company, was shown to induce intrinsic apoptosis. D112 was found to bind to mtDNA and inhibit electron flow through ETC resulting in ROS production, mtDNA damage, activation of pro-apoptotic proteins and eventually apoptosis [267].

1.6.4 Dequalinium chloride

Dequalinium is a quaternary ammonium cation that contains two quaternary quinolinium units linked by an N-decylene chain (Figure 1.33). It is most commonly available as a dichloride salt and used as an active ingredient in antibiotics for treating vaginal bacterial infections. Dequalinium chloride (DQA) has been reported to demonstrate potent anticancer activity *in vitro* and *in vivo* in different malignancies [268]. Several studies have suggested that the cytotoxicity mechanism of DQA is related to mitochondrial dysfunction due to the damage to mitochondrial DNA and the inhibition of mitochondrial complex I [267]. It has also been reported that DQA triggers cell death in the HeLa cells by selective depletion of mtDNA [269]. Moreover, it has been postulated that DQA causes human cancer cell death by affecting the redox balance [270–272].

Sancho *et al.* [270] observed in human leukaemia cells that DQA-induced apoptosis was mediated via the intrinsic mitochondrial pathway triggered by mitochondrial DQA accumulation which subsequently led to loss of ΔΨm, cytochrome *c* release and ROS overproduction. They also showed that elevated ROS caused apoptotic cell death in the early phase of DQA exposure when sufficient levels of intracellular ATP were detected, whereas necrosis was the main cell death mechanism in the later phases when ATP became significantly reduced. Similar results were observed in a study conducted with the PC-3 cells (human prostate cancer) in which DQA induced oxidative stress and apoptosis, followed by necrosis secondary to apoptosis [272]. Another study by Sancho *et al.* [271] showed that DQA rendered the cell cycle arrest in G2/M phase in the NB4 cells (human leukaemia) before the cells underwent apoptosis and necrosis.

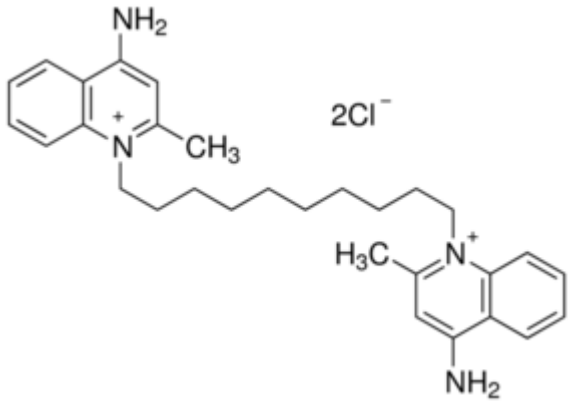

Figure 1.33. Chemical structure of Dequalinium Chloride. Dequalinium is a delocalised lipophilic cation that is able to enter mitochondrial membranes, and preferentially into those of cancer cells due to their more negative mitochondrial transmembrane potential (governed by the Nernst equation). Since DLCs are toxic at high concentration, the accumulation of such molecules in cancer cells leads to targeted cell death [255].

1.7 Need for efficient predictive biomarkers in cancer therapy

Cancer biomarkers can be classified into three categories according to their usage: *predictive biomarkers* which can predict the response to specific therapeutic interventions; *prognostic biomarkers* which aim to give the physicians indication of clinical outcomes such as disease progression or cancer recurrence in the future; *diagnostic biomarkers* which are used to identify a specific disease condition (reviewed in Ref. [273]).

Several predictive biomarkers for human cancers are currently in clinical use. For example, overexpression of HER2, a member of the EGFR family, is predictive of a patient's response to the HER2 monoclonal antibodies such as pertuzumab and trastuzumab in breast cancer therapy. Phase III trials have confirmed that breast cancer patients with HER2 overexpression show improved disease-free and overall survival rates when anti-HER2 therapy is administrated [274,275]. Overexpression of HER2 is also predictive of response to trastuzumab in patients with advanced gastric or gastro-oesophageal junction cancer [276]. In terms of the anti-EGFR therapy for treating colorectal cancer, the mutation status of KRAS is a predictive biomarker of patients' response, because KRAS-activating mutations are associated with resistance to EGFR inhibitors such as cetuximab [277,278]. In breast cancer, overexpression of oestrogen receptor (ER) is tested in order to predict response to anti-endocrine therapies such as tamoxifen [279]. Other major predictive biomarkers as well as those described above are listed in Table 1.1.

Table 1.1. Predictive biomarkers in clinical use. HER2: Human epidermal growth factor receptor 2; ER: Oestrogen receptor; GIST: Gastrointestinal stromal tumour; CML: Chronic myeloid leukaemia; NSCLC: Non-small cell lung cancer; EGFR: Epidermal growth factor receptor.

Organ	Cancer	Biomarker	Associated Target and Drug	Ref.
Breast	Breast Cancer	HER2: Overexpression	HER2: Trastuzumab, Pertuzumab, Ado-trastuzumab emtansine	[274,275]
		ER: Overexpression	ER: Endocrine therapy (Tamoxifen, Aromatase inhibitors)	[280]
Gastrointestinal	Colorectal Cancer	KRAS: Mutations	EGFR: Cetuximab, Panitumumab	[277,281]
	GIST	KIT: Mutation	BCR-ABL: Imatinib	[282]
	Esophago-gastric adenocarcinoma	HER2: Overexpression	HER2: Trastuzumab	[276]
Haematological	CML	BCR-ABL	BCR-ABL: Imatinib, Dasatinib, Nilotinib	[283]
Lung	NSCLC	EGFR (HER1): Mutations	EGFR: Erlotinib, Gefitinib, Afatinib	[284]
	Lung adenocarcinoma	EGFR (HER1): Mutations	EGFR: Erlotinib, Gefitinib, Afatinib, Cetuximab	[285]
		HER2: Overexpression	HER2: Neratinib, Lapatinib, Trastuzumab	[285]
		KRAS: Mutations	KRAS: Erlotinib, Tivantinib, Everolimus, Ridaforalimus, Selumetinib	[285]
Skin	Melanoma	BRAF: Mutations	BRAF: Vemurafenib, Dabrafenib	[286]

Currently, numerous predictive biomarkers based on single genes are in phase II or III trials (Table 1.2). In light of the increasing clinical significance of efficient predictive biomarkers, identifying novel biomarkers to help develop enhanced therapeutic strategies is becoming a trend.

Table 1.2. Predictive biomarkers currently under clinical evaluation with their companion therapeutic agents and registered with ClinicalTrials.gov (https://clinicaltrials.gov/ct2/home).

Organ	Cancer	Biomarker	Associated Drug	Phase	Clinicaltrials.gov identifier
Breast	Breast cancer	BRCA1/2	Olaparib	III	NCT02000622
		HER2 (negative in tumour but positive in circulating tumour cells)	Lapatinib	III	NCT01619111
Gastrointestinal	Colorectal	RAS	FOLFOXIRI, Bevacizumab	II	NCT02350530
	Esophagogastric	HER2	Afatinib, Trastuzumab	II	NCT01522768
Head and Neck	Squamous cell carcinoma	HER and KRAS	Poziotinib	II	NCT02216916
Lung	NSCLC	ROS1	Crizotinib	II	NCT02183870
		BRAF	Dabrafenib, Trametinib	II	NCT01336634
Skin	Melanoma	BRAF	Trametinib, Binimetinib	II	NCT02196181

Mitochondria are well known to play a fundamental role in various physiological aspects of cells. Besides being the major source of ATP generation, they are also involved in numerous metabolic reactions and play a pivotal role in apoptosis. Therefore, it is not surprising that mitochondrial dysfunction has been associated with a wide range of human diseases including cancer. Nevertheless, specific mutations within the mitochondrial genome might provide significant and important biomarkers in the detection of cancer, cancer classification and prediction of cancer recurrence. MtDNA mutations could also be used as efficient markers in personalised readjustment of chemotherapy, since the currently accepted markers for clinical use (e.g. nodal status, size of tumour and histological grade) are unable to adequately indicate patients' outcome and/or assess their risk levels of recurrence. Therefore, correlations between mitochondrial genetic abnormalities and clinicopathological classification of the tumours should be further established (reviewed in Ref. [66]).

Despite its strong side effects and high incidence of resistance, conventional chemotherapy is still widely used in clinical practice. Therefore, developing novel pharmacological approaches and targets in the treatment of cancer becomes a high priority in chemotherapy to overcome its existing issues.

Currently, increased information obtained at the level of mitochondria aims to broaden the knowledge of cisplatin resistance and optimistically lead to the identification of predicative biomarkers that might be utilised as an early indicator of cisplatin therapy response. Once the specific mechanisms associated with cisplatin activity have been elucidated, new regimen could be developed for a synergic combination with cisplatin (reviewed in Ref. [17]).

1.8 Project significance, hypotheses, aims and objectives

One of the biggest challenges in treating cancer is to avoid drug resistance and minimise the side effects of chemotherapy by delivering the minimal dosage of drugs required to achieve an adequate cancer cell death. Although the mitochondrial genome mutation spectra are highly variable between different cancer types, impact of mtDNA mutations on the diverse mitochondrial activities and cellular behaviours including response to anticancer treatment is not well investigated. The results of this PhD project provide a better understanding as to how we can utilise intracellular ROS and mitochondrial genetic abnormalities as novel biomarkers to predict drug efficacy.

Hypothesis

ROS-mediating agents that target mitochondria can enhance therapeutic efficacy and intracellular ROS level as well as certain mitochondrial genetic abnormalities (mtDNA mutation and mtDNAcn change) are effective biomarkers to predict drug sensitivity in cancer cells.

Aims

1. Investigate the impact of intracellular ROS on drug response and the underlying molecular mechanisms.
2. Investigate the link between mitochondrial genetic abnormalities and intracellular ROS level.
3. Evaluate ROS-mediating agents as potential synergistic anti-cancer drugs in combination with conventional chemotherapy.

Objectives

1. Measure the baseline intracellular ROS and mitochondrial superoxide levels in a number of cancer and non-cancerous cell lines
2. Measure the cytotoxicity effect of the conventional chemotherapy (cisplatin, CDDP) and mitochondria-targeting compound (dequalinium chloride hydrate, DQA) on the cell lines
3. Measure the relative mitochondrial DNA (mtDNA) copy number in the cell lines
4. Identify mutations in the whole mtDNA genome in the cell lines
5. Predict functional mutations within the mtDNA-encoded OXPHOS subunits by 3D protein modelling
6. Evaluate mitochondrial genetic alternations as biomarkers to predict drug response

Chapter 2

Materials and Methods

2.1 Cell culture and drug treatment

2.1.1 Human cell lines

The human cell lines used in this study were obtained from the departmental cell bank at the University of Portsmouth; five cancer cell lines including Ishikawa/endometrium, MDA-MB-231/breast, Caco-2/colon, PC-3/prostate, Caki-2/kidney and two non-cancerous cell lines including PNT-2/prostate and HEK-293/kidney were enrolled in the study. All cell lines were originally purchased from the European Collection of Authenticated Cell Cultures (Ishikawa, MDA-MB-231, Caco-2, PNT-2 and Caki-2) or the American Type Culture Collection (PC-3 and HEK-293). All cell lines were authenticated using PowerPlex 16 HS System (Promega, Southampton, UK) for short tandem repeat (STR) profiling and screened for mycoplasma contamination using the PCR Mycoplasma Test Kit (PromoCell, Heidelberg, Germany), over the period of the investigation.

2.1.2 Maintenance of cell lines

The Caco-2, MDA-MB-231 and HEK-293 cells were grown in DMEM (Gibco, Fisher Scientific, Loughborough, UK) supplemented with 10% fetal bovine serum (FBS, Merck, Dorset, UK). The Ishikawa cells were grown in DMEM supplemented with 5% FBS. Caki-2 cells were grown in McCoy's 5A (Gibco) supplemented with 10% fetal bovine serum. The PC-3 and PNT-2 cells were grown in a mixture (1:1) of RPMI 1640 and Ham's F-12 (Gibco) supplemented with 10% FBS. Culture media are summarised in Table 2.1. All media contained 1% Amphotericin B/Penicillin/Streptomycin (Fisher Scientific).

Table 2.1. Cell lines and their culture media employed in the study.

Cell line	Origin	Culture media
Ishikawa	Endometrium	DMEM + FBS 5%
MDA-MB-231	Breast	DMEM + FBS 10%
Caco-2	Colon	DMEM + FBS 10%
Caki-2	Kidney	McCoy's 5A + FBS 10%
HEK-293	Kidney	DMEM + FBS 10%
PC-3	Prostate	RPMI 45% + HAM'S F12 45% + FBS 10%
PNT-2	Prostate	RPMI 45% + HAM'S F12 45% + FBS 10%

All cells were grown in humidified incubator at 37°C under 5% CO_2, and culture medium was changed twice per week. At 90% confluence, the culture medium was removed and the cells were washed with 5 mL of phosphate buffered saline (PBS, Gibco). The cells were detached following the incubation with 3 mL of the TrypLE Express solution (Gibco) for 5 min at 37°C. The trypsin enzymatic reaction was terminated by adding 7 mL of complete medium to the cell culture flask, then the cell solution was collected in a centrifuge tube and centrifuged at 1,150 rpm for 5 min. The supernatant was decanted and the cell pellet was re-suspended in 8 mL of fresh complete medium to be used for all the downstream procedures.

2.1.3 Cell counting

Cells were counted using an automated cell counting device, Moxi™ Z (ORFLO Technologies, Idaho, USA). For each counting, 75 µL of cell suspension was loaded into the designated cassette and the cell concentration (cell number/mL) was automatically calculated and displayed on the screen of the device.

2.1.4 Population doubling time

Population doubling time (PDT) was measured for all cell lines by plating an equal number of cells (50,000 cells/well) and then counting them using the automated cell counter at 24, 48 and 72 hours post seeding. The values of 3 separate experiments were plotted and the average population doubling time for each cell line was calculated using the Graphpad Prism version 8.0 software.

2.1.5 Drug treatment

Stock solutions of cisplatin (CDDP, Merck) and dequalinium chloride hydrate (DQA, Merck) were prepared at 100 mM in DMSO and 2 mM in distilled water respectively. Both drugs were added to the cells (separately or jointly) at various working concentrations, and the cells were incubated for specific durations according to the nature of the experiments (described in the relevant subsections below). The IC50s (IC50: the half maximal inhibitory concentration) of CDDP and DQA were determined following the drug treatment for 24 hours. Concentrations of CDDP and DQA used to determine the IC50 of each drug and the new IC50 of CDDP in combination with DQA at half of its IC50, are summarised in Table 2.2.

After the CDDP and DQA IC50s were determined, cells were treated with either CDDP IC50, DQA IC50 or combined treatment of CDDP and DQA at half of their IC50 concentrations for different incubation times up to 24 hours in all subsequent experiments.

Table 2.2. Concentrations of CDDP and DQA used to determine IC50s.

CDDP (μM)	DQA (μM)	CDDP (μM) + ½ DQA IC50 (μM)*
5	1	5 + ½ DQA IC50
10	5	10 + ½ DQA IC50
50	10	50 + ½ DQA IC50
100	25	100 + ½ DQA IC50
250	50	250 + ½ DQA IC50
500	75	500 + ½ DQA IC50
750	100	750 + ½ DQA IC50
1000	200	1000 + ½ DQA IC50

* The ½ DQA IC50 was 89.6 μM for Caco-2 and 7.2 μM for Ishikawa respectively.

N-Acetyl-L-cysteine (NAC, Merck), a powerful antioxidant, was dissolved in distilled water at the concentration of 100 mM shortly before each experiment and the pH was adjusted to 7.4 using sodium hydroxide before diluting the solution to the working concentration (10 mM) with complete cell culture medium. Cells were pre-incubated with NAC (10 mM) for 1 hour before the CDDP and DQA treatments were applied. All experiments related to NAC followed the same procedure as described in the sections below.

2.2 Functional assays

2.2.1 Cell viability assay (MTS assay)

Cell viability was measured colorimetrically using the [3-(4,5-dimethylthiazol-2-yl)-5-(3-carboxymethoxyphenyl)-2-(4-sulfophenyl)-2H-tetrazolium] (MTS) solution (CellTiter 96 Aqueous) (Promega) in the presence of phenazine methosulfate (PMS, Merck). The MTS assay assesses the metabolic activity by detecting the mitochondrial dehydrogenase activity (Figure 2.1). Viable cells are able to reduce tetrazolium salt to a blue formazan whereas dead cells are unable to. The generated signal is proportional to the number of viable cells (reviewed in Ref. [287]).

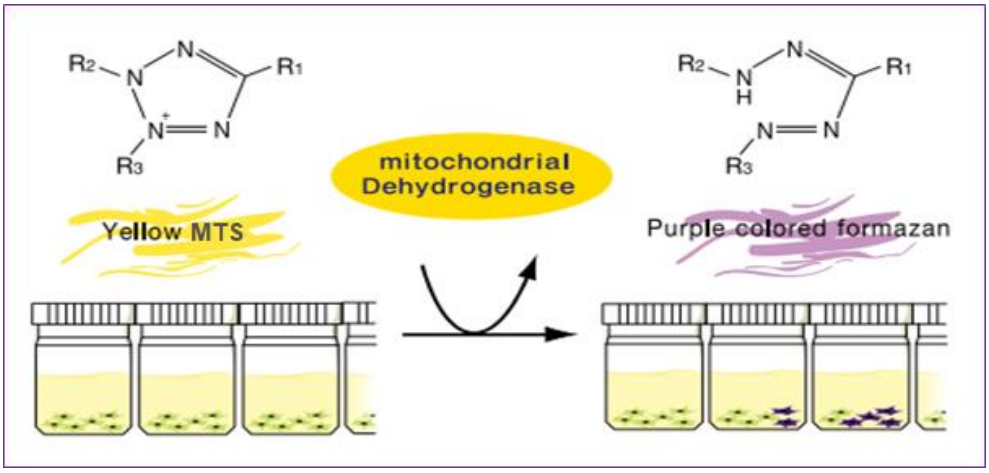

Figure 2.1. The MTS assay is based on the conversion of yellow MTS tetrazolium compound into blue formazan by living cells, which determines mitochondrial activity and reflects the number of viable cells present [288].

For the MTS assay, 90 µL of cell suspension containing 10,000 cells was added in each well of the 96-well plate (VWR, Pennsylvania, USA), and the plate was incubated for 24 hours at 37°C with 5% CO_2 in a fully humid environment. Cells were treated with 10 µL of the 10 × drug (working solution) for the desired amount of time (24 hours to determine the IC50 of the drugs and 1, 3, 5 and 24 hours for time course experiments). At the end of the experiment, the medium was replaced with 100 µL of fresh medium containing MTS and PMS (final concentrations: 0.4 µM and 0.3 nM respectively), and the 96-well plate was incubated for 90-180 minutes at 37°C with 5% CO_2 according to the cell type. Absorbance was measured using the microplate reader (Multiskan® GO, ThermoFisher Scientific, Loughborough, UK) at 490 nm. Viability changes upon treatments were determined as percentage of untreated wells after background subtraction.

IC50 was calculated as the concentration of the drug that caused a 50% loss of metabolic activity using the Graphpad Prism version 8.0 software.

2.2.1.1 Combination Index for synergism assessment

Analysis of drug synergy was performed by calculating the Combination Index (CI) to assess how drug combination might have influenced the therapeutic efficacy (CI > 1 – Antagonistic; CI = 1 – Additive; CI < 1 – Synergistic) at different combinations according to the median-effect principle of the Chou and Talalay method, using the CompuSyn software 1.4 [289].

2.2.2 Cell viability/cytotoxicity assay (ApoTox-Glo™ Triplex)

The ApoTox-Glo™ Triplex Assay Kit (Promega) was used to assess the viability and cytotoxicity events by measuring two protease activities; one is a marker for cell viability and the other is a marker for cytotoxicity. The activity of live-cell protease is restricted to the intact viable cells and measured using a cell permeant fluorogenic substrate (GF-AFC/glycylphenylalanyl-aminofluoroumarin). The substrate enters intact cells where it is cleaved by the activity of live-cell protease to release AFC and generates a fluorescent signal proportional to the number of living cells. This live-cell protease becomes inactive upon loss of cell membrane integrity and leakage into the surrounding culture medium. A second fluorogenic yet cell impermeant substrate (bis-AAF-R110/bis-alanyl-alanyl phenylalanyl-rhodamine 110) is used to measure the activity of dead-cell protease which is released from cells that have lost membrane integrity (Figure 2.2). Because bis-AAF-R110 is not cell-permeant, subsequently no signal from this substrate is generated by intact, viable cells. The live- and dead-cell proteases produce different products, AFC and R110, which have different excitation and emission spectra, allowing them to be detected simultaneously [290].

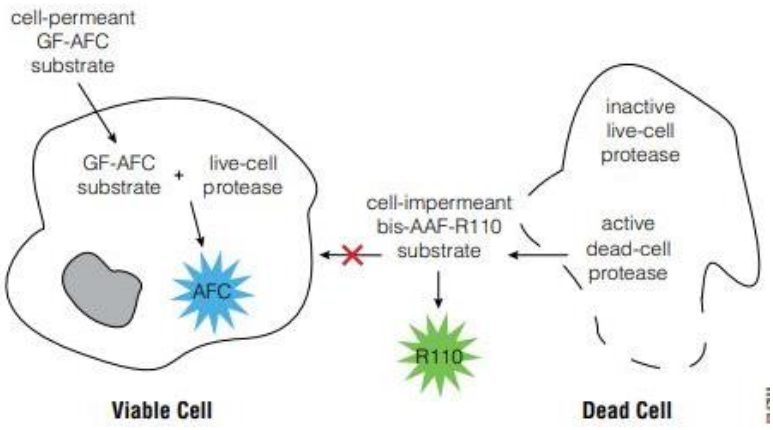

Figure 2.2. The biology of the viability/cytotoxicity assay (diagram taken from the manufacturer's protocol: https://www.promega.co.uk/products/cell-health-assays/apoptosis-assays/apotox_glo-triplex-assay/?catNum=G6320#protocols).

According to the manufacturer's protocol, 90 µL of cell suspension containing 10,000 cells was added in each well of the 96-well black-wall plate (Corning, NY, USA), and the plate was incubated overnight. Cells were treated with 10 µL of the 10 × drug (working solution) for 24 hours. At the end of the experiment, the freshly prepared viability/cytotoxicity reagent (a mixture of GF-AFC and bis-AAF-R110 in the assay buffer) (20 µL) was added to each well, and the plate was shaken at 400 rpm for 30 seconds and incubated for 60 minutes at 37°C. Fluorescence was then measured at two wavelength sets using the microplate reader (POLARstar Omega, BMG LABTECH Ltd., Ortenberg, Germany): 380 nm (excitation) / 510 nm (emission) for viability and 485 nm (excitation) / 520 nm (emission) for cytotoxicity. Viability and cytotoxicity changes upon treatments were determined as percentage of untreated wells after background subtraction.

2.2.3 Intracellular ROS assays

Baseline intracellular ROS levels were measured in a 96-well-plate format using the Cellular Reactive Oxygen Species Detection Assay Kit (Abcam, Cambridge, UK) based on the fluorogenic dye 2',7'-dichlorofluorescin (DCFDA). After diffusion into the cells, DCFDA is deacetylated by cellular esterases to a non-fluorescent compound which is later oxidised by ROS into dichlorofluorescein (DCF), a highly fluorescent compound which can be detected by fluorescence spectroscopy [291].

According to the manufacturer's protocol (https://www.abcam.com/dcfda--h2dcfda-cellular-ros-assay-kit-ab113851-protocols.html#top-500), 25,000 cells were seeded in each well of the 96-well black-wall plate overnight prior to the experiments. After 24 hours, the cells were washed with 150 µL of HBSS (Gibco), then 100 µL of the staining buffer (20 µM of DCFDA in HBSS) was added to each well, and the plate was incubated for 40 minutes at 37 °C. The cells were then washed twice with 150 µL of HBSS, and 100 µL of HBSS was added to each well following the second wash. Fluorescence was measured using the microplate reader (POLARstar Omega) at 485 nm (excitation) and 535 nm (emission).

For determining intracellular ROS levels upon drug treatments, the staining buffer was added for 40 min at 37 °C. The cells were then washed twice with 150 µL of HBSS and treated with 100 µL of phenol red-free media containing the therapeutic compound(s) of interest.

The plate was then incubated for 1, 3, 5, 7, 16, 20 and 24 hours before fluorescence was measured. ROS changes upon treatments were determined as percentage of untreated wells after background subtraction.

The tert-Butyl hydrogen peroxide (TBHP) solution (provided in the Kit) was used as a positive control in each experiment. Four hours prior to the completion of the drug treatment, fresh TBHP (500 µM) was prepared in the phenol red-free media and added to the designated positive control wells to achieve the final concentration of 50 µM.

2.2.4 Mitochondrial superoxide assay

2.2.4.1 Plate reader based assay

To measure mitochondrial superoxide, the same procedure was conducted as described above using a mitochondrial ROS-specific dye, MitoSOX™ (Life Technologies, Fisher Scientific), instead of DCFDA. MitoSOX™ permeates live cells where it selectively targets mitochondria. It is rapidly oxidised by superoxide but not by other reactive oxygen species. The cells were incubated with 5 µM of MitoSOX in HBSS for 30 minutes. Fluorescence was measured using the same microplate reader at 510 nm (excitation) and 580 nm (emission). Mitochondrial superoxide changes upon treatments were determined as percentage of untreated wells after background subtraction.

2.2.4.2 Fluorescence microscopy based assay

The presence of mitochondrial superoxide was visualised with a confocal laser-scanning microscope (LSM710; Zeiss, Oberkochen, Germany) using a Plan Apochromatic 20 × DIC objective (NA0.8) (pixel size 0.42 µm). For the sample preparation, 15,000 cells were seeded in each well of an 8-well chamber slide (Nunc™ Lab-Tek™ II Chamber Slide™, ThermoFisher Scientific) overnight prior to the experiments. In the following day, the cells were washed with 300 µL of HBSS, then 200 µL of the staining buffer (5 µM of MitoSOX™ in HBSS) was added to each well, and the slide was incubated for 30 minutes at 37 °C. The cells were then washed twice with 300 µL of HBSS and incubated with the drug treatments for 6 hours before imaging. All images presented represent a single optical section. These images were acquired using sequential acquisition of the different channels to avoid cross-talk between fluorophores, with the pinholes adjusted to one airy unit. Images were processed with the software Zen2009 Light Edition and exported into Adobe Photoshop. Only brightness and contrast were adjusted for the whole frame, and no part of a frame was enhanced or modified in any way.

2.2.5 Mitochondria quantification by fluorescent staining

The level of mitochondria was measured in a 96-well plate format using MitoTracker™ Red CMXRos (Invitrogen, ThermoFisher Scientific). MitoTracker™ is a red fluorescent dye that passively diffuses across the plasma membrane and accumulates in active mitochondria.

According to the manufacturer's protocol (https://www.thermofisher.com/order/catalog/product/M7512#/M7512), 25,000 cells were seeded in each well of the 96-well black-wall plate overnight prior to the experiments. In the following day, the cells were washed with 150 µL of HBSS, then 100 µL of the staining buffer (0.1 µM of MitoTracker™ in HBSS) was added to each well, and the plate was incubated for 40 minutes at 37 °C. The cells were then washed twice with 150 µL of HBSS, and 100 µL of HBSS was added to each well following the second wash. Fluorescence was measured using the microplate reader (POLARstar Omega) at 584 nm (excitation) and 620 nm (emission).

2.2.6 Mitochondrial transmembrane potential assay

MMP was measured by staining the cells with the JC-10 fluorescent dye (Enzo Life Sciences, Exeter, UK). In healthy cells, JC-10 concentrates in the mitochondrial matrix where it forms red fluorescent aggregates. However, in apoptotic and necrotic cells, JC-10 diffuses out of mitochondria where it changes to monomeric form and stains cells in green fluorescence. The ratio of red to green fluorescence intensity depends on the transmembrane potential and can reflect the maintenance of cellular health and viability. For example, a decrease in the red/green ratio indicates reduced transmembrane potential as seen in apoptotic and necrotic cells when mitochondrial membrane disintegrates.

Based on the manufacturer's protocol (https://www.enzolifesciences.com/ENZ-52305/jc-10-ultra-pure/), 90 µL of the cell suspension containing 25,000 cells was added in each well of the 96-well black-wall plate, and the plate was incubated overnight at 37°C with 5% CO_2. In the next day, the cells were treated with 10 µL of the 10 × drug solution for 1, 3, 5 and 24 hours. At the end of the experiment, the cells were washed with 150 µL of HBSS, then 100 µL of the staining buffer (20 µM of JC-10 in HBSS) was added to each well and the plate was incubated for 40 min at 37°C. The cells were then washed twice with 150 µL of HBSS and 100 µL of HBSS was added to each well following the second wash.

Red and green fluorescent signals were measured using the microplate reader (POLARstar Omega) at 540 nm (excitation) / 590 nm (emission) and 490 nm (excitation) / 525 nm (emission) respectively. MMP was calculated as ratio of red/green, and MMP changes upon treatments were determined as percentage of untreated wells.

2.2.7 Caspase activity assay

Caspase-3/7 activity was measured using the Caspase-Glo® 3/7 Reagent (a mixture of the Caspase-Glo 3/7 lysis buffer and a luminogenic substrate) from the ApoTox-Glo™ Triplex Assay Kit (Promega). The Caspase-Glo® 3/7 Reagent causes cell lysis, followed by caspase cleavage of the substrate and generation of a luminescent signal. Luminescence is proportional to the amount of caspase activity present.

According to the manufacturer's protocol, 90 µL of cell suspension containing 10,000 cells was added in each well of the 96-well black-wall plate, and the plate was incubated at 37°C overnight. The next day, the cells were treated with 10 µL of the 10 × drug solution for 24 hours. At the end of the experiment, the freshly prepared Caspase-Glo 3/7® Reagent (100 µL) was added to each well, and the plate was shaked at 400 rpm for 30 seconds and incubated for 60 minutes at room temperature. Luminescence was then measured using the microplate reader (POLARstar Omega). Caspase activities upon treatments were determined as percentage of untreated wells after background subtraction.

2.2.8 Apoptotic or necrotic cell death evaluation

Apoptosis was also analysed by studying the translocation of the membrane phosphatidylserine (PS) from the inner face of the plasma membrane to the cell surface. For this purpose, cells were double stained with fluorescent conjugate of Annexin V (Annexin V-FITC) and propidium iodide (PI) using the Annexin V-FITC Apoptosis Staining / Detection Kit (Abcam).

Live cells correspond to Annexin V-FITC negative and PI negative (A^-/PI^-). Cells with intact cell membrane integrity do not uptake PI which is impermeable to such cells, and therefore cells stained with Annexin V-FITC only (A^+/PI^-) are considered to be in an early stage of apoptosis. In late apoptosis or necrosis secondary to apoptosis, cell membrane loses its integrity hence cells will be stained with both Annexin V-FITC and PI (A^+/PI^+). Cells with PI staining alone (A^-/PI^+) are considered necrotic.

According to the manufacturer's protocol (https://www.abcam.com/annexin-v-fitc-apoptosis-staining--detection-kit-ab14085.html), 300,000 cells were plated in each well of a standard 6-well cell culture plate (VWR). The plate was incubated overnight and then exposed to drug treatments for 24 hours. At the end of the experiment, the cells were washed with PBS, trypsinised, collected by centrifugation and re-suspended in 500 µL of the binding buffer provided in the Kit. The cells were double stained by adding 5 µL of Annexin V-FITC and 5 µL of propidium iodide and incubated at room temperature for 10 minutes in the dark. The samples were then analysed by flow cytometry using BD FACSCalibur™ (BD Biosciences, New Jersey, USA) according to the standard procedure (PI: 493 nm (excitation) / 636 nm (emission), Annexin V-FITC: 488 nm (excitation) / 530 nm (emission)), and the generated data were analysed using the FlowJo-V10 software.

2.2.9 Lactate assay

Baseline lactate concentrations were measured in a 96-well-plate format using the Lactate Colorimetric Assay Kit (Abcam) where lactate is oxidised by LDH to generate pyruvate that interacts with the water-soluble tetrazolium salts probe (WST) and produces a colour change.

According to the manufacturer's protocol (https://www.abcam.com/l-lactate-assay-kit-colorimetric-ab65331-protocols.html#top-0), 2×10^6 cells were harvested, washed with cold PBS (4°C) and re-suspended in 200 µL of the lactate assay buffer. The tubes containing the cell suspension were vortexed on the highest setting for 15 seconds to fully re-suspend the cells and then centrifuged at 14,000 × *g* for 5 minutes at 4°C. The soluble supernatants were transferred into new Eppendorf tubes and kept on ice. Endogenous LDH was removed from the samples to avoid the degradation of lactate by using the Deproteinizing Sample Preparation Kit – TCA (Abcam). Basically, 15 µL of ice-cold trichloroacetic acid (TCA) was added to the sample and left on ice for 15 minutes. The tubes were later vortexed at 12,000 × *g* for 5 minutes at 4°C and the soluble supernatants were transferred into new Eppendorf tubes and kept on ice. Then 10 µL of ice-cold Neutralization Solution (provided in the Kit) was added to neutralise excess trichloroacetic acid in the samples, and the tubes were left on ice for 5 min.

To determine the lactate concentrations of the samples, a standard curve was prepared by measuring a series of diluted Lactate Standard solutions at 20, 40, 60, 80 and 100 µM. The test samples were diluted 1:1 in the provided assay buffer, and 50 µL of each test sample as well as each of the standard solutions was loaded in the same 96-well plate (all samples were loaded in duplicate). Then 50 µL of the reaction mix (46:2:2, Assay buffer: lactate substrate: lactate enzyme) was added to the standard and the test samples. The plate was incubated at room temperature for 30 minutes before absorbance was measured using the microplate reader (Multiskan® GO) at 450 nm. The absorbance readings of the Lactate Standards were utilised to generate a standard curve to determine the lactate concentration of each test sample.

2.3 Molecular biology techniques

2.3.1 DNA extraction

Total DNA was isolated from 300,000 cells (either untreated or treated for 24 hours) using the QIAmp DNA Mini Kit (QIAGEN, Hilden, Germany) according to the manufacturer's protocol (https://www.qiagen.com/gb/resources/resourcedetail?id=566f1cb1-4ffe-4225-a6de-6bd3261dc920&lang=en) . In the last step, DNA was eluted with 100 µL of the AE buffer. The purity and concentration of isolated DNA were assessed using an automated spectrophotometer (ND-1000; NanoDrop Technologies, Wilmington, DE, USA). Based on the spectrophotometry results, DNA samples were diluted accordingly in order to achieve an equal concentration of all the DNA samples used in the SYBR Green qPCR experiments (i.e. 14 ng/µL; Table 2.3).

2.3.2 Measurement of mtDNA copy number by SYBR Green real-time PCR

Relative quantification of mtDNAcn was performed using the QuantiTect SYBR Green PCR Kit (QIAGEN), and the qPCR was run on the LightCycler® 96 System (Roche, Basel, Switzerland). According to the manufacturer's protocol (https://www.qiagen.com/dk/shop/new-products/quantitect-sybr-green-pcr-kits/), two 70-µL reaction mixes were prepared for each test sample, one containing D-loop primers and the other *β*-actin primers (Table 2.3), then 20 µL of each reaction mix was added to the 96-well qPCR plate in triplicate for each test sample.

Table 2.3. Reaction setup for SYBR Green real-time PCR.

Component	Volume (µL)	Volume (µL)
Nuclease-free water	19.4	19.4
2 × QuantiTect SYBR Green PCR Master Mix	35	35
Primers set 1 (D-loop primers, 5 µM)	5.6	-
Primers set 2 (*β*-actin primers, 5 µM)	-	5.6
DNA (14 ng/µL)	10	10
Total volume per reaction	**70 µL**	**70 µL**

The amplification procedure entailed 95°C for 10 seconds, followed by 30 cycles of 95°C for 30 seconds, 58°C for 30 seconds and 72°C for 90 seconds. Two sets of primers were used based on a previous study [292], one to amplify the D-loop region (1232 bp) within the mitochondrial genome and the other to amplify the housekeeping gene, *β*-actin (318 bp) (Table 2.4).

Table 2.4. SYBR Green qPCR primers to amplify the D-loop and *β*-actin fragments [292].

Primers set 1	D-loop (forward)	5′ CTCCACCATTAGCACCCAAAG 3′
	D-loop (reverse)	5′ GTGATGTGAGCCCGTCTAAAC 3′
Primers set 2	*β*-actin (forward)	5′ ATCATGTTTGAGACCTTCAACA 3′
	β-actin (reverse)	5′ CATCTCTTGCTCGAAGTCCA 3′

The relative quantity of mtDNA content in each sample was calculated by normalising the copy number of mtDNA against that of *β*-actin. The data from qPCR were analysed based on the $2^{-\Delta\Delta CT}$ method (CT: cycle threshold). ΔCT was first calculated as the average D-loop CT value deducted by the average *β*-actin CT value of the same sample. The relative mtDNAcn fold change in the drug-treated samples was calculated by normalising against the untreated samples in which ΔΔCT was the ΔCT value of the treated sample deducted by the ΔCT value of the untreated sample. Three independent experiments were carried out and all the samples were run in triplicates in each experiment.

2.3.3 RNA extraction

Total RNA was isolated from 300,000 cells (either untreated or treated for 24 hours) using the RNeasy Mini Kit (QIAGEN) according to the manufacturer's protocol (https://www.qiagen.com/gb/resources/resourcedetail?id=0e32fbb1-c307-4603-ac81-a5e98490ed23&lang=en). In the last step, RNA was eluted with 40 μL of RNA–free sterile water. The purity and concentration of isolated RNA were assessed using an automated spectrophotometer (ND-1000; NanoDrop Technologies). Based on the spectrophotometry results, RNA samples were diluted accordingly in order to provide an equal concentration of all the RNA samples in the complementary DNA synthesis experiments (i.e. 0.1 μg/μL; Table 2.5).

2.3.4 Synthesis of complementary DNA

Complementary DNA (cDNA) was synthesised using the High-Capacity cDNA Reverse Transcription Kit (Applied Biosystems, California, USA). Based on the manufacturer's protocol (https://www.thermofisher.com/order/catalog/product/4368813#/4368813), a 20-µL reaction mix was prepared for each RNA sample (Table 2.5).

Table 2.5. Reaction setup for cDNA synthesis.

Component	Volume (µL)
10 × RT Buffer	2
25 × dNTP Mix (100 mM)	0.8
10 × RT Random Primers	2
MultiScribe™ Reverse Transcriptase	1
Nuclease-free water	4.2
RNA sample (0.1 µg/µL)	10
Total volume per reaction	**20 µL**

The cDNA synthesis reaction was carried out on the T100™ Thermal Cycler (Bio-Rad, Watford, UK). Conditions for the thermal cycling were: 25°C for 10 min, 37°C for 120 min, 85°C for 5 min then 4°C infinitely. Synthesised cDNA samples were used directly in TaqMan qPCR assays or stored at -20°C for later use.

2.3.5 TaqMan real-time quantitative polymerase chain reaction

TaqMan real-time qPCR (RT-qPCR) was performed using the FastStart Essential DNA Probes Master reagents (Roche) in 96-well plates, and the assays were run on the LightCycler® 96 System (Roche). The pre-designed primer/probe mixes for all the target genes (i.e. genes of interest) were purchased from Integrated DNA Technologies (IDT, Leuven, Belgium), whereas the primer/probe mix for the endogenous control gene (i.e. housekeeping gene) was obtained from Life Technologies (Table 2.6).

The primer/probe mixes of the target and housekeeping genes were labelled with FAM and VIC fluorophores respectively, which enabled a duplex reaction for simultaneous determination of the expression levels of both genes.

Table 2.6. The pre-designed primer/probe mixes for all the target genes.

Gene	Ref Sequence	Source
SOD1	NM_000454(1)	IDT
SOD2	NM_001024466(3)	IDT
CAT	NM_001752(1)	IDT
GPX1	NM_000581(2)	IDT
Nrf2	NM_006164(1)	IDT
NOX1	NM_001271815(3)	IDT
NOX2	NM_000397(1)	IDT
NOX3	NM_015718(1)	IDT
NOX4	NM_016931	IDT
NOX5	NM_001184779(5)	IDT
DUOX1	NM_175940(1)	IDT
OPA1	NM_130835(2)	IDT
PINK1	NM_032409(1)	IDT
BCL-XL	NM_001191(2)	IDT
BAX	NM_138764(1)	IDT
APAF1	NM_181868(5)	IDT
Cyt C	NM_018947(1)	IDT
MDR1	NM_000927(1)	IDT
OGG1	NM_002542(8)	IDT
RRM2B	NM_015713(1)	IDT
ENDOG	NM_004435(1)	IDT
PDK1	NM_002610(1)	IDT
GAPDH	NM_001686.3	Life Technologies

According to the manufacturer's protocol (https://lifescience.roche.com/en_gb/products/faststart-essential-dna-probes-master.html#documents), a 20-µL reaction mix was prepared for each TaqMan qPCR reaction (Table 2.7), then 10 µL of the reaction mix was added to the 96-well qPCR plate in duplicate for each test sample.

Table 2.7. Reaction setup for TaqMan qPCR.

Component	Volume (µL)
Nuclease-free water	3
10 × Primer-probe mix (gene of interest)	1
10 × Primer-probe mix (housekeeping gene)	1
2 × Master Mix	10
cDNA sample	5
Total per reaction	**20 µL**

The amplification procedure entailed a pre-incubation step at 95°C for 10 minutes and 45 cycles of 95 °C for 10 seconds followed by 60 °C for 30 seconds. For each TaqMan qPCR reaction, GAPDH was utilised as the endogenous control gene. Three independent experiments were carried out and all the samples were run in duplicates in each experiment. The TaqMan qPCR data were analysed based on the same $2^{-\Delta\Delta CT}$ principle as described above in Section 2.3.2.

2.3.6 Western blotting

2.3.6.1 Cell lysis and protein extraction

Based on the standard protocol, 300,000 cells (either untreated or treated for 24 hours) were washed twice with ice-cold PBS and lysed in ice-cold RIPA lysis buffer (pH 8.0) (150 mM NaCl, 1% Triton X-100, 0.5% sodium deoxycholate, 0.1% sodium dodecyl sulfate/SDS and 50 mM Tris) supplemented with the Protease Inhibitor Cocktail solution (Fisher scientific). The cells were incubated at 4°C on a shaker for 60 minutes then the cell lysates were collected and transferred into labelled tubes. The tubes were vortexed on the highest setting for 3 minutes and incubated on ice for 40 minutes. Another round of vortex was carried out and the lysates were centrifuged at 14,000 × *g* for 10 minutes at 4°C. The soluble supernatants which contained the total cellular proteins were transferred into new Eppendorf tubes and stored at -20°C until required.

To study the release of cytochrome *c* from mitochondria, cytoplasmic protein extract was prepared using the NE-PER™ Nuclear and Cytoplasmic Extraction Reagents (Fisher Scientific). According to the manufacturer's protocols (https://www.thermofisher.com/order/catalog/product/78833#/78833), 300,000 cells (either untreated or treated for 24 hours) were harvested and transferred to labelled tubes, and the pellets were washed twice with ice-cold PBS. The cells were then lysed using 200 µL of ice-cold Cytoplasmic Extraction Reagent I (CER I) supplemented with the Protease Inhibitor Cocktail solution (Fisher scientific). The tubes were vortexed on the highest setting for 15 seconds to fully re-suspend the cells and incubated on ice for 10 minutes. Then 11 µL of Cytoplasmic Extraction Reagent II (CER II) was added to the tubes that were later vortexed for 15 seconds on the highest setting and incubated on ice for 1 minute. Another round of vortex was carried out and the lysates were centrifuged at 14,000 × *g* for 10 minutes at 4°C. The soluble supernatants that contained the cytoplasmic proteins were transferred into new Eppendorf tubes and stored at -20°C until required.

2.3.6.2 Protein quantification

Protein concentrations were determined using the BCA (bicinchoninic acid) protein assay. Bovine serum albumin (BSA) (1 mg/mL stock; Merck) was diluted with distilled water to achieve protein standard concentrations of 10, 20, 30, 40 and 50 µg/mL. Later, 25 µl of each standard solution was loaded into a 96-well plate in duplicate.

For each protein sample, the whole cell lysate was diluted 1:10 with distilled water and 25 µl of the diluted sample was loaded into the same 96-well plate in duplicate. Then 200 µl of the BCA working reagent {50:1, reagent A (bicinchoninic acid solution): reagent B (copper sulfate solution)} was added to the standard and sample wells. The plate was incubated at 37°C for 30 minutes before absorbance was measured using the microplate reader (Multiskan® GO) at 562 nm. The absorbance readings of the BSA standards were utilised to generate a standard curve to determine the protein concentration of each test sample.

Based on the BCA assay results, protein samples were diluted accordingly in order to result in an equal concentration for all samples.

2.3.6.3 Sodium dodecyl sulfate polyacrylamide gel electrophoresis

A 10% SDS-PAGE gel solution was prepared according to the established protocol (Table 2.8) and poured into the designated glass plates. Once the gel was set, the comb was removed and the electrophoresis reservoir was filled with 1 × running buffer (pH 8.3) (25 mM Tris base, 190 mM glycine and 0.1% SDS). Each cell lysate was mixed with 4 × loading buffer [0.3 M Tris-HCl (pH 6.8), 50% glycerol, 10% SDS and 0.05% bromophenol blue] supplemented with 5 mM Dithiothreitol (DTT), and the samples were heated for 5 minutes at 95°C. Then 25 µL of the heated sample was loaded into each lane; 10 µL of PageRuler™ Plus Prestained 10-250 kDa Protein Ladder (Fisher Scientific) was loaded on the same gel as size standards. The samples were run on 100 volts through the stacking gel then the voltage was increased to 200 V through the resolving gel.

All chemicals in the running and loading buffers were purchased from Fisher scientific.

Table 2.8. Western blot gels preparation.

Volume (mL) required for				**Source**
Running gel (10%)		**Stacking gel (4%)**		
Protogel	3.3	Protogel	1.2	Fisher Scientific
2M Tris PH 8.8	2	0.5M Tris PH 6	1.4	Fisher Scientific
60% Sucrose	2	60% Sucrose	2	Fisher Scientific
20% SDS	0.025	20% SDS	0.025	Fisher Scientific
TEMED	0.005	TEMED	0.01	Merck
Distilled water	2.64	Distilled water	5.33	In house
10% APS	0.03	10% APS	0.03	Fisher Scientific
Total volume	**10 mL**	**Total volume**	**10 mL**	

SDS: Sodium dodecyl sulfate. TEMED: Tetramethylethylenediamine; APS: Ammonium persulfate

2.3.6.4 Protein transfer

The separated proteins were transferred onto an activated polyvinylidene fluoride membrane (PVDF; Millipore, Nottingham, UK) using a wet transfer method. Prior to transferring, the membrane and the gel and the blotting paper pads were soaked with the transfer buffer (25 mM Tris base, 200 mM Glycine, 0.04% SDS and 0.005% Tween-20). Transfer occurred by applying 300 mA for 2.5 hours at 4°C. Following the transfer, non–specific protein binding was blocked by incubating the PVDF blots for 1 hour in 3% fat-free milk/TBST (tris-buffered saline and Tween 20) when blotting for total proteins and in 3% BSA/TBST when blotting for phospho–proteins. The membranes were incubated overnight at 4°C with the primary antibody diluted in appropriate blocking buffer (Table 2.9) then incubated with the corresponding secondary antibody (Table 2.10) for 2 hours at room temperature. Between each step, the membranes were washed three times with TBST buffer.

The immunoreactive proteins were detected by incubating the membrane with the Immobilon Forte Western HRP substrate (Millipore) for three minutes with no direct light and visualised with a high sensitivity CCD (charge-coupled device) camera imaging platform, i.e. the ChemiDoc™MP Gel Imaging System (Bio-Rad). The ImageJ software was used for the densitometric quantification of the western blot bands [293].

Table 2.9. List of primary antibodies used in western blotting.

Protein	Antibody Code	Species	Dilution	Source
SOD1	SC-101523	Mouse monoclonal	1:500	Santa Cruz, USA
SOD2	SC-130345	Mouse monoclonal	1:500	Santa Cruz
CAT	SC-271803	Mouse monoclonal	1:250	Santa Cruz
BCL-XL	MAB894	Rabbit monoclonal	1:500	R&D systems, USA
BAX	SC-20067	Mouse monoclonal	1:250	Santa Cruz
OGG1	SC-376935	Mouse monoclonal	1:250	Santa Cruz
ATR	SC-515173	Mouse monoclonal	1:500	Santa Cruz
pATR	D5K8W	Rabbit monoclonal	1:1000	Cell Signalling, USA
Chk1	SC-8408	Mouse monoclonal	1:500	Santa Cruz
pChk1	D12H3	Rabbit monoclonal	1:1000	Cell Signalling
Cytochrome *c*	MA5-11674	Mouse monoclonal	1:500	ThermoFisher
VDAC1	SC-390996	Mouse monoclonal	1:500	Santa Cruz
***β*-Actin**	MAB8929	Mouse monoclonal	1: 2000	R&D systems

Table 2.10. List of secondary antibodies used in western blotting.

Antibody	Dilution	Source
Anti-rabbit HRP	1:2000	Dako, Denmark
Anti-mouse HRP	1:5000	Dako

2.4 MtDNA mutation analysis

2.4.1 Polymerase chain reaction

To assess the mtDNA mutations of the cell lines enrolled in our study, sufficient mtDNA templates were required for the sequencing analysis. Therefore, seventeen primer pairs were designed using Primer-BLAST (https://www.ncbi.nlm.nih.gov/tools/primer-blast/index.cgi) to amplify the entire mitochondrial genome in overlapping fragments of ~ 1.1 kb (Table 2.11).

Table 2.11. List of the primers designed to amplify 17 overlapping mtDNA fragments.

Primer ID	Sequence	Length	Start	End	Size (bp)
F1	CCCTATTAACCACTCACGGG	20	17	36	1139
R1	CTGTGGCTCGTAGTGTTCTG	20	1155	1136	
F2	GATACCCCACTATGCTTAGCC	21	1079	1099	1114
R2	TTGGTGGCTGCTTTTAGGC	19	2192	2174	
F3	CTGGTGATAGCTGGTTGTCC	20	2006	2025	1131
R3	CTTGTCCTTTCGTACAGGGAG	21	3137	3117	
F4	GATCTGAGTTCAGACCGGAG	20	3063	3082	1103
R4	GTATGAGTTGGTCGTAGCGG	20	4165	4146	
F5	AACATATGACGCACTCTCCC	20	4041	4060	1108
R5	TCGTGGTGCTGGAGTTTAAG	20	5148	5129	
F6	ACCGTACAACCCTAACATAACC	22	5051	5072	1150
R6	GTTGTTTATGCGGGGAAACG	20	6200	6181	
F7	CCAGGCAACCTTCTAGGTAAC	21	6033	6053	1099
R7	CGTAGGTTTGGTCTAGGGTG	20	7131	7112	
F8	TGTAGCCCACTTCCACTATG	20	7022	7041	1109
R8	GTTTGGTTTAGACGTCCGGG	20	8130	8111	
F9	GTAGTACTCCCGATTGAAGCC	21	8009	8029	1153
R9	TAGGCTTGGATTAAGGCGAC	20	9161	9142	
F10	CATTACTGCAGGCCACCTAC	20	9015	9034	1136
R10	ATGTAGCCGTTGAGTTGTGG	20	10150	10131	
F11	ATAATCAACACCCTCCTAGCC	21	10080	10100	1070
R11	CAAGGTGGGGATAAGTGTGG	20	11149	11130	
F12	TCCAGTGAACCACTATCACG	20	11012	11031	1114
R12	CGGTAATGATGTCGGGGTTG	20	12125	12106	
F13	ACACCTATCCCCCATTCTCC	20	12076	12095	1072
R13	GGCTATTTTCTGCTAGGGGG	20	13147	13128	
F14	CAGCCCAATTAGGTCTCCAC	20	13007	13026	1168
R14	TAATTGAGATTGCTCGGGGG	20	14174	14155	
F15	TCCATCATCACCTCAACCCA	20	14056	14075	1081
R15	GCCTATGAAGGCTGTTGCTA	20	15136	15117	
F16	CAGAAACCTGAAACATCGGC	20	15075	15094	1112
R16	GGGTTTTGATGTGGATTGGG	20	16186	16167	
F17	GACTCACCCATCAACAACCG	20	16065	16084	1150
R17	TTTATGGGGTGATGTGAGCC	20	645	626	

All PCR amplifications were performed using GoTaq® G2 Hot Start Polymerase (Promega). Briefly, a 50-µL reaction mix was prepared for each set of primers (Table 2.12). A negative control was included in every PCR experiment where water was used to replace the template DNA.

Table 2.12. Reaction setup for PCR amplifications.

Component	Volume (µL)
5 × PCR buffer	10
$MgCl_2$ (25 mM)	3
dNTPs (5 mM)	2
Primers set (5 µM)	2
GoTaq® G2 Hot Start Polymerase (5 U/µL)	0.25
Nuclease-free water	22.75
DNA (20 ng/µL)	10
Total volume per reaction	**50 µL**

The PCR tubes were vortexed, followed by a pulse spin and placed on ice until ready to load onto the T100™ Thermal Cycler (Bio-Rad). The amplification procedure entailed 95°C for 15 min, followed by 35 cycles of 95°C for 40 seconds, 60°C for 40 seconds and 72°C for 2 min with a final elongation step for 10 min at 72°C.

2.4.2 Agarose gel electrophoresis

To check whether the amplification of the 17 amplicons was successful, PCR products were run using agarose gel electrophoresis to confirm the bands before the products being sequenced. A 1.2% gel solution was prepared by dissolving 1.2 g of agarose in 100 mL of 1 × TBE buffer (Fisher Scientific). The gel solution was heated by microwave to fully dissolve the agarose and left to cool down before adding 10 µL of the DNA stain, SafeView (NBS Biologicals, Huntingdon, UK). The gel solution was then poured into the gel tank. Once the gel was set, the comb was removed and the electrophoresis reservoir was filled with 1 × TBE buffer.

After 20 µL of the PCR product was mixed with 5 µL of 5 × DNA Gel Loading Buffer (Eppendorf, Stevenage, UK), the sample was loaded into the gel. In addition, 10 µL of exACTGene™ DNA Ladders (Fisher Scientific) was used as size standards.

The gel was run on 125 V for 50 minutes. Once the electrophoresis was completed, the gel was viewed with the Gel Doc™ EZ System (Bio-Rad).

2.4.3 Sanger sequencing

Sanger sequencing for the PCR products was performed by Eurofins Genomics (Ebersberg, Germany).

2.4.4 Mutation analysis

Mutations in the mitochondrial genome were identified by comparing the obtained sequences with the NCBI Human Mitochondrial Reference Sequence (NC_012920.1; https://www.ncbi.nlm.nih.gov/nuccore/251831106/) using the Nucleotide BLAST software (https://blast.ncbi.nlm.nih.gov/Blast.cgi). Identified mtDNA mutations were annotated and their disease association was analysed using online tools and databases including MitoWheel (http://mitowheel.org/mitowheel.htmL), MitoMAP (https://www.mitomap.org/MITOMAP) and Human Mitochondrial DataBase (HmtDB; http://www.hmtdb.uniba.it/hmdb/index.jsp).

2.4.4.1 MitoWheel

MitoWheel displays a circular graphical representation of the human mitochondrial genome. The entire genome is displayed as a wheel that can be viewed by spinning the wheel allowing users to scan through and browse different regions of the genome. The sequence used is the NCBI Human Mitochondrial Reference Sequence (NC_012920.1).

The MitoWheel tool was used to identify the location of the mutation on the mitochondrial genome and whether the regions containing variants were protein or non-protein coding. If the mutations were identified as protein coding, the amino acid changes (if applicable) were recorded (Figure 2.3).

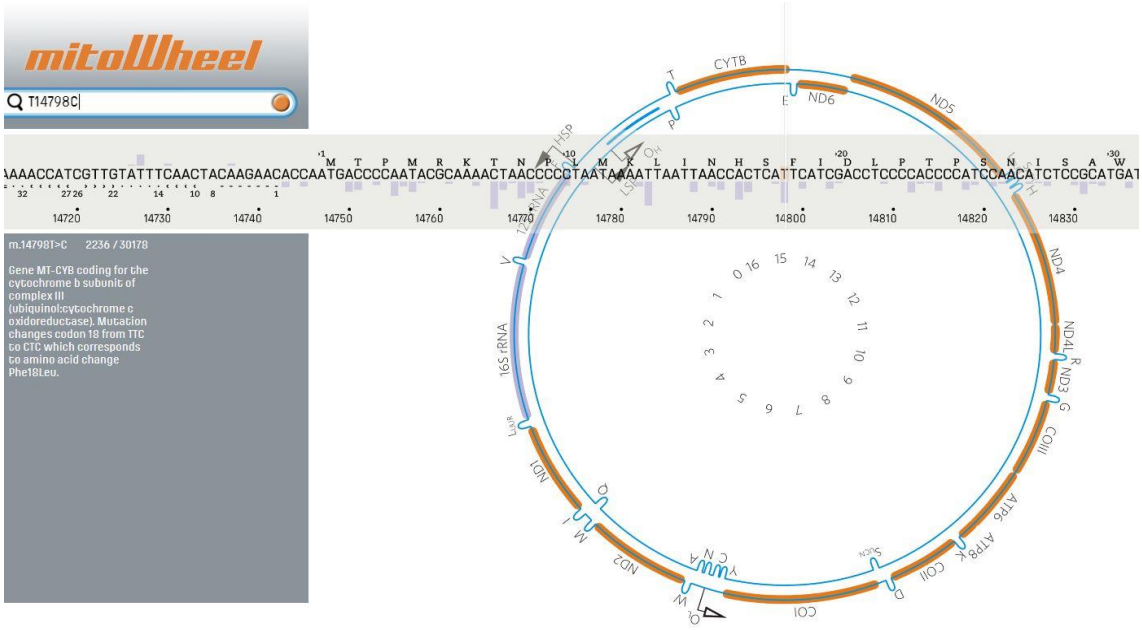

Figure 2.3. A screenshot of the MitoWheel search tool using the T14798C mutation as an example.

2.4.4.2 MitoMap

MitoMap is a human mitochondrial genome database containing a compendium of polymorphisms and mutations in the human mitochondrial genome. MitoMap reports published data on human mitochondrial variants and mutations [294].

The Allele Search tool in MitoMap was used to record any diseases previously associated with the observed mutations along with their specific references (Figure 2.4).

Allele Search - Search the Mitomap database for quick variant information

Enter a single nucleotide position in the **Start** box or use both **Start** and **End** boxes to enter a range (up to 101 bps).

Start: 14798 End: 14798 Search

Searched nucleotide position(s): **14798 - 14798**

MITOMAP: mtDNA Coding Region Sequence Variants

Nucleotide Position	Locus	Nucleotide Change	Codon Number	Codon Position	Amino Acid Change	MitoTIP †
14798	MT-CYB	T-C	18	1	non-syn:F-L	N/A

MITOMAP: mtDNA Somatic Variants

Nucleotide Position	Locus	Nucleotide Change	Homoplasmy	Heteroplasmy	Amino Acid Change	Cell or Tissue Type
14798	MT-CYB	T-C	+	-	F-L	glioblastoma

Figure 2.4. The screenshot of the MitoMap's Allele Search tool showing reported variants and mutations at the 14798 bp position of mtDNA.

2.4.4.3 Human Mitochondrial DataBase

Human Mitochondrial DataBase (HmtDB) is a human mitochondrial genome database hosting human mitochondrial genome sequences annotated with population and variability data (Figure 2.5). HmtDB was also used to record any diseases previously associated with the observed mutations along with their specific references.

2.4.5 *In silico* protein structure mapping and analysis

A three-dimensional (3D) protein structure mapping and analysis tool (developed and validated by Lloyd and McGeehan) [45] was used to predict the functional impact of all non-synonymous mitochondrial DNA mutations identified in protein coding regions. The 3D structure modelling provides a powerful tool for assessing the impact of mtDNA mutations on protein structure and therefore its function by allowing the amino acid changes to be visualised [45].

2.4.5.1 Selection of OXPHOS structures

Because of their complex nature and location within the inner mitochondrial membrane, the respiratory chain proteins were difficult to be crystallised. Since not all structures of human respiratory chain complexes are well defined, some homologous structures have been used in parallel with the human ones for the purpose of analysing human mtDNA mutations.

In this PhD project, the human mitochondrial protein sequences were used to choose the best quality, latest and most similar OXPHOS complex structures for complexes I, III, IV and V available from the Research Collaboratory for Structural Bioinformatics Protein Data Bank (RCSB PDB, http://www.rcsb.org/).

The RCSB PDB (or it's short form, the PDB) is a global archive for experimentally determined, atomic level 3D structures of biological macromolecules (DNA, RNA and proteins) [295].

Homologous structures were selected if they had a good atomic resolution and were in an organism whose protein sequence had a high level of identity to the human one.

FASTA sequences of the potential homologous respiratory chain complexes (downloaded from the PDB) were aligned with their respective human sequences (NC_012920.1) using Clustal Omega, a multiple sequence alignment program that generates alignments between several sequences (https://www.ebi.ac.uk/Tools/msa/clustalo/).

Sequences with the level of structure identity greater than 60% were considered suitable for the 3D structural analysis (Table 2.13).

Table 2.13. List of the complex structures obtained from the RCSB PDB.

Complex	PDB accession code	Organism	Subunit	Sequence identity (%)	Ref.
Complex I	5XTD	Homo sapiens	ND1	99.37	[46]
			ND2	99.71	
			ND3	98.26	
			ND4	99.56	
			ND4L	97.94	
			ND5	99.50	
			ND6	99.43	
	5LC5	Bos taurus	ND1	77.96	[38]
			ND2	63.37	
			ND3	72.97	
			ND4	73.96	
			ND4L	72.63	
			ND5	69.77	
			ND6	61.40	
Complex III	5XTE	Homo sapiens	MT-CYB	100	[46]
	1NTZ	Bos taurus	MT-CYB	78.89	[44]
Complex IV	5Z62	Homo sapiens	COI	100	[47]
			COII	100	
			COIII	100	
Complex V	5ARA	Bos taurus	ATP 6	77.42	[51]

All the alignments of the reference protein sequences used in the 3D modelling analyses are listed in Appendix Figures 1-7, with the identified mutation positions marked in rectangular boxes.

2.4.5.2 Creating structural files for mutation analysis

The atomic co-ordinates of each respiratory chain complex were downloaded from the PDB and opened using PyMol (the PyMOL Molecular Graphics System/Version 1.8, distributed by Schrödinger, LLC, NY, USA). The PDB files were also opened using the COOT software (Crystallographic Object-Oriented Toolkit), a program used to display and manipulate atomic models of macromolecules, typically proteins or nucleic acids [296]. COOT was used in our project to create PDB files containing all non-synonymous mutations identified by Sanger sequencing. Each residue in the non-human structures was carefully checked before mutating it to make sure that it was homologous with the human protein sequence. A new PDB file was generated for each mutation as well as for each complex containing all mutations.

2.4.5.3 Mapping and analysis of non-synonymous mutations

All identified non-synonymous mutations were mapped to their locations on the protein structures using PyMol. PDB files including the mutations (created by COOT) were also opened with PyMol. The whole structure was displayed in a cartoon style, and each mutation was identified and displayed in the stick and sphere format.

Detailed analysis of the effect of each mutation on protein structure was performed by examining the location of the amino acid change within the protein. Proximity to important catalytic regions, such as active sites, binding pockets and subunit interfaces, as well as whether the amino acid substitution could be accommodated or not at a specific position were analysed using PyMol. Such information and the type of amino acid change (Figure 2.6) were then used to predict the functionality of the associated mutations. Each of the mutations was also classified into one of the five structural classes previously defined by Lloyd and McGeehan: 1) Frameshift; 2) Active site; 3) Binding pocket; 4) Protein interaction region; 5) Non-functional [45].

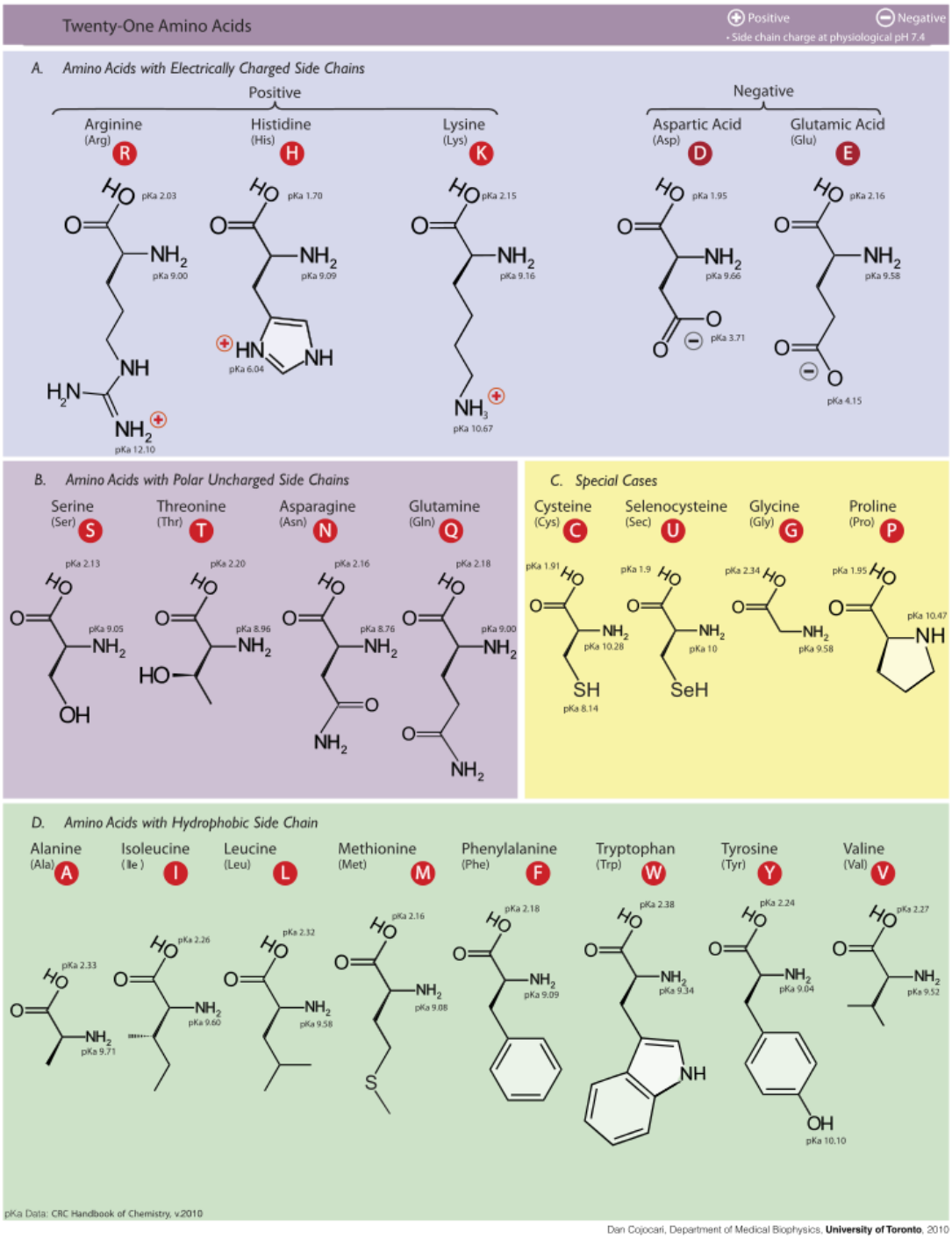

Figure 2.5. The structures of the 21 amino acids. Amino acids are grouped in A) amino acids with electrically charged side chains, B) amino acids with polar uncharged side chains, C) amino acids with different side chains and D) amino acids with hydrophobic side chains. Figure created by Dr Dan Cojocari, University of Toronto and taken from https://commons.wikimedia.org/wiki/File:Molecular_structures_of_the_21_proteinogenic_amino_acids.svg.

2.5 Statistical Analysis

Data were analysed with the GraphPad Prism version 8.0 (Graphpad Software, CA, USA) and presented as the mean ± SEM of at least two independent experiments. Specific statistical tests used to analyse various data sets are described in the associated figure legends in the following chapters. Differences between groups were considered statistically significant based on the following criteria: *p<0.05, **p<0.01, ***p<0.001 and ****p<0.0001.

Potential linear correlation between two variables was assessed by Pearson correlation coefficient method using SPSS (2015) software. Pearson's ***r*** has a value between +1 and −1, where +1 indicates a total positive linear correlation, 0 indicates a non-linear correlation, and -1 indicates a total negative linear correlation.

Chapter 3
Mitochondria-targeting/ROS-mediating agents as novel synergistic drugs for improved cancer-specific therapy

3.1 Introduction

Mitochondria are the primary source of intracellular ROS as side-products of the mitochondrial electron transport chain reaction during cellular respiration [160]. ROS play important roles in cell signalling pathways such as growth, differentiation, metabolism and apoptosis [160,297]. They are also regarded as a double-edged sword in cancer cells since low doses of ROS can promote cell proliferation and invasion, whereas excessive levels of ROS cause oxidative damage to biomolecules which consequently induce cell death [168,196]. Therefore, a slight increase of ROS is associated with the initiation and progression of cancer [144,160], but high levels of ROS can induce cell death by activating several signalling pathways resulting in cell apoptosis [168,196].

Despite its strong side effects, chemotherapy is still widely used in clinical practice. Many chemotherapy drugs cause cell death by a direct damage to the nucleic acids while others disrupt the redox balance within the cell. Some chemotherapeutic agents can cause an excessive accumulation of ROS either via an overproduction of ROS or by supressing their elimination in tumour cells by the antioxidant systems (reviewed in Ref. [175]).

Cisplatin (CDDP) is one of the most commonly used chemotherapeutic agents employed in the treatment of various human cancers. It is a highly reactive molecule which forms various types of adducts by binding to DNA, RNA and proteins [209]. Moreover, previous studies have demonstrated that cisplatin accumulates in mitochondria and causes significant changes in mitochondrial structure and metabolic function [209,240]. Recent reports evinced that cisplatin-induced apoptosis could be inhibited by compounds that interfere with ROS generation. These observations elucidate that the killing effect is correlated to increased ROS generation [240]. However, the clinical use of cisplatin is limited because of its severe irreversible side effects including neurotoxicity, ototoxicity and nephrotoxicity which has been reported as the main limitation of cisplatin [298].

Recently, due to their critical role in metabolism, ATP synthesis and redox status, and because of their involvements in many pathways related to the cell death, mitochondria have become one of the main interests in developing cancer treatments. Since cancer cells generally have higher levels of ROS compared to normal cells, and because of the differences in the mitochondrial transmembrane potential between cancer and normal cells, a direct targeting on mitochondrial functions could be an effective approach to triggering cancer-specific cell death.

Delocalised lipophilic cations (DLCs), a group of small membrane permeable agents driven by negative potential across the mitochondrial membrane, accumulate in mitochondria and are more toxic to cancer cells compared to normal cells (reviewed in Ref. [255]). This characteristic attracts researchers to evaluate DLCs for selective cancer cell elimination [299]. Within a wide range of DLCs, dequalinium (DQA) has been reported to demonstrate a potent anticancer activity *in vitro* and *in vivo* in different malignancies [270]. Several studies have suggested that the cytotoxicity mechanism of DQA is related to mitochondrial dysfunction due to the damage of mitochondrial DNA and the inhibition of mitochondrial complex I [267].

Given the merit of mitochondria-targeting therapy, the combination of conventional chemotherapy drugs such as cisplatin with mitochondria-targeting agents (e.g. DQA) may offer a promising strategy for enhanced anticancer therapy [300].

In this chapter, we report our investigation on how baseline ROS level might influence cells' response to ROS-stimulating therapy. The potential synergistic effect of cisplatin and dequalinium chloride in killing cancer cells was also assessed.

3.2 Results

3.2.1 Overproduction of intracellular ROS and mitochondrial superoxide in cancer cells

Initially, in advance of the first ROS experiments, a population-doubling-time (PDT) analysis was performed for all the cell lines enrolled in the study so that cell lines with comparable PDT values could be selected to avoid potential interference of disparate proliferation rates with the downstream work.

Results in Figure 3.1 show that the average doubling times were 27.2, 34.7, 34.3, 33.2, 32.1, 35.9 and 40.2 hours for Caki-2, Ishikawa, Caco-2, PC-3, MDA-MB-231, PNT-2 and HEK-293 cells, respectively. According to these results, Ishikawa, Caco-2, PC-3, MDA-MB-231 and PNT-2 cells were selected due to their comparable doubling times.

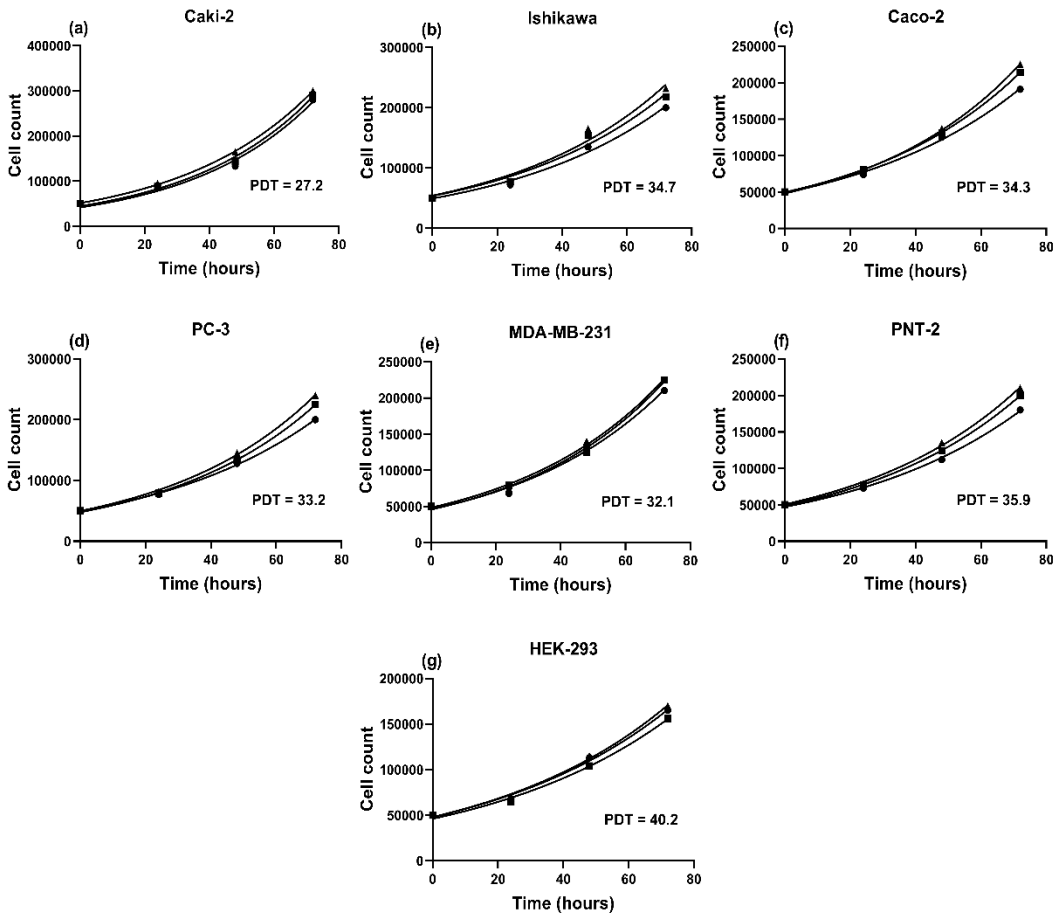

Figure 3.1. Cell line doubling times illustrated by graphs with cell number plotted against culture time.

After establishing this phenotypic characteristic of the cells, comparative analyses of the baseline intracellular ROS level and mitochondrial superoxide across the various cell types were performed. As shown by DCFDA and MitoSOX assays in Figure 3.2 a & b, all cancer cell lines had increased baseline intracellular ROS and mitochondrial superoxide levels compared to the non-cancerous cells (PNT-2). Amongst the cancer cell lines, Caco-2 had the highest baseline intracellular ROS and mitochondrial superoxide levels whereas Ishikawa had the lowest. Moreover, the baseline mitochondrial superoxide and the overall intracellular ROS levels were positively correlated in all the cell lines (Figure 3.2 c).

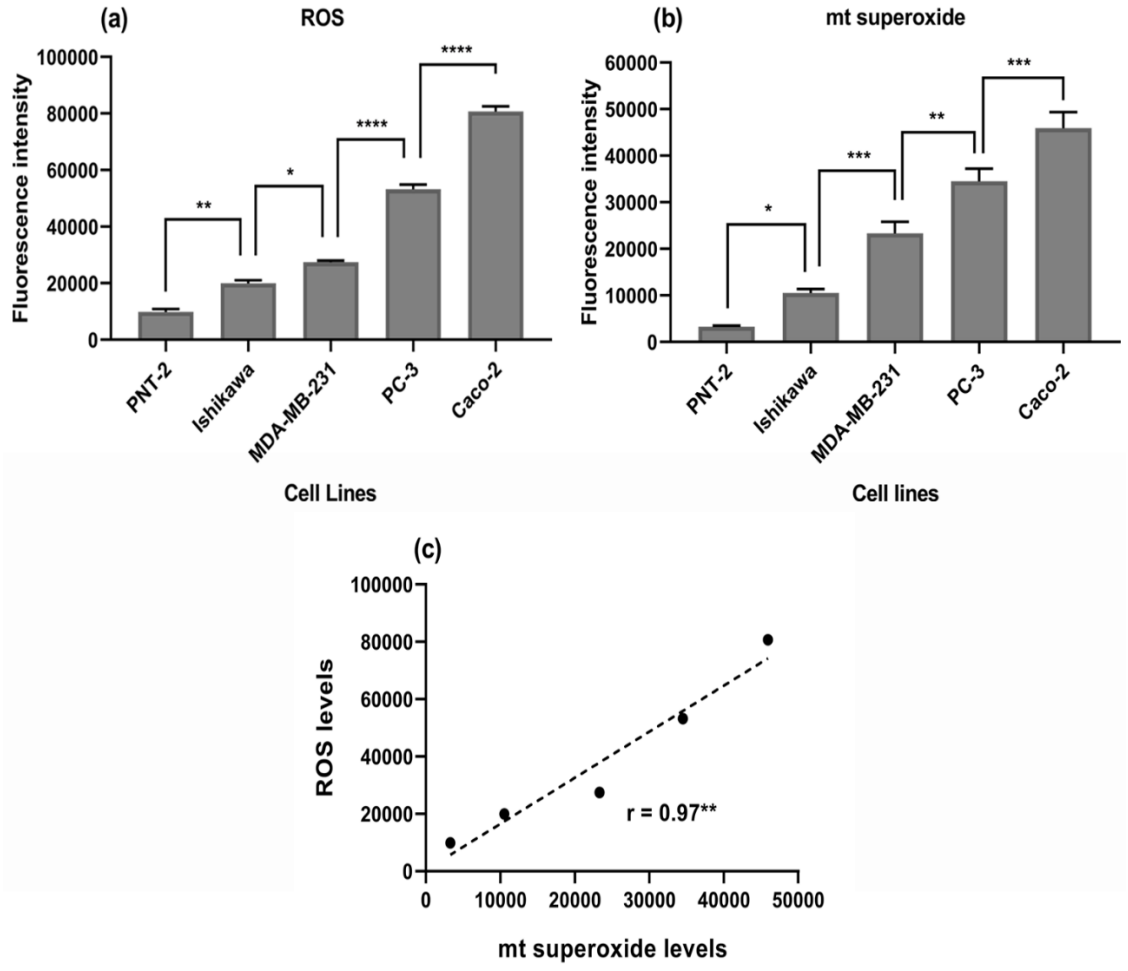

Figure 3.2. Correlation between the baseline mitochondrial superoxide and intracellular ROS levels. Intracellular ROS (**a**) and mitochondrial superoxide (**b**) levels of the PNT-2, Ishikawa, MDA-MB-231, PC-3 and Caco-2 cell lines are represented by the fluorescence intensity of DCFDA and MitoSOX respectively. Data are mean ± SEM (*N*=3 separate experiments); *p* values were calculated using one-way ANOVA with Tukey multiple comparison post-hoc analysis; **p*<0.05, ***p*<0.01, ****p*<0.001 and *****p*<0.0001. (**c**) Positive correlation between the baseline mitochondrial superoxide and intracellular ROS levels. Data points representing the cell lines are in the same sequence as the columns in panels **a** and **b**. r and *p* values were calculated using the Pearson correlation coefficient method; ***p*<0.01.

3.2.2 Increased drug resistance in cancer cells

To evaluate the drug sensitivity of all the cell lines towards cisplatin (CDDP) and dequalinium chloride hydrate (DQA), cells were treated with various concentrations of CDDP and DQA for 24 hours (described in Chapter 2, 2.1.5).

The MTS assay results showed that the PNT-2 cells were more sensitive to both drugs compared to the cancer cells with Caco-2 being the most resistant whereas Ishikawa the most sensitive amongst the cancer cells (Figure 3.3 a & b). The IC50s of CDDP were 34.31±2.5, 84.96±3, 158.9±8.2, 372.7±17.5 and 499.5±15.1 μM for PNT-2, Ishikawa, MDA-MB-231, PC-3 and Caco-2 respectively, whereas the IC50s of DQA were 9.07±0.66, 14.24±0.59, 57.85±3.59, 93.31±3.21 and 179.2±5.2 μM respectively for the above cell lines.

Interestingly, the increased IC50s of both CDDP and DQA among the cell lines followed the same trend as that of the baseline intracellular ROS levels. This indicates that the baseline intracellular ROS levels were positively correlated with the resistance levels to both drugs in the cell lines (Figure 3.3 c & d).

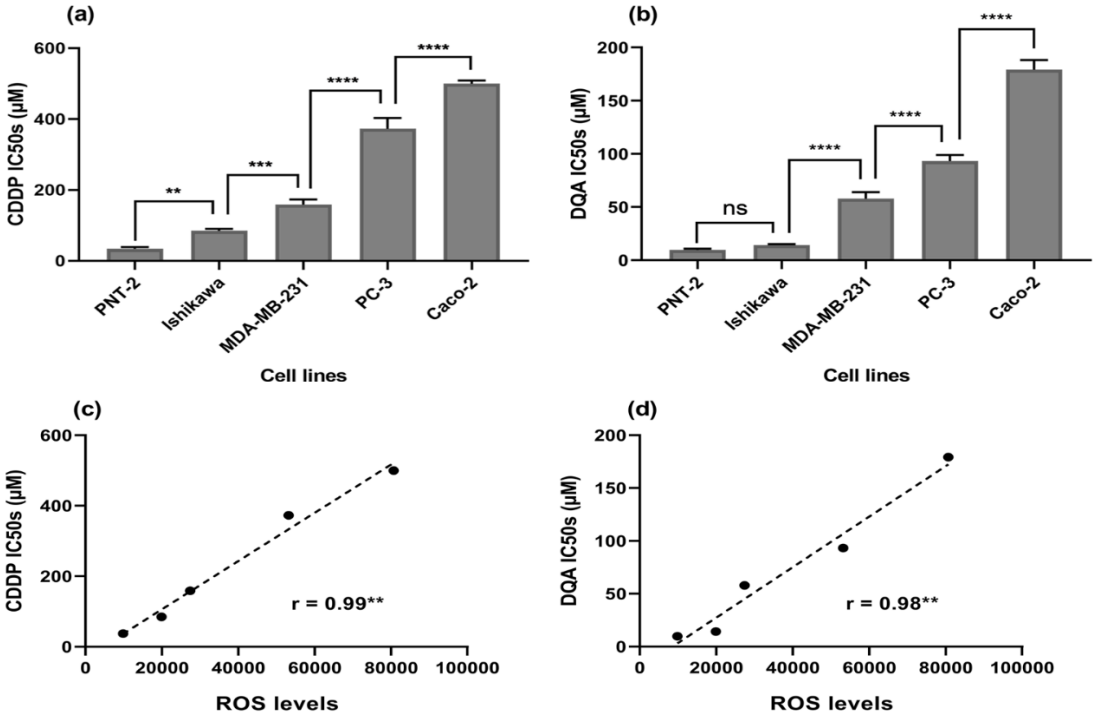

Figure 3.3. Comparison of the CDDP IC50s and the DQA IC50s amongst the 5 cell lines. The columns represent the CDDP IC50s (**a**) and the DQA IC50s (**b**) in the all cell lines. Data are mean ± SEM (N=3 separate experiments); p values were calculated using one-way ANOVA with Tukey multiple comparison post-hoc analysis; ns, not significant, **p<0.01, ***p<0.001 and ****p<0.0001. Positive correlation between the baseline intracellular ROS levels and drug resistance levels against CDDP (**c**) and DQA (**d**). Data points representing the cell lines are in the same sequence as the columns in panels **a** and **b**. r and p values were calculated using the Pearson correlation method; **p<0.01.

Based on these observations, Caco-2 and Ishikawa were chosen to represent the most resistant and sensitive cell lines respectively in the downstream experiments to investigate the synergistic effect of CDDP and DQA as well as the underlying killing mechanisms that might be influenced by baseline intracellular ROS levels, since Caco-2 and Ishikawa also represented cancer cells with the highest and the lowest ROS levels in this study.

3.2.3 Synergistic effect of cisplatin and dequalinium chloride observed in Ishikawa and Caco-2

In order to study the synergistic effect of cisplatin and dequalinium chloride hydrate, the Caco-2 and Ishikawa cells were incubated with a combined treatment of CDDP and DQA at half of their IC50 concentrations for 24 hours. Such treatments resulted in a marked reduction of cell viability in both Caco-2 and Ishikawa cells, compared to the cells treated with a single drug (either CDDP or DQA) at its IC50 (Figure 3.4 a & b).

Moreover, treating cells with various concentrations of CDDP (5, 10, 50, 100, 250, 500, 750 and 1000 μM) in combination with DQA at half of its IC50 (i.e. 89.6 μM for Caco-2 and 7.2 μM for Ishikawa) resulted in a significant decrease of CDDP IC50 for the Caco-2 (384±8.3 μM) and Ishikawa (21.8±.91 μM) cells (Figure 3.4 c & d).

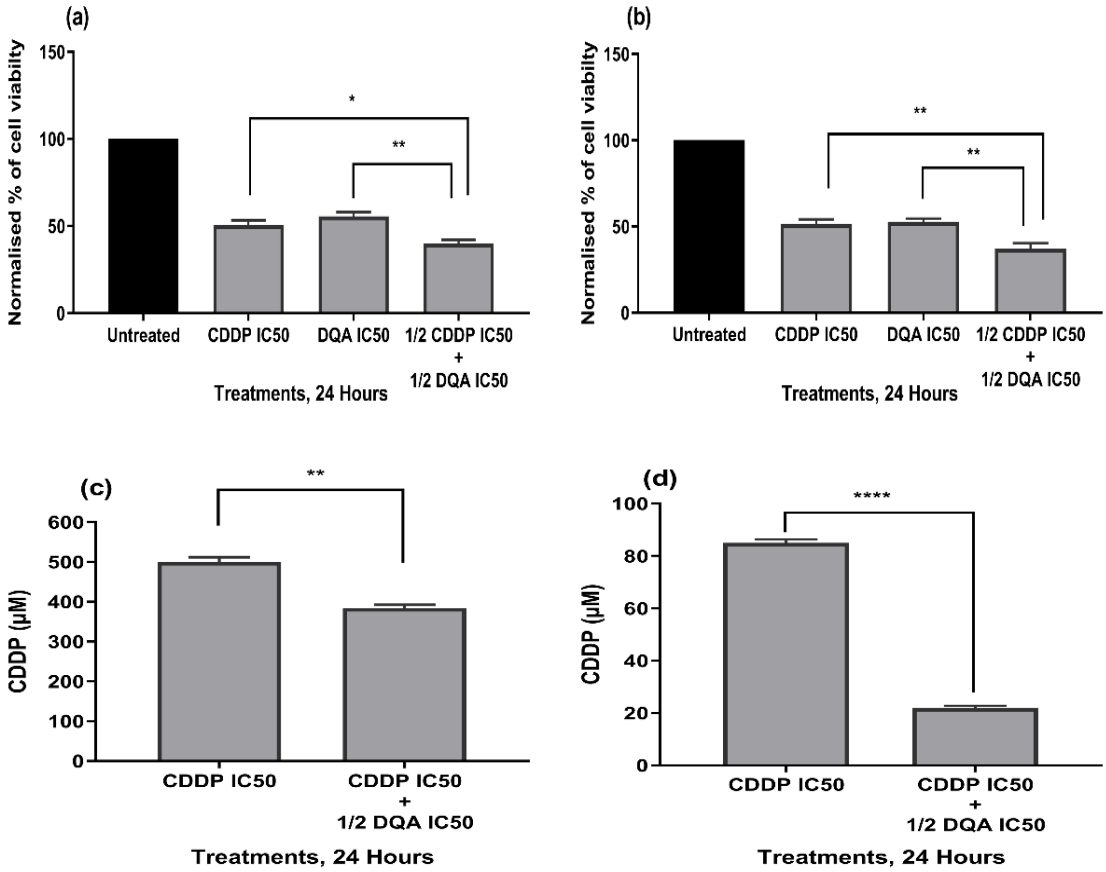

Figure 3.4. Comparison of Caco-2 (**a**) and Ishikawa (**b**) cell viability upon treatments with CDDP and DQA at their IC50 concentrations, and a combination of ½ IC50 of both drugs at 24 hours. The columns represent cell viability under various treatment conditions normalised against the untreated controls. Data are mean ± SEM (*N*=3 separate experiments); *p* values comparing single and combined treatments were calculated using one-way ANOVA with Tukey multiple comparison post-hoc analysis; **p*<0.05, ***p*<0.01. (**c**) Comparison between the CDDP IC50 (499.5 µM) in single drug treatment and the new CDDP IC50 (384 µM) in combination with ½ DQA IC50 in the Caco-2 cells. (**d**) Comparison between the CDDP IC50 (84.9 µM) in single drug treatment and the new CDDP IC50 (21.8 µM) in combination with ½ DQA IC50 in the Ishikawa cells. Data are mean ± SEM (*N*=3 separate experiments); *p* values comparing single and combined treatments were calculated using a two-tailed t-test; ***p*<0.01 and *****p*<0.0001.

Furthermore, to elucidate the influence of drug combination on therapeutic efficacy (i.e. Antagonistic, Additive or Synergistic), the Combination Index (CI) was calculated at different combinations according to the median-effect principle of the Chou and Talalay method, using the CompuSyn software.

Data from the CompuSyn analysis (Table 3.1) indicate synergistic effects of the compounds in both cell lines. However, the Ishikawa cells demonstrated higher synergistic effects within the whole concentration range for CDDP in combination with DQA at half of its IC50 (7.2 µM), whereas the Caco-2 cells demonstrated lower synergistic effects of the compounds and only within the concentration range of 5–250

μM for CDDP in combination with DQA at half of its IC50 (89.6 μM). Antagonistic effects of the compounds were observed only in the Caco-2 cells treated with 500–1000 μM of CDDP in combination with DQA. No additive effects were observed in either Ishikawa or Caco-2 with the concentrations of the compounds used in the study.

Table 3.1. The Measurement of Combination Index (CI).

Caco-2			
Dose CDDP / μM	**Dose DQA / μM**	**Effect**	**CI**
5	89.6	0.66	0.99136
10	89.6	0.64	0.92967
50	89.6	0.60	0.94462
100	89.6	0.55	0.92323
250	89.6	0.45	0.90660
500	89.6	0.39	1.07629
1000	89.6	0.33	1.37327
Ishikawa			
Dose CDDP / μM	**Dose DQA / μM**	**Effect**	**CI**
5	7.2	0.66	0.72731
10	7.2	0.59	0.63296
42.5	7.2	0.38	0.57506
50	7.2	0.34	0.55585
85	7.2	0.28	0.65842
100	7.2	0.25	0.66588
500	7.2	0.01	0.21071
1000	7.2	0.01	0.41721

3.2.4 Intracellular ROS and mitochondrial superoxide levels increased upon treatments

To evaluate the impact of the compounds on ROS production upon treatment, the Caco-2 and Ishikawa cells were continuously exposed to CDDP and DQA at their IC50 concentrations and to the combination of both drugs at half of their IC50 concentrations for 24 hours. Such treatments resulted in significant increases of intracellular ROS and mitochondrial superoxide levels in both Caco-2 and Ishikawa cells in a time-dependent manner (Figure 3.5). Significant increases in intracellular ROS were observed in the Caco-2 cells at 5 hours following initial exposures to CDDP and the combined therapy (Figure 3.5 a & c), and at 7 hours following DQA treatment (Figure 3.5 b).

ROS levels increased continuously up to 24 hours in the Caco-2 cells under all treatments. Earlier increases of intracellular ROS were observed in the Ishikawa cells, i.e. at 3 hours following initial exposures to CDDP and DQA (Figure 3.5 d & e), and at 1 hour with the combined therapy (Figure 3.5 f). Parallel increases in mitochondrial superoxide were observed in both cell lines (Figure 3.5 a-f).

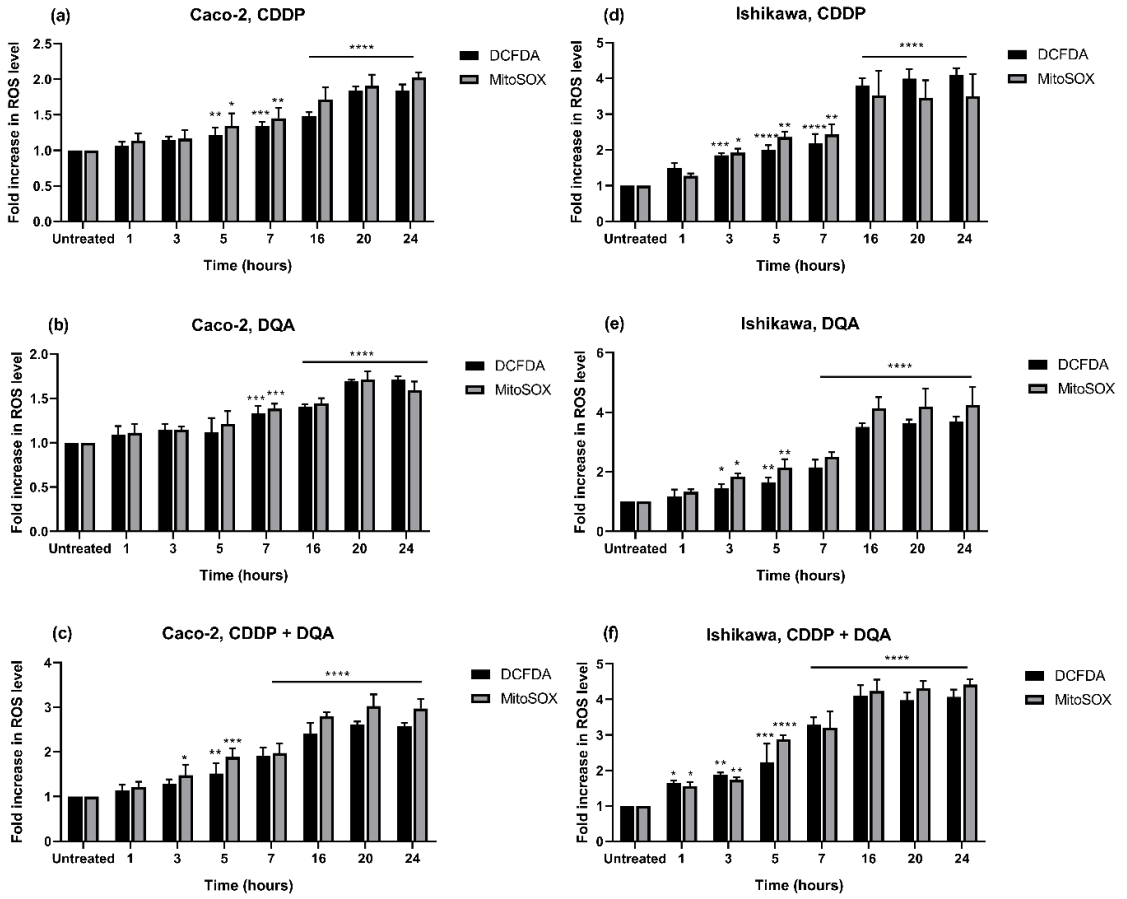

Figure 3.5. Increases in the intracellular ROS and mitochondrial superoxide levels in the Caco-2 and Ishikawa cells upon treatments during a 24-hour period. The columns represent the fold changes of intracellular ROS (DCFDA) and mitochondrial superoxide (MitoSOX) respectively normalised against the untreated controls. Data are mean ± SEM (N=3 separate experiments); p values comparing treated and untreated cells were calculated using one-way ANOVA with Tukey multiple comparison post-hoc analysis; *p<0.05, **p<0.01, ***p<0.001 and ****p<0.0001.

Furthermore, greater increases in intracellular ROS and mitochondrial superoxide were observed with the combined therapy compared to single treatment of CDDP or DQA in the Caco-2 cells at 24 hours (Figure 3.6 a & b). On the contrary, ROS and mitochondrial superoxide productions were equally elevated in the Ishikawa cells under all treatment conditions (Figure 3.6 c & d). However, the Ishikawa cells showed markedly higher increases in intracellular ROS and mitochondrial superoxide upon treatments compared to Caco-2 (Figure 3.6 e & f).

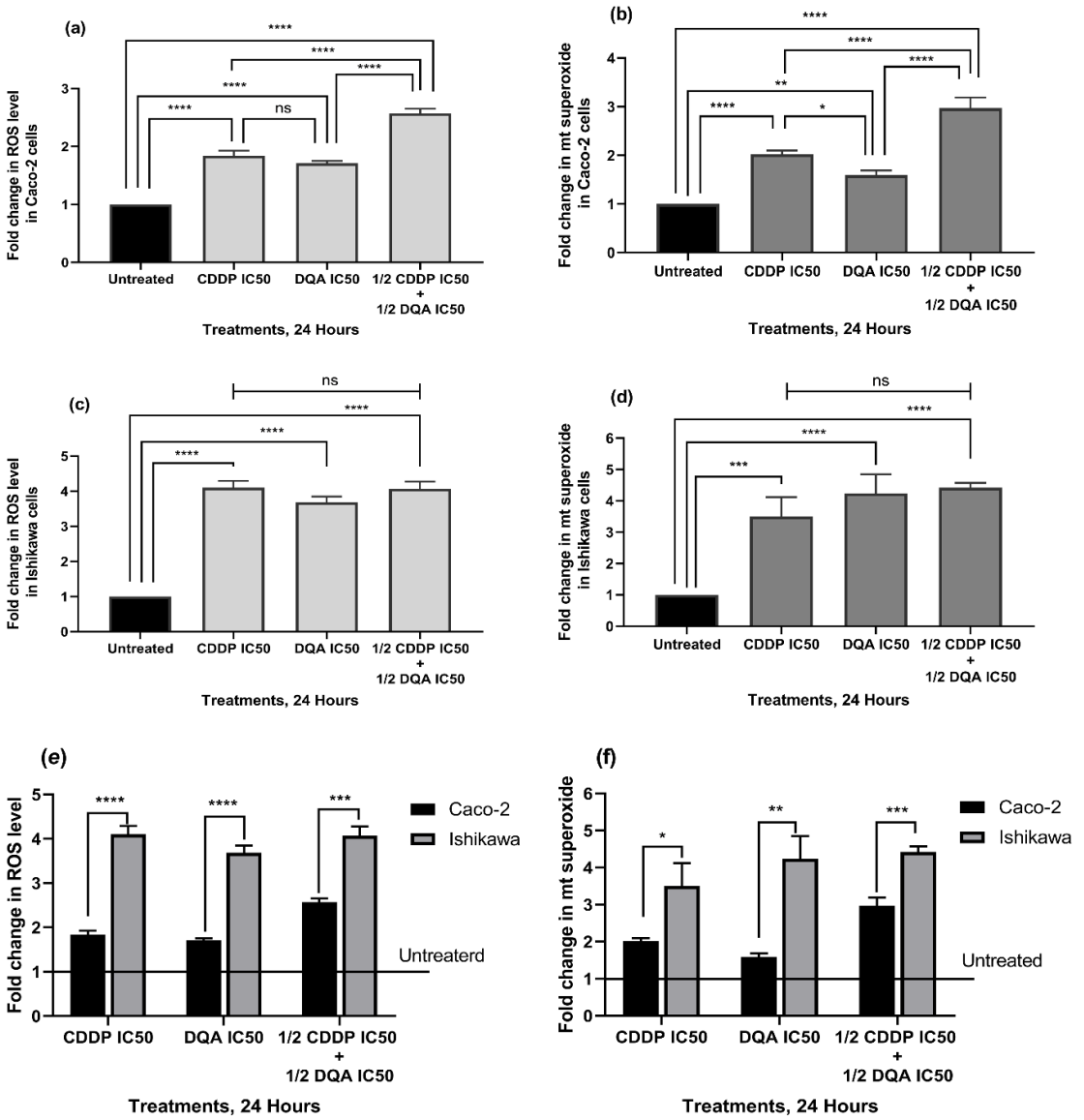

Figure 3.6. Increases of intracellular ROS and mitochondrial superoxide levels in the Caco-2 (**a** & **b**) and Ishikawa (**c** & **d**) cells upon treatments at 24 hours. The columns represent the fold changes of ROS and mitochondrial superoxide normalised against the untreated controls. Data are mean ± SEM (*N*=3 separate experiments); *p* values comparing treated and untreated cells were calculated using one-way ANOVA with Tukey multiple comparison post-hoc analysis; ns, not significant, **p*<0.05, ***p*<0.01, ****p*<0.001 and *****p*<0.0001. (**e**) Comparison of intracellular ROS level changes upon treatments between the Caco-2 and Ishikawa cells at 24 hours. (**f**) Comparison of mitochondrial superoxide changes upon treatments between the Caco-2 and Ishikawa cells at 24 hours. Data are mean ± SEM (*N*=3 separate experiments); *p* values comparing the Caco-2 and Ishikawa cells were calculated using a two-tailed t-test; **p*<0.05, ***p*<0.01, ****p*<0.001 and *****p*<0.0001.

The presence and production of mitochondrial superoxide upon treatments were also confirmed using fluorescence microscopy. Fluorescence staining with MitoSOX showed significantly increased production of mitochondrial superoxide in the Caco-2 and Ishikawa cells upon treatments with CDDP and DQA at their IC50 concentrations and with the combination of both drugs at half of their IC50 concentrations (Figure 3.7). The highest levels of mitochondrial superoxide were observed following the combined drug treatment in Caco-2 whereas comparable mitochondrial superoxide productions were observed under all treatment conditions in Ishikawa (Figure 3.7 b & c).

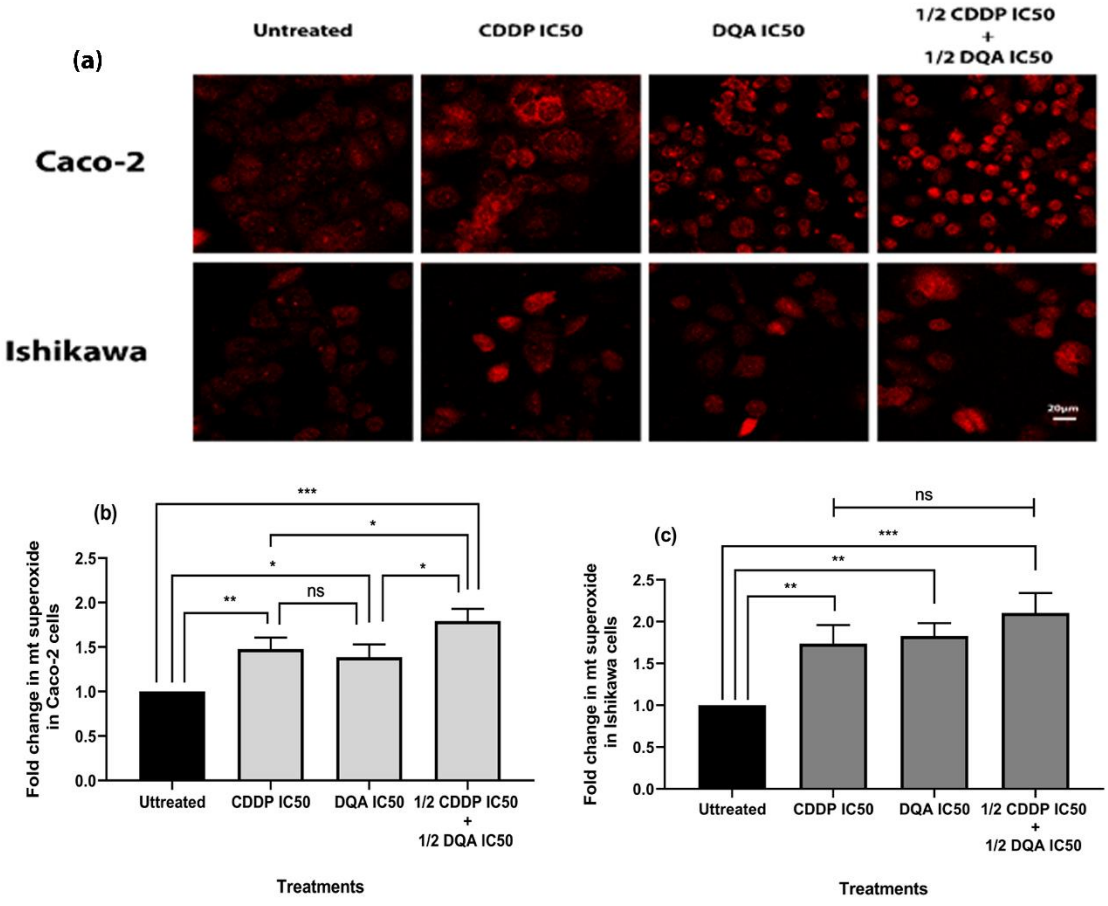

Figure 3.7. (**a**) Visualisation of mitochondrial superoxide stained by the MitoSOX probe upon treatments at 6 hours using confocal laser-scanning microscopy. Magnification of these images was ×20 and the scale bar represents 20 µm. (**b** & **c**) Quantification of the increased MitoSOX staining in treated cells. The columns represent the fold changes of mitochondrial superoxide normalised against the untreated controls. Data are mean ± SEM (*N*=3 separate experiments); *p* values comparing treated and untreated cells were calculated using one-way ANOVA with Tukey multiple comparison post-hoc analysis; ns, not significant, **p*<0.05, ***p*<0.01 and ****p*<0.0001. Fluorescence intensity was normalised to the number of cells per field of view in order to account for variations in the number of cells in each image.

3.2.5 Cell viability and mitochondrial transmembrane potential reduction along the same timeline as increased ROS generation

Continuous exposure to CDDP and DQA at their IC50 concentrations and to the combination of both drugs at half of their IC50 concentrations for 24 hours resulted in significant reduction of cell viability in both Caco-2 and Ishikawa cells in a time-dependent manner (Figure 3.8). MTS assay showed marked reductions of cell viability at 3 hours for CDDP and the combined therapy in both cell lines with cell viability continuously decreasing up to 24 hours, whereas marked reductions of cell viability were observed at 5 hours for DQA in both cell lines.

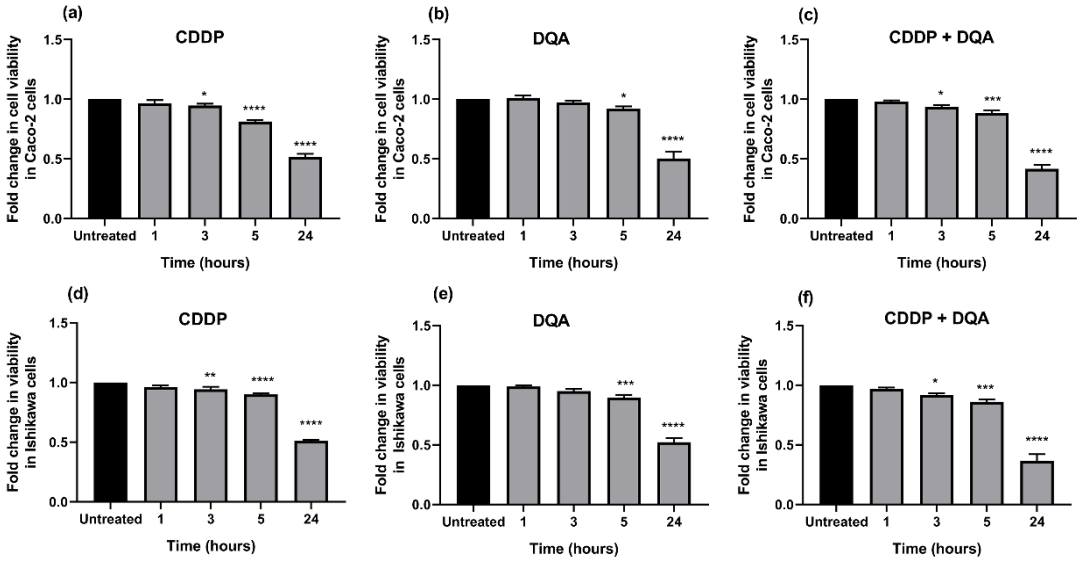

Figure 3.8. Effects of CDDP and DQA at their IC50 concentrations and a combination of both drugs at 1/2 IC50 concentrations, on cell viability in the Caco-2 (**a**, **b**, **c**) and Ishikawa (**d**, **e**, **f**) cells over a 24-hour treatment period. The columns represent the fold changes of cell viability normalised against the untreated controls. Data are mean ± SEM (N=3 separate experiments); p values comparing treated and untreated cells were calculated using one-way ANOVA with Tukey multiple comparison post-hoc analysis; *p<0.05, **p<0.01, ***p<0.001 and ****p<0.0001.

MMP was evaluated using the JC-10 fluorescence dye whose red/green fluorescence ratio depends only on the transmembrane potential (described in Chapter 2, 2.2.6). It was observed that the fluorescence changed from red to green following the treatments in both cell lines in a time-dependent manner. Data in Figure 3.9 show that CDDP noticeably depolarised mitochondrial potential at 1 and 3 hours in Ishikawa and Caco-2 respectively, and MMP continued to reduce up to 24 hours in both cell lines. Interestingly, cells treated with DQA and the combined therapy showed significantly greater mitochondrial depolarisation at the 1-hour time point compared to the CDDP treatment in both cell lines, predominantly in Ishikawa.

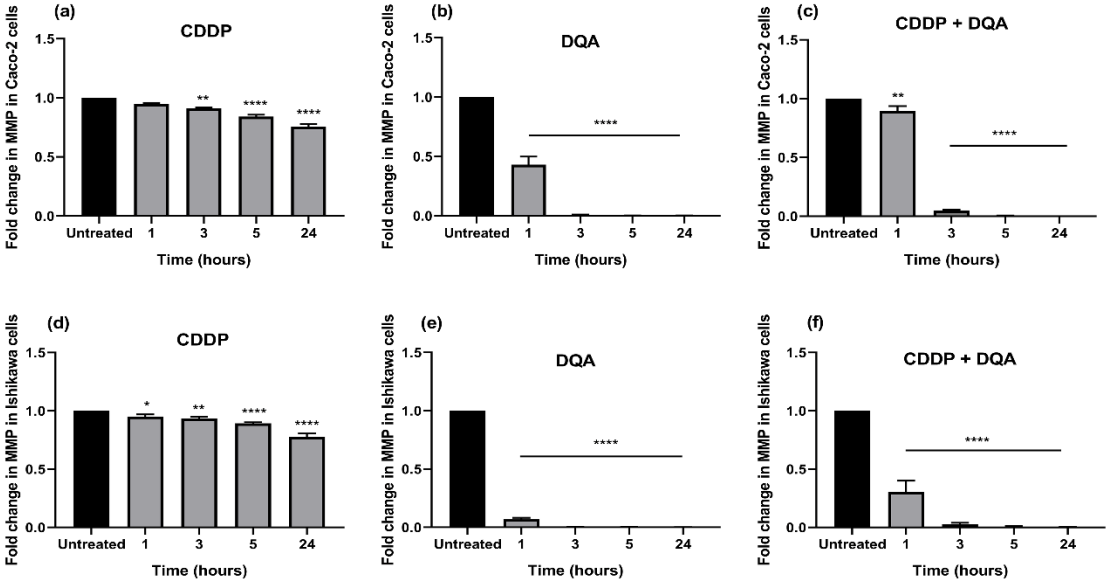

Figure 3.9. Effects of CDDP and DQA at their IC50 concentrations, and a combination of both drugs at 1/2 IC50 concentrations, on mitochondrial membrane potential in the Caco-2 (**a**, **b**, **c**) and Ishikawa (**d**, **e**, **f**) cells over a 24-hour treatment period. The columns represent the fold changes of MMP normalised against the untreated controls. Data are mean ± SEM (*N*=3 separate experiments); *p* values comparing treated and untreated cells were calculated using one-way ANOVA with Tukey multiple comparison post-hoc analysis; **p*<0.05, ***p*<0.01, ****p*<0.001 and *****p*<0.0001.

It is worth noting that the aforementioned changes in cell viability, MMP and ROS (both intracellular and mitochondria-specific) levels showed good correlations in the same time-dependent manner over the 24-hour treatment period (Figures 3.5, 3.8 and 3.9).

3.2.6 MtDNAcn decreased upon treatments

Using SYBR Green real-time PCR, the relative content of mtDNA in respect of the *β*-actin gene was determined in Caco-2 and Ishikawa upon the treatments. As shown in Figure 3.10, incubation with CDDP, DQA and their combination for 24 hours resulted in a marked reduction of mtDNAcn in both cell lines. The SYBR Green qPCR results showed that the mtDNAcn in both cell lines decreased significantly upon the treatments and reached its lowest value in the combined therapy at 24 hours, especially in Caco-2 (Figure 3.10 a).

The mtDNAcn data of all the cell lines are presented and discussed in Chapter 6 (6.2.1).

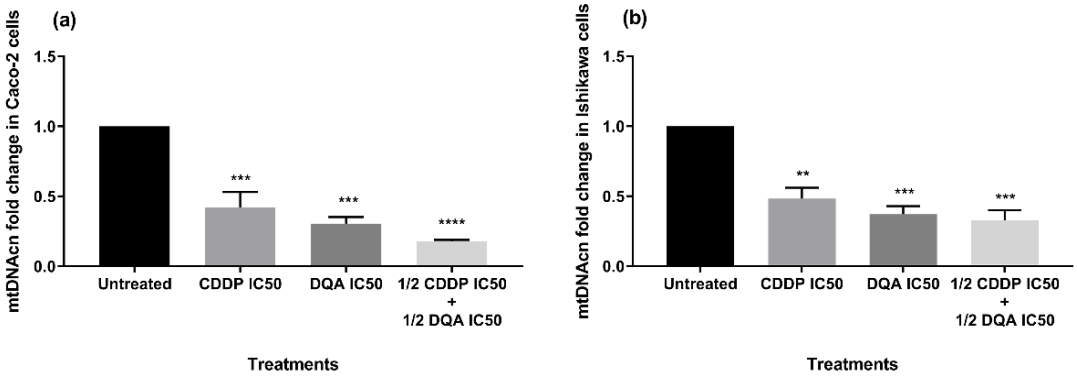

Figure 3.10. Decreases of mtDNAcn of the Caco-2 (**a**) and Ishikawa (**b**) cells upon treatments at 24 hours. The columns represent the fold changes of mtDNAcn that were normalised against the untreated controls. Data are mean ± SEM (*N*=3 separate experiments); *p* values comparing treated and untreated cells were calculated using one-way ANOVA with Tukey multiple comparison post-hoc analysis; ***p*<0.01, ****p*<0.001 and *****p*<0.0001.

3.2.7 Cancer-preferential uptake of dequalinium chloride

To elucidate the impact of higher MMP in cancer cells on DQA uptake, and how this can provide a window opportunity to achieve cancer-specific targeting by using delocalised lipophilic cations such as DQA, one pair of normal-cancer cell lines of prostate origin (PNT-2 and PC-3) was used in the cancer-preferential uptake experiments. The JC-10 assay results indicated that the PC-3 cell line (prostate cancer) had indeed significantly higher MMP compared to PNT-2 (non-cancerous counterpart) (Figure 3.11 a). Applying 10 µM of DQA to both cell lines resulted in far more rapid mitochondrial depolarisations in the PC-3 cells compared to the PNT-2 cells within the 3-hour incubation period (Figure 3.11 b).

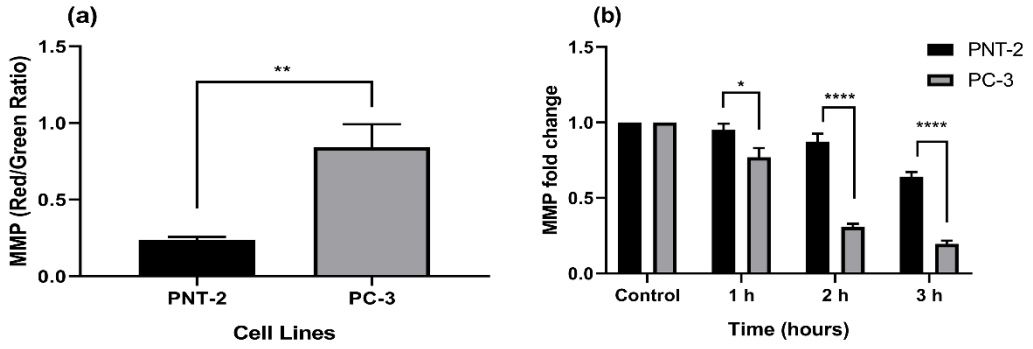

Figure 3.11. (**a**) Mitochondrial membrane potential of the PNT-2 and PC-3 cells. The columns represent the red/green ratio of fluorescence intensity. Data are mean ± SEM (*N*=3 separate experiments); *p* values comparing PNT-2 and PC-3 was calculated using a two-tailed t-test; ***p*<0.01. (**b**) Effects of DQA (10 µM) on mitochondrial membrane potential in the PNT-2 and PC-3 cells. The columns represent the fold changes of MMP normalised against the untreated controls. Data are mean ± SEM (*N*=3 separate experiments); *p* values comparing the PNT-2 and PC-3 cells were calculated using a two-tailed t-test; **p*<0.05 and *****p*<0.0001.

3.3 Discussion

Elevated level of ROS has been associated with various disease processes including cancer, and the unlimited growth of cancer cells in response to accumulation of ROS has been the focus of interest in recent studies. However, it has also been established that beside their mitogenic effect on tumorigenesis, excessive levels of ROS can induce damage in cancer cells and trigger apoptosis if not counteracted by antioxidant systems (reviewed in Ref. [175]).

Therefore, further increase of ROS levels using ROS stimulators in cancer therapy has attracted more attention in the past decades and various strategies of utilising ROS in the treatments of cancer have been developed [160].

This PhD project investigated the role of baseline intracellular ROS level in modulating the effect of anticancer drug treatment in various human cancer cell lines. In this Chapter, the initial screening of ROS levels among the cancer cell lines and their responses to ROS-stimulating agents are presented and discussed.

3.3.1 Correlation between baseline ROS levels and drug resistance

Several previous studies have demonstrated that various types of cancer cell lines have elevated levels of ROS compared to non-cancerous cell lines [301–303]. Our own intracellular ROS and mitochondrial superoxide assays were conducted with one pair of non-cancerous - cancer cell lines (PNT-2 and PC-3) of the same origin to verify this previous observation. Indeed, our results confirmed it to be the case and also demonstrated that all cancer cell lines involved in this study showed higher ROS levels compared to the non-cancerous cell line (PNT-2). Interestingly, results from the DCFDA and MitoSOX assays showed the same trend of both intracellular ROS and mitochondrial superoxide levels among the cell lines. This observation confirmed that mitochondria are the main source of ROS production in the cells employed in the study.

It has been postulated that cisplatin increases the generation of intracellular ROS which may cause damage to DNA, proteins and lipids leading to apoptosis [209]. Several previous studies also related the mechanism of the anti-tumour effect of dequalinium to an impairment of mitochondrial function and the associated ROS generation [270,271,304]. Therefore, the potential link between the baseline ROS levels in cancer cells and their drug response towards cisplatin and dequalinium was investigated in the present study.

Population doubling time results showed that all cell lines enrolled in this study had comparable doubling times (≈ 34 hours). Therefore, the 24-hour drug incubation period was considered appropriate in the toxicity experiments conducted to measure the IC50s because the same number of cells of each cell line had been seeded in the beginning of the experiments and the populations remained comparable among the cell lines during the 24-hour incubation period which was significantly shorter than the doubling times.

Our results showed that the IC50s of both CDDP and DQA at 24 hours were significantly greater in cancer cells with higher baseline intracellular ROS levels. On the contrary, cancer cells with the lowest baseline ROS level (i.e. Ishikawa) required the lowest doses of both treatments to achieve 50% of cell death. Consequently, our data suggested that the drug resistance levels of those cancer cells were correlated with their baseline ROS levels, and that cancer cells with a low intracellular ROS level were more sensitive to both cisplatin and dequalinium, whereas cancer cells with high baseline ROS levels were significantly more resistant. These results were in agreement with a study conducted by Yang *et al.* [267] who observed a positive correlation between baseline levels of ROS and drug resistance to photo activation of the delocalised lipophilic cation D112. Therefore, baseline ROS levels could be utilised to predict drug response of cancer cells.

Based on the above findings, the Ishikawa and Caco-2 cell lines were employed as *in vitro* models in the downstream investigations to represent cancer cells with the lowest and highest baseline intracellular ROS levels respectively.

3.3.2 Synergistic effect of cisplatin and dequalinium chloride

Neurotoxicity, ototoxicity and nephrotoxicity have been previously reported as the main limitations in the use of cisplatin (reviewed in Ref. [305]). Therefore, it is plausible to apply a lower dose of cisplatin in combination with another anticancer agent in order to reduce the side effects of cisplatin while enhancing the therapeutic efficacy. In this study, the effect of combining CDDP and DQA was evaluated by applying a combined treatment of both drugs at half of their IC50 concentrations to the Ishikawa and Caco-2 cell lines.

Our data showed that the combined therapy significantly caused a further reduction in the cell viability compared to the single treatment with CDDP and DQA at their IC50 concentrations. Moreover, incubating cells with various concentrations of CDDP in combination with DQA at half of its IC50 resulted in a significant decrease of CDDP IC50 in both Caco-2 and Ishikawa cells.

It is noteworthy that the extent of reduction in the CDDP IC50 under the combined treatment was far more obvious in Ishikawa (75%) than that in Caco-2 (25%). This correlates with the observation that the Caco-2 cells were most resistant to the drugs whereas the Ishikawa cells were most sensitive amongst the 4 cancer lines that we initially screened for drug response. In other words, the Ishikawa cells showed a much greater level of sensitivity towards the combined treatment compared to Caco-2.

In this study, significant synergistic effects of CDDP and DQA were also observed in both Caco-2 and Ishikawa cells when the cytotoxicity data were analysed using the CompuSyn software. We did not observe any additive or antagonistic effects in Ishikawa within the dose range of 5-1000 μM (as indicated by the CI values of Ishikawa in Table 3.1 which are all <1). This further confirms high sensitivity of Ishikawa to the treatments. Interestingly, an antagonistic effect was observed in Caco-2 within the dose range of 500-1000 μM. This antagonistic effect could explain the much greater resistant levels of Caco-2 towards both DQA and CDDP compared to Ishikawa, and it might be a result of competition between the two compounds over the cell membrane influx system at higher drug concentrations. Furthermore, our CompuSyn data from Caco-2 suggest that an additive effect may well occur if the Caco-2 cells are exposed to CDDP at a concentration between 250 μM and 500 μM in combination with 90 μM of DQA. (As indicated by the CI values of Caco-2 in Table 3.1; i.e. CI=0.90660 at 250 μM and CI=1.07629 at 500 μM).

Our observations were in alignment with previous findings that mitochondria are a promising target for anticancer therapy [52], and our data clearly suggest that combining mitochondria-targeting agents could provide improved efficacy while reducing side effects of conventional therapy in treating cancer.

3.3.3 Cell viability and mitochondrial transmembrane potential reduction along the same timeline as increased ROS generation

Cancer cells are highly sensitive to ROS-stimulating agents due to an elevated oxidative stress environment. To investigate treatment-induced ROS production in our study and its contribution to cell killing, the intracellular ROS and mitochondrial superoxide levels in the Ishikawa and Caco-2 cells were measured upon the treatments with CDDP, DQA and their combination. Interestingly, the present study revealed a significant difference between the Caco-2 and Ishikawa cells in terms of their response and behaviour to the treatments at cellular and molecular levels.

Our data showed significant increases in the intracellular ROS and mitochondrial superoxide levels in a time-dependent manner up to 24 hours following the continuous exposure to the treatments in both cell lines. However, ROS production upon drug exposure was significantly elevated in Ishikawa compared to Caco-2, and the onset of ROS production was far more rapid in Ishikawa than that in Caco-2. In addition, the Caco-2 cells responded most significantly to the combined therapy, whereas similar levels of increased ROS generation were observed in the Ishikawa cells across all treatments.

These results suggested that CDDP, DQA and their combination could stimulate greater ROS production in cells with relatively low baseline levels of intracellular ROS. As elevated ROS can trigger cell death, this explains the significantly higher sensitivity of the Ishikawa cells towards those treatments compared to the Caco-2 cells.

For cells with relatively high baseline ROS levels, the combined treatment of CDDP and DQA could have a greater impact on ROS production compared to the single treatment of the same compounds. This is in line with our aforementioned observation that combining CDDP with DQA had a synergistic effect in killing cancer cells. Since cancer cells with higher baseline ROS levels could be more resistant to CDDP, combining CDDP and DQA might warrant a new strategy to tackle such resistance issues in the future.

It is worth mentioning that DQA caused morphological changes to the cells such as irregular cell shape and reduced cell size. These changes were predominantly observed in the Caco-2 cells but not Ishikawa, and might be attributed to the increased cell membrane permeability due to the severe damages of the cell membrane components by excessive ROS in Caco-2. However further investigation is needed to elucidate the actual causes of this phenomenon.

Since mitochondrial membrane depolarisation is an early key feature of cell death and also could affect respiration and increase ROS generation (reviewed in Ref. [24]), changes in mitochondrial transmembrane potential due to the treatments were examined in the present study. Indeed, depolarisations occurred in both cell lines upon treatments in a time-dependent manner, which indicated that both CDDP and DQA affected the mitochondrial transmembrane potential and interfered with ROS generation.

A far more rapid and overwhelming depolarisation upon DQA treatment and its combination with CDDP was observed in both cell lines compared to the MMP changes observed in cells treated with CDDP alone. It should be noted that unlike the synergistic

effects on ROS production and cytotoxicity, the combined treatment did not have a synergistic effect on mitochondrial depolarisation in both cell lines. In fact, although the combined treatment had a profound impact on mitochondrial transmembrane potential, cells treated with DQA alone showed the most rapid and significant depolarisation upon the treatment. This could be attributed to the positive charge of DQA which led to its prompt and excessive accumulation within mitochondria, consequently neutralising the negative electric potential on the inner mitochondrial membrane at a speedy pace. Such swift changes in MMP were observed in our time course experiments. The impact on MMP was less severe from the combined treatment compared to that from DQA alone during the early phase of the time course particularly at the 1-hour and 3-hour time points. This could be due to the fact that only half of the DQA dosage was administrated to the cells in the combined treatment, which affected the speed and extent of depolarisation in those cells.

Furthermore, changes in cell viability upon the treatments were examined in the present study. Interestingly, the time-dependent changes in ROS and MMP matched the time course of cell death as shown by the relevant time course data. Indeed, decrease in cell viability occurred in both cell lines in a time-dependent manner and followed the same time points for ROS overproduction upon the treatments, which indicated that both cell death and ROS generation are linked.

A previous study showed that dequalinium induced a selective depletion of mitochondrial DNA in carcinoma cells [269]. Other reports also demonstrated that cisplatin accumulated in mitochondria formed adducts in mtDNA that interfered with mtDNA transcription and replication, and caused ATP deficiency which then led to cell death [209,307,308]. Our results showed significant decreases of mtDNAcn in both cancer cell lines upon the treatments and the relative mtDNAcn value reached the lowest in samples that had undergone the combined therapy. Such mtDNA depletion would reduce the expression levels of mtDNA-encoded complex subunits of the electron transport chain (ETC) and cause more leakage of electrons during OXPHOS, consequently leading to an excessive generation of ROS.

All together, these data indicate that CDDP and DQA and their combination exert cancer cell killing via mitochondrial dysfunction and ROS-induced cell death.

It should be emphasised that another advantage of using mitochondria-targeting cations in anticancer therapy, apart from the synergistic killing effect, is that those compounds preferentially enter mitochondria in cancer cells which generally have higher transmembrane potential compared to that of mitochondria in normal cells. This allows cations to selectively target cancer cells and accumulate more rapidly in their mitochondria (reviewed in Ref. [255]). Our data comparing the prostate cancer (PC-3) and non-cancerous (PNT-2) cell lines confirmed the preferential targeting of cancer cells by DQA. This *in vitro* phenomenon needs to be investigated *in vivo* to evaluate the potential of DLCs in clinical practice. If proven, DLCs could offer cancer-specific therapy with significantly reduced side effects. MKT-077 was the first DLC to be tested in clinical trials which were terminated due to renal toxicity [255,267]. Therefore, more suitable DLCs still need to be trialled.

3.4 Summary

The intracellular redox imbalance and the abnormal levels of ROS within the cell may lead to damages to macromolecules cell dysfunction, activation of protein kinases and inhibition of protein phosphatases resulting in malignant transformation and cancer development and progression. These events are accompanied by activation of transcription factors, accumulation of defective proteins, and adaptation to high levels of ROS and resistance to ROS-dependent apoptosis. Moreover, prolonged operation of cells at abnormal steady-state levels of ROS provokes genetic mutations, which makes the cells well adapted to oxidative stress by mobilising a set of adaptive mechanisms such as activating anti-oxidant systems to counteract the oxidative stress and inhibiting apoptosis. Recent evidences suggest that such adaptation contributes to malignant transformation, metastasis and resistance to anticancer drugs (reviewed in Ref. [168]). The aforementioned data might explain the increased resistance observed in cancer cells with higher baseline intracellular ROS levels.

This chapter focused on the different baseline intracellular ROS levels among the cancer cells and their impact on the cytotoxic efficacy of cisplatin and dequalinium. It was concluded that cancer cells with lower baseline ROS levels are more sensitive to ROS-stimulating agents whereas cells with higher baseline ROS levels are more resistant. Moreover, it was suggested that a robust increase in ROS production might explain the remarkable sensitivity of the Ishikawa cells to CDDP and DQA compared to other cancer cells. It is also possible that the Ishikawa cells are ill adapted to dealing with rapidly elevated oxidative stress upon ROS-stimulating therapy due to their relatively low baseline ROS level. In comparison, the Caco-2 cells are able to survive excess ROS production much better because those cells have already adapted to living under a relatively high level of ROS.

In summary, the present study suggests that baseline ROS level in cancer cells could be an efficient predictive biomarker for drug response. Since measuring ROS in tissues is technically challenging, a more efficient biomarker linked to ROS to indicate the response to ROS-stimulating agents is still needed (please see further results and discussion in Chapter 6). This study also supports the theory that combining conventional chemotherapy with mitochondria-targeting therapy enhances cell death and allows reduced doses of the conventional drug.

Chapter 4

Understanding the implication of cellular redox and apoptosis status in ROS-mediated cell death using Ishikawa and Caco-2 as *in vitro* models

4.1 Introduction

In healthy tissues, the intracellular ROS are preserved at a steady and low level by the equilibrium between ROS production and enzymatic elimination by antioxidants such as cytoplasmic superoxide (SOD1), mitochondrial superoxide (SOD2), catalase (CAT), peroxiredoxins (PRxs) and glutathione peroxidases (GPxs). Free radical activity can also be eliminated non-enzymatically through the interaction between ROS and their substrates such as glutathione (GSH) (reviewed in Ref.s [65,166,175]).

Generally, cancer cells have a constant metabolic oxidative stress compared to normal cells, and the elevated levels of ROS during cell transformation are due to high metabolic rate in mitochondria resulting in increased electron leakage and ROS generation [164]. Furthermore, cancer cells express relatively low levels of antioxidants compared to non-cancerous cells, which renders higher ROS levels in cancer cells (reviewed in Ref. [65]). However, cancer cells are capable of compensating the excessive levels of ROS by increasing the antioxidant capacity and reprograming the metabolic pathways to overcome oxidative stress and enhance tumour survival/growth [164]. Therefore, inducing further increase of intracellular ROS levels by ROS stimulators as a novel approach to cancer therapy has attracted more attention in the past decades, and various strategies for ROS-stimulating therapy have been developed (reviewed in Ref.s [144,160]).

Although cancer cells generally have higher ROS levels compared to their normal counterparts, they exhibit various levels of intracellular ROS due to differences in their tissue origin, genetic background, energy metabolic activity and microenvironment. Moreover, different capacity of the antioxidant system among cancer cells may also render their different levels of ROS.

On the other hand, cancer cells exhibit different levels of sensitivity to ROS-stimulating agents. Variations in the efficiency of the mitochondrial apoptosis signalling pathways among the cancer cells may also explain their different responses to the drugs.

The Ishikawa and Caco-2 cell lines were employed as *in vitro* models in the downstream investigations to represent cancer cells with the lowest and highest baseline intracellular ROS levels respectively, with the aim of understanding why cancer cells with different baseline ROS levels also respond differently to ROS-induced cell death.

In this chapter, we report our investigation on the link between the relative expression levels of the antioxidant enzymes and the baseline intracellular ROS level in both cell lines. Implications of the key genes associated with the mitochondrial apoptosis pathway and drug resistance were also assessed.

4.2 Results

4.2.1 Comparable mitochondrial organelle content levels in Ishikawa and Caco-2 with higher mitochondrial DNAcn in Caco-2

To correlate the differences in the baseline intracellular ROS level between the Ishikawa and Caco-2 cells to the mitochondrial function of each cell line, the baseline physical mitochondrial content level and mitochondrial DNA copy number in both cell lines were measured. MitoTracker™ Red CMXRos, a red-fluorescent dye that passively diffuses across the plasma membrane and accumulates in active mitochondria was used to determine mitochondrial content level.

As shown in Figure 4.1, comparable mitochondrial content levels were detected in the Ishikawa and Caco-2 cells with higher mtDNAcn observed in the Caco-2 cells.

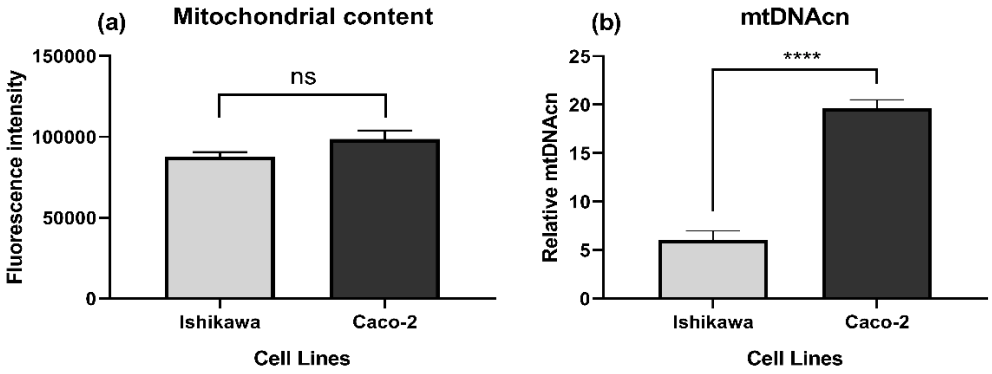

Figure 4.1. Mitochondrial content level and mitochondrial DNA copy number in Ishikawa and Caco-2. (**a**) Mitochondrial content levels of the Ishikawa and Caco-2 cells measured by MitoTracker. (**b**) Relative copy numbers of mtDNA in Ishikawa and Caco-2 normalised against the house keeping gene (β-actin). Data are mean ± SEM (N=3); p value comparing Caco-2 and Ishikawa was calculated using a two-tailed t-test; ns, not significant and ***p<0.001.

4.2.2 Higher NADPH oxidases expression in Ishikawa

The membrane-bound enzyme family of NADPH oxidases (NOXs) is an important group of signalling mediators associated with the generation of ROS. To elucidate their influence on the baseline intracellular ROS levels between the Ishikawa and Caco-2 cells, the relative baseline expression levels of the *NOX* isoforms were investigated by quantitative reverse transcription polymerase chain reaction (TaqMan qPCR) in both cell lines.

As shown in Figure 4.2, the relative baseline expression levels of *NOX1*, *2*, *5* and *DUOX1* were significantly higher in the Ishikawa cells compared to the Caco-2 cells with *NOX1* being the most expressed isoform. *NOX3* and *NOX4* were not detected in either of the two cell lines.

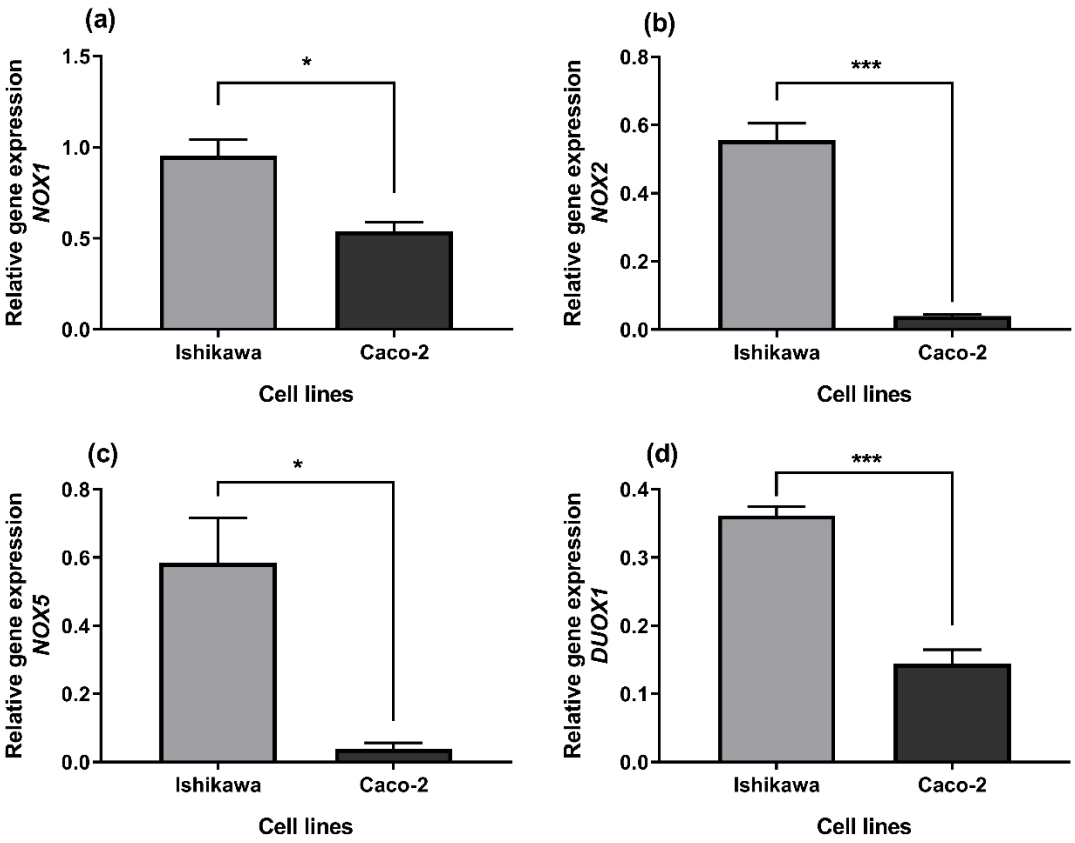

Figure 4.2. Comparison of the relative expression levels of *NOX* family between the untreated Ishikawa and Caco-2 cells. The columns represent the relative gene expression levels of the *NOX1* (**a**), *NOX2* (**b**), *NOX5* (**c**) and *DUOX1* (**d**) using TaqMan qPCR. Data are mean ± SEM (*N*=3 separate experiments); *p* values comparing Ishikawa and Caco-2 were calculated using two-tailed t-test; ns, not significant, **p*<0.05 and ****p*<0.001.

4.2.3 Higher anti-oxidants expression observed in Ishikawa

To demonstrate the influence of the antioxidant system on the differences in the redox status between the Ishikawa and Caco-2 cells, the antioxidant profiles of the two cell lines were compared.

The TaqMan qPCR results showed that the relative baseline gene expression levels of the four antioxidant genes, *SOD1*, *SOD2*, *CAT* and *GPx*, were significantly higher in the Ishikawa cells compared to the Caco-2 cells. Moreover, the relative baseline expression level of the nuclear factor erythroid 2-related factor 2 (*Nrf2*), a prime regulator of redox homeostasis in response to oxidative stress, was also significantly higher in the Ishikawa cells (Figure 4.3 a-e). The mRNA expression patterns of *SOD1*, *SOD2* and *CAT* genes in the Ishikawa and Caco-2 cells were largely mirrored at the protein expression level as observed by western blot (Figure 4.3 f-h). However, the protein expression of GPx and Nrf2 were not analysed in this study due to technical issues with the antibodies.

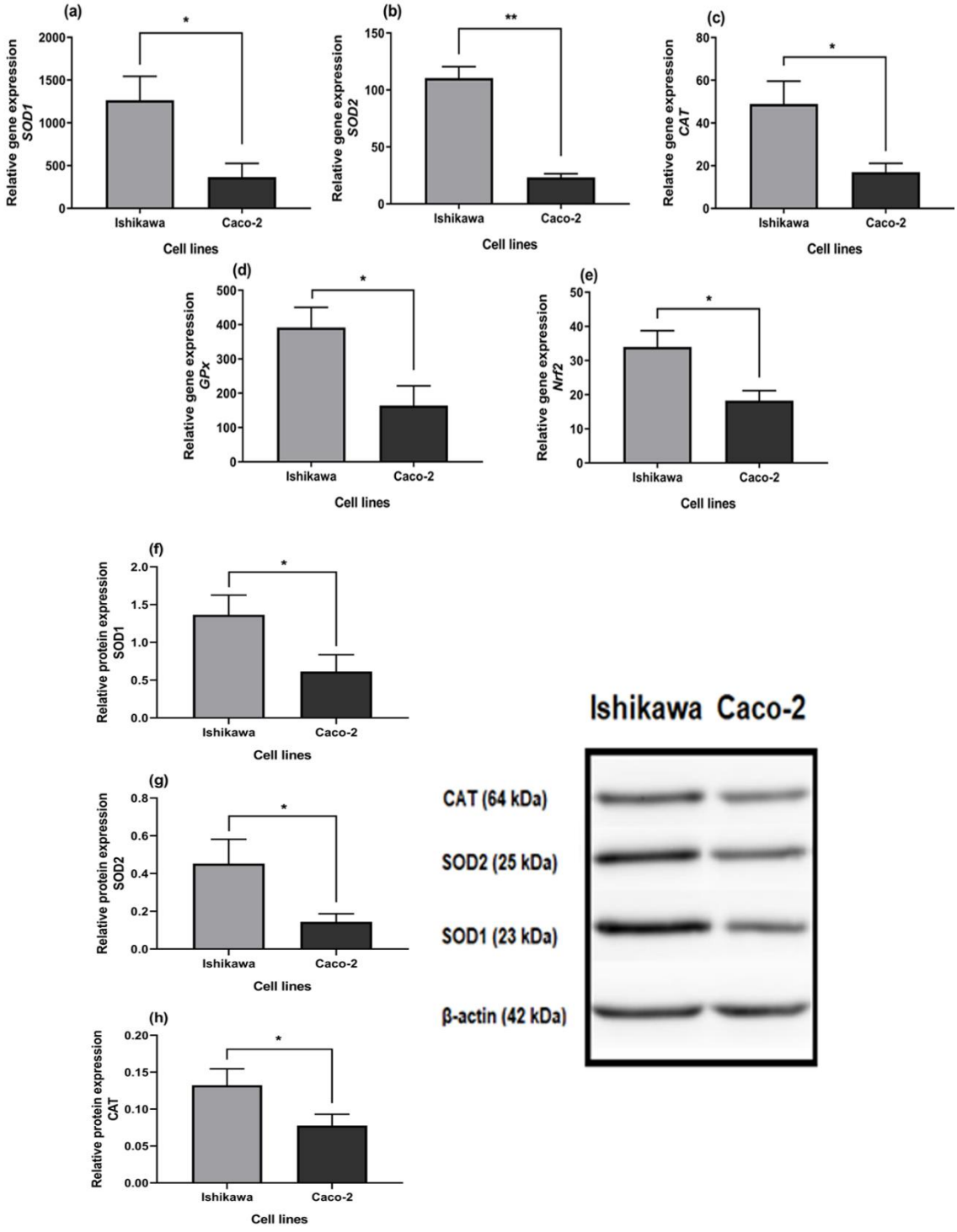

Figure 4.3. Comparison of the relative expression levels of antioxidants between the untreated Ishikawa and Caco-2 cells. The columns represent the relative gene expression levels of the *SOD1* (**a**), *SOD2* (**b**), *CAT* (**c**), *GPx* (**d**) and *Nrf2* (**e**) using TaqMan qPCR. Western blots showing the protein levels of SOD1 (**f**), SOD2 (**g**) and CAT (**h**) in the Ishikawa and Caco-2 cells. The columns represent the protein levels normalised against the loading control protein β-actin. Data are mean ± SEM (N=3 separate experiments); p values comparing Ishikawa and Caco-2 were calculated using two-tailed t-test; *p<0.05 and **p<0.01.

4.2.4 Upregulation of mitochondria-related survival genes in Caco-2

To elucidate the impact of the variations in baseline ROS level on the mitochondrial dynamics, some key mitochondrial adaptation mechanisms were studied in Ishikawa and Caco-2.

The relative baseline expression levels of genes related to mitochondria conservation and protection of cells from stress-induced mitochondrial dysfunction such as optic atrophy 1 (*OPA1*) and PTEN-induced kinase 1 (*PINK1*) were evaluated using TaqMan qPCR. The results showed that the expression levels of both *OPA1* and *PINK1* genes were significantly higher in the Caco-2 cells compared to the Ishikawa cells (Figure 4.4).

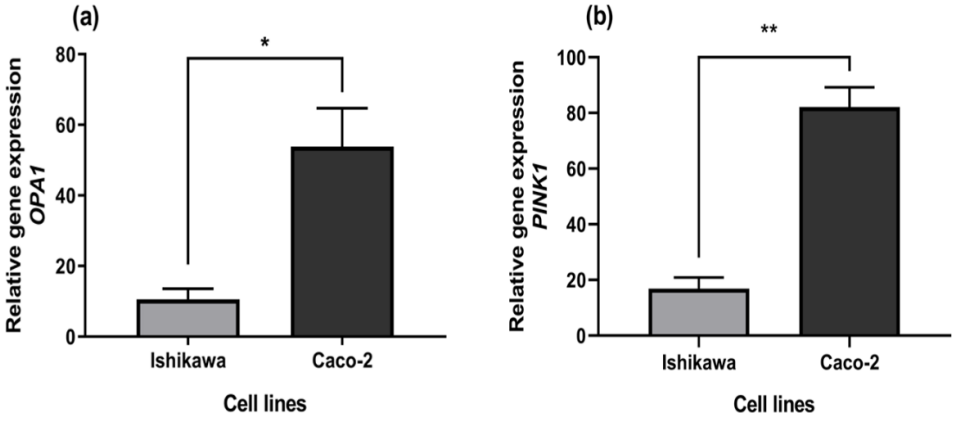

Figure 4.4. Comparison of the relative expression levels of the *OPA1* (**a**) and *PINK1* (**b**) genes between the untreated Ishikawa and Caco-2 cells. The columns represent the relative expression levels of the genes using TaqMan qPCR. Data are mean ± SEM (*N*=3 separate experiments); *p* values comparing Ishikawa and Caco-2 were calculated using two-tailed t-test; **p*<0.05 and ***p*<0.01.

4.2.5 Higher levels of pro-apoptotic proteins and drug resistance gene expression in Ishikawa

To gain further insights into the reasons for different sensitivity levels between the Ishikawa and Caco-2 cells towards the treatments, the relative baseline expression levels of some key genes involved in the intrinsic apoptosis pathway were investigated.

The TaqMan qPCR results showed that the relative baseline expression level of the anti-apoptotic gene *BCL-XL* was significantly higher in the Caco-2 cells (Figure 4.5 a) whereas all pro-apoptotic genes, *BAX*, *APAF-1* and cytochrome *c*, were significantly higher in the Ishikawa cells (Figure 4.5 b-d). The mRNA expression patterns of the *BCL-XL* and *BAX* genes in the Ishikawa and Caco-2 cells were largely mirrored at the protein expression level as observed by western blot (Figure 4.5 e-f). However, the protein expression of APAF-1 and cytochrome *c* were not analysed in this study due to technical issues.

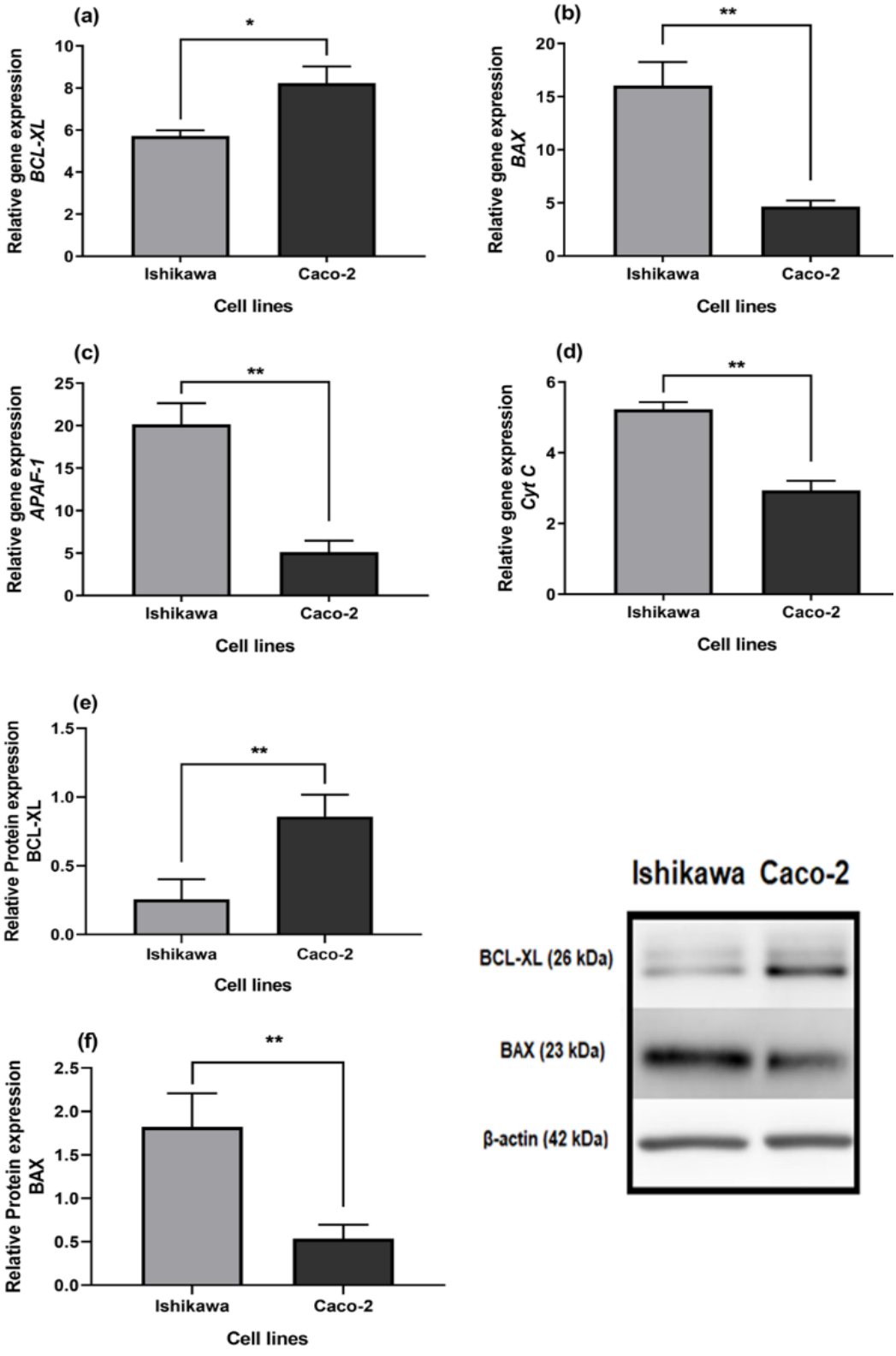

Figure 4.5. Comparison of the relative expression levels of apoptosis-associated genes between the untreated Ishikawa and Caco-2 cells. The columns represent the relative gene expression levels of the *BCL-XL* (a), *BAX* (**b**), *APAF-1* (**c**) and *Cyt C* (**d**) using TaqMan qPCR. Western blots showing the protein levels of BCL-XL (**e**) and BAX (**f**) in the Ishikawa and Caco-2 cells. The columns represent the protein levels normalised against the loading control protein *β*-actin. Data are mean ± SEM (*N*=3 separate experiments); *p* values comparing Ishikawa and Caco-2 were calculated using two-tailed t-test; **p*<0.05 and ***p*<0.01.

The multi-drug resistance protein 1 (MDR1) is an important protein of the cell membrane that acts as an efflux pump for many foreign substrates. Therefore, the expression level of *MDR1* was investigated to elucidate its impact on the differences in drug sensitivity between the Ishikawa and Caco-2 cells towards the treatments. The TaqMan qPCR results showed that the relative baseline expression level of the *MDR1* gene was significantly higher in the Ishikawa cells compared to the Caco-2 cells (Figure 4.6).

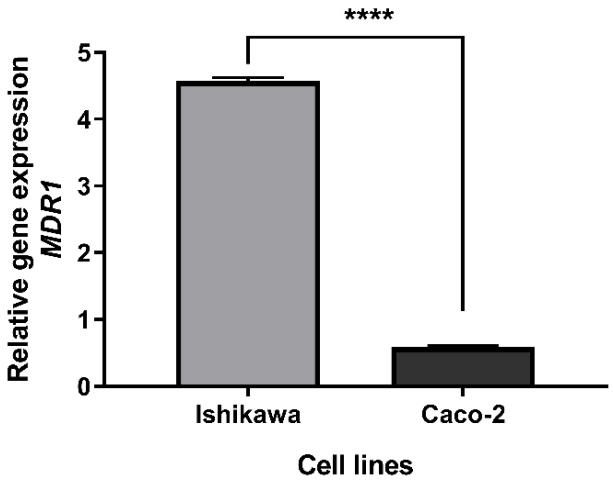

Figure 4.6. Comparison of the relative gene expression levels of the *MDR1* gene between the untreated Ishikawa and Caco-2 cells. The columns represent the relative expression levels of the gene using TaqMan qPCR. Data are mean ± SEM (*N*=3 separate experiments); *p* values comparing Ishikawa and Caco-2 were calculated using two-tailed t-test; ****$p<0.0001$.

4.2.6 Enhanced DNA repair in Caco-2

Cells with higher baseline ROS levels are expected to have higher potential for DNA damage, and therefore cells enhance their DNA repair systems to avoid the accumulation of DNA damage and grant cell survival. To elucidate the impact of the variations in baseline ROS level on cell's response to DNA damage, the activation of the ATR-Chk1 pathway and expression levels of a key player engaged in other DNA repair mechanisms (OGG1) were analysed and compared in the Ishikawa and Caco-2 cells.

The TaqMan qPCR and western blotting results showed that the relative baseline expression levels of the OGG1 gene and protein were significantly higher in the Caco-2 cells compared to the Ishikawa cells (Figure 4.7 a & b).

Western blotting results showed that the phosphorylated proteins of Chk1 at Ser-317 and ATR at The-1989 were significantly higher in the Caco-2 cells (Figure 4.7 c & d) indicating that the ATR-Chk1 pathway was markedly over activated in the Caco-2 cells compare to the Ishikawa cells.

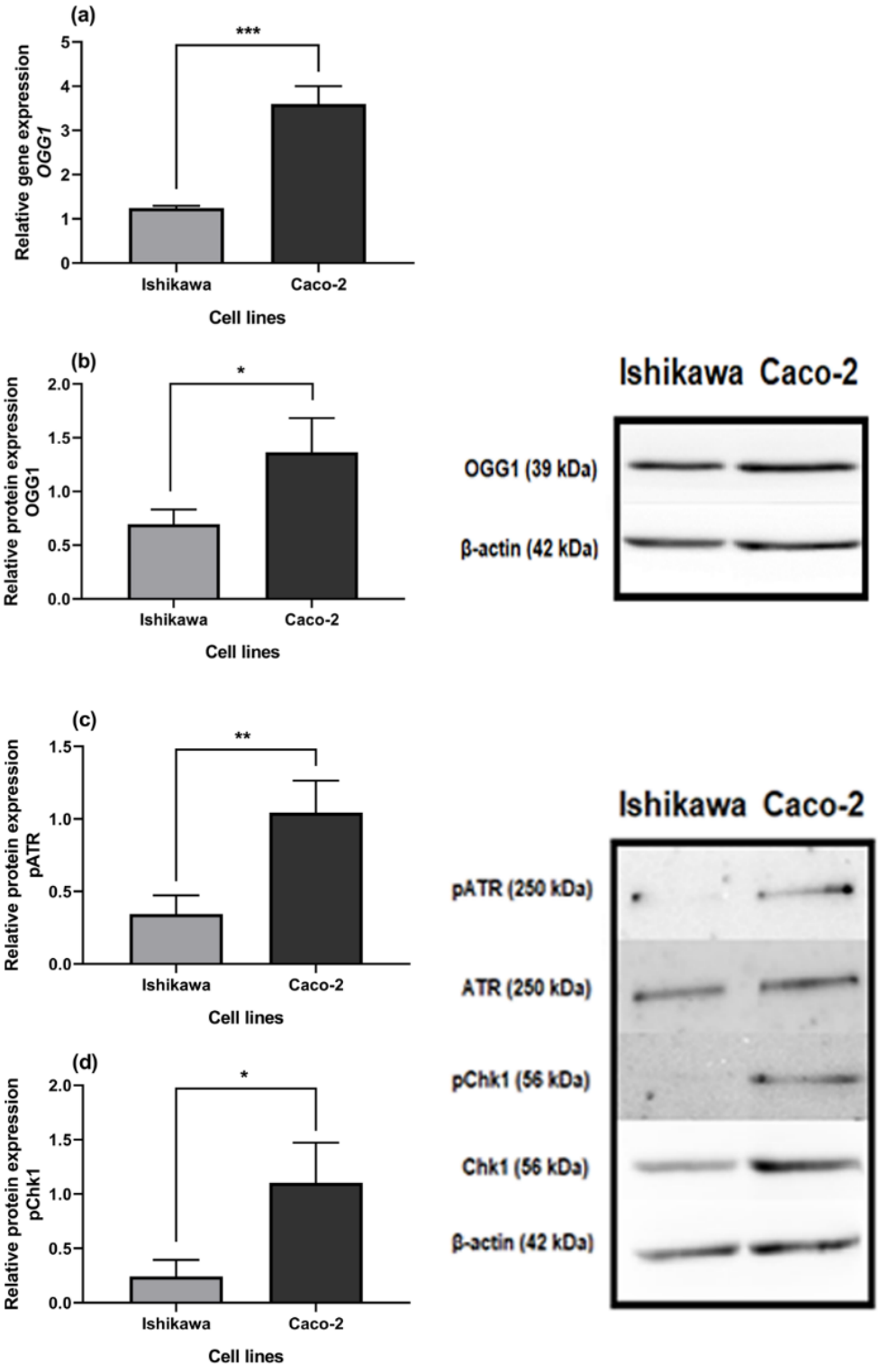

Figure 4.7. Comparison of the relative expression levels of OGG1 and the activation of the ATR-Chk1 pathway between the untreated Ishikawa and Caco-2 cells. (**a**) Comparison of the relative gene expression levels of the *OGG1* gene between untreated Ishikawa and Caco-2. The columns represent the relative gene expression levels of the *OGG1* using TaqMan qPCR. Western blots showing the protein levels of OGG1 (**b**) and phosphorylated ATR (pATR) (**c**) and phosphorylated Chk1 (pChk1) (**d**) in Ishikawa and Caco-2. The columns represent the protein levels normalised against the loading control protein *β*-actin for OGG1, and total ATR and Chk1 for pATR and pChk1, respectively. Data are mean ± SEM (N=3 separate experiments); p values comparing Ishikawa and Caco-2 were calculated using two-tailed t-test; *p<0.05, **p<0.01 and ***p<0.001.

4.3 Discussion

Among the cancer cell lines enrolled in our study, Ishikawa (endometrium) and Caco-2 (colon) were employed as *in vitro* models in the downstream investigations to represent cancer cells with the lowest and highest baseline intracellular ROS levels respectively. Given that both cell lines belong to different tissue origins, certain cellular and molecular factors might have led to the variations in the baseline intracellular ROS level as well as the sensitivity towards ROS-stimulating agents between these two cell lines.

In this chapter, such differences between the Caco-2 and Ishikawa cells are explained based on some of the key molecular mechanisms for ROS-related drug resistance.

4.3.1 Higher intracellular ROS level linked to higher mtDNAcn

Mitochondria are well known to be the powerhouse of the cell, and the amount of ATP produced in mitochondria is influenced by the abundance of the organelles and the number of mtDNA copies according to the cell type and the physiological conditions [105].

Since mitochondria are the primary source of intracellular ROS as side-products of the mitochondrial electron transport chain reaction during cellular respiration (reviewed in Ref. [65]), it was necessary to compare the mitochondrial content levels between Ishikawa and Caco-2 in order to evaluate the impact of mitochondrion quantity on their ROS levels. Interestingly, comparable mitochondrial content levels were detected in the Ishikawa and Caco-2 cells using the MitoTracker™ Red CMXRos staining in our study. This result indicates that the difference in the baseline ROS level between Ishikawa and Caco-2 may be independent of the abundance of mitochondria within the cells. This finding also suggests that the baseline ROS level (either intracellular or mitochondrial superoxide) might be more indicative of drug response compared to the abundance of the organelles in the cells.

Generally, cancer cells with a higher demand for ATP can increase their mtDNAcn in each mitochondrion to produce more subunits for the OXPHOS or upregulate mitochondrial fission to produce additional copies of the existing organelles; either of the two mechanisms helps the cell achieve the required energy. Therefore, it appears that the Caco-2 cells require a higher level of cellular energy compared to the Ishikawa cells, and this is achieved by increasing the mtDNAcn only without the need for mitochondrial replication.

It is widely acknowledged that each mitochondrion can contain 2-10 copies of the mitochondrial genome [87], and its copy number is preserved within a stable range to achieve the required energy of the cell and hence to ensure normal physiological functions [146]. Therefore, since the Caco-2 cells had higher mtDNAcn compared to the Ishikawa cells, we speculate that the average copy number of mtDNA per mitochondrion must be far greater in a single Caco-2 cell than that in a single Ishikawa cell. In addition, our data suggest that the copy number of the cell's mtDNA, rather than its mitochondrion quantity, may have a more influential role in mitochondrial superoxide production.

4.3.2 Different redox statuses between Caco-2 and Ishikawa

The NADPH oxidases (NOXs) are important sources of cellular reactive oxygen species. Seven NOX homologues are present in the human genome: *NOX1-5*, *DUOX1* and *DUOX2* which differ in their expression level and type of ROS release (reviewed in Ref. [309]). It has been reported that ROS generated by the NOXs are essential for cell growth in prostate cancer cells [208]. Therefore, the relationship between the baseline ROS levels and the mRNA expression levels of the NOX isoforms in Ishikawa and Caco-2 was determined.

Interestingly, our results showed that *NOX1*, *NOX2*, *NOX5* and *DUOX1* were significantly overexpressed in the Ishikawa cells compared to the Caco-2 cells whereas *NOX3* and *NOX4* were not expressed in either of the cell lines. This observation could have been translated into the outcome that Ishikawa should be the cell line with the higher ROS level, which was not the case in our study (our DCFDA and MitSOX results showed that Caco-2 had the highest ROS level among the 4 cancer cell lines). This finding suggests that the overexpression of *NOXs* in the Ishikawa cells has not resulted in an overall high level of intracellular ROS in Ishikawa. It also indicates that mitochondria are the main source of ROS generation in the cells investigated in our study. Collectively, the above observations strongly indicate that mitochondrial genetic abnormalities would have been the main influencer in ROS production (further discussion will be covered in Chapter 6).

To gain further insight into the reason behind the different baseline ROS levels between the Ishikawa and Caco-2 cells, the expression levels of four antioxidant enzymes, SOD1, SOD2, CAT and GPx, and the expression level of the transcription factors Nrf2 which regulates the expression of genes involved in the cellular antioxidant system were

analysed. Our data showed that the expression levels of these antioxidant genes were significantly lower in the naïve Caco-2 cells compared to Ishikawa. This could explain the differences in the baseline ROS level between the two cell lines, since cells producing less antioxidants are expected to have an inefficient ROS scavenging system, resulting in higher baseline ROS level in those cells.

All the aforementioned data elucidate that different ROS levels in the two cell lines are related to the variations in their mitochondrial function and antioxidant systems, making them good candidates for our *in vitro* study.

4.3.3 Greater adaptability of Caco-2 to oxidative stress

To test our theory that the different ROS-associated drug sensitivity levels seen in Ishikawa and Caco-2 were affected by the variations in their mitochondrial abnormalities, the expression levels of genes related to mitochondrial function were evaluated by TaqMan qRT-PCR.

The optic atrophy 1 (OPA1) is a nuclear-encoded mitochondrial protein. It localises on the inner mitochondrial membrane and helps regulate mitochondrial stability and energy output. It also mediates the fusion of inner membranes to facilitate the union of two mitochondria into one mitochondrion. This fusion phenomenon helps cells moderate stress by sharing multiple elements that sustain mitochondrial biology [9]. Moreover, stabilisation of mitochondrial cristae by OPA1 protects cells from mitochondrial dysfunction, cytochrome *c* release and ROS-induced damage, thus preventing cell death [310].

Indeed, our results showed that the *OPA1* gene was overexpressed in the Caco-2 cells compared to the Ishikawa cells confirming the adaption of the Caco-2 cells to the escalated oxidative stress condition, which may result in their enhanced resistance to ROS-stimulating agents.

Our result was in agreement with that reported by Fang *et al*. [311] who showed that lung cancer cells with higher *OPA1* expression were more resistant to cisplatin. Moreover, a study conducted by Santin *el al*. demonstrated that *OPA1*-mediated mitochondrial fusion was responsible for cisplatin resistance in the neuroblastoma B50 rat cells, and silencing the expression of *OPA1* mitigated the cisplatin resistance [312].

Mitophagy is a fundamental process which contributes to mitochondrial quality control and exploits the same core machinery of autophagy through the formation of autophagosomes and autolysosomes (reviewed in Ref. [313]). However, several mitophagy effectors have been identified including the mitophagy receptors such as NIX, BNIP3 and FUDNC1 and several mediators in the PINK1/Parkin pathway [15,314].

PTEN-induced kinase 1 (PINK1) is a mitochondrial serine/threonine-protein kinase encoded by the *PINK1* gene that plays a role in protecting cells from stress-induced mitochondrial dysfunction. PINK1 is involved with mitochondrial quality control by identifying damaged mitochondria and targeting specific mitochondria for degradation. Its activity causes the parkin protein (a ubiquitin ligase that plays a critical role in ubiquitination) to bind to depolarised mitochondria and subsequently induce selective autophagy of those mitochondria (mitophagy) [315,316]. PINK1 has also been shown to facilitate the generation of mitochondria-derived vesicles which can shuttle ROS toward lysosomes for degradation [317].

Indeed, our results showed that *PINK1* gene was overexpressed in the Caco-2 cells compared to the Ishikawa cells, indicating the greater capability of Caco-2 to adapt to the increased oxidative stress condition. This was achieved by upregulating the pro-survival mechanism through the elimination of the dysfunctional mitochondria, and as a result of it, the Caco-2 cells also became more resistant to ROS-stimulating agents.

Our observation was echoed by Su *et al.* [318] who demonstrated that triggering mitophagy by overexpression of galactin-1 (Gal-1, a protein encoded by the *LGALS1* gene and involved in many biological processes such as cell proliferation, differentiation and tumour progression) resulted in cisplatin resistance in hepatocellular carcinoma. This study showed that Gal-1 was capable of reducing the loss of mitochondrial potential and apoptosis induced by cisplatin treatment by inducing mitophagy via BNIP3 upregulation [318]. Moreover, other studies demonstrated that inhibition of the mitophagy pathways and downregulation of the mitophagy receptors such as BNIP3 and FUDNC1 chemosensitised cancer cells [319,320]. A study by Datta *et al*. [321] has also shown that inhibition of autophagy with chloroquine prevented the development of paclitaxel resistance and potentiated the effect of paclitaxel by increased accumulation of superoxide-producing damaged mitochondria.

A recent study by Green *et al*. [322] has shown that telomerase, beside its role in telomere stabilisation, seems to play a role in the response to oxidative stress. Results suggest that the cells expressing the mutant telomerase had significant increases in autophagy markers as a response to H_2O_2 challenge. These results suggest that the loss of hTERT in mitochondria initiates a signalling cascade that allows for cells to adapt to and cope with the lack of mitochondrial telomerase. Such effects also influence the cellular response to oxidative damage.

Given that both *OPA1* and *PINK1* are overexpressed in the Caco-2 cells compared to the Ishikawa cells, it is speculated that the Caco-2 cells have greater potential to cope with severe oxidative stress induced by the treatments and therefore are more resistant than Ishikawa.

4.3.4 Higher resistance in Caco-2

Many mechanisms may contribute to cisplatin resistance including the inhibition of apoptosis, increased drug efflux, upregulation of DNA repair and other survival mechanisms (reviewed in Ref. [323]). However, different cancer cells display various levels of resistance according to the efficiency of their mechanisms. Therefore, how Ishikawa and Caco-2 responded to ROS-induced apoptosis was investigated with a focus on the pro- and anti-apoptotic pathways.

Beside their vital role in biosynthetic processes such as ATP generation, mitochondria play a central role in apoptotic cell death (reviewed in Ref. [52]). The mitochondrial intrinsic pathway is highly regulated by certain members of the BCL-2 protein family which control the release of pro-apoptotic proteins that facilitate the activation of caspase 9, such as cytochrome *c*, leading to apoptosis [26].

Given the importance of the role of mitochondria in apoptosis, it is not surprising that downregulation of pro-apoptotic BCL-2 family proteins as well as overexpression of anti-apoptotic BCL-2 family proteins have the propensity to allow cells to acquire resistance to apoptosis [35]. Several studies have shown that cancer cells overexpress anti-apoptotic proteins (e.g. BCL-XL) that inhibit the function of the key apoptotic effectors BAX or BAK and consequently prevent the formation of permeable pores and the release of pro-apoptotic molecules such as cytochrome *c* (reviewed in Ref. [52]).

To correlate the drug sensitivity level to the apoptosis condition in the Ishikawa and Caco-2 cells, the relative mRNA and protein levels of the key apoptosis mediators were analysed. Our data showed that the expression level of the anti-apoptotic protein BCL-XL was significantly lower in the naïve Ishikawa cells whereas all pro-apoptotic proteins BAX, APAF-1 and cytochrome *c* were significantly lower in the Caco-2 cells. Taken together, these results may explain the different drug responses of the two cell lines, Ishikawa being more vulnerable to oxidative stress due to higher pro-apoptotic activities and low levels of anti-apoptotic proteins whereas Caco-2 being more resistant thanks to the more powerful anti-apoptotic mechanisms.

The correlation between inhibition of apoptosis and drug resistance does not only apply to cisplatin but also extends to ROS-stimulating agents generally. As mentioned earlier (Section 1.3.6), excessive ROS level is a key factor in facilitating MPTP opening by promoting the ubiquitination of the anti-apoptotic protein BCL-2, thus allowing the activation and oligomerisation of BAX and BAK resulting in permeabilisation of mitochondrial membranes and the release of apoptosis-inducing proteins such as cytochrome *c* (reviewed in Refs. [99,160]). Therefore, it is not surprising that cells with higher expression of BCL-XL require more drug to produce sufficient ROS level to abate its anti-apoptotic activity.

On the other hand, enhanced drug efflux can also contribute to the drug-resistance phenotype by affecting a net decrease in drug intake. The ABC superfamily is the most abundant trans-membrane protein family that plays essential roles in pumping chemo drugs out of the cells, leading to reduced drug concentrations in the cells and thus resulting in the failure of chemotherapy (reviewed in Ref. [324]). So far, 49 members of the ABC superfamily have been discovered and ABCB1, also known as multidrug resistance protein 1 (MDR1), is considered as the predominant member because of its special role in chemo resistance (reviewed in Refs. [325,326]). MDR1 is a 170 kDa ATP-dependent membrane transporter that is widely distributed throughout the body and pumps many foreign substances out of the cells (reviewed in Ref. [327]). Overexpression of *MDR1* has been associated with various types of cancers, and several previous studies have revealed that cisplatin resistance is correlated with increased expression of *MDR1* and downregulation of *MDR1* attenuates cisplatin resistance [328,329].

In our study, since the Caco-2 cells were more resistant to cisplatin compared to the Ishikawa cells, we speculated that the Caco-2 cells would have a higher expression level of *MDR1*. Surprisingly, our results showed that the expression level of *MDR1* was significantly higher in the Ishikawa cells. This observation indicates that the enhanced drug efflux in the Ishikawa cell line could not account for its greater cisplatin sensitivity compared to Caco-2. It also further confirms that cellular redox status is the main regulator of drug response between the two cell lines. However, since only 1 out of 49 of the ABC superfamily members was investigated in this study, it is possible that other ABC proteins might be overexpressed in the Caco-2 cells rendering their higher resistance to the treatments. Further investigation into the expression levels of other key members of the ABC superfamily would shed some light on this theory.

The increased rate of repair of cisplatin-induced DNA damages constituting an essential mechanism of cisplatin resistance and the consequential decrease in cisplatin-mediated cell death has been demonstrated in several human tumour cell lines (reviewed in Ref. [330]). Generally, once cisplatin-induced DNA lesions occur, cells must remove them otherwise those DNA damages will lead to massive cell death. Several DNA repair systems are involved in removing cisplatin-induced DNA damage including nucleotide excision repair (NER), mismatch repair (MMR) and base excision repair (BER) [331].

Since cells have different baseline ROS levels, it is speculated that those with higher ROS levels are more vulnerable to oxidative DNA damage and therefore require an enhanced correction mechanism to avoid the accumulation of DNA lesions and to evade cell death. Indeed, our results showed that the Caco-2 cells had higher expression level of OGG1 which mainly removes 8oxoG adducts (the most dominant mutagenic lesions generated by ROS) [73]. As mentioned earlier, it has been postulated that the anti-tumour effect of cisplatin and dequalinium is associated to ROS generation [270,271,304,332]. Therefore, the efficiency of the mechanism responsible for correcting DNA lesions generated by ROS could contribute to drug resistance. Having a higher baseline expression level of OGG1 might have rendered the higher resistance to ROS-stimulating agents in the Caco-2 cells compared to the Ishikawa cells.

DNA lesions alter the transcription and synthesis of DNA, which in turn triggers an orchestrated signal transduction cascade to clear the lesions. Once the cell cycle is arrested, adequate time for DNA repair is provided to remove the lesions through various mechanisms, or cell death occurs if DNA damage is irreversible (reviewed in Ref. [249]).

ATR (ataxia telangiectasia and Rad3-related) is essential for sensing DNA damage and activating the DNA damage checkpoint, resulting in cell cycle arrest [333]. Once ATR is activated in the cell due to DNA damage, it phosphorylates checkpoint kinase 1 (Chk1) which facilitates DNA damage repair by activating several repair factors such as PCNA, Rad51 and FANCE [196]. ROS-stimulating agents are well known to cause DNA damages, and therefore the efficiency of the ATR-Chk1 pathway is highly susceptible to influence the level of response to the treatments. The best way to evaluate the correlation of the cisplatin / dequalinium resistance with the ATR-Chk1 pathway is to examine and compare the activation state of ATR-Chk1 in both Ishikawa and Caco-2 cells.

Our results showed that the phosphorylation of ATR and Chk1 was significantly higher in the naïve Caco-2 cells compared to the Ishikawa cells. Knowing that the Caco-2 cells have a higher baseline ROS level which might result in a higher rate of DNA damage, it would be well acceptable to conclude that the elevated ROS production has reinforced the active status of the ATR-Chk1 pathway in the Caco-2 cells for them to survive high frequency of DNA damage compared to Ishikawa.

Taking all together, higher baseline ROS levels act as a driving force to promote resistance to ROS-stimulating agents by activating the ATR-Chk1 pathway.

4.4 Summary

This chapter focused on the differential cellular and molecular profiles of the Ishikawa and Caco-2 cells and their impact on baseline intracellular ROS levels as well as drug sensitivity observed in both cell lines.

It was concluded that the variable ROS levels were mainly due to specific mitochondrial abnormalities and antioxidant system capacity of the cells.

Moreover, it was suggested that higher adaptability for oxidative stress via enhanced DNA repair mechanisms and upregulated anti-apoptotic pathways might explain increased resistance to ROS-stimulating agents, as observed in the Caco-2 cells in comparison with the Ishikawa cells.

Therefore, although the Ishikawa and Caco-2 cells belong to different tissue origins, which may cause some limitations to our study, the aforementioned data assert that the Ishikawa and Caco-2 cells are good *in vitro* models to investigate the possible underlying mechanisms of differential response to ROS-stimulating therapy.

Chapter 5

Cellular and molecular regulatory pathways in ROS-mediated cell death

5.1 Introduction

Playing a critical role in the regulation of apoptosis pathways makes mitochondria an attractive target for cancer therapy. Therefore, several therapeutic approaches have been proposed to target mitochondria for tumour elimination (reviewed in Ref. [99]).

The anti-apoptotic BCL-2 family proteins are well known to be overexpressed in many cancers and associated with cancer initiation and resistance to therapy by their attenuating the release of cytochrome *c* and inactivating other pro-apoptotic proteins. Therefore, preventing the interaction between the anti-apoptotic proteins (e.g. BCL-XL) and the apoptosis effectors (such as BAK and BAX) to allow pore formation in outer mitochondrial membrane (OMM) is one of the main strategies in cancer treatments (reviewed in Ref. [217]).

In this respect, elevated ROS levels have been shown to abate the anti-apoptotic activity of BCL-2 and to abrogate the ubiquination of BAX and BAD, thus allowing the activation and oligomerisation of BAX and BAK that result in the formation of a VDAC (voltage-dependent anion channel)-containing pore and permeabilisation of mitochondrial membranes to facilitate cytochrome *c* release (reviewed in Ref. [160]). Moreover, excessive ROS production has been shown to be a key factor in facilitating the induction of mitochondrial permeability transition (MPT) following oxidative modification of ANT (adenine nucleotide translocase), a major component of the MPT pore, thus resulting in cytochrome *c* release (reviewed in Ref. [99]).

Modulating the mitochondrial respiratory chain activity is another approach to cancer treatment (reviewed in Ref. [99]). Inhibition of OXPHOS by several inhibitors or by targeting the mitochondrial genome to form drug-mtDNA adducts has been shown to induce apoptosis mediated by ROS overproduction [86,99].

In this chapter, we report our investigation on the contribution of treatment-induced intracellular ROS to cell death. The modes of action of the two compounds and their combination were also assessed.

5.2 Results

5.2.1 Reduced cell death upon elimination of ROS

To elucidate the role of elevated intracellular ROS in cell death, cell viability of the Ishikawa and Caco-2 cells was evaluated upon the elimination of treatment-induced ROS by ROS scavenger. The MTS assay results showed that the cell death induced by CDDP, DQA and the combined treatment was significantly reduced by pre-incubation with N-Acetylcysteine (NAC; a powerful antioxidant) (Figure 5.1 a & b). Those data showed that cell death attenuation with the combined therapy in Caco-2 was more significant than that with the single treatments, whereas the attenuation in Ishikawa was comparable amongst different treatments. Furthermore, cell death attenuation upon pre-incubation with NAC was more significant in Ishikawa compared to Caco-2 (Figure 5.1 c).

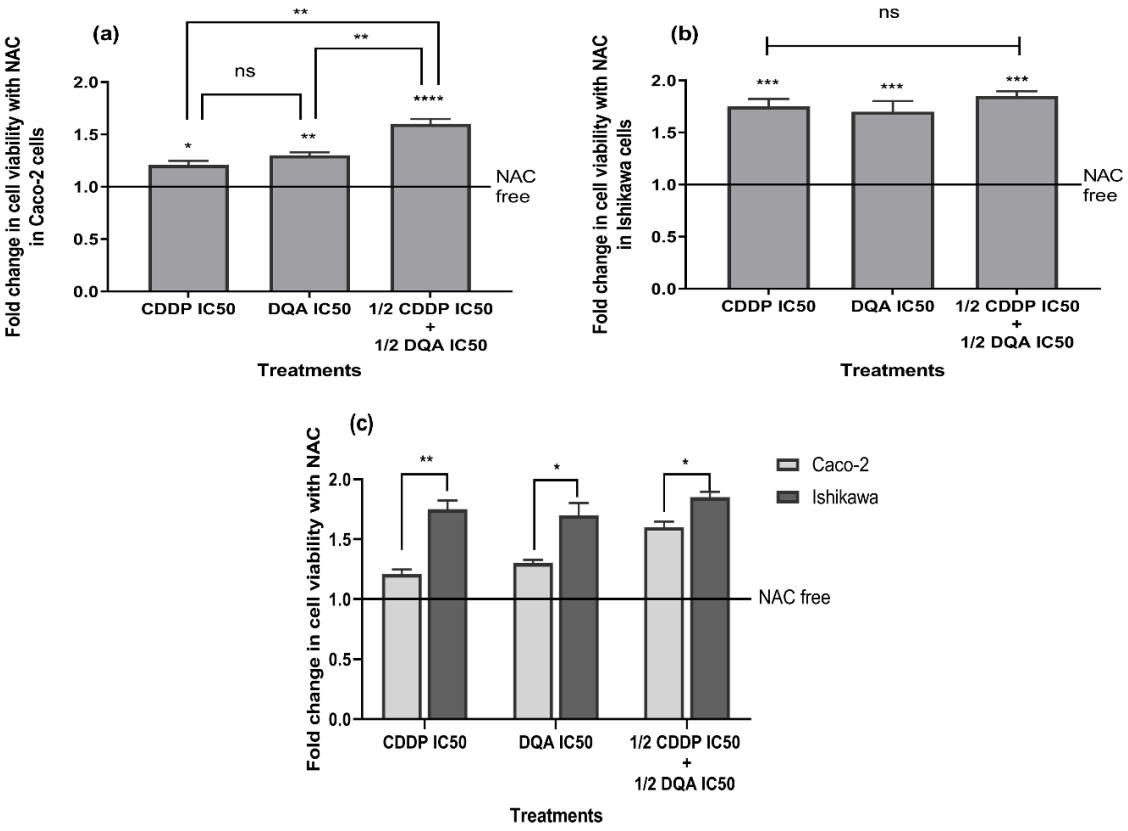

Figure 5.1. Effect of ROS generation on cell viability in the Caco-2 and Ishikawa cells detected by MTS assay. (**a** & **b**) Increased cell viability of Caco-2 and Ishikawa upon pre-incubation with NAC (10 mM) prior to the drug treatments. The columns represent the fold changes in cell viability normalised against NAC-free treatment. Data are mean ± SEM (*N*=3 separate experiments); *p* values comparing NAC-free and NAC-pre-incubated cells were calculated using one-way ANOVA with Tukey multiple comparison post-hoc analysis; ns, not significant, **p*<0.05, ***p*<0.01, ****p*<0.001 and *****p*<0.0001. (**c**) Comparison of the changes in cell viability between Caco-2 and Ishikawa upon pre-incubation with NAC. Data are mean ± SEM (*N*=3 separate experiments); *p* values comparing Caco-2 and Ishikawa were calculated using two-tailed t-test; **p*<0.05 and ***p*<0.01.

The same trend of results was observed using the ApoTox-Glo™ Triplex Assay kit where cell viability and cytotoxicity were assessed by measuring two protease activities; one is a marker for cell viability and the other a marker for cytotoxicity. Results might not be statistically significant as they present data from just two experiments, however they appear to be consistent with the previous results.

Data in Figure 5.2 a & b confirm that the IC50s of CDDP and DQA (determined using MTS assay) caused 50% cell death and the combined treatment of CDDP and DQA at half of their IC50 concentrations resulted in further cell death in both cell lines. Data in Figure 5.2 c & d also show that the combined treatment of CDDP and DQA at half of their IC50 concentrations caused a marked increase in cytotoxicity compared to the single treatment in both cell lines. More importantly, the pre-incubation with NAC resulted in attenuations in cell death and cytotoxicity in both cell lines, more observed in the Ishikawa cells (Figure 5.2 a-d).

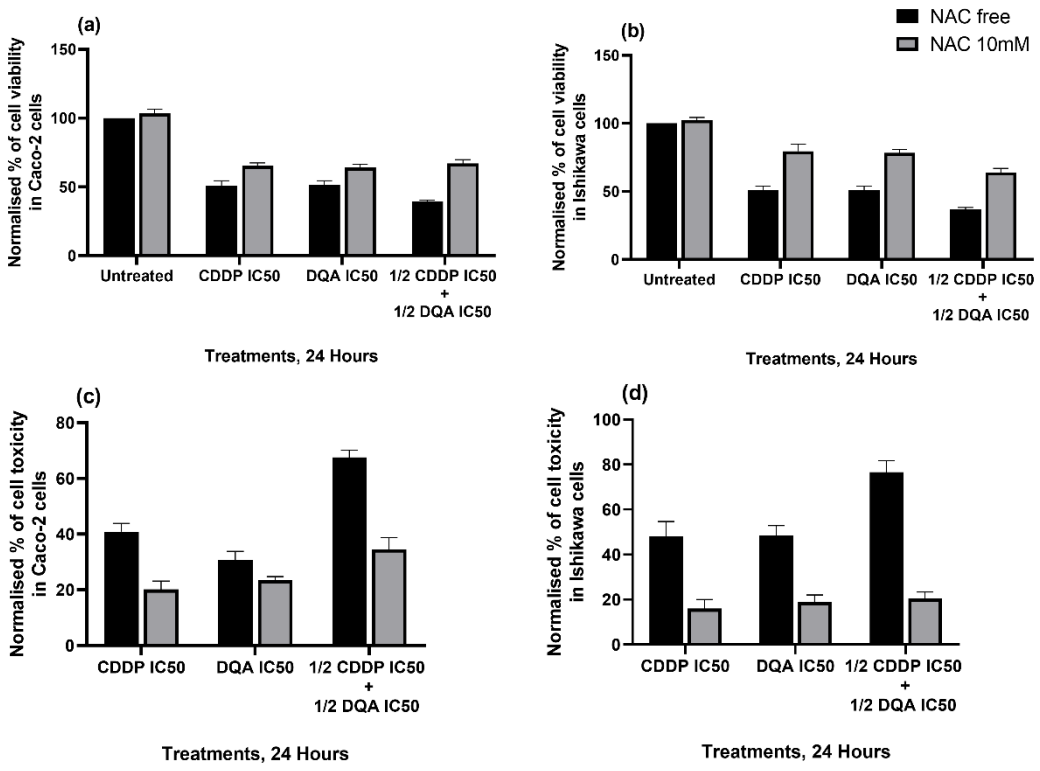

Figure 5.2. Effect of ROS generation on cell viability and cytotoxicity in the Caco-2 and Ishikawa cells detected using the ApoTox-Glo™ Triplex Assay kit. (**a** & **b**) Increased cell viability of Caco-2 and Ishikawa upon pre-incubation with NAC (10 mM) prior to the drug treatments. The columns represent cell viability under various treatment conditions normalised against the untreated controls. (**c** & **d**) Decreased cytotoxicity of Caco-2 and Ishikawa upon pre-incubation with NAC (10 mM) prior to the drug treatments. The columns represent cytotoxicity under various treatment conditions normalised against the untreated controls. Data are mean ± SEM (*N*=2 separate experiments).

5.2.2 Apoptosis events revoked upon elimination of ROS

Apoptosis and necrosis events were analysed by determining the cell surface exposure of phosphatidylserine (PS) and measuring propidium iodide (PI)-stained cells using flow cytometry. Early (annexin V-FITC (+)/PI (-)) and late (annexin V-FITC (+)/PI (+)) apoptosis events were significantly observed in both cell lines after 24 hours of incubation with CDDP, DQA and their combination. Data in Figure 5.3 show that pre-incubation with NAC resulted in a significant decrease in apoptosis events. Greater degrees of attenuation in apoptosis were clearly observed in the Ishikawa cells compare to the Caco-2 cells in all treatments.

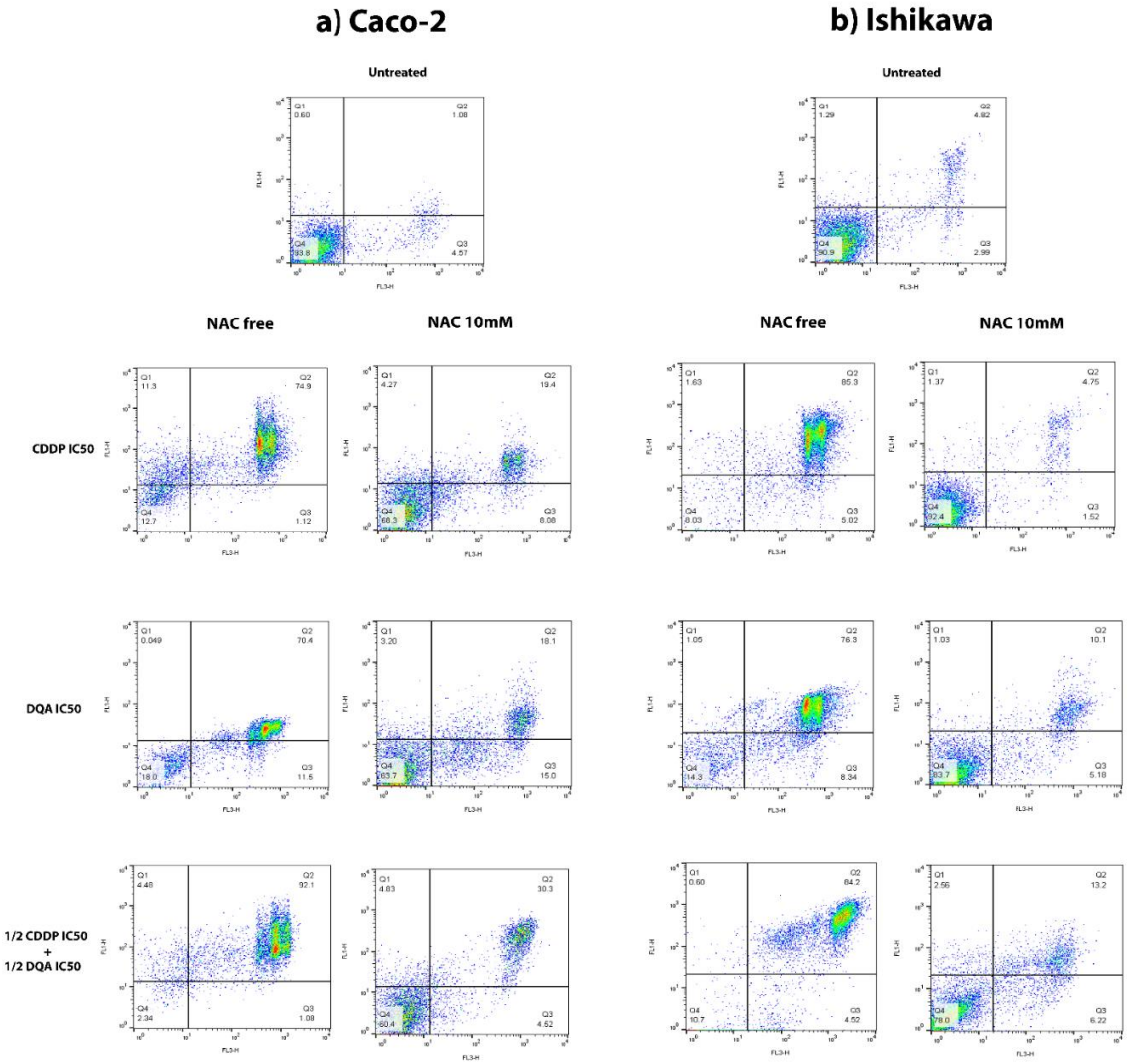

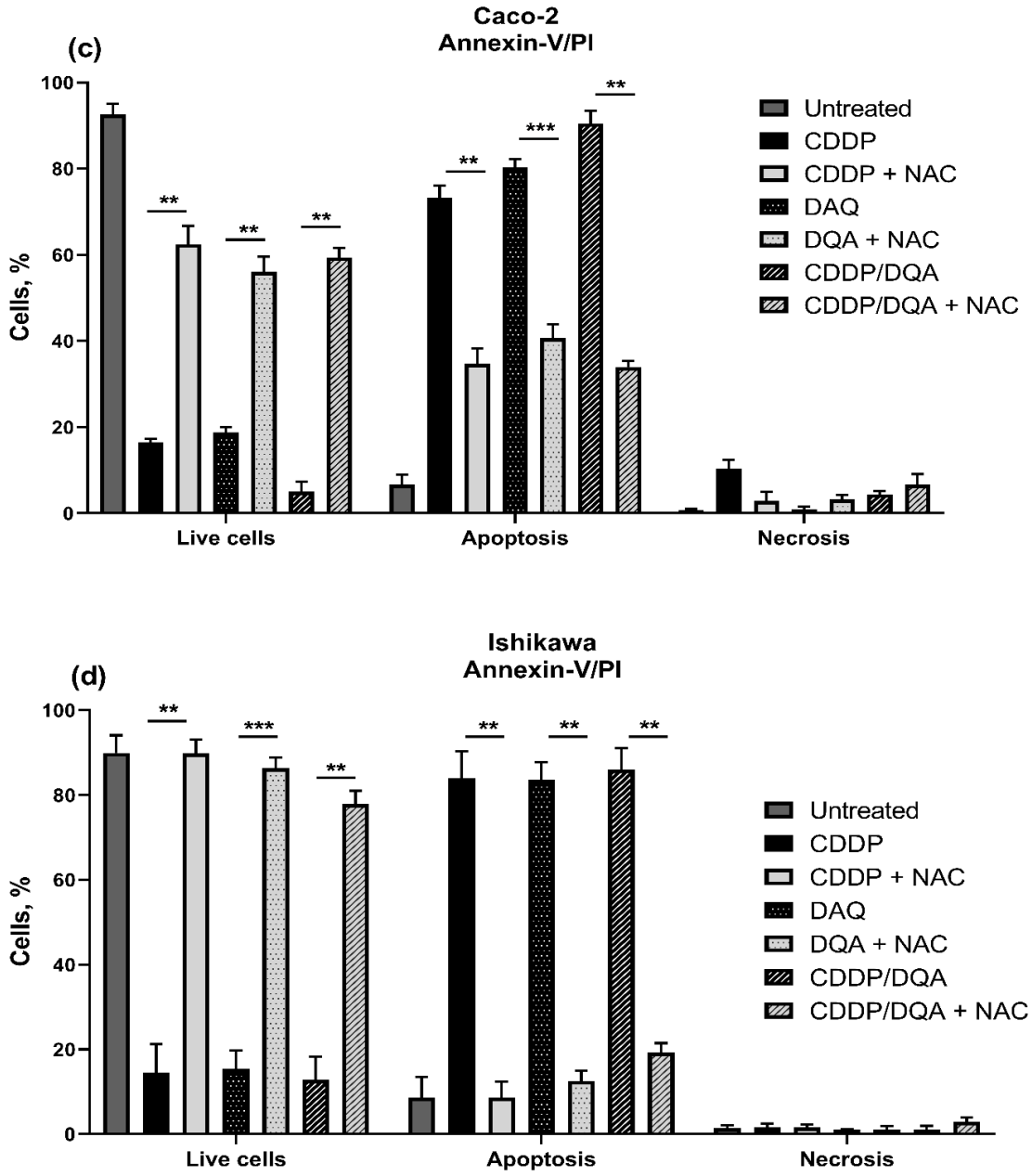

Figure 5.3. Effect of ROS generation on apoptotic cell death in the Caco-2 and Ishikawa cells detected by Annexin V-FITC/PI double staining. (**a** & **b**) Representative dot plot diagrams of flow cytometry assays with Annexin V-FITC/PI double staining of untreated cells, treated cells with/without NAC pre-incubation for Caco-2 and Ishikawa. Dots in the lower left quadrant area represented intact cells which were A^-/PI^-; dots in the lower right quadrant area represented early apoptotic cells which were A^+/PI^-; dots in the upper right quadrant area represented late apoptotic or necrotic cells which were A^+/PI^+; dots in the upper left quadrant area represented necrotic cells which were A^-/PI^+. (**c** & **d**) Percentage of cells obtained from the corresponding dot plot diagrams of Caco-2 and Ishikawa. Percentages are presented as the mean ± SEM (*N*=3 separate experiments); *p* values comparing NAC-free and NAC-pre-incubated cells undergone the same CDDP/DQA treatments were calculated using two-tailed t-test; $^{**}p<0.01$ and $^{***}p<0.001$.

To confirm apoptosis cascades and the impact of ROS generation induced by the treatments, caspase activation was measured using the ApoTox-Glo™ Triplex Assay kit. Data in Figure 5.4 a & b show a marked level of caspase-3/7 activation upon the treatments which was suppressed by NAC pre-incubation in both cell lines. Results might not be statistically significant as they present data from just two experiments, however they appear to be consistent with the previous results.

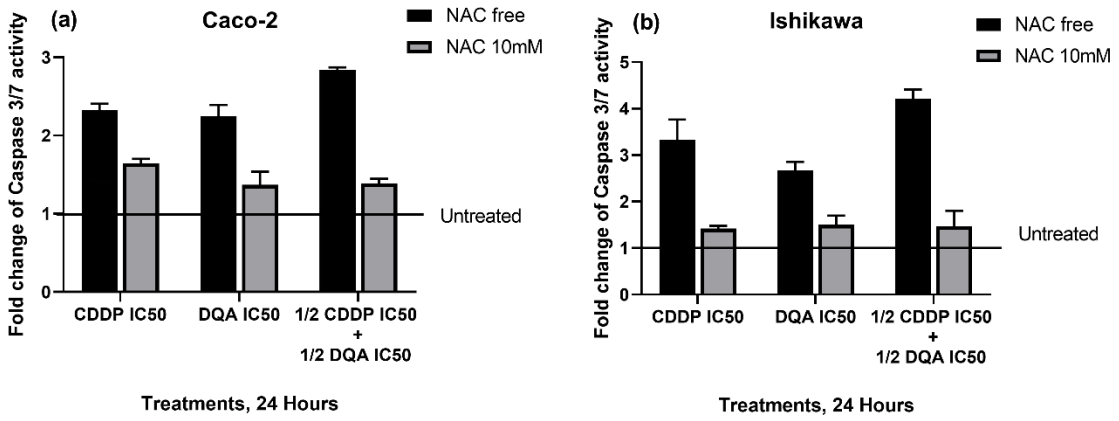

Figure 5.4. Effect of ROS generation on caspase activation. Caspase activity assay showing changes in caspase-3/7 activity in the Caco-2 (**a**) and Ishikawa (**b**) cells upon the treatments for 24 h and the effect of NAC pre-incubation in attenuating these changes in both cell lines. The columns represent the fold changes of caspase-3/7 activity normalised against the untreated cells. Data are mean ± SEM ($N = 2$ separate experiments); *p* values comparing CDDP/DQA-treated and -untreated cells without NAC pre-incubation were calculated using one-way ANOVA with Tukey multiple comparison post-hoc analysis; $^{**}p<0.01$ and $^{***}p<0.001$. *p* values comparing NAC-free and NAC-pre-incubated cells undergone the same CDDP/DQA treatments were calculated using two-tailed t-test; $^{*}p<0.05$ and $^{**}p<0.01$.

5.2.3 Excessive level of ROS provoked intrinsic apoptosis pathway

To further confirm that the cell death was due to ROS-induced apoptosis upon the treatments, apoptosis-associated proteins were measured in cells with or without the pre-incubation of NAC. For the cells without NAC pre-incubation, western blotting data showed significant decreases in the anti-apoptotic protein, BCL-XL, upon the treatments in both cell lines ($p<0.0001$; Figure 5.5 a & b), whereas the release of cytochrome *c* was significantly increased upon the treatments ($p<0.0001$; Figure 5.5 c & d). All the above events were significantly attenuated by NAC pre-incubation (Figure 5.5).

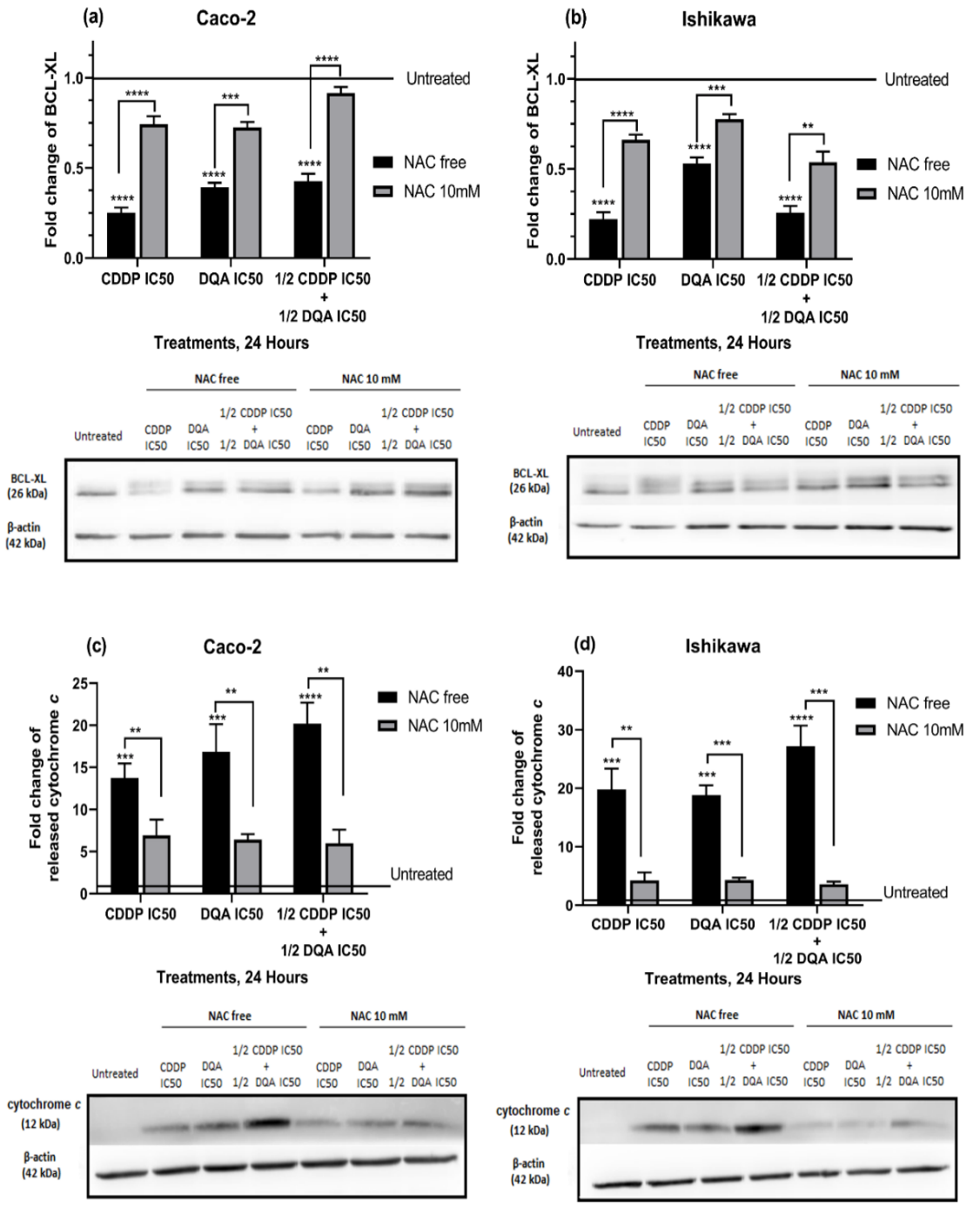

Figure 5.5. Effect of ROS generation on apoptosis-related proteins. Western blots showing changes in the protein levels of BCL-XL (lower bands, **a** & **b**) and the release of cytochrome *c* (**c** & **d**) in the Caco-2 and Ishikawa cells upon the treatments at 24 h and the effect of NAC pre-incubation in attenuating these changes. The columns represent the fold changes of the protein levels normalised against the loading control protein, *β*-actin. Data are mean ± SEM ($N = 3$ separate experiments); *p* values comparing CDDP/DQA-treated and -untreated cells without NAC pre-incubation were calculated using one-way ANOVA with Tukey multiple comparison post-hoc analysis; ***p<0.001 and ****p<0.0001. *p* values comparing NAC-free and NAC-pre-incubated cells undergone the same CDDP/DQA treatments were calculated using two-tailed t-test; **p<0.01, ***p<0.001 and ****p<0.0001.

Mitochondrial permeability transition pore (MPTP) is a mega channel complex involved in the intrinsic apoptosis process by releasing cytochrome *c* from intermembrane space (IMS) to cytosol. The main components of MPTP are VDAC in the outer mitochondrial membrane and ANT in the inner mitochondrial membrane (IMM) (reviewed in Ref. [334]). To determine the effect of the treatments on the structure of MPTP and the possible changes in MPTP caused by increased ROS production, the expression level of the voltage-dependent anion channel 1 (VDAC1) protein was measured in cells with or without the pre-incubation of NAC.

Western blotting data showed no significant changes in the VDAC1 protein expression upon the treatments irrespective of NAC pre-incubation in both cell lines (Figure 5.6 a & b).

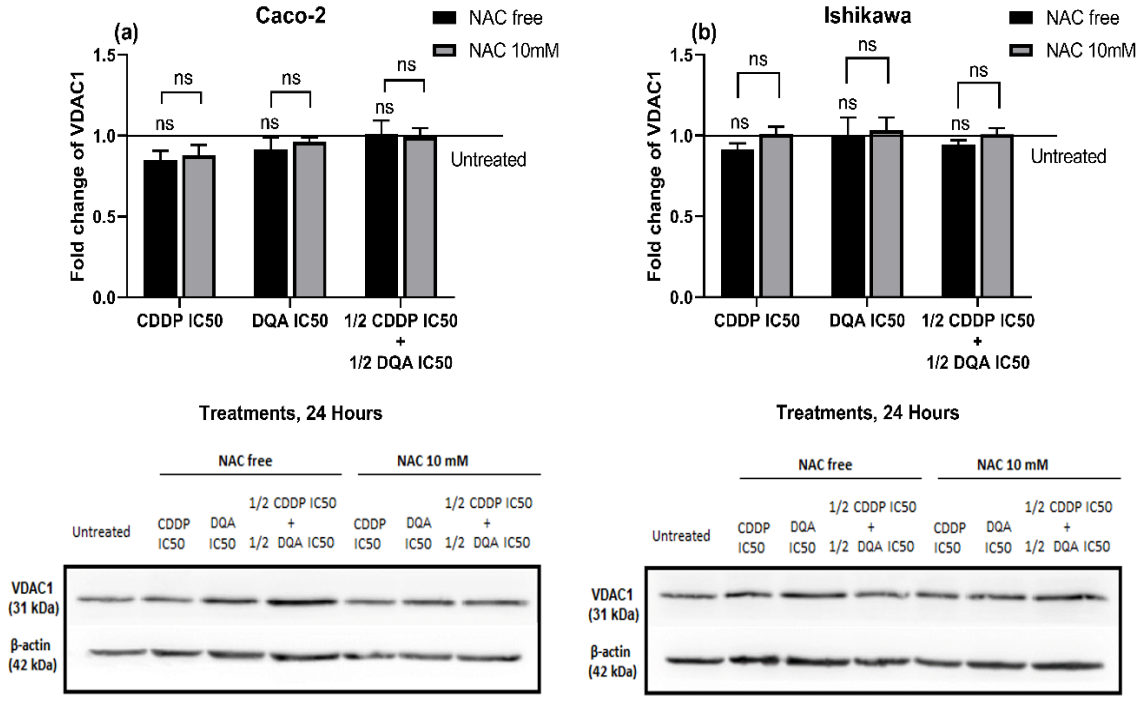

Figure 5.6. Effect of ROS generation on the VDAC1 protein expression. Western blots showing no significant changes in the protein levels of VDAC1 in the Caco-2 (**a**) and Ishikawa (**b**) cells upon treatments at 24 h and no obvious effect of NAC pre-incubation in both cell lines. The columns represent the fold changes of the protein levels normalised against the loading control protein, *β*-actin. Data are mean ± SEM ($N = 3$ separate experiments); *p* values comparing CDDP/DQA-treated and -untreated cells without NAC pre-incubation were calculated using one-way ANOVA with Tukey multiple comparison post-hoc analysis; ns, not significant. *p* values comparing NAC-free and NAC-pre-incubated cells undergone the same CDDP/DQA treatments were calculated using two-tailed t-test; ns, not significant.

5.2.4 Expression levels of mitochondrial function-associated genes altered upon the treatments

To assess potential mitochondrial dysfunction caused by the treatments, the expression levels of optic atrophy 1 (*OPA1*), endonuclease G (*ENDOG*) and ribonucleotide reductase regulatory TP53 inducible subunit M2B (*RRM2B*) were evaluated by TaqMan qPCR.

OPA1 was downregulated in the Caco-2 and Ishikawa cells in the presence of all treatments with a further decrease in the combined therapy in both cell lines (Figure 5.7 a & d). *ENDOG* was upregulated in both cell lines in the presence of all treatments with a further elevation in the DQA-alone and the combined treatments in Caco-2 (Figure 5.7 b), and in the cisplatin-alone treatment in Ishikawa (Figure 5.7 e). *RRM2B* was also upregulated in both cell lines with a further increase in the DQA-treated Caco-2 cells (Figure 5.7 c & g).

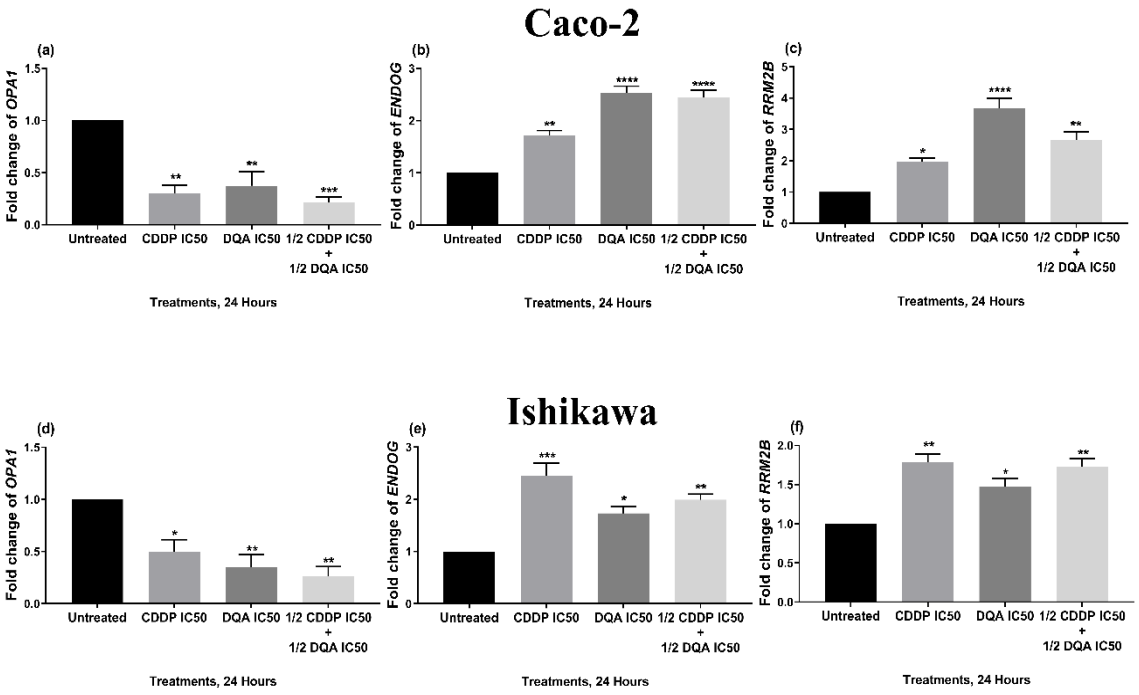

Figure 5.7. Expression level changes of the *OPA1*, *ENDOG* and *RRM2B* genes in the Caco-2 (**a-c**) and Ishikawa (**d-f**) cells upon the treatments at 24 h. The columns represent the fold changes of the relative expression levels of the genes normalised against the untreated controls. Data are mean ± SEM ($N = 3$ separate experiments); p values comparing treated and untreated cells were calculated using one-way ANOVA with Tukey multiple comparison post-hoc analysis; ns, not significant, *p<0.05, **p<0.01, ***p<0.001 and ****p<0.0001.

5.2.5 Expression levels of anti-oxidant genes altered upon treatments

To gain further insight into the mechanisms underlying treatment-induced ROS production, the expression levels of the antioxidant genes upon the treatments were investigated by TaqMan qPCR.

Interestingly, all genes were significantly upregulated in the Caco-2 cells in the presence of DQA but no significant changes were observed with CDDP or the combined therapy for *SOD1, SOD2* and *CAT* (Figure 5.8 a-c). However, the *GPx* and *Nrf2* genes were significantly upregulated in the presence of all treatments (Figure 5.8 d & e).

In the Ishikawa cells, *SOD1* was significantly upregulated in the presence of CDDP, whereas a significant downregulation in the combined therapy was observed (Figure 5.8 f). *SOD2* did not show any significant changes upon the treatments (Figure 5.8 g) while *CAT* was significantly downregulated in the presence of all treatments with a further decrease in the combined therapy (Figure 5.8 h). *GPx* was significantly upregulated only in the presence of CDDP (Figure 5.8 i) while *Nrf2* showed a significant upregulation only with DQA (Figure 5.8 j).

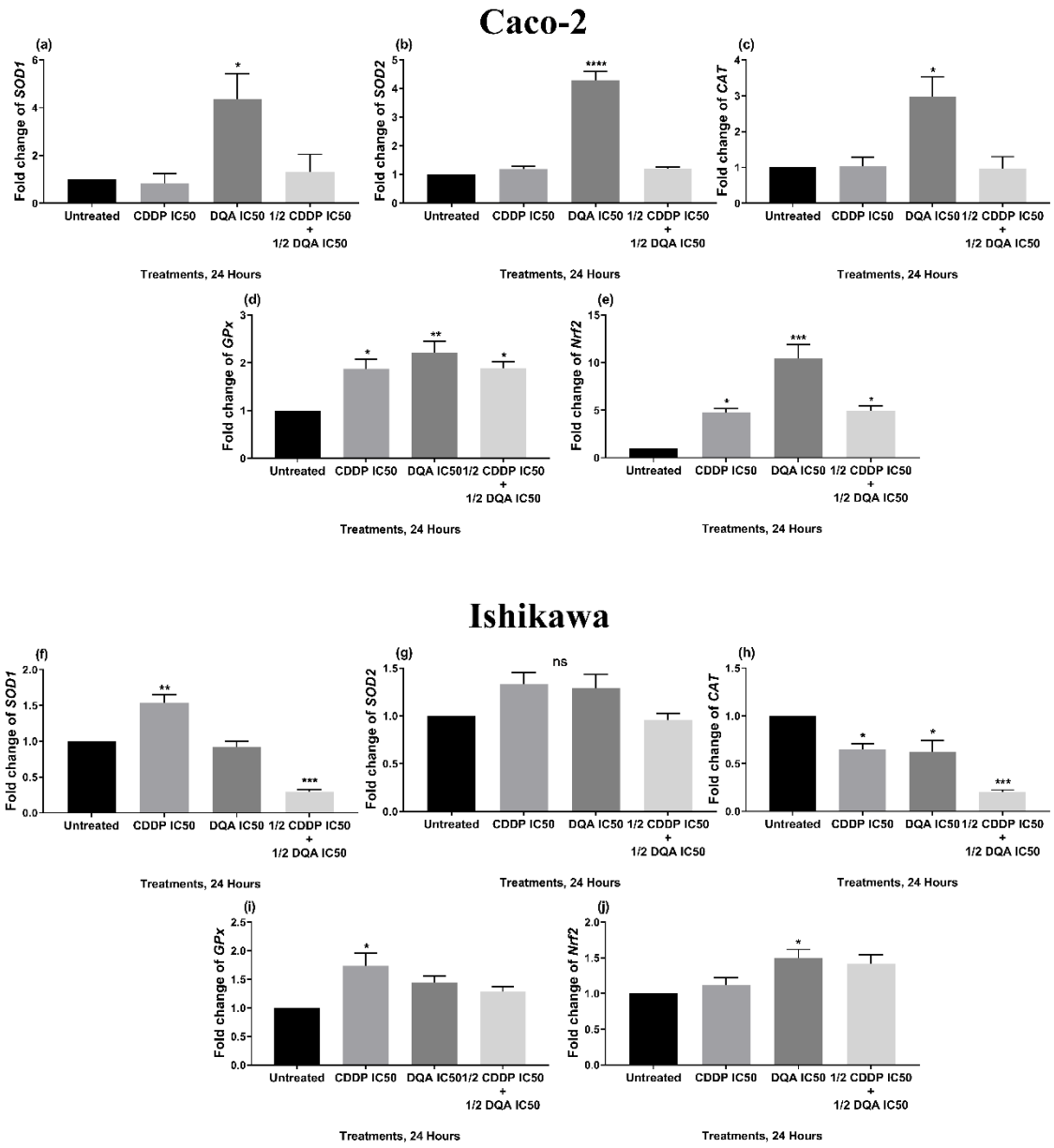

Figure 5.8. Changes in expression levels of major antioxidant genes in the Caco-2 (**a-e**) and Ishikawa (**f-j**) cells upon the treatments at 24 h. The columns represent the fold changes of the relative expression levels of the genes normalised against the untreated controls. Data are mean ± SEM ($N = 3$ separate experiments); p values comparing treated and untreated cells were calculated using one-way ANOVA with Tukey multiple comparison post-hoc analysis; ns, not significant, *p<0.05, **p<0.01 and ***p<0.001.

5.3 Discussion

As previously reported, CDDP and DQA accumulate in mitochondria and exert their antitumor effect through increased ROS generation and mitochondrial disruption [240,267,270]. To confirm this, NAC was administered to the cells prior to the drug treatments to elucidate the role of treatment-induced ROS in cell death.

In this chapter, the implication of ROS production upon the treatments in cell death is analysed and discussed.

5.3.1 ROS as the main contributor in cell death

When NAC was administered to the cells prior to the drug treatments, cell viability was significantly restored, indicating the critical role of enhanced ROS production in triggering cell death upon various CDDP and DQA treatments. It should be noted that in the Caco-2 cells, the rescue of cell viability with the combined therapy was more significant than that with the single treatment, which was in alignment with the highest ROS production level upon the combined treatment as compared to the single treatment (discussed in Chapter 3). However, comparable rescue effects were observed in the Ishikawa cells irrespective of the treatments, indicating an equal (or non-treatment-specific) production level of ROS following the treatments, which was indeed the case as supported by the ROS data of the Ishikawa cells (discussed in Chapter 3). Furthermore, the rescue of cell viability by NAC was generally more effective for Ishikawa compared to Caco-2, indicating that ROS had a more important role in mediating cell death in Ishikawa.

Those results were further confirmed by a parallel trend in terms of the rescue of cell viability and the attenuation of cell toxicity with NAC pre-incubation, as indicated by data from the ApoTox-Glo™ Triplex Assay experiments.

Once the cytotoxic effects of CDDP/DQA on the Caco-2 and Ishikawa cells were demonstrated, the capacity of CDDP/DQA to induce cell death by apoptosis or necrosis was analysed. The translocation of PS to the external layer of the cell membrane (the characteristic early event of apoptosis; [335]) and the membrane permeability were analysed through the annexin V-FITC/PI double staining.

The mode of CDDP/DQA-induced cell death after 24 hours in the Caco-2 and Ishikawa cells seems to be apoptosis followed by necrosis secondary to apoptosis. It has been described that a fundamental difference between necrosis and apoptosis lies in the kinetics of membrane integrity loss during these types of cell death [335]. Apoptotic cells exclude dyes for several hours whereas necrotic cells undergo rapid swelling and lysis within minutes. The annexin V-FITC/PI double staining assay showed the presence of cells in the late apoptosis and necrosis-secondary-to-apoptosis phases which demonstrated PS exposure on the cell surface as well as membrane permeability allowing the entry of PI (i.e. A^+/PI^+). Apoptotic cell death was further confirmed by measuring caspase-3/7 activation which is a typical event during apoptosis.

Our data showed a significant attenuation in apoptosis events and caspase-3/7 activation in both cell lines when the cells were pre-incubated with NAC. Those data proved that the mode of action of the two compounds and their combination was through ROS-induced apoptosis. Moreover, it is worth mentioning that the attenuation in the apoptosis related events by NAC was more effective for Ishikawa compared to Caco-2, which is in alignment with the results regarding the rescue of cell viability by NAC.

Those results collectively confirm that baseline ROS levels could influence how cancer cells respond to the same treatment, as demonstrated by the Caco-2 and Ishikawa cells in this study. Moreover, our data highlight the fact that cancer cells with lower baseline levels of intracellular ROS would respond better to ROS-stimulating therapy by generating more ROS compared to cells with higher baseline levels of ROS. Hence, the excessive ROS induced by the treatments could be the main cause of cell death in cells with low baseline ROS, whereas different mechanisms might play a role in parallel with ROS in causing cell death in cells with high baseline ROS.

5.3.2 BCL-XL as the main target of ROS

The anti-apoptotic protein BCL-XL antagonises the pro-apoptotic family of proteins such as BAX and BAK. This antagonism prevents the activation and oligomerisation of BAX and BAK, which in turn inhibits the formation of MPTP and the release of cytochrome *c* that plays a central role in the execution of apoptosis. Once cytochrome *c* is released from mitochondria, various events will lead to the activation of caspase-3 which is considered as the non-return point in the apoptotic signalling cascade (reviewed in Ref. [35]).

As mentioned previously (Chapter 1, 1.3.6), excessive ROS level is a key factor in facilitating MPTP opening by promoting the ubiquitination of the anti-apoptotic BCL-2 proteins, thus allowing the activation and oligomerisation of BAX / BAK and the release of cytochrome *c* (reviewed in Refs. [99,160]). It has been reported that oxidation of ANT, a main component of MPTP, by ROS is also linked to the regulation of the MPTP opening (reviewed in Ref. [160]). However, the expression of ANT was not covered in this study.

In order to confirm that the observed cytotoxicity was caused by ROS-induced mitochondria-dependent apoptosis pathway, changes in the protein expression of BCL-XL and VDAC1 and the release of cytochrome *c* were analysed in the Caco-2 and Ishikawa cells.

Indeed, our data showed a significant decrease in the BCL-XL protein expression at 24 hours of the treatments in both cell lines followed by marked cytochrome *c* release and caspase-3 activation. Our results indicate that the reduced BCL-XL protein level resulted either in the activation and oligomerisation of proapoptotic proteins (BAX and BAK) leading to formation of the pores on the OMM, or in less suppression of VDAC1 allowing its oligomerisation and consequently the formation of VDAC-containing pore.

As mentioned earlier, it is well documented that ROS cause a direct damage to ANT by oxidation, however little is known about the direct impact of excessive levels ROS on VDAC1. It worth mentioning that no changes were observed in the VDAC1 protein expression either upon the treatments or with NAC pre-incubation in both cell lines. This observation indicates that the confirmation state of VDAC1 (homodimerisation or heterodimerisation with proapoptotic proteins) rather that its oxidation and degradation regulates the MPTP opening. Moreover, the observed changes in BCL-XL protein levels upon treatments further confirmed the pivotal role of the BCL-2 proteins in the formation of MPTP by facilitating VDAC1 oligomerisation, rather than regulating VDAC1 expression.

All those aforementioned changes in BCL-XL, cytochrome *c* and caspase-3 were reversed when the cells were pre-incubated with NAC. Such findings clearly suggest that ROS-induced BCL-XL oxidation and degradation facilitates the formation of a channel complex with sufficient pore size capable of releasing cytochrome *c* from the IMS to the cytosol and consequently triggers caspase-initiated apoptosis. Moreover, these

observations indicate that BCL-XL protein is the main target of ROS and further prove that the mode of action of the two compounds is through ROS-induced apoptosis.

5.3.3 Mitochondria as the main target of ROS

As mentioned previously, CDDP and DQA accumulate in mitochondria so certain mitochondrial damage is expected in cells exposed to the treatments. To test this hypothesis, three key markers of mitochondrial damage (*OPA1*, *RRM2B* and *ENDOG*) have been investigated in our study.

The OPA1 protein is well known to regulate mitochondrial fusion and to stabilise cristae structure for maintenance of normal mitochondrial activities [336]. It has been reported that stabilisation of mitochondrial cristae by OPA1 prevents mitochondrial dysfunction and protects the cell from intrinsic apoptosis [310]. Our data showed that the *OPA1* gene was downregulated in the presence of all treatments in both cell lines, which is in alignment with the observed cytochrome *c* release upon the treatments.

As mentioned earlier, RRM2B plays an important role in DNA damage repair and maintenance of mtDNA content [28,29]. In addition, Kuo *et al.* [337] evidenced that *RRM2B* was induced upon oxidative stress to protect the mtDNA content. Our data demonstrated that *RRM2B* was upregulated in the presence of all the treatments in both cell lines, which could be a counteract mechanism by the cells against the observed mtDNA depletions upon the treatments (discussed in Chapter 3).

On the other hand, ENDOG has a pro-apoptotic function and participates in apoptosis via DNA degradation [338]. Under oxidative stress, ENDOG is released from mitochondria and migrates to the nucleus where it degrades DNA to effect apoptosis. Therefore, maintaining low levels of *EndoG* could prevent cell death caused by stress conditions [339].

Our data showed that *ENDOG* was upregulated in the presence of all the treatments in both cell lines, which is in alignment with the observed caspase activation upon the treatments.

All aforementioned results are in agreement with a study conducted by Choi *et al.* [240] who observed downregulation of *OPA1* and upregulation of *RRM2B* and *ENDOG* upon the treatment with CDDP in the HEK-2 cells.

Our microscopic analysis (Chapter 3) revealed an enhanced ROS generation upon the treatments largely localised within mitochondria causing MMP disruption, mtDNA depletion, downregulation of mitochondrial stability markers and upregulation of mitochondrial DNA damage markers (demonstrated through qPCR data). Hence, it was evident from these results that CDDP/DQA induced mitochondrial damage through oxidative stress.

Having established the critical role of excessive ROS in cell death in our study, the potential antioxidant systems counteracting treatment-induced ROS production were investigated by analysing the expression levels of the antioxidant genes.

Interestingly, all the antioxidant genes and *Nrf2* were significantly upregulated in the Caco-2 cells treated with DQA, whereas only *GPx* and *Nrf2* were significantly upregulated in the Caco-2 cells undergone all the treatments. Those results indicated that DQA treatment provoked wider antioxidant responses in the Caco-2 cells while some of the genes remained silent upon exposure to CDDP. It is possible (as seen in our study) that in the Caco-2 cells, CDDP and its combination with DQA had a direct regulatory impact only on specific antioxidants such as *GPX* and certain transcription factors such as *Nrf2* which regulates the expression of genes involved in the cellular antioxidant system [164,166].

As to the Ishikawa cells, the expression profiles of the tested antioxidant genes were less consistent compared to those in the Caco-2 cells. However, both *SOD1* and *CAT* were significantly downregulated in Ishikawa upon the combined treatment whereas no significant changes occurred in the expression levels of *SOD2*, *GPX* and *Nrf2* in any of the treatments except for CDDP and DQA in *GPX* (upregulated) and *Nrf2* (upregulated) respectively.

Our results presented in Chapter 4 suggest that cancer cells with high baseline ROS levels might have relatively low expressions of antioxidant genes. However, upon ROS-stimulating treatments, those cells could upregulate their antioxidants significantly as a protective mechanism, rendering them more resistant to the treatment. On the other hand, cells with low baseline ROS levels might have saturated their antioxidant system, and therefore could not defend themselves efficiently against ROS-stimulating compounds, as demonstrated by the significantly higher sensitivity levels of Ishikawa compared to those of Caco-2 in this study.

5.4 Summary

The above observations indicate that excessive intracellular ROS induced by CDDP/DQA is the essential mediator of mitochondrial dysfunction and cell death, which are in line with previous studies where scavenging of ROS by antioxidants results in the attenuation in cell death.

More importantly, this chapter has demonstrated that cells with lower baseline ROS levels respond better to ROS scavengers when undergoing ROS-stimulating treatment, which grants better cell death attenuation. This indicates that excessive ROS could be the main cause of cell death in cells with relatively low baseline ROS levels, whereas other mechanisms might play a role alongside with ROS in killing cells with relatively high baseline ROS levels. Our results also highlight the possibility of achieving greater efficacy of ROS-stimulating agents in treating cancers with low baseline ROS levels compared to those with high baseline ROS levels.

Chapter 6

Evaluation of mitochondrial genetic abnormalities as effective biomarkers to predict drug sensitivity in cancer cells

6.1 Introduction

Cancer is considered as a group of multi-process and multifactorial genetic diseases, and it has been revealed that all cancer cells accumulate somatic mutations in both mitochondrial and nuclear genomes that drive normal cells to become progressively malignant [340]. As previously described, mtDNA is independent of nuclear DNA and consists of protein-coding regions for 13 mitochondrial complex subunits, 22 tRNA and 2 rRNA sequences as well as the D-loop region that regulates mtDNA replication and transcription (discussed in Chapter 1).

Mitochondria are implicated in many cellular processes such as cell communication, differentiation and apoptosis so a little mitochondrial dysfunction can lead to the development of several human diseases, including cancers [26]. Mitochondrial dysfunction can be associated with mtDNA alterations such as mutations and changes in the mtDNAcn (reviewed in Ref.s [65,160]). This chapter focuses on the implications of mtDNA abnormalities in ROS related cancer cell death/survival and drug resistance.

It is well known that mitochondria are considered a primary intracellular site of ROS generation via OXPHOS during ATP generation [297]. ROS play important roles in cell signalling pathways such as growth, differentiation, metabolism and death signalling (reviewed in Ref. [160]). MtDNA mutations could influence intracellular ROS levels, and consequently be responsible for mitochondrial dysfunction and genome instability [76,341]. In particular, mutations in complexes I and III coding regions in both nDNA and mtDNA can affect the normal function of corresponding complexes. Since these two complexes are the main ROS generation sites, mutations in their coding regions can have an impact on ROS production (reviewed in Ref. [163]). Moreover, researchers have indicated the existence of particular mutation patterns in mtDNA of various types of cancer, and abnormal apoptotic procedures are considered a consequence of these mutations [79]. It is known that dysregulation of apoptosis contributes to cancer cell survival and drug resistance.

In addition, as mtDNA is continuously exposed to ROS and lacks protective histones and efficient DNA repair machinery, it is more susceptible to ROS-induced mutations and has a mutation rate 10 times higher than nDNA (reviewed in Ref. [65]).

Furthermore, mitochondrial DNA copy number (mtDNAcn) per cell is preserved within a stable range to achieve the required cellular energy and hence ensure normal physiological functions. It ranges among the population from 10^3 to 10^4 per cell type [145]. Such variations also reflect the imbalance between ROS production and the antioxidant capacity, so mtDNAcn has been considered as a potential diagnostic and prognostic biomarkers for several cancer types (discussed in Chapter 1) [146].

To date, mitochondrial dysfunction and various mtDNA alterations including point mutations, large deletions and copy number changes have been observed in several human cancers such as breast, colon, stomach, kidney, thyroid, head and neck and ovarian cancers [18,80,81]. Mitochondrial genetic abnormalities have also been strongly linked to oxidative stress, risk of metastasis and resistance of cancer cells to apoptosis (reviewed in Ref.s. [53,78,342]).

ROS have been purported to have a double-edged-sword effect in living cells since low levels of ROS can play a critical role in promoting cell proliferation and invasion, whereas excessive levels of ROS can cause oxidative damage to intracellular bio-macromolecules and consequently induce cell death (reviewed in Ref.s [168,196]). Therefore, it is speculated that induction of ROS may be a promising approach to cancer therapy (reviewed in Ref.s [144,160]). Indeed, some conventional chemotherapies and mitochondria-targeting agents have been proven to cause cell death by affecting the redox balance via excessive accumulation of ROS [175,271]. However, due to the strong side effects of the chemotherapies and different levels of response to the treatments, their clinical use is limited (reviewed in Ref. [305]). For that reason, finding effective biomarkers to predict response to ROS-stimulating therapy is a main objective of this PhD study.

This chapter aimed to explore the mitochondrial genetic abnormalities in all the cell lines enrolled in this study and also to investigate the implications of certain mitochondrial DNA mutations in ROS levels and other mitochondrial functional parameters, as well as in cells' response to cisplatin and dequalinium.

6.2 Results

6.2.1 Increased mitochondrial DNA copy number in cancer cells

As shown in Figure 6.1 a, cancer cell lines had increased mtDNAcn compared to the non-cancerous cells (PNT-2). Amongst the cancer cell lines, Caco-2 had the highest mtDNAcn whereas Ishikawa had the lowest.

It is worth noting that the mtDNAcn values showed the same trend as those of the intracellular ROS and mitochondrial superoxide levels observed in the cell lines. These results demonstrated positive correlations between mtDNAcn and ROS levels as well as mitochondrial superoxide levels in the cell lines (Figure 6.1 b & c).

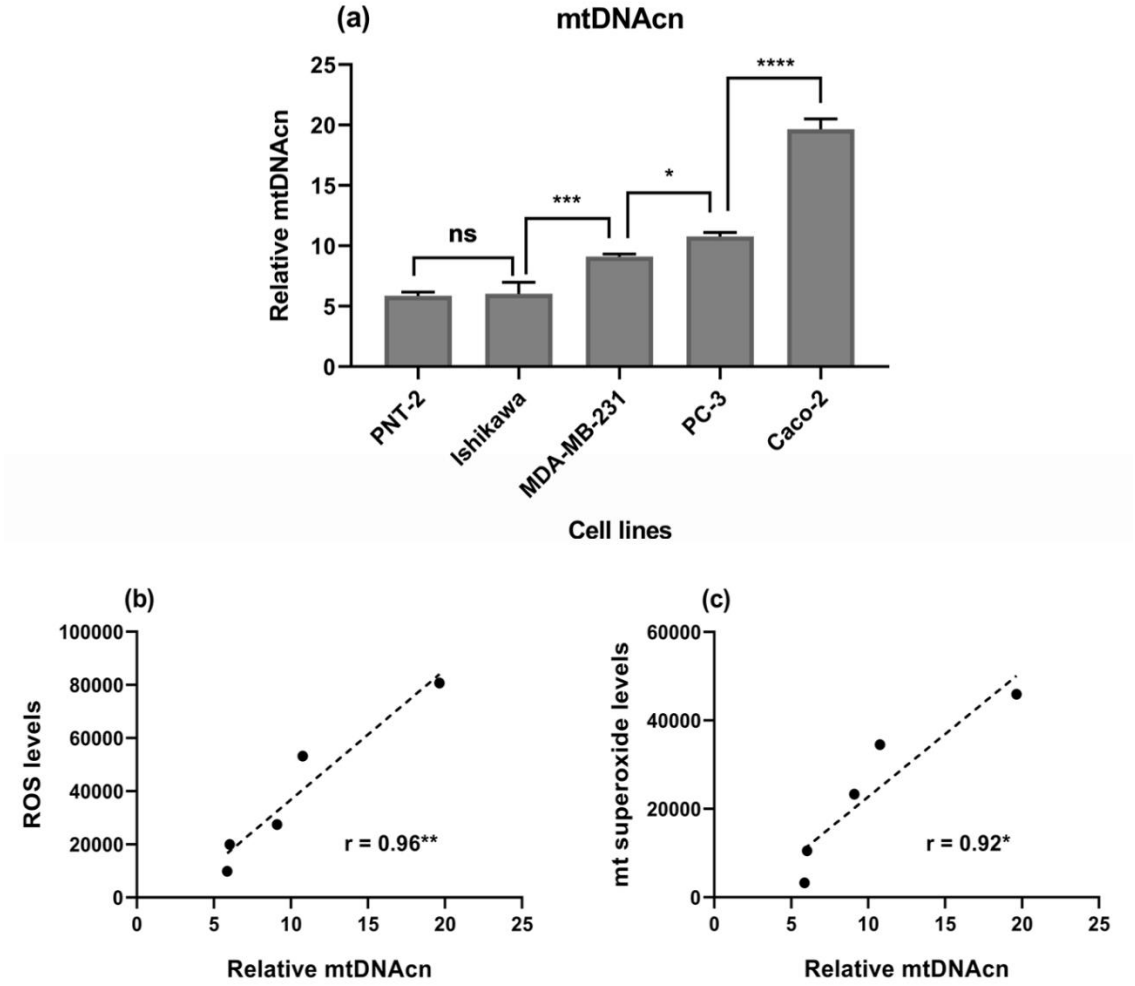

Figure 6.1. Relative content of mtDNA in PNT-2, Ishikawa, MDA-MB-231, PC-3 and Caco-2 normalised against the house keeping gene (β-actin). The columns represent the relative mtDNAcn of the cell lines. Data are mean ± SEM (N=3 separate experiments); *p* values were calculated using one-way ANOVA with Tukey multiple comparison post-hoc analysis; ns, not significant, **p*<0.05, ****p*<0.001 and *****p*<0.0001. Positive correlation between the relative content of mtDNAcn and the baseline intracellular ROS levels (**b**) and mitochondrial superoxide levels (**c**). Data points representing the cell lines are in the same sequence as the columns in panel **a**. r and *p* values were calculated using the Pearson correlation method; **p*<0.05 and ***p*<0.01.

6.2.2 Increased number of non-synonymous mutations in the mtDNA protein coding regions in cancer cells

The complete mitochondrial genome of each cell line was PCR amplified via 17 overlapping amplicons (in-house primers and PCR sizes listed in Chapter 2), and the expected PCR product sizes were confirmed by agarose gel electrophoresis (a representative gel image is shown in Figure 6.2).

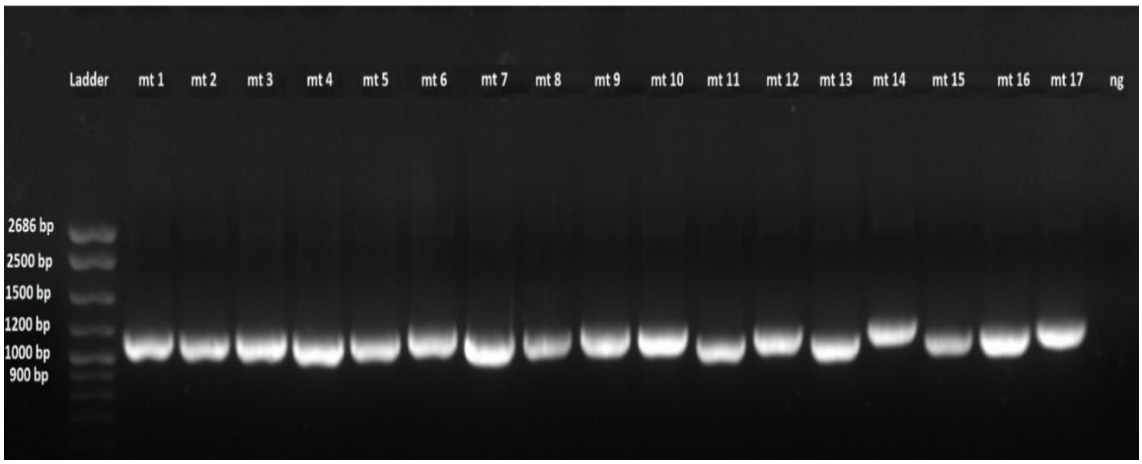

Figure 6.2. Representative image of agarose gel electrophoresis of PCR products amplified using 17 pairs of primers. mt 1-17: seventeen fragments (~ 1,1 kb) of mitochondrial genome; ng: negative control.

Sequencing data revealed that the total number of mtDNA mutations in each cancer cell line was comparable (30, 25, 26 and 36 mutations in Ishikawa, MDA-MB-231, PC-3 and Caco-2, respectively). However, these numbers were significantly higher than that in the non-cancerous cell line (PNT-2), in which only 9 mutations were identified (Figure 6.3 a). Progressive increases in the number of non-synonymous point mutations in complexes I and III (1, 3, 4, 5 and 9 mutations) and in the whole coding regions (2, 4, 5, 6, 11) were observed in PNT-2, Ishikawa, MDA-MB-231, PC-3 and Caco-2, respectively (Figure 6.3 b & c).

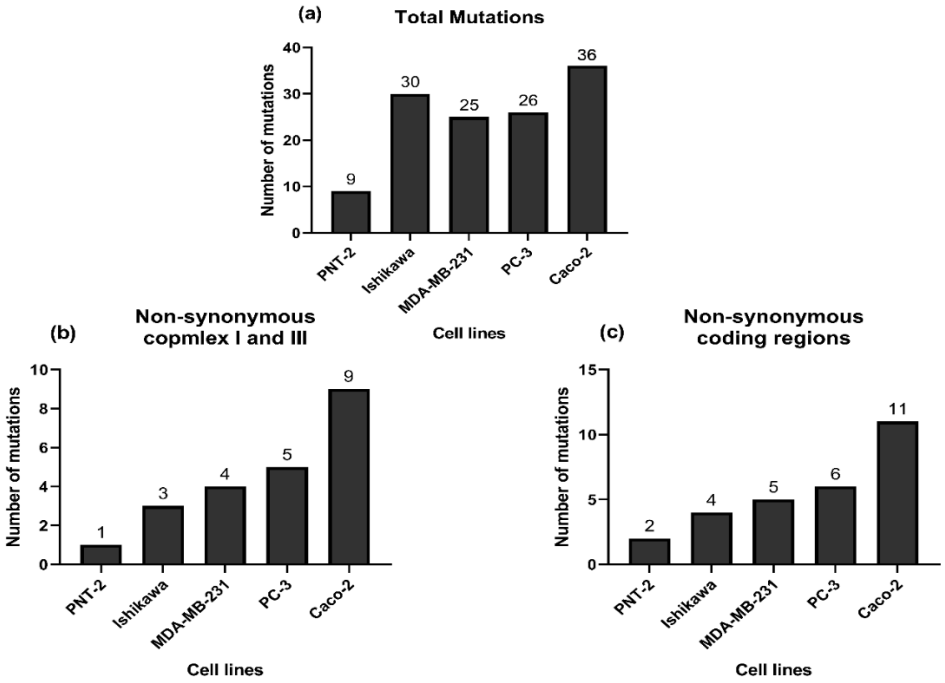

Figure 6.3. Number of mutations identified in the mitochondrial genome by Sanger sequencing. (**a**) Number of the total mutations observed in the cell lines. (**b**) Number of non-synonymous mutations observed in mtDNA coding regions for complex I and III subunits. (**c**) Number of non-synonymous mutations observed in the whole mtDNA coding regions.

Numerous common mutations in cell lines were observed within the mitochondrial genome (Appendix Table 1). Our results indicated that the A8860G mutation was detected in all the cell lines whereas C14766T was detected only in the cancer cells. G13708A was identified only in the PC-3 and Caco-2 cells, whereas A15326G was a common mutation in the PNT-2, Ishikawa, MDA-MB-231 and Caco-2 cells. On the contrary, greater numbers of unique mutations, mainly in complexes I and III, were observed in the cancer cells (Appendix Table 2). The T3394C point mutation was found only in the Ishikawa cells; C12084T and A13966G were found only in the MDA-MB-231 cells; T11120C, C13802T and A14793G were found only in the PC-3 cells. Caco-2 had the highest number of unique mutations including T4216C, G7977C, A10398G, A13681G, T14798C, A14927G and C15452A. No unique mutations within complexes I and III were found in the non-cancerous cells (PNT-2).

All the identified mutations within the mitochondrial DNA protein coding regions and their disease association using MitoMAP and Human Mitochondrial DataBase (HmtDB) are listed in Appendix Table 3.

Briefly, all of the identified mutations have been previously reported in different diseases including cancers, and some of the mutations have been linked to escalated ROS production (discussed below in 6.3.3).

6.2.3 Mapping of complexes I, III, IV and V mutations

In total 37 mutations were identified in complexes I, III, IV and V, amongst which 17 were non-synonymous (i.e. causing amino acid changes). Nine non-synonymous substitutions were found in complex I, of which 2 were present in ND1, 1 in ND3, 2 in ND4 and 4 in ND 5. A total of 6 MT-CYB substitutions were identified in complex III. One substitution was identified in complex IV located in MT-COII and one substitution was identified in complex V located in ATP6 (Figure 6.4).

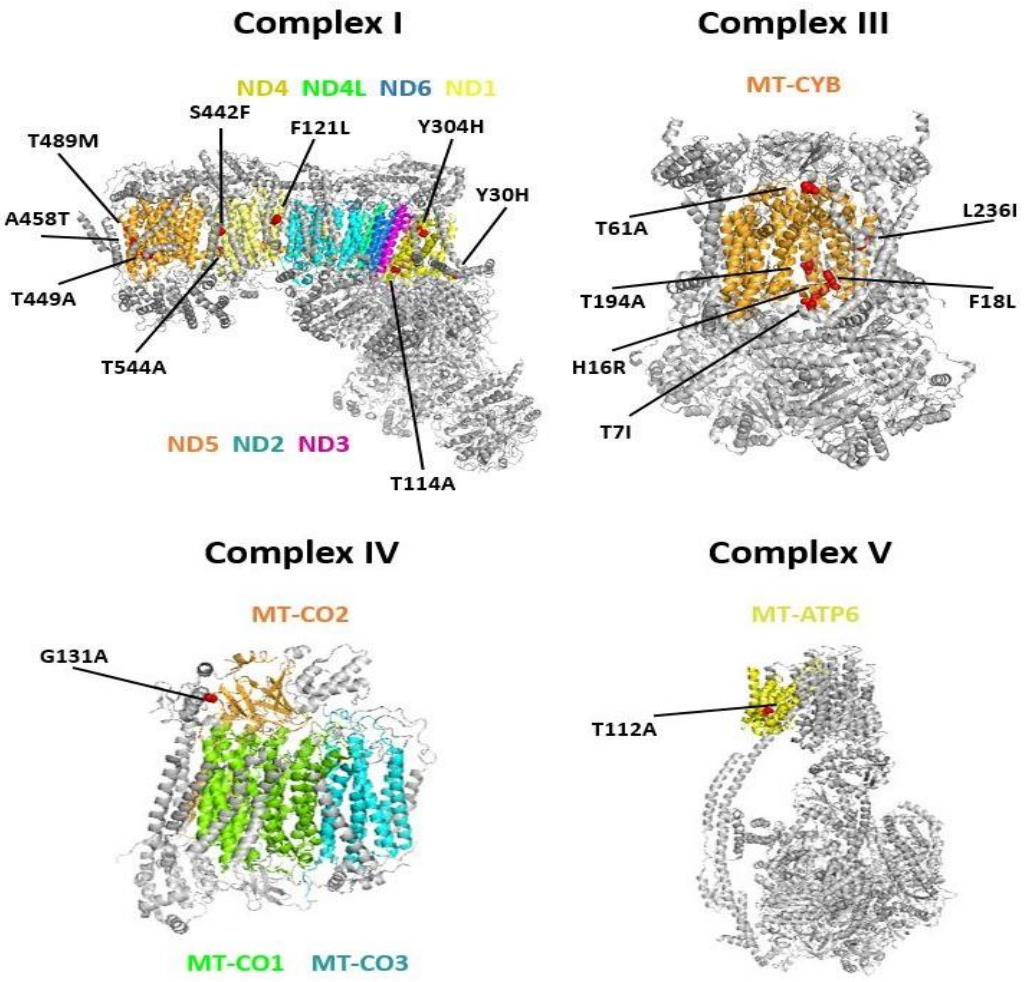

Figure 6.4. Mapping of all the identified non-synonymous mutations in the mitochondrial OXPHOS protein complexes. Mutations are mapped to *Homo sapiens* complex I homolog [PDB:5XTD], *Homo sapiens* complex III homolog [PDB:5XTE], *Homo sapiens* complex IV homolog [PDB:5Z6N] and *Bos taurus* complex V homolog [PDB:5ARA]. All complexes are depicted as ribbon models. The nuclear DNA encoded subunits are coloured in grey whereas the mitochondrial DNA encoded subunits are coloured differently. Mutation sites are highlighted as red spheres.

6.2.4 Prediction of functional mutations

6.2.4.1 Complex I functional mutations

The A10398G mutation could cause the disruption of complex I assembly and stability by affecting the association of ND3 and ND1. The replacement of T114 by A114 removes the polar sidechain property of threonine, which is likely to affect the formation of hydrogen bonds with the ND1 residue (N382) and weaken the interaction between the two subunits, and consequently affect the assembly of the two subunits and the stability of complex I (Figure 6.5). Similarly, the A13681G, C13802T and A13966G mutations cause the disruption of ND5 subunit stability. The replacements of T449 by A449, T489 by M489 and T544 by A544 result in the loss of the hydrogen bonds formed with the W106, Y485 and L540 residues in the ND5 subunit, respectively. Consequently, these mutations weaken the interaction within the subunit, hence affect the stability of complex I.

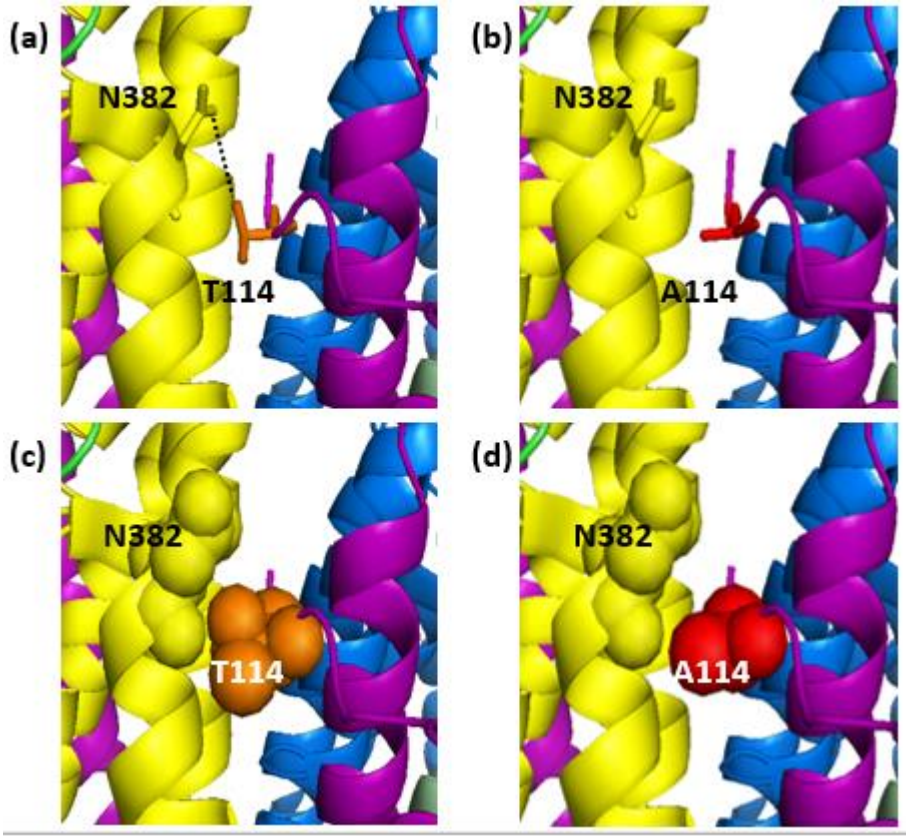

Figure 6.5. Detailed view of the complex I mutation A10398G (T114A). T114 is located at the surface of complex I within the mitochondrial DNA encoded ND3 subunit. ND3 is shown in purple and ND1, an adjacent subunit, in yellow. The *wild type* T114 is shown in orange as sticks and spheres (**a** & **c**, respectively) and the mutant A114 is shown in red (**b** & **d**). Alanine is non-polar and smaller than threonine in size meaning the change is likely to hinder the interaction with the N382 residue of ND1, and therefore affect the association of the two subunits and consequently the stability of complex I.

The C12084T mutation results in the disruption of ND4 stability. This mutation replaces serine with phenylalanine (a larger amino acid) at position 442 (S442F) which is unlikely to be accommodated within the structure. Apart from being of a larger size, this phenylalanine at position 442 may disrupt and repel another phenylalanine nearby within the ND4 subunit (i.e. F438) and consequently affect the stability of complex I (Figure 6.6). Similarly, the T1120C and G13708A mutations cause the disruption of the ND4 and ND5 subunits respectively. The replacement of F121 by L121 is unlikely to be accommodated within the structure due to the orientation of the leucine side chain at position 121 which protrudes and results in its intra-subunit interaction with methionine at position 108 (M108) within the same subunit. The replacement of A458 with T458 is also unlikely to be accommodated within the structure, since the larger size of threonine may well disrupt and repel leucine at position 445 (L455) within the same subunit. These intra-subunit disruptions could interfere with the stabilisation of the ND4 and ND5 subunits and consequently affect the stability of complex I.

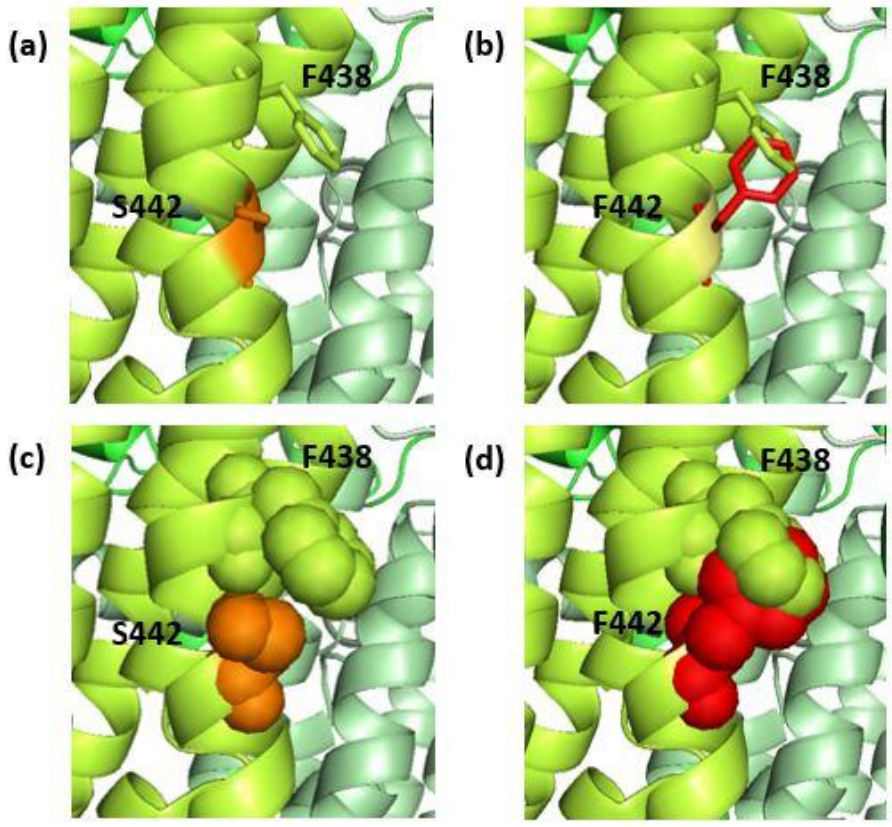

Figure 6.6. Detailed view of the complex I mutation C12084T (S442F). S442 is located at the core of complex I within the mitochondrial DNA encoded ND4 subunit. ND4 is shown in bright green. The *wild type* S442 is shown in orange sticks and spheres (**a** & **c**, respectively) and the mutant F442 is shown in red (**b** & **d**). Phenylalanine is bigger than serine due to its aromatic side chain and is likely to disrupt and repel the hydrophobic F438 residue within ND4, which is predicted to affect the stability of complex I.

6.2.4.2 Complex III functional mutations

T14798C that results in the amino acid change F18L is located at the ubiquinone-binding site (i.e. the Q_i site) of the MT-CYB subunit. Phenylalanine (F) is one of the residues that form the entrance of the Q_i site of complex III [44]. Both phenylalanine (F) and leucine (L) are hydrophobic. However, they differ in their side chains. Leucine does not have an aromatic side chain which makes it smaller than phenylalanine. Therefore, this substitution is likely to alter the shape and size of the Q_i site because it results in a larger cavity at the entrance to the site (Figure 6.7). Such a change may interfere with the binding of ubiquinone and consequently the electron transfer from heme b_H. Hence, the T14798C mutation is predicted to be functional as it may alter the activity of complex III.

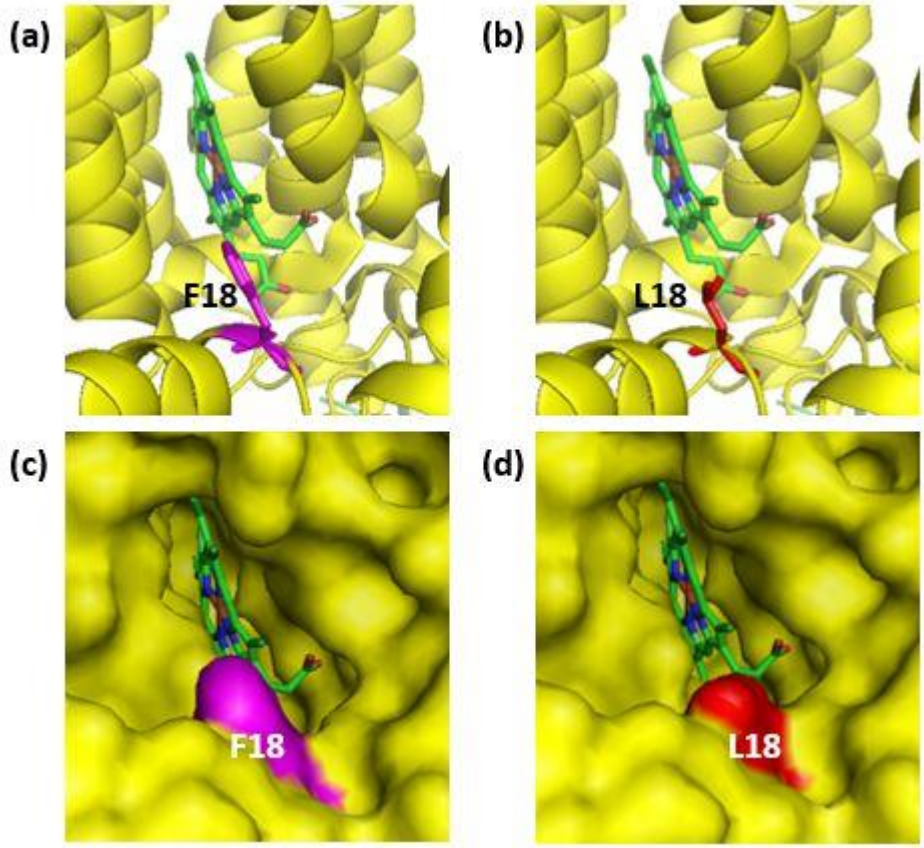

Figure 6.7. Detailed view of the complex III mutation T14798C (F18L). F18 is located at the entrance of the ubiquinone-binding site (Q_i site) within the mitochondrial DNA encoded cytochrome *b* subunit (MT-CYB). MT-CYB is shown in yellow and ubiquinone in green. The *wild type* F18 is shown in purple sticks and spheres (**a** & **c**, respectively) and the mutant L18 is shown in red (**b** & **d**). Phenylalanine is a much larger residue than leucine, suggesting that this change is likely to affect the shape and structure of the binding site and consequently alter the activity of complex III.

All functional mutations predicted by 3D-structural modelling and their occurrences in the cell lines are summarised in Table 6.1

Table 6.1. List of functional mutations predicted by 3D-structural modelling identified in the 5 cell lines.

Mutations	PNT-2	Ishikawa	MDA-MB-231	PC-3	Caco-2	Locus	Amino acid change
A10398G					✔	Complex I	T114A
T11120C				✔		Complex I	F121L
C12084T			✔			Complex I	S442F
A13681G					✔	Complex I	T449A
G13708A				✔	✔	Complex I	A458T
C13802T				✔		Complex I	T489M
A13966G			✔			Complex I	T544A
T14798C					✔	Complex III	F18L

6.2.5 Non-functional mutations in protein-coding regions

Of the seventeen non-synonymous mutations identified within the mtDNA protein-coding regions, nine were predicted to be non-functional. These were: T3394C (Y30H) and T4216C (Y304H) in complex I; C14766T (T7I), A14793G (H16R), A14927G (T61A), A15326G (T194A) and C15452A (L236I) in complex III; G7977C (G131A) in complex IV; A8860G (T112A) in complex V. The structural analysis revealed that all those residues were distal from any known electron or proton route or major catalytic sites, and did not have any direct interaction with amino acids from neighbouring mitochondrial or nuclear subunits. There also appeared to be sufficient room to accommodate the amino acid change in each case.

To summarise, all the mutations predicted to be non-functional locate on the surface of the subunits and could therefore affect their interaction with the inner mitochondrial membrane and the formation of the MRC super-complexes [343]. However, this hypothesis is difficult to prove because currently, none of the 3D structures of the MRC super-complexes is available to have them sufficiently characterised. With improved understanding of the structures and the complex-membrane interactions, it is possible that the aforementioned predictions can be validated in the future.

All the non-synonymous mutations and their structural modelling data are summarised in Table 6.2.

Table 6.2. Summary of the non-synonymous mutations and the 3D structural modelling results.

Mutations	Locus	Complex	Amino Acid change	Sequence	Location	Interaction	Prediction
T3394C	ND1	I	Y30H	Conserved	Surface	None	Non-functional
T4216C	ND1	I	Y304H	Non-conserved	Surface	None	Non-functional
A10398G	ND3	I	T114A	Non-conserved	Surface	ND3-ND1	Functional
T11120C	ND4	I	F121L	Conserved	Surface	ND4 intra-subunit	Functional
C12084T	ND4	I	S442F	Conserved	Core	ND4 intra-subunit	Functional
A13681G	ND5	I	T449A	Conserved	Surface	ND5 Intra-subunit	Functional
G13708A	ND5	I	A458T	Conserved	Core	ND5 Intra-subunit	Functional
C13802T	ND5	I	T489M	Conserved	Surface	ND5 Intra-subunit	Functional
A13966G	ND5	I	T544A	Conserved	Surface	ND5 Intra-subunit	Functional
C14766T	CYB	III	T7I	Conserved	Surface	None	Non-functional
A14793G	CYB	III	H16R	Conserved	Surface	None	Non-functional
T14798C	CYB	III	F18L	Conserved	Surface	Substrate binding site	Functional
A14927G	CYB	III	T61A	Conserved	Surface	None	Non-functional
A15326G	CYB	III	T194A	Conserved	Surface	None	Non-functional
C15452A	CYB	III	L236I	Conserved	Surface	None	Non-functional
G7977C	CO2	IV	G131A	Conserved	Surface	None	Non-functional
A8860G	ATP6	V	T112A	Non-conserved	Surface	None	Non-functional

6.2.6 D-loop region as a hotspot for mtDNA mutations

The sequencing data revealed that the D-loop region was a hotspot for mutations identified in the present study. Ishikawa, PC-3 and Caco-2 showed greater numbers of mutations in this region compared to PNT-2 and MDA-MB-231 (Figure 6.8).

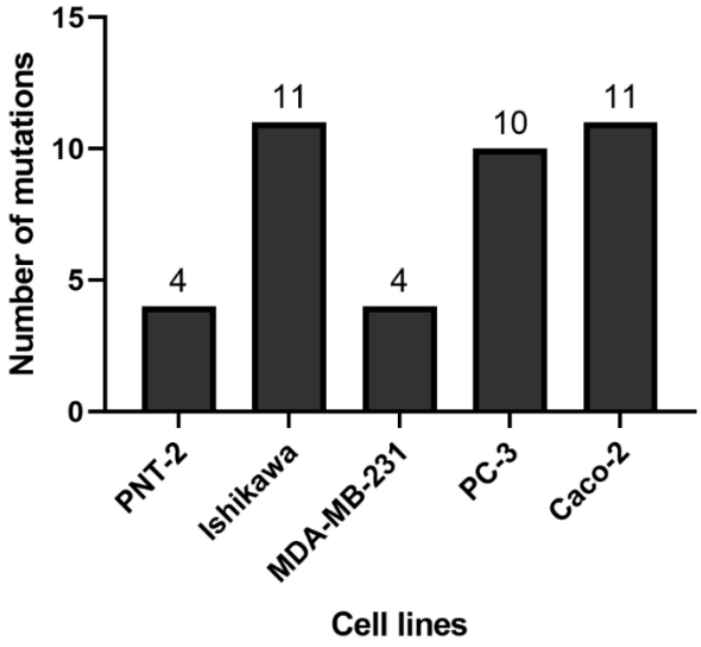

Figure 6.8. Number of mutations identified in the D-loop region in the 5 cell lines.

Numerous mutations common amongst the cancer cell lines were observed in the D-loop region (summarised in Appendix Table 1). Our results indicated that A73G was detected in Ishikawa, PC-3 and Caco-2; T195C was identified only in MDA-MB-231 and PC-3; A263G was a common mutation in all the cancer cell lines; 310insC was observed only in Ishikawa, PC-3 and MDA-MB-231; T16172C was detected in Ishikawa and PC-3; C16261T occurred in Ishikawa and Caco-2. None of the common mutations seen in the cancer cells was detected in the non-cancerous cell line (PNT-2).

On the other hand, each cell line harboured a number of unique mutations in the D-loop region (listed in Appendix Table 2). 513insCA, G16319A, T16325C and T16519C were found only in the PNT-2 cells; C150T, C338T, C16223T, C16257A, T16304C and A16497G were found only in Ishikawa; A153G was found only in MDA-MB-231; T195C, C16192T, C16256T, C16270T, C16320T and A16399G were found only in PC-3; G47A, G185A, G228A, C295T, C462T, T489C, C16069T and T16126C were found only in Caco-2.

All the identified D-loop mutations and their disease association using MitoMAP and Human Mitochondrial DataBase (HmtDB) are listed in Appendix Table 3.

Briefly, majority of the identified mutations have been previously reported in different diseases including cancers, and some of the mutations (C16223T, A16399G and C295T) have been associated with increased mtDNAcn, (discussed below in 6.3.5).

6.2.7 Mutations outside the protein coding and D-loop regions

Our sequencing data also revealed several mutations outside the protein coding and D-loop regions with certain common mutations amongst the cancer cell lines (summarised in Appendix Table 1). A750G was a common mutation in all the cancer and non-cancerous cell lines; A1438 was detected in PNT-2, Ishikawa, PC-3 and Caco-2; 2800insA occurred in Ishikawa and MDA-MB-231; 3107delN was observed only in Ishikawa, MDA-MB-231 and Caco-2. A750G and A1438 are mutations affecting the coding sequence for the 12S ribosomal RNA subunit whereas A2706, 2800insA and 3107delN are mutations affecting the 16S rRNA sequence.

On the other hand, each cell line harboured a number of unique mutations outside the protein coding and D-loop regions (listed in Appendix Table 2). T691C and A1937C were found only in the Ishikawa cells; 646insA, 653insT, G709A and G1719A were found only in MDA-MB-231; A12308G was found only in PC-3. None of these unique mutations was detected in Caco-2 or the non-cancerous cell line (PNT-2). T691C, 653insT and G709A are located in the coding region for the 12S ribosomal RNA subunit, whereas A1937C and G1719A affect the 16S ribosomal RNA sequence, and 646insA and A12308G affect tRNA-Phe and tRNA-Leu respectively.

6.2.8 Increased lactate production and *PDK1* expression in cancer cells

To investigate whether there was an association between the number of non-synonymous mutations observed within the mitochondrial genome of cancer cells and mitochondrial functional alterations, the baseline lactate levels of the cells were measured. Lactate is produced during glycolysis following the catalysis of pyruvate by lactate dehydrogenase (LDH), and can be measured to assess the efficiency of glycolysis.

Using a colorimetric assay, the relative content of lactate in respect of the total cellular protein was determined in all the cell lines enrolled in the study. As shown in Figure 6.9, the 4 cancer cell lines had increased lactate compared to the non-cancerous line (PNT-2). Amongst the cancer cell lines, Caco-2 had the highest lactate level whereas Ishikawa had the lowest. These results demonstrated a positive correlation between lactate levels and numbers of non-synonymous mutations.

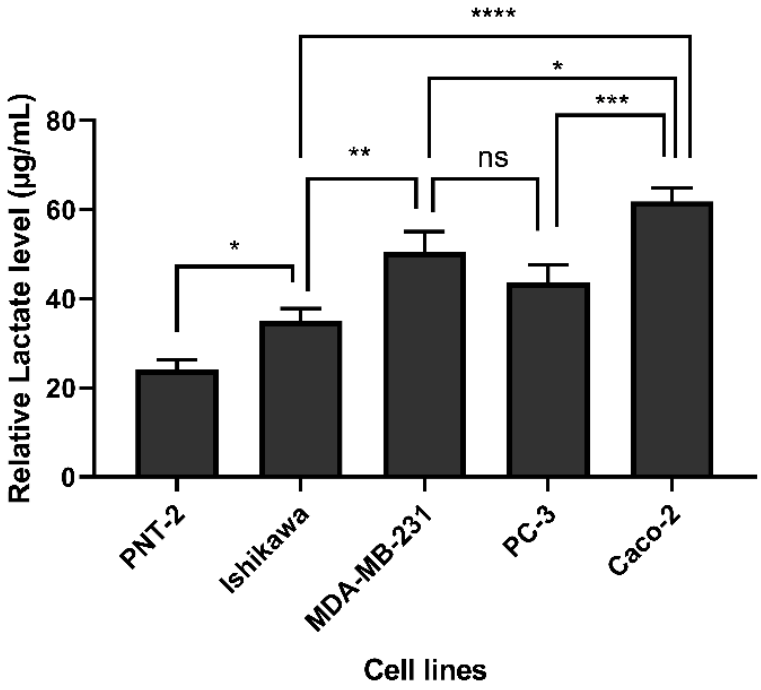

Figure 6.9. Relative lactate levels in the PNT-2, Ishikawa, MDA-MB-231, PC-3 and Caco-2 cells normalised against the total protein content. The columns represent the relative lactate level. Data are mean ± SEM (*N*=3 separate experiments); *p* values were calculated using one-way ANOVA with Tukey multiple comparison post-hoc analysis; ns, not significant, **p*<0.05, ***p*<0.01, ***p<0.001 and *****p*<0.0001.

Transformation between OXPHOS and glycolysis is controlled by the relative activities of pyruvate dehydrogenase (PDH) and lactate dehydrogenase (LDH). Given the fact that pyruvate dehydrogenase kinase 1 (PDK1), a key suppressor of PDH and an indirect activator of LDH, is highly regulated by oxidative stress and since Ishikawa and Caco-2 had been selected in this study to represent cancer cells with the lowest and the highest baseline levels of ROS, the expression level of *PDK1* was investigated in both cell lines to elucidate its impact on the difference in glycolysis efficiency observed in this study and also to confirm the correlation between the oxidative status and the metabolic profile.

The TaqMan qPCR results showed that the relative gene expression level of *PDK1* was significantly higher in the Caco-2 cells compared to the Ishikawa cells (Figure 6.10).

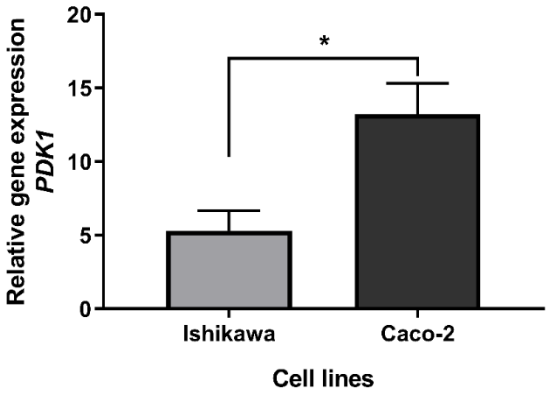

Figure 6.10. Comparison of the relative baseline expression levels of the *PDK1* gene between the untreated Ishikawa and Caco-2 cells. The columns represent the relative expression levels of the gene using TaqMan qPCR. Data are mean ± SEM (*N*=3 separate experiments); *p* values comparing the Ishikawa and Caco-2 cells were calculated using two-tailed t-test; *$p<0.05$.

6.2.9 Implication of mitochondrial DNA mutations in baseline ROS level, drug resistance and lactate production

In order to investigate how mitochondrial genetic abnormalities might affect the baseline ROS level and drug response in the cancer cells, linear regression was employed to model the relationship between the numbers of non-synonymous mutations and redox statues as well as CDDP/DQA IC50s and baseline lactate levels.

Data in Figure 6.11 show that numbers of non-synonymous mutations identified in the coding regions for all the mitochondrial OXPHOS subunits were positively correlated with the overall ROS and mitochondrial superoxide levels (Figure 6.11 a & b). Those non-synonymous mutation numbers were also positively correlated with the IC50s of both CDDP and DQA (Figure 6.11 c & d). Moreover, they were positively correlated with the baseline lactate levels (Figure 6.11 e).

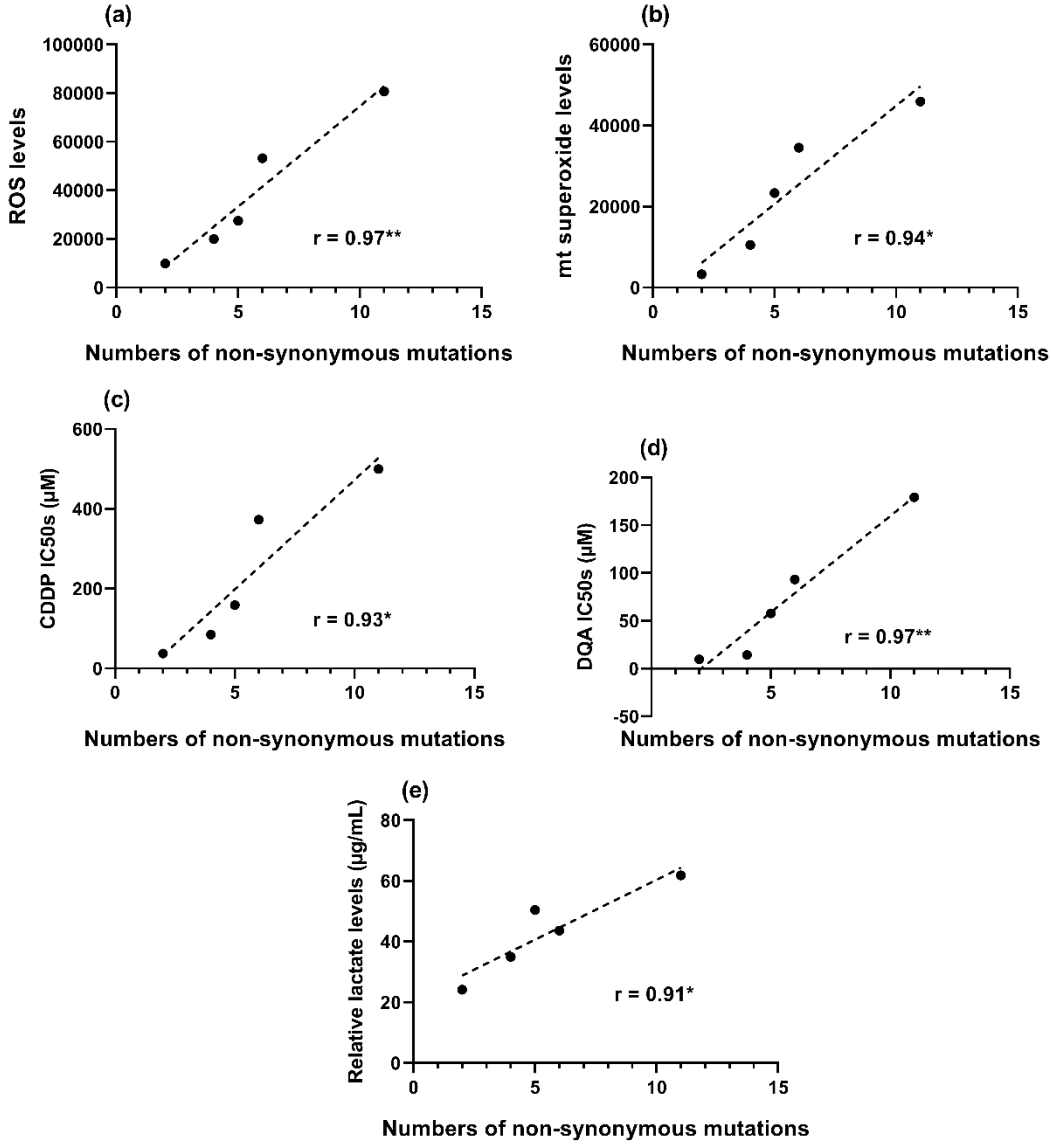

Figure 6.11. Positive correlations between the numbers of non-synonymous mutations identified in the protein coding regions and baseline ROS levels (**a**), mitochondrial superoxide levels (**b**), CDDP IC50s (**c**), DQA IC50s (**d**) and relative lactate levels (**e**). Data points representing the cell lines are in the sequence of PNT-2, Ishikawa, MDA-MB-231, PC-3 and Caco-2. r and *p* and values were calculated using the Pearson correlation coefficient method; **p*<0.05 and ***p*<0.01.

Similarly, numbers of non-synonymous mutations identified only in the complexes I and III coding regions were also positively correlated with ROS, mitochondrial superoxide, CDDP/DQA IC50s and relative lactate levels (Figure 6.12).

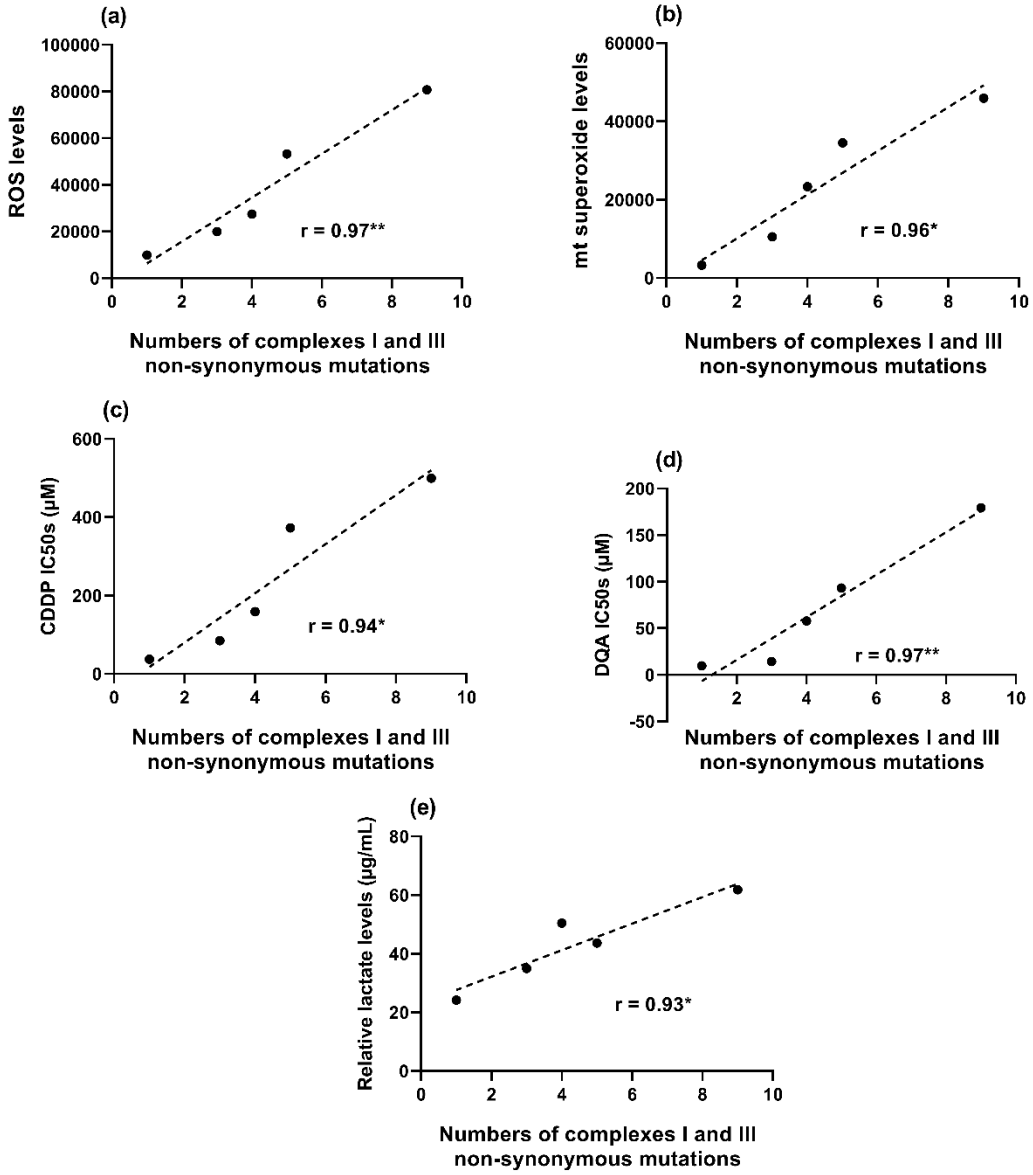

Figure 6.12. Positive correlations between the numbers of non-synonymous mutations identified in the complexes I & III coding regions and baseline ROS levels (**a**), mitochondrial superoxide levels (**b**), CDDP IC50s (**c**), DQA IC50s (**d**) and relative lactate levels (**e**). Data points representing the cell lines are in the sequence of PNT-2, Ishikawa, MDA-MB-231, PC-3 and Caco-2. r and *p* and values were calculated using the Pearson correlation coefficient method; **p*<0.05 and ***p*<0.01.

Interestingly, numbers of non-synonymous mutations predicted to be functional in our study by 3D-structural modelling were also positively correlated with ROS, mitochondrial superoxide, CDDP/DQA IC50s and relative lactate levels (Figure 6.13).

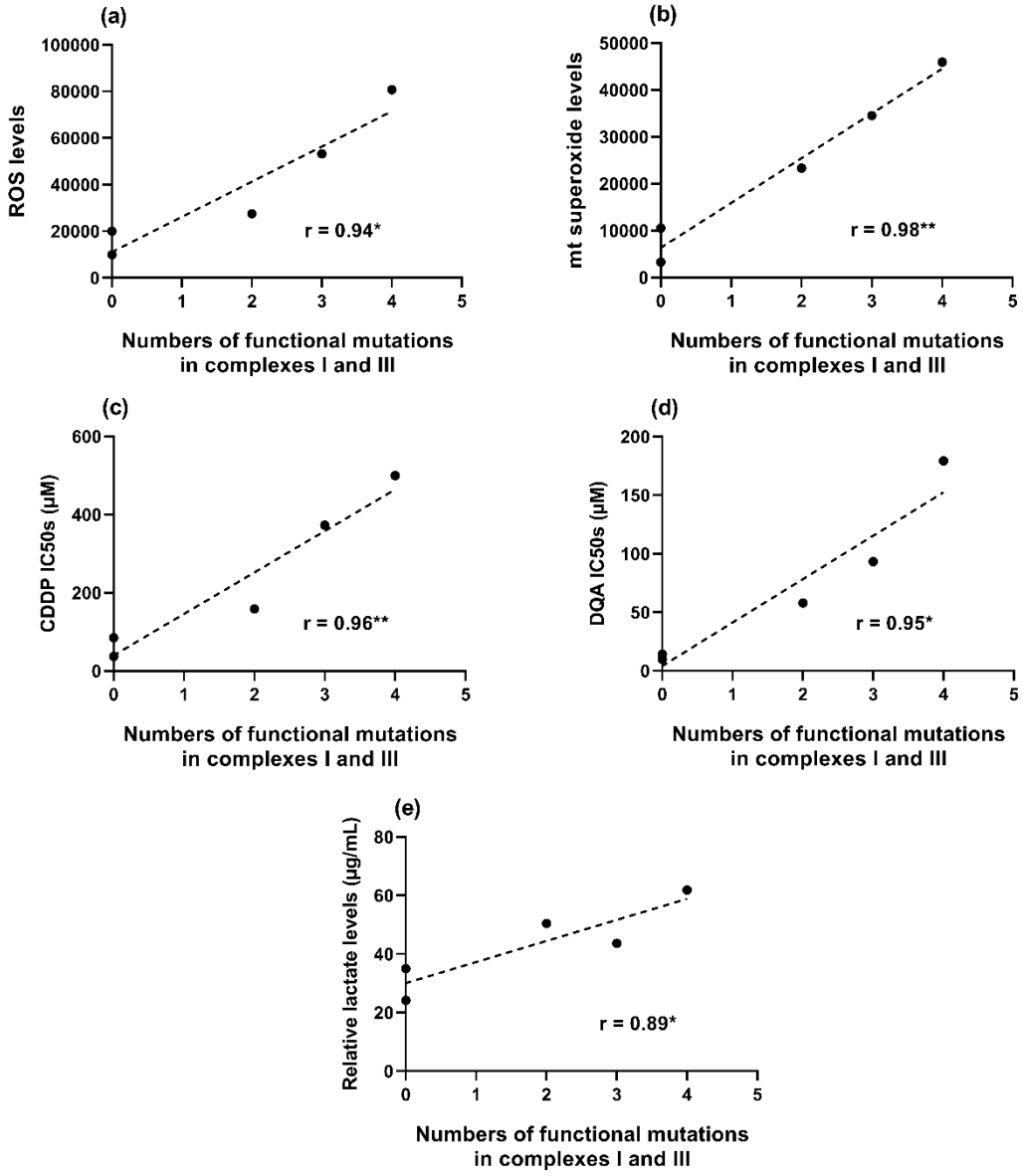

Figure 6.13. Positive correlations between the numbers of functional mutations identified in the complex I & III coding regions and baseline ROS levels (**a**), mitochondrial superoxide levels (**b**), CDDP IC50s (**c**), DQA IC50s (**d**) and lactate levels (**e**). Data points representing the cell lines are in the sequence of PNT-2, Ishikawa, MDA-MB-231, PC-3 and Caco-2. r and *p* and values were calculated using the Pearson correlation coefficient method; **p*<0.05 and ***p*<0.01.

6.3 Discussion

ROS can be generated from both endogenous and exogenous sources, and mitochondria are considered a primary intracellular site of ROS generation when some of the electrons in the mitochondrial electron transport chain escape from the mitochondrial respiratory complexes (mainly I and III) and react with oxygen to generate ROS (reviewed in Ref. [160]). Results presented in Chapters 3, 4 and 5 suggested a correlation between the baseline intracellular ROS levels and drug responses in human cancer cell lines, and addressed how different levels of ROS can influence drug sensitivity. Therefore, ROS was proposed as a novel biomarker to predict drug sensitivity. However, since measuring ROS in tissues is technically challenging, a more efficient biomarker to indicate the response to ROS-stimulating agents is still needed.

In this chapter, specific mitochondrial genetic mutations in cancer cells were identified, and the possibility that mitochondrial genetic alterations could be utilised to predict drug sensitivity is discussed. The discussion will focus on the link between mtDNAcn and baseline intracellular ROS and the implication of mutations in the mitochondrial OXPHOS subunits coding regions as well as in the D-loop region.

6.3.1 Correlation between mitochondrial copy numbers and ROS levels

Cancer cells have various levels of mtDNAcn which are strictly correlated to the demand of ATP generated by OXPHOS, "the major site of ROS production" [302,303]. Indeed, our data showed a positive correlation between mtDNAcn and baseline intracellular ROS and mitochondrial superoxide levels amongst the non-cancerous and 4 cancer cell lines of different tissue origins, which confirmed the previous observation that cells containing larger mtDNAcn also have higher levels of ROS [344].

Moreover, our result confirmed that the prostate cancer cell line (PC-3) had higher mtDNAcn compared to the non-cancerous counterpart cell line (PNT-2), which is in agreement with previous observations obtained from prostate cancer cells and their non-cancerous counterparts (Discussed in Chapter 1, 1.2.6) [345]. Interestingly, all the cancer cell lines in this study showed higher levels of mtDNAcn compared to PNT-2. However, to confirm a greater mtDNAcn in each of the other 3 cancer cell lines (i.e. Ishikawa, MDA-MB-231 and Caco-2), a head-to-head comparison with their non-cancerous counterpart of the same tissue origin is still needed (not conducted in the PhD study).

As discussed above, the good correlation between mtDNAcn and baseline intracellular ROS levels in naïve cancer cells also means that mtDNAcn could be measured instead to indicate the response to mitochondria-targeting therapy, and therefore make a potential biomarker to indicate drug sensitivity.

6.3.2 Correlation between numbers of non-synonymous mutation and ROS levels/drug response in cancer cells

Our data have shown that the non-cancerous cell line, PNT2, had the lowest number of mutations compared to the cancer lines including PC-3. Moreover, the total numbers of non-synonymous mutations within the mitochondrial genome, in particular those in complexes I and III, are strongly correlated with baseline ROS levels and the associated drug resistance. In our study, the conventional chemotherapy (cisplatin) and mitochondria-targeting therapy (dequalinium) compounds as well as their combination caused cell death through the excessive production of ROS as seen in the previous Chapters. A progressive increase in the number of non-synonymous mutations in complexes I and III was observed in Ishikawa (3), MDA-MB-231 (4), PC-3 (5) and Caco-2 (9) cells, which showed the same trend as the baseline ROS level and drug resistance among those cells. Based on these results, it is speculated that cancer cells generally carry more mutations in their mitochondrial genome than non-cancerous cells, which renders higher baseline ROS levels in cancer cells and consequently increased drug resistance/cell survival.

6.3.3 Correlation between numbers of non-synonymous mutation and glycolysis

It is well known that cancer cells reprogramme their energy metabolism by depending more on glycolysis instead of OXPHOS in order to optimise ROS levels and thereby improve survival. Cells under high stress will try to reduce ROS to avoid apoptosis by either upregulating antioxidant enzymes or increasing glycolysis (reviewed in Ref. [303]). Otto Warburg was the first to characterise cancer as preferably utilising glycolysis for ATP production due to mitochondrial dysfunction, a phenomenon coined the “Warburg Effect” (reviewed in Ref. [17]).

The cancer cells enrolled in our study exhibited different levels of mitochondrial dysfunction as indicated by the elevated number of mitochondrial genetic abnormalities compared to the normal cells. Those genetics data were in alignment with increased levels

of intracellular ROS in the cancer cells. Therefore, it was well expected that cells with higher number of non-synonymous mutations within complexes I and III would rely more on glycolysis for ATP generation due to dysfunctional OXPHOS.

The best way to determine the shift between mitochondrial respiration and cytoplasmic glycolysis for ATP generation is to measure oxygen consumption rate and extracellular acidification rate. However, since lactate is produced through glycolysis following the catalysis of pyruvate by lactate dehydrogenase, it can be measured to assess the level of glycolysis in the cytoplasm. Indeed, our data showed a positive correlation between the numbers of non-synonymous mutations in the mitochondrial genome and the glycolysis levels, confirming the metabolic adaption by the cells undergoing oxidative stress.

Since reactive oxygen species are by-products of OXPHOS, cells that are more glycolysis dependent should have less ROS production. Interestingly, this was not the case in our study. Our explanation is that cells with a high baseline ROS level (likely due to mitochondrial dysfunction and relatively low antioxidant activities) will in fact upregulate glycolysis for ATP generation in order to avoid extra ROS generation through OXPHOS. However, the Warburg Effect does not imply a complete switch from OXPHOS to glycolysis. Therefore, a certain level of OXPHOS is expected to occur alongside the enhanced glycolysis in those cancer cells.

As previously described, the metabolic switch between OXPHOS and glycolysis is controlled by the relative activities of pyruvate dehydrogenase (PDH) and lactate dehydrogenase (LDH) (reviewed in Ref. [99]). TCA cycle dysfunction and the resultant oxidative stress have been demonstrated to activate hypoxia-inducible factor 1 (HIF-1) which is well known to catalyses key steps of glycolysis by regulating the expression of glycolytic enzymes (reviewed in Ref. [101]). HIF-1 has been reported to induce pyruvate dehydrogenase kinase 1 (PDK1) that inactivates PDH and consequently supresses the Krebs cycle and mitochondrial respiration (reviewed in Ref. [99]).

In this respect, the expression of *PDK1* in Ishikawa and Caco-2 was examined to confirm the correlation between the oxidative status and the metabolic profile. Our data showed that the Caco-2 cells had significantly upregulated expression of *PDK1* compared to the Ishikawa cells, which supported the higher glycolysis level observed in Caco-2. Considering a much higher ROS level compared to Ishikawa, the Caco-2 cells may well

have an overexpression of ROS-activated HIF-1 and consequently an upregulation of *PDK1* and glycolysis.

6.3.4 Previously reported non-synonymous mutations confirmed by the present study

All the identified non-synonymous mutations in the present study were transitions while only one cytosine → adenine transversion (C15452A) was detected in the Caco-2 cells. A8860G, defined as a polymorphism in complex V in the Human Mitochondrial Genome Database [346,347], was found in all the cell lines involved in the study. A15326G, another known polymorphism located in complex III [348], was found in all the cell lines except PC-3. Both mutations had been previously reported to have negligible impact on mitochondrial function [348]. The C14766T mutation in the cytochrome *b* subunit of complex III causes a threonine to isoleucine change in the protein product. This mutation was found only in the 4 cancer cell lines, indicating that this mutation could interfere with complex III function and contribute to the elevated levels of ROS in the cancer cell lines. However, no previous reports can be found on C14766T. G13708A in complex I has been reported in various types of cancer such as breast and colorectal cancer [349,350]. This mutation was identified only in the PC-3 and Caco-2 cells, which may account for the significantly higher levels of ROS in these two cell lines compared to other cell lines.

Several non-synonymous mutations in complexes I and III observed in the cancer cell lines but not in the non-cancerous PNT-2 cells might have contributed to the elevated levels of ROS in the cancer cells. For example, the T3394C mutation which resulted in the substitution of tyrosine with histidine in complex I was found only in the Ishikawa cells. This variation was previously observed in the tumour lesion but not in the adjacent normal mucosa of non-small cell lung carcinoma (NSCLC) and colon cancer [351]. It was also identified in Leber's Hereditary Optic Neuropathy (LHON) [352]. Both previous studies suggested an association between T3394C and reduced complex I activity [351,352]. It is, therefore, possible that T3394C could interfere with complex I function and as a result, increase electron leakage and ROS generation. The C12084T and A13966G mutations in complex I were found only in the MDA-MB-231 cells in the present study. Both mutations were previously reported to be responsible for reduced complex I activity and enhanced metastatic potential in the MDA-MB-231 cells [353,354]. In fact, mitochondrial respiration defects and ROS overproduction induced by

certain mtDNA mutations can manipulate the malignant transformation of tumour cells in order to promote metastasis. It has been shown that C12084T and A13966G can induce complex I defects in mouse lung carcinoma cells and increase the cells' metastatic potential via ROS overproduction and the resultant overexpression of *Hif-1α* [353].

The T11120C and C13802T mutations in complex I and the A14793G mutation in complex III were found only in the PC-3 cells. A14793G has not been reported in the literature, but both T11120C and C13802T were previously reported in the PC-3 cell line [355]. Given the fact that mtDNA mutations which inhibit the electron transport chain (ETC) and increase ROS production could act as both tumour initiators and promoters, the study suggested that reversing the C13802T mutation to the *wild type* sequence might reduce the tumorigenic potential of the PC-3 cells. Furthermore, increased frequency of complex I mutation in PC-3 was found to inhibit OXPHOS and increase ROS production, and consequently promote tumour growth *in vivo* when those PC-3 cells were injected into nude mice [355].

The highest number of non-synonymous mutations was observed in the Caco-2 cells. Such mutations include T4216C, G7977C, A10398G, A13681G, T14798C, A14927G and C15452A. Amongst these 7 unique mutations, A10398G results in the substitution of threonine with alanine in complex I. This mutation was reported in various types of cancer including brain, breast and cervical cancer, and strongly associated with elevated levels of ROS [356–359]. T14798C results in the substitution of phenylalanine with leucine alanine in complex III. A study conducted by Kathleen *et al.* [21] demonstrated that T14798C carriers amongst patients with glioblastoma had elevated oxidative stress.

The remaining mutations unique to Caco-2 were also observed in several types of cancer [79,360,361] but so far, no published data on their involvement in ROS production are available. However, since the Caco-2 cells had the highest ROS level amongst the cancer cells tested in this study and the previously reported A10398G and T14798C mutations were only identified in Caco-2, we speculate that the other 5 unique non-synonymous mutations found in Caco-2 are likely to be also functional and may have an impact on ROS production.

6.3.5 Potential biomarkers highlighted by structural analysis

One weakness in the aforementioned previous studies is that the researchers could only observe a collective effect of mtDNA mutation on ROS production. It was not clear how individual mutations might have interfered with the ROS level independently. Therefore, it was not possible to rely on the literature only to establish an accurate list of mutations as efficient biomarkers for the prediction of response to ROS-stimulating agents. Cytoplasmic hybrid (cybrid) experiments allow the examination of the impact of a single mutation on the cell's redox status. However, cybrid experiments were not performed in this study due to time and funding limitations. In order to investigate the impact of each non-synonymous mutation identified in our study on ROS production, *in silico* three-dimensional protein structure mapping [21,42,45,48] was used to assess how those mutations could potentially affect the structure and function of the corresponding protein subunit and complex.

One previous study has shown that online predictive algorithms such as SIFT, Mutation Assessor and PolyPhen are not always accurate in predicting the impact of mitochondrial mutations located in subunit interaction regions, since those algorithms are designed for analysing nuclear DNA mutations [45]. Instead, 3D-structural modelling using programmes such as PyMol and Coot provides a detailed visualisation of the complete protein and can take into account of the close interactions between mitochondrial subunits. 3D-strucutral modelling also allows amino acid changes to be visualised. Therefore, it can be a powerful tool for predicting the impact of individual mtDNA mutations on protein structure and function.

Each of the complex I, III, IV and V mutations was analysed using PyMol and Coot as described in Chapter 2, 2.4.5. The location of the changed amino acid was examined and its proximity to the important catalytic regions within the subunit such as binding pockets and active sites was studied. Consequently, the prediction was made according to whether the amino acid change could be tolerated or not at a specific position.

Of the 17 complex I, III, IV and V mutations studied, 9 were predicted to be non-functional mutations. Our predictions for T4216C, C14766T, A14793G, A15326G and C15452A as non-functional mutations were in agreement with previous studies conducted by Lloyd *et al.* and McGeehan *et al.* [42,48] on mitochondrial genomes isolated from glioblastoma cell lines and tissues.

On the other hand, eight mutations were predicted to be functional and the most represented class of functional mutation was Subunit Interaction Mutation whilst only one Binding Pocket Mutation was identified (i.e. T14798C). Our prediction for T14798C as a functional mutation aligns with previous reports by Lloyd *et al.* and Katthleen *et al.* [21,48] where they observed that patient derived glioblastoma multiforme (GBM) cell cultures and primary tissues harboured the T14798C mutation and showed elevated ROS compared to the non-carrier cancer cells.

Interestingly, all the predicted functional mutations locate in complexes I and III. As both complexes are the main producers of ROS, it is well accepted that alterations to those complexes would affect their normal function and lead to changes in ROS production. It is worth noting that the numbers of functional complexes I and III mutations (predicted by 3D-structural modelling) are positively correlated with ROS levels among the cancer cells. This confirms the efficiency of 3D-structural modelling in predicting the impact of these mutations on ROS production. More importantly, it allows us to screen for such mutations as potentially effective biomarker to predict cancer cells' redox status and response to ROS-stimulating agents.

6.3.6 Implication of D-loop mutations in mtDNAcn variations and redox status

The D-loop region consists of two hypervariable regions: hypervariable region 1 (HVR1) located at positions 16,024-16,383 and hypervariable region 2 (HVR2) at positions 57-372; both HV regions exhibit a high frequency of mtDNA mutations [362]. Since the D-loop region is a major control site for mtDNA replication and transcription, mutations in this region can alter the sequence of the light and heavy strand promoters, rendering the loss of their binding affinities to the initiators and modulators of mtDNA transcription, thus, disturbing the rate of transcription, RNA primer synthesis as well as mtDNA replication at the H-strand origin of replication (O_H) [363]. Various studies have documented that D-loop mutations are associated with several multi-factorial genetic diseases, and higher mtDNAcn has also been reported in various types of cancer carrying D-loop mutations [364,365].

Indeed, the D-loop region was a hotspot for mutations identified in the present study. It is difficult to speculate the role of these mutations on mtDNAcn changes due to the limited information in the literature. Moreover, none of the identified mutations was located in the L-strand origin of replication (O_L) and only one mutation (i.e. 310insC) was

in one of the three conserved sequence blocks (CSB 1, 2 and 3) within the H-strand origin of replication (O_H) that harbours critical functional motifs for the initiation and regulation of H-strand replication (Figure 1.4).

Interestingly, the 310insC mutation located in CSB2 was a common mutation in Ishikawa, MDA-MB-231 and PC-3. Given that insertion mutations have a real fundamental impact on DNA function, as they completely change the sequence of the region and result in the shift of the original functional motifs, it is likely that the 310insC mutation may interfere with DNA-primer interaction and have a negative impact on the replication of the H-strand in those cell lines. This observation might explain why the above cell lines had lower mtDNA copy numbers compared to Caco-2 that did not harbour this insertion.

Nevertheless, it is worth mentioning that a few mutations outside the CSBs but still within the O_H were identified in the cancer cells but not the non-cancerous cells (PNT-2) in this study. This might explain the higher copy numbers of mtDNA observed in the cancer cells since those mutations might interfere with the replication of the mitochondrial genome.

However, we were unable to explain the reason behind the different levels of mtDNAcn in the cancer cells as they all had a comparable total number of mutations in the O_H region as well as in the whole D-loop region. It is still worth mentioning that the Caco-2 cells harboured the highest number of unique mutations within the O_H, which may indicate that those Caco-2-specific mutations could be responsible for the highest mtDNAcn observed.

Some mutations identified in our study have already been reported to be associated with increased mtDNAcn, such as C16223T, A16399G and C295T in the Ishikawa, PC-3 and Caco-2 cells respectively [366–368]. Amongst these three mutations, only C295T locates in the O_H region and was identified in Caco-2 only. This observation supports our previous suggestion that the Caco-2-specific mutations might be implicated in the highest mtDNAcn detected in the Caco-2 cells in comparison to other cell lines.

Since the mtDNA mutations in the cells were identified using the Sanger sequencing method, it has not been possible to ascertain whether those mutations were homoplasmy or heteroplasmy. However, the fact that those mutations were successfully detected by Sanger sequencing indicates that they are significantly abundant in the collective mitochondrial genome and may well be pathogenic. Nevertheless, a more advanced technique such as Next Generation Sequencing (NGS) would be able to provide

information on the heteroplasmy rate of those mutations. Furthermore, some of the mutations identified in the cell lines are previously reported SNPs. Unfortunately, it was not realistic to obtain matched white blood cell (WBC) samples of the donors from whose tissues the commercial cell lines were derived. Without the sequencing data from the matched WBC DNA that represents the germline genome of the donor, somatic mutations and SNPs in the derived cell line cannot be differentiated. This is an inherent weakness of the present study because commercial cell lines were employed. In order to keep the terminology simple, all identified mtDNA variants were described as mutations in this thesis.

6.4 Summary

The above observations indicate that high frequency of non-synonymous mutations in complexes I and III would result in increased baseline ROS level and reprogramming of the metabolic pathways to overcome oxidative stress. The positive correlation between the numbers of non-synonymous complexes I/III mutations and ROS/drug response in cancer cells suggests that such mitochondrial genetic abnormalities could be an efficient biomarker to indicate the response to mitochondria-targeting therapy. Indeed, a comprehensive literature search following the structural analysis revealed that a panel of specific mutations within the mitochondrial genome, including A10398G, T11120C, C12084T, A13681G, G13708A, C13802T, A13966G and T14798C, could be used to indicate elevated intracellular ROS and therefore to predict drug resistance to ROS-stimulating agents.

In addition, mtDNA copy number also showed a good correlation with baseline ROS levels. Therefore, mtDNA copy number could be another useful biomarker to predict cancer cells' response to mitochondria-targeting therapy.

Chapter 7
Summary of key findings and future directions

7.1 General discussion of key findings

This study focused on the different baseline intracellular ROS levels among the cancer cells and their impact on the cytotoxic efficacy of cisplatin (CDDP) and dequalinium chloride hydrate (DQA).

The intracellular redox imbalance and the abnormal levels of ROS within the cell may lead to damages to macromolecules that are important for maintaining normal cell functions. Such damages can cause activation of protein kinases and inhibition of protein phosphatases resulting in malignant transformation and cancer development and progression. These events are accompanied by activation of transcription factors, accumulation of defective proteins, and adaptation to high levels of ROS and resistance to ROS-dependent apoptosis. Moreover, prolonged operation of cells at abnormal yet steady-state levels of ROS provokes genetic mutations, which makes the cells well adapted to oxidative stress by mobilising a set of adaptive mechanisms such as activating anti-oxidant systems to mitigate the oxidative stress and inhibit ROS-induced apoptosis. Recent evidences suggest that such adaptation contributes to malignant transformation, metastasis and resistance to anticancer drugs (reviewed in Ref. [168]). The aforementioned data might explain the increased resistance observed in cancer cells with higher baseline intracellular ROS levels.

It is suggested from this study that cancer cells exhibit different baseline intracellular ROS levels due to cell-specific mitochondrial abnormalities and antioxidant capacity. It is concluded that cancer cells with low baseline ROS levels are more sensitive to ROS-stimulating agents compared to cells with high baseline ROS levels. It is possible that cells with low baseline ROS levels are poorly adapted to a robust increase in oxidative stress upon ROS-stimulating therapy and hence become more sensitive, whereas cells with high baseline ROS levels are well adapted to oxidative stress via their developed mitochondrial adaptation mechanisms, enhanced DNA repair mechanisms and upregulated anti-apoptotic pathways to resist ROS-induced cell death.

Observations in this study confirmed that CDDP/DQA exerted their cytotoxic effects through excessive production of ROS. It was revealed that an enhanced ROS generation upon the treatments was largely localised within mitochondria and caused MMP disruption, mtDNA depletion, downregulation of mitochondrial stability markers and

upregulation of mtDNA damage markers. Hence, it was evident from these results that CDDP/DQA induced mitochondrial damage through oxidative stress.

It is also indicated that excessive intracellular ROS induced by the treatments is the essential mediator of mitochondrial dysfunction and cell death, which are in line with previous studies where scavenging of ROS by antioxidants results in the attenuation in cell death. More importantly, this study has demonstrated that cells with lower baseline ROS levels respond better to ROS scavengers when undergoing ROS-stimulating treatment, which grants better cell death attenuation. This indicates that excessive ROS could be the main cause of cell death in cells with relatively low baseline ROS levels, whereas other mechanisms might play a role alongside with ROS in killing cells with relatively high baseline ROS levels.

Our results support the theory that combining conventional chemotherapy with mitochondria-targeting therapy enhances cell death and allows reduced doses of the conventional drug. They also clearly suggest that combining mitochondria-targeting agents could provide improved efficacy while reducing side effects of conventional therapy in treating cancer. Our study highlights the possibility of achieving greater synergistic efficacy of ROS-stimulating agents in treating cancers especially those with low baseline ROS levels compared to others with high baseline ROS levels.

In conclusion, the present study suggests that baseline ROS level in cancer cells could be an efficient predictive biomarker for drug response [369]. However, since measuring ROS in tissues is technically challenging, more efficient biomarkers linked to ROS to indicate the response to ROS-stimulating agents were also investigated in this study.

Mitochondrial dysfunction can be associated with mtDNA alterations such as mutations and changes in the mtDNAcn (reviewed in Ref.s [65,160]). Therefore, this study also focused on the implications of mtDNA abnormalities in ROS related cancer cell death/survival and drug response. Indeed, our data showed a positive correlation between mtDNAcn and baseline intracellular ROS level, which confirmed previous observations that cells containing larger mtDNAcn also have higher levels of ROS. The positive correlation between mtDNAcn and baseline intracellular ROS levels in naïve cancer cells also means that mtDNAcn could be measured instead to indicate the response to mitochondria-targeting therapy, and therefore could be utilised as a potential biomarker to indicate drug sensitivity.

Our data have also shown that the total numbers of non-synonymous mutations within the mitochondrial genome, in particular those in complexes I and III, are strongly correlated with baseline ROS levels and the associated drug resistance. It is speculated that cancer cells generally carry more mutations in their mitochondrial genome than non-cancerous cells, which renders higher baseline ROS levels in cancer cells and consequently increased drug resistance/cell survival. These observations indicate that high frequency of non-synonymous mutations in complexes I and III would result in increased baseline ROS level and reprogramming of the metabolic pathways to overcome oxidative stress. The positive correlation between the numbers of non-synonymous complexes I/III mutations and ROS/drug response in cancer cells suggests that such mitochondrial genetic abnormalities could be an efficient biomarker to indicate the response to mitochondria-targeting therapy. Indeed, a comprehensive literature search following the structural analysis revealed that a panel of specific mutations within the mitochondrial genome could be used to indicate elevated intracellular ROS and hence to predict drug resistance to ROS-stimulating agents.

To our knowledge, this is the first study showing that baseline intracellular ROS levels of cancer cells are associated with drug response and specific mtDNA mutations (e.g. A10398G, T11120C, C12084T, A13681G, G13708A, C13802T, A13966G and T14798C) as well as large mtDNA copy numbers could be linked to elevated intracellular ROS and therefore utilised as biomarkers to predict drug resistance to ROS-stimulating agents.

7.2 Future directions

As the above conclusions have been drawn based on limited *in vitro* work, further studies engaging a wider range of cell lines and ROS-stimulating agents, patient-derived primary cell cultures and tissues, and *in vivo* experiments will be required to validate the present findings.

One of the limitations in this study is that only one non-cancerous cell line (PNT-2) was used in our investigation, which restricted us to compare the redox statuses and genetic profiles of the cancer cell lines from different origins to the same non-cancerous cell line. Therefore, using matched normal–cancer primary cultures or tissues from the same patient will allow more accurate and efficient comparisons in future studies. More importantly, testing those matched samples will enable us to differentiate somatic mutations from germline variations for the mtDNA sequence changes identified in the cancer tissue. In addition, the predicted functional mtDNA mutations and the correlation between mtDNAcn and drug responses observed in this study also need to be tested and verified in clinical samples.

Another limitation of the study lies in the fact that all the cancer cell lines carried multiple mutations in their mitochondrial genomes, which had made it impossible to ascertain any physiobiological impact of those individual mtDNA mutations predicted to be functional by the 3D modelling work. Advanced technologies could be employed in future studies where targeted single mutations would be introduced to the *wild type* mtDNA in non-cancerous cells, and the genetically modified mitochondria would replace their counterpart organelles in cancer cells to generate cybrids. Those cybrid cells can be useful tools to investigate the biological behaviour of cancer cells carrying a specific single mtDNA mutation or a combination of several specific mutations.

Finally, since mitochondrial respiratory chain complexes are composed of both mitochondrial and nuclear subunits to form this elegant molecular machine, screening for functional mutations within the nuclear subunits should be also considered.

Nevertheless, this study has provided an insight into understanding the influence of intracellular ROS on drug sensitivity, and may lead to the development of new therapeutic strategies to improve anticancer drug efficacy.

References

References

1. Frey TG, Mannella CA. The internal structure of mitochondria. *Trends Biochem Sci*. **2000**;25(7):319-24.
2. Taanman JW. The mitochondrial genome: structure, transcription, translation and replication. *Biochim Biophys Acta.* **1999**;1410(2):103-23.
3. Jeng JY, Yeh TS, Lee JW, Lin SH, Fong TH, Hsieh RH. Maintenance of mitochondrial DNA copy number and expression are essential for preservation of mitochondrial function and cell growth. *Cell Biochem.* **2008**;103(2):347-57.
4. Shadel GS, Clayton DA. Mitochondrial DNA maintenance in vertebrates. *Annu Rev Biochem*. **1997**;66:409-35.
5. Sherratt HS. Mitochondria: structure and function. *Rev Neurol*. **1991**;147(6-7):417-30.
6. Arnould T, Michel S, Renard P. Mitochondria Retrograde Signaling and the UPR mt: Where Are We in Mammals? *Int J Mol Sci.* **2015**;16(8):18224-51.
7. Chan DC. Mitochondrial fusion and fission in mammals. *Annu Rev Cell Dev Biol.* **2006**;22:79-99.
8. Okamoto K, Shaw JM. Mitochondrial morphology and dynamics in yeast and multicellular eukaryotes. *Annu Rev Genet.* **2005**;39:503-36.
9. Quintana-Cabrera R, Quirin C, Glytsou C, Corrado M, Urbani A, Pellattiero A, *et al*. The cristae modulator Optic atrophy 1 requires mitochondrial ATP synthase oligomers to safeguard mitochondrial function. *Nat Commun.* **2018**;9(1):1-13.
10. Hoppins S, Nunnari J. The molecular mechanism of mitochondrial fusion. *Biochim Biophys Acta*. **2009**;1793(1):20-6.
11. Eisner V, Lenaers G, Hajnóczky G. Mitochondrial fusion is frequent in skeletal muscle and supports excitation-contraction coupling. *J Cell Biol.* **2014**;205(2):179-95.
12. Twig G, Elorza A, Molina AJ, Mohamed H, Wikstrom JD, Walzer G, *et al*. Fission and selective fusion govern mitochondrial segregation and elimination by autophagy. *EMBO J*. **2008**;27(2):433-46.
13. Wieder SY, Serasinghe MN, Sung JC, Choi DC, Birge MB, Yao JL, *et al*. Activation of the Mitochondrial Fragmentation Protein DRP1 Correlates with BRAF(V600E) Melanoma. *J Invest Dermatol.* **2015**;135(10):2544-47.
14. Van der Bliek AM, Shen Q, Kawajiri S. Mechanisms of mitochondrial fission and fusion. *Cold Spring Harb Perspect Biol.* **2013**;5(6):1-16.
15. Zhang T, Xue L, Li L, Tang C, Wan Z, Wang R, *et al*. BNIP3 Protein Suppresses PINK1 Kinase Proteolytic Cleavage to Promote Mitophagy. *J Biol Chem.* **2016**;291(41):21616-29.
16. Chen G, Kroemer G, Kepp O. Mitophagy: An Emerging Role in Aging and Age-Associated Diseases. *Front Cell Dev Biol*. **2020**;8:200.
17. Cocetta V, Ragazzi E, Montopoli M. Mitochondrial Involvement in Cisplatin Resistance. *Int J Mol Sci.* **2019**;20(14):1-17.
18. Dang S, Qu Y, Wei J, Shao Y, Yang Q, Ji M, *et al*. Low copy number of mitochondrial DNA (mtDNA) predicts worse prognosis in early-stage laryngeal cancer patients. *Diagn Pathol.* **2014**;9(28):1-9.
19. Keogh MJ, Chinnery PF. Mitochondrial DNA mutations in neurodegeneration. *Biochim Biophys Acta*. **2015**;1847(11):1401-11.
20. Lee W, Johnson J, Gough DJ, Donoghue J, Cagnone GL, Vaghjiani V, *et al*. Mitochondrial DNA copy number is regulated by DNA methylation and demethylation of POLGA in stem and cancer cells and their differentiated progeny. *Cell Death Dis.* **2015**;6(2):1-11.
21. Keatley K, Stromei-Cleroux S, Wiltshire T, Rajala N, Burton G, Holt WV, *et al*. Integrated Approach Reveals Role of Mitochondrial Germ-Line Mutation F18L in Respiratory Chain, Oxidative Alterations, Drug Sensitivity, and Patient Prognosis in Glioblastoma. *Int J Mol Sci.* **2019**;20(13):1-20.
22. Falkenberg M. Mitochondrial DNA replication in mammalian cells: overview of the pathway. *Essays Biochem*. **2018**;62(3):287-96.
23. Mohamed Yusoff AA. Role of mitochondrial DNA mutations in brain tumors: A mini-review. *J Cancer Res Ther.* **2015**;11(3):535-44.
24. Attardi G. Animal mitochondrial DNA: an extreme example of genetic economy. *Int Rev Cytol*. **1985**;93:93-145.
25. Szczepanowska K, Trifunovic A. Different faces of mitochondrial DNA mutators. *Biochim Biophys Acta.* **2015**;1847(11):1362-72.

26. Mei H, Sun S, Bai Y, Chen Y, Chai R, Li H. Reduced mtDNA copy number increases the sensitivity of tumor cells to chemotherapeutic drugs. *Cell Death Dis.* **2015**;6(4):1-11.
27. Lu B, Lee J, Nie X, Li M, Morozov YI, Venkatesh S, *et al*. Phosphorylation of human TFAM in mitochondria impairs DNA binding and promotes degradation by the AAA+ Lon protease. *Mol Cell.* **2013**;49(1):121-32.
28. Guittet O, Håkansson P, Voevodskaya N, Fridd S, Gräslund A, Arakawa H, *et al*. Mammalian p53R2 protein forms an active ribonucleotide reductase in vitro with the R1 protein, which is expressed both in resting cells in response to DNA damage and in proliferating cells. *J Biol Chem.* **2001**;276(44):40647-51.
29. Bourdon A, Minai L, Serre V, Jais JP, Sarzi E, Aubert S, *et al*. Mutation of RRM2B, encoding p53-controlled ribonucleotide reductase (p53R2), causes severe mitochondrial DNA depletion. *Nat Genet.* **2007**;39(6):776-80.
30. Gorman GS, Taylor RW. RRM2B-Related Mitochondrial Disease. In: Adam MP, Ardinger HH, Pagon RA, Wallace SE, Bean LJH, Stephens K, *et al*., (editors). GeneReviews® [Internet]. Seattle (WA): University of Washington, Seattle; 2014. 1993-2020. Available from: https://www.ncbi.nlm.nih.gov/books/NBK195854/.
31. Shutt TE, Gray MW. Bacteriophage origins of mitochondrial replication and transcription proteins. *Trends Genet.* **2006**;22(2):90-5.
32. D'Souza AR, Minczuk M. Mitochondrial transcription and translation: overview. *Essays Biochem.* **2018**;62(3):309-20.
33. Gammage PA, Frezza C. Mitochondrial DNA: the overlooked oncogenome?. *BMC Biol.* **2019**;17(53):1-10.
34. Park CB, Larsson NG. Mitochondrial DNA mutations in disease and aging. *J Cell Biol.* **2011**;193(5):809-18.
35. Indran IR, Tufo G, Pervaiz S, Brenner C. Recent advances in apoptosis, mitochondria and drug resistance in cancer cells. *Biochim Biophys Acta.* **2011**;1807(6):735-45.
36. Cormio A, Sanguedolce F, Musicco C, Pesce V, Calò G, Bufo P, *et al*. Mitochondrial dysfunctions in bladder cancer: Exploring their role as disease markers and potential therapeutic targets. *Crit Rev Oncol Hematol*. **2017**;117:67-72.
37. Nadege B, Patrick L, Rodrigue R. Mitochondria: from bioenergetics to the metabolic regulation of carcinogenesis. *Frontiers in Bioscience.* **2009**;14:4015-34.
38. Zhu J, Vinothkumar KR, Hirst J. Structure of mammalian respiratory complex I. *Nature*. **2016**;536(7616):354-8.
39. Fiedorczuk K, Letts JA, Degliesposti G, Kaszuba K, Skehel M, Sazanov LA. Atomic structure of the entire mammalian mitochondrial complex I. *Nature*. **2016**;538(7625):406-10.
40. Baradaran R, Berrisford JM, Minhas GS, Sazanov LA. Crystal structure of the entire respiratory complex I. *Nature*. **2013**;494(7438):443-8.
41. Bezawork-Geleta A, Rohlena J, Dong L, Pacak K, Neuzil J. Mitochondrial Complex II: At the Crossroads. *Trends Biochem Sci*. **2017**;42(4):312-25.
42. McGeehan RE, Cockram LA, Littlewood DTJ, Keatley K, Eccles DM, An Q. Deep sequencing reveals the mitochondrial DNA variation landscapes of breast-to-brain metastasis blood samples. *Mitochondrial DNA Part A.* **2018**;29(5):703-13.
43. Song Z, Laleve A, Vallières C, McGeehan JE, Lloyd RE, Meunier B. Human Mitochondrial Cytochrome b Variants Studied in Yeast: Not All Are Silent Polymorphisms. *Hum Mutat*. **2016**;37(9):933-41.
44. Gao X, Wen X, Esser L, Quinn B, Yu L, Yu CA, *et al*. Structural basis for the quinone reduction in the bc1 complex: a comparative analysis of crystal structures of mitochondrial cytochrome bc1 with bound substrate and inhibitors at the Qi site. *Biochemistry*. **2003**;42(30):9067-80.
45. Lloyd RE, McGeehan JE. Structural analysis of mitochondrial mutations reveals a role for bigenomic protein interactions in human disease. *PLoS One*. **2013**;8(7):1-14.
46. Guo R, Zong S, Wu M, Gu J, Yang M. Architecture of Human Mitochondrial Respiratory Megacomplex $I_2III_2IV_2$. *Cell*. **2017**;170(6):1247-57.
47. Zong S, Wu M, Gu J, Liu T, Guo R, Yang M. Structure of the intact 14-subunit human cytochrome c oxidase. *Cell Res*. **2018**;28(10):1026-34.

48. Lloyd RE, Keatley K, Littlewood DT, Meunier B, Holt WV, An Q, *et al*. Identification and functional prediction of mitochondrial complex III and IV mutations associated with glioblastoma. *Neuro Oncol*. **2015**;17(7):942-52.
49. Muramoto K, Hirata K, Shinzawa-Itoh K, Yoko-o S, Yamashita E, Aoyama H, *et al*. A histidine residue acting as a controlling site for dioxygen reduction and proton pumping by cytochrome c oxidase. *Proc Natl Acad Sci U S A*. **2007**;104(19):7881-6.
50. Rich PR. Mitochondrial cytochrome c oxidase: catalysis, coupling and controversies. *Biochem Soc Trans*. **2017**;45(3):813-29.
51. Zhou A, Rohou A, Schep DG, Bason JV, Montgomery MG, Walker JE, *et al*. Structure and conformational states of the bovine mitochondrial ATP synthase by cryo-EM. *Elife*. **2015**;4:1-15.
52. Lopez J, Tait SW. Mitochondrial apoptosis: killing cancer using the enemy within. *Br J Cancer*. **2015**;112(6):957-62.
53. Desler C, Marcker ML, Singh KK, Rasmussen LJ. The importance of mitochondrial DNA in aging and cancer. *J Aging Res*. **2011**;2011:1-9.
54. Bras M, Queenan B, Susin SA. Programmed cell death via mitochondria: different modes of dying. *Biochemistry*. **2005**;70(2):231-9.
55. Matés JM, Segura JA, Alonso FJ, Márquez J. Oxidative stress in apoptosis and cancer: an update. *Arch Toxicol*. **2012**;86(11):1649-65.
56. Pradelli LA, Bénéteau M, Ricci JE. Mitochondrial control of caspase-dependent and -independent cell death. *Cell Mol Life Sci*. **2010**;67(10):1589-97.
57. Wang C, Youle RJ. The role of mitochondria in apoptosis. *Annu Rev Genet*. **2009**;43:95-118.
58. Huang H, Hu X, Eno CO, Zhao G, Li C, White C. An interaction between Bcl-xL and the voltage-dependent anion channel (VDAC) promotes mitochondrial Ca2+ uptake. *J Biol Chem*. **2013**;288(27):19870-81.
59. Liu Z, Luo Q, Guo C. Bim and VDAC1 are hierarchically essential for mitochondrial ATF2 mediated cell death. *Cancer Cell Int*. **2015**;15(34):1-14.
60. Camara AKS, Zhou Y, Wen PC, Tajkhorshid E, Kwok WM. Mitochondrial VDAC1: A Key Gatekeeper as Potential Therapeutic Target. *Front Physiol*. **2017**;8(460):1-18.
61. Shimizu S, Ide T, Yanagida T, Tsujimoto Y. Electrophysiological study of a novel large pore formed by Bax and the voltage-dependent anion channel that is permeable to cytochrome c. *J Biol Chem*. **2000**;275(16):12321-5.
62. Leist M, Single B, Castoldi AF, Kühnle S, Nicotera P. Intracellular adenosine triphosphate (ATP) concentration: a switch in the decision between apoptosis and necrosis. *J Exp Med*. **1997**;185(8):1481-6.
63. Formigli L, Papucci L, Tani A, Schiavone N, Tempestini A, Orlandini GE, *et al*. Aponecrosis: morphological and biochemical exploration of a syncretic process of cell death sharing apoptosis and necrosis. *J Cell Physiol*. **2000**;182(1):41-9.
64. Li H, Slone J, Fei L, Huang T. Mitochondrial DNA Variants and Common Diseases: A Mathematical Model for the Diversity of Age-Related mtDNA Mutations. *Cells*. **2019**;8(6):608-28.
65. Tokarz P, Blasiak J. Role of mitochondria in carcinogenesis. *Acta Biochim Pol*. 2014;61(4):671-8.
66. Czarnecka AM, Kukwa W, Krawczyk T, Scinska A, Kukwa A, Cappello F. Mitochondrial DNA mutations in cancer--from bench to bedside. *Front Biosci*. **2010**;15:437-60.
67. Taylor RW, Taylor GA, Durham SE, Turnbull DM. The determination of complete human mitochondrial DNA sequences in single cells: implications for the study of somatic mitochondrial DNA point mutations. *Nucleic Acids Res*. **2001**;29(15):1-8.
68. Li H, Slone J, Huang T. The role of mitochondrial-related nuclear genes in age-related common disease. *Mitochondrion*. **2020**;53:38-47.
69. Kauppila JH, Stewart JB. Mitochondrial DNA: Radically free of free-radical driven mutations. *Biochim Biophys Acta.* **2015**;1847(11):1354-61.
70. Gredilla R. DNA damage and base excision repair in mitochondria and their role in aging. *J Aging Res.* **2010**;2011:1-9.
71. Bjelland S, Seeberg E. Mutagenicity, toxicity and repair of DNA base damage induced by oxidation. *Mutat Res*. **2003**;531(1-2):37-80.

72. Sheng Z, Oka S, Tsuchimoto D, Abolhassani N, Nomaru H, Sakumi K, *et al*. 8-Oxoguanine causes neurodegeneration during MUTYH-mediated DNA base excision repair. *J Clin Invest*. **2012**;122(12):4344-61.
73. David SS, O'Shea VL, Kundu S. Base-excision repair of oxidative DNA damage. *Nature*. **2007**;447(7147):941-50.
74. Zharkov DO, Mechetin GV, Nevinsky GA. Uracil-DNA glycosylase: Structural, thermodynamic and kinetic aspects of lesion search and recognition. *Mutat Res*. **2010**;685(1-2):11-20.
75. Ocampo MT, Chaung W, Marenstein DR, Chan MK, Altamirano A, Basu AK, *et al*. Targeted deletion of mNth1 reveals a novel DNA repair enzyme activity. *Mol Cell Biol*. **2002**;22(17):6111-21.
76. Chomyn A, Attardi G. MtDNA mutations in aging and apoptosis. *Biochem Biophys Res Commun*. **2003**;304(3):519-29.
77. Ishikawa K, Takenaga K, Akimoto M, Koshikawa N, Yamaguchi A, Imanishi H, *et al*. ROS-generating mitochondrial DNA mutations can regulate tumor cell metastasis. *Science*. **2008**;320(5876):661-4.
78. Kulawiec M, Owens KM, Singh KK. Cancer cell mitochondria confer apoptosis resistance and promote metastasis. *Cancer Biol Ther*. **2009**;8(14):1378-85.
79. Akouchekian M, Houshmand M, Akbari MH, Kamalidehghan B, Dehghan M. Analysis of mitochondrial ND1 gene in human colorectal cancer. *J Res Med Sci*. **2011**;16(1):50-5.
80. Park JS, Sharma LK, Li H, Xiang R, Holstein D, Wu J, *et al*. A heteroplasmic, not homoplasmic, mitochondrial DNA mutation promotes tumorigenesis via alteration in reactive oxygen species generation and apoptosis. *Hum Mol Genet*. **2009**;18(9):1578-89.
81. Jiang WW, Rosenbaum E, Mambo E, Zahurak M, Masayesva B, Carvalho AL, *et al*. Decreased mitochondrial DNA content in posttreatment salivary rinses from head and neck cancer patients. *Clin Cancer Res*. **2006**;12(5):1564-9.
82. Cooper GM. Mitochondria. In: The Cell: A Molecular Approach. 2nd Edition [Internet]. Sinauer Associates. 2000. Available from: https://www.ncbi.nlm.nih.gov/books/NBK9896/.
83. Blagosklonny MV. How cancer could be cured by 2015. *Cell Cycle*. **2005**;4(2):269–78.
84. Hanahan D, Weinberg RA. Hallmarks of cancer: the next generation. *Cell*. **2011**;144(5):646-74.
85. Housman G, Byler S, Heerboth S, Lapinska K, Longacre M, Snyder N, *et al*. Drug resistance in cancer: an overview. *Cancers*. **2014**;6(3):1769-92.
86. Zhang E, Zhang C, Su Y, Cheng T, Shi C. Newly developed strategies for multifunctional mitochondria-targeted agents in cancer therapy. *Drug Discov Today*. **2011**;16(3-4):140-6.
87. Seyfried TN. Cancer as a mitochondrial metabolic disease. *Front Cell Dev Biol*. 2015;3:43.
88. Koura M, Isaka H, Yoshida MC, Tosu M, Sekiguchi T. Suppression of tumorigenicity in interspecific reconstituted cells and cybrids. *Gan*. **1982**;73(4):574-80.
89. Israel BA, Schaeffer WI. Cytoplasmic suppression of malignancy. *In Vitro Cell Dev Biol*. **1987**;23(9):627-32.
90. Singh KK, Kulawiec M, Still I, Desouki MM, Geradts J, Matsui S. Inter-genomic cross talk between mitochondria and the nucleus plays an important role in tumorigenesis. *Gene*. **2005**;354:140-6.
91. Petros JA, Baumann AK, Ruiz-Pesini E, Amin MB, Sun CQ, Hall J, *et al*. mtDNA mutations increase tumorigenicity in prostate cancer. *Proc Natl Acad Sci U S A*. **2005**;102(3):719-24.
92. Cruz-Bermúdez A, Vallejo CG, Vicente-Blanco RJ, Gallardo ME, Fernández-Moreno MÁ, Quintanilla M, *et al*. Enhanced tumorigenicity by mitochondrial DNA mild mutations. *Oncotarget*. **2015**;6(15):13628-43.
93. Li L, Connelly MC, Wetmore C, Curran T, Morgan JI. Mouse embryos cloned from brain tumors. *Cancer Res*. **2003**;63(11):2733-6.
94. Hu Y, Lu W, Chen G, Wang P, Chen Z, Zhou Y, *et al*. K-ras(G12V) transformation leads to mitochondrial dysfunction and a metabolic switch from oxidative phosphorylation to glycolysis. *Cell Res*. **2012**;22(2):399-412.
95. Warburg O. On the Nature of Cancer Cells. *Science*. 1956;123(3191):309-14.
96. Hanahan D, Weinberg RA. The hallmarks of cancer. *Cell*. **2000**;100(1):57-70.
97. Pavlova NN, Thompson CB. The Emerging Hallmarks of Cancer Metabolism. *Cell Metab*. **2016**;23(1):27-47.

98. Hammond EM, Giaccia AJ. The role of p53 in hypoxia-induced apoptosis. *Biochem Biophys Res Commun*. **2005**;331(3):718-25.
99. Gogvadze V, Orrenius S, Zhivotovsky B. Mitochondria as targets for cancer chemotherapy. *Semin Cancer Biol*. **2009**;19(1):57-66.
100. Wang GL, Semenza GL. General involvement of hypoxia-inducible factor 1 in transcriptional response to hypoxia. *Proc Natl Acad Sci U S A*. **1993**;90(9):4304-8.
101. Kim HK, Noh YH, Nilius B, Ko KS, Rhee BD, Kim N, *et al*. Current and upcoming mitochondrial targets for cancer therapy. *Semin Cancer Biol*. 2017;47:154-67.
102. Wang Y, Agarwal E, Bertolini I, Ghosh JC, Seo JH, Altieri DC. IDH2 reprograms mitochondrial dynamics in cancer through a HIF-1α-regulated pseudohypoxic state. *FASEB J*. **2019**;33(12):13398-411.
103. Kim JW, Dang CV. Cancer's molecular sweet tooth and the Warburg effect. *Cancer Res*. **2006**;66(18):8927-30.
104. Kim JW, Dang CV. Multifaceted roles of glycolytic enzymes. *Trends Biochem Sci.* **2005**;30(3):142-50.
105. Lin CS, Lee HT, Lee MH, Pan SC, Ke CY, Chiu AW, *et al*. Role of Mitochondrial DNA Copy Number Alteration in Human Renal Cell Carcinoma. *Int J Mol Sci*. **2016**;17(6):1-14.
106. Lu F. Reactive oxygen species in cancer, too much or too little?. *Med Hypotheses.* **2007**;69(6):1293-8.
107. Kroemer G, Galluzzi L, Brenner C. Mitochondrial membrane permeabilization in cell death. *Physiol Rev*. **2007**;87(1):99-163.
108. Beroukhim R, Mermel CH, Porter D, Wei G, Raychaudhuri S, Donovan J, *et al*. The landscape of somatic copy-number alteration across human cancers. *Nature*. **2010**;463(7283):899-905.
109. Brenner C, Cadiou H, Vieira HL, Zamzami N, Marzo I, Xie Z, *et al*. Bcl-2 and Bax regulate the channel activity of the mitochondrial adenine nucleotide translocator. *Oncogene*. **2000**;19(3):329-36.
110. Haupt S, Berger M, Goldberg Z, Haupt Y. Apoptosis - the p53 network. *J Cell Sci*. **2003**;116(20):4077-85.
111. Galluzzi L, Morselli E, Kepp O, Vitale I, Rigoni A, Vacchelli E, *et al*. Mitochondrial gateways to cancer. *Mol Aspects Med*. **2010**;31(1):1-20.
112. Gama V, Swahari V, Schafer J, Kole AJ, Evans A, Huang Y, *et al*. The E3 ligase PARC mediates the degradation of cytosolic cytochrome c to promote survival in neurons and cancer cells. *Sci Signal*. **2014**;7(334):1-11.
113. Polyak K, Li Y, Zhu H, Lengauer C, Willson JK, Markowitz SD, *et al*. Somatic mutations of the mitochondrial genome in human colorectal tumours. *Nat Genet*. **1998**;20(3):291-3.
114. Richard SM, Bailliet G, Páez GL, Bianchi MS, Peltomäki P, Bianchi NO. Nuclear and mitochondrial genome instability in human breast cancer. *Cancer Res*. **2000**;60(15):4231-7.
115. Sharma LK, Fang H, Liu J, Vartak R, Deng J, Bai Y. Mitochondrial respiratory complex I dysfunction promotes tumorigenesis through ROS alteration and AKT activation. *Hum Mol Genet*. **2011**;20(23):4605-16.
116. Lu J, Sharma LK, Bai Y. Implications of mitochondrial DNA mutations and mitochondrial dysfunction in tumorigenesis. *Cell Res*. **2009**;19(7):802-15.
117. Sanchez-Cespedes M, Parrella P, Nomoto S, Cohen D, Xiao Y, Esteller M, *et al*. Identification of a mononucleotide repeat as a major target for mitochondrial DNA alterations in human tumors. *Cancer Res.* **2001**;61(19):7015-9.
118. Lee HC, Li SH, Lin JC, Wu CC, Yeh DC, Wei YH. Somatic mutations in the D-loop and decrease in the copy number of mitochondrial DNA in human hepatocellular carcinoma. *Mutat Res*. **2004**;547(1-2):71-8.
119. Huang XW, Zhao Q, Chen DZ, Zhang LS. Mutations in the D-loop region of mitochondrial DNA and the ROS level in the tissue of hepatocellular carcinoma. *Yi Chuan*. **2005**;27(1):14-20.
120. Lee HC, Yin PH, Lin JC, Wu CC, Chen CY, Wu CW, *et al*. Mitochondrial genome instability and mtDNA depletion in human cancers. *Ann N Y Acad Sci*. **2005**;1042:109-22.
121. Lièvre A, Chapusot C, Bouvier AM, Zinzindohoué F, Piard F, Roignot P, *et al*. Clinical value of mitochondrial mutations in colorectal cancer. *J Clin Oncol*. **2005**;23(15):3517-25.

122. Yu M, Shi Y, Zhang F, Zhou Y, Yang Y, Wei X, *et al*. Sequence variations of mitochondrial DNA D-loop region are highly frequent events in familial breast cancer. *J Biomed Sci*. **2008**;15(4):535-43.
123. Lorenc A, Bryk J, Golik P, Kupryjańczyk J, Ostrowski J, Pronicki M, *et al*. MELAS A3243G mtDNA mutation in a colon cancer sample. *Mitochondrion*. **2003**;3(2):119-24.
124. Lombès A, Bories D, Girodon E, Frachon P, Ngo MM, Breton-Gorius J, *et al*. The first pathogenic mitochondrial methionine tRNA point mutation is discovered in splenic lymphoma. *Hum Mutat*. **1998**;1:175-83.
125. Máximo V, Soares P, Lima J, Cameselle-Teijeiro J, Sobrinho-Simões M. Mitochondrial DNA somatic mutations (point mutations and large deletions) and mitochondrial DNA variants in human thyroid pathology: a study with emphasis on Hürthle cell tumors. *Am J Pathol*. **2002**;160(5):1857-65.
126. Fliss MS, Usadel H, Caballero OL, Wu L, Buta MR, Eleff SM, *et al*. Facile detection of mitochondrial DNA mutations in tumors and bodily fluids. *Science*. **2000**;287(5460):2017-9.
127. Jerónimo C, Nomoto S, Caballero OL, Usadel H, Henrique R, Varzim G, *et al*. Mitochondrial mutations in early stage prostate cancer and bodily fluids. *Oncogene*. **2001**;20(37):5195-8.
128. Jones JB, Song JJ, Hempen PM, Parmigiani G, Hruban RH, Kern SE. Detection of mitochondrial DNA mutations in pancreatic cancer offers a "mass"-ive advantage over detection of nuclear DNA mutations. *Cancer Res*. **2001**;61(4):1299-304.
129. Tan DJ, Chang J, Chen WL, Agress LJ, Yeh KT, Wang B, *et al*. Somatic mitochondrial DNA mutations in oral cancer of betel quid chewers. *Ann N Y Acad Sci*. **2004**;1011:310-6.
130. Prior SL, Griffiths AP, Baxter JM, Baxter PW, Hodder SC, Silvester KC, *et al*. Mitochondrial DNA mutations in oral squamous cell carcinoma. *Carcinogenesis*. **2006**;27(5):945-50.
131. Mayr JA, Meierhofer D, Zimmermann F, Feichtinger R, Kögler C, Ratschek M, *et al*. Loss of complex I due to mitochondrial DNA mutations in renal oncocytoma. *Clin Cancer Res*. **2008**;14(8):2270-5.
132. Bonora E, Porcelli AM, Gasparre G, Biondi A, Ghelli A, Carelli V, *et al*. Defective oxidative phosphorylation in thyroid oncocytic carcinoma is associated with pathogenic mitochondrial DNA mutations affecting complexes I and III. *Cancer Res*. **2006**;66(12):6087-96.
133. Vogel R, Nijtmans L, Ugalde C, van den Heuvel L, Smeitink J. Complex I assembly: a puzzling problem. *Curr Opin Neurol*. **2004**;17(2):179-86.
134. Ricci JE, Muñoz-Pinedo C, Fitzgerald P, Bailly-Maitre B, Perkins GA, Yadava N, *et al*. Disruption of mitochondrial function during apoptosis is mediated by caspase cleavage of the p75 subunit of complex I of the electron transport chain. *Cell*. **2004**;117(6):773-86.
135. Parrella P, Xiao Y, Fliss M, Sanchez-Cespedes M, Mazzarelli P, Rinaldi M, *et al*. Detection of mitochondrial DNA mutations in primary breast cancer and fine-needle aspirates. *Cancer Res*. **2001**;61(20):7623-6.
136. Taylor RW, Barron MJ, Borthwick GM, Gospel A, Chinnery PF, Samuels DC, *et al*. Mitochondrial DNA mutations in human colonic crypt stem cells. *J Clin Invest*. **2003**;112(9):1351-60.
137. Máximo V, Sobrinho-Simões M. Hürthle cell tumours of the thyroid. A review with emphasis on mitochondrial abnormalities with clinical relevance. *Virchows Arch*. 2000;437(2):107-15.
138. Liu VW, Shi HH, Cheung AN, Chiu PM, Leung TW, Nagley P, *et al*. High incidence of somatic mitochondrial DNA mutations in human ovarian carcinomas. *Cancer Res*. **2001**;61(16):5998-6001.
139. Dasgupta S, Hoque MO, Upadhyay S, Sidransky D. Mitochondrial cytochrome B gene mutation promotes tumor growth in bladder cancer. *Cancer Res*. 2008;68(3):700-6.
140. Singh RK, Saini SK, Prakasam G, Kalairasan P, Bamezai RNK. Role of ectopically expressed mtDNA encoded cytochrome c oxidase subunit I (MT-COI) in tumorigenesis. *Mitochondrion*. **2019**;49:56-65.
141. Vives-Bauza C, Gonzalo R, Manfredi G, Garcia-Arumi E, Andreu AL. Enhanced ROS production and antioxidant defenses in cybrids harbouring mutations in mtDNA. *Neurosci Lett*. **2006**;391(3):136-41.
142. Shidara Y, Yamagata K, Kanamori T, Nakano K, Kwong JQ, Manfredi G, *et al*. Positive contribution of pathogenic mutations in the mitochondrial genome to the promotion of cancer by prevention from apoptosis. *Cancer Res*. **2005**;65(5):1655-63.

143. Simonnet H, Alazard N, Pfeiffer K, Gallou C, Béroud C, Demont J, *et al*. Low mitochondrial respiratory chain content correlates with tumor aggressiveness in renal cell carcinoma. *Carcinogenesis*. **2002**;23(5):759-68.
144. Guo ZS, Jin CL, Yao ZJ, Wang YM, Xu BT. Analysis of the Mitochondrial 4977 Bp Deletion in Patients with Hepatocellular Carcinoma. *Balkan J Med Genet*. **2017**;20(1):81-6.
145. Veltri KL, Espiritu M, Singh G. Distinct genomic copy number in mitochondria of different mammalian organs. *J Cell Physiol*. **1990**;143(1):160-4.
146. Mondal R, Ghosh SK, Choudhury JH, Seram A, Sinha K, Hussain M, *et al*. Mitochondrial DNA copy number and risk of oral cancer: a report from Northeast India. *PLoS One*. **2013**;8(3):1-8.
147. Tong H, Zhang L, Gao J, Wen S, Zhou H, Feng S. Methylation of mitochondrial DNA displacement loop region regulates mitochondrial copy number in colorectal cancer. *Mol Med Rep*. **2017**;16(4):5347-53.
148. Wang Y, Liu VW, Xue WC, Tsang PC, Cheung AN, Ngan HY. The increase of mitochondrial DNA content in endometrial adenocarcinoma cells: a quantitative study using laser-captured microdissected tissues. *Gynecol Oncol*. **2005**;98(1):104-10.
149. Jiang WW, Masayesva B, Zahurak M, Carvalho AL, Rosenbaum E, Mambo E, *et al*. Increased mitochondrial DNA content in saliva associated with head and neck cancer. *Clin Cancer Res*. **2005**;11(7):2486-91.
150. Lynch SM, Weinstein SJ, Virtamo J, Lan Q, Liu CS, Cheng WL, *et al*. Mitochondrial DNA copy number and pancreatic cancer in the alpha-tocopherol beta-carotene cancer prevention study. *Cancer Prev Res*. **2011**;4(11):1912-9.
151. Feng S, Xiong L, Ji Z, Cheng W, Yang H. Correlation between increased copy number of mitochondrial DNA and clinicopathological stage in colorectal cancer. *Oncol Lett*. **2011**;2(5):899-903.
152. Purdue MP, Hofmann JN, Colt JS, Hoxha M, Ruterbusch JJ, Davis FG, *et al*. A case-control study of peripheral blood mitochondrial DNA copy number and risk of renal cell carcinoma. *PLoS One*. **2012**;7(8):1-5.
153. Mambo E, Chatterjee A, Xing M, Tallini G, Haugen BR, Yeung SC, *et al*. Tumor-specific changes in mtDNA content in human cancer. *Int J Cancer*. **2005**;116(6):920-4.
154. Bai RK, Chang J, Yeh KT, Lou MA, Lu JF, Tan DJ, *et al*. Mitochondrial DNA content varies with pathological characteristics of breast cancer. *J Oncol*. **2011**;2011:1-11.
155. Morten KJ, Ashley N, Wijburg F, Hadzic N, Parr J, Jayawant S, *et al*. Liver mtDNA content increases during development: a comparison of methods and the importance of age- and tissue-specific controls for the diagnosis of mtDNA depletion. *Mitochondrion*. **2007**;7(6):386-95.
156. Wang Y, Liu VW, Xue WC, Cheung AN, Ngan HY. Association of decreased mitochondrial DNA content with ovarian cancer progression. *Br J Cancer*. **2006**;95(8):1087-91.
157. Cerritelli SM, Frolova EG, Feng C, Grinberg A, Love PE, Crouch RJ. Failure to produce mitochondrial DNA results in embryonic lethality in Rnaseh1 null mice. *Mol Cell*. **2003**;11(3):807-15.
158. Wang J, Silva JP, Gustafsson CM, Rustin P, Larsson NG. Increased in vivo apoptosis in cells lacking mitochondrial DNA gene expression. *Proc Natl Acad Sci U S A*. **2001**;98(7):4038-43.
159. Phaniendra A, Jestadi DB, Periyasamy L. Free radicals: properties, sources, targets, and their implication in various diseases. *Indian J Clin Biochem*. **2015**;30(1):11-26.
160. Zou Z, Chang H, Li H, Wang S. Induction of reactive oxygen species: an emerging approach for cancer therapy. *Apoptosis*. **2017**;22(11):1321-35.
161. Hancock JT, Desikan R, Neill SJ. Role of reactive oxygen species in cell signalling pathways. Biochem Soc *Trans*. **2001**;29(2):345-50.
162. Birben E, Sahiner UM, Sackesen C, Erzurum S, Kalayci O. Oxidative stress and antioxidant defense. *World Allergy Organ J*. **2012**;5(1):9-19.
163. Finkel T, Holbrook NJ. Oxidants, oxidative stress and the biology of ageing. *Nature*. **2000**;408(6809):239-47.
164. Kumari S, Badana AK, G MM, G S, Malla R. Reactive Oxygen Species: A Key Constituent in Cancer Survival. *Biomark Insights*. **2018**;13:1-9.
165. Cross AR, Segal AW. The NADPH oxidase of professional phagocytes--prototype of the NOX electron transport chain systems. *Biochim Biophys Acta*. **2004**;1657(1):1-22.

166. Chio IIC, Tuveson DA. ROS in Cancer: The Burning Question. *Trends Mol Med*. **2017**;23(5):411-29.
167. Gupta RK, Patel AK, Shah N, Chaudhary AK, Jha UK, Yadav UC, *et al*. Oxidative stress and antioxidants in disease and cancer: a review. *Asian Pac J Cancer Prev*. **2014**;15(11):4405-9.
168. Georgieva E, Ivanova D, Zhelev Z, Bakalova R, Gulubova M, Aoki I. Mitochondrial Dysfunction and Redox Imbalance as a Diagnostic Marker of "Free Radical Diseases". *Anticancer Res*. **2017**;37(10):5373-81.
169. Oka S, Hayashi M, Taguchi K, Hidaka M, Tsuzuki T, Sekiguchi M. ROS control in human iPS cells reveals early events in spontaneous carcinogenesis. *Carcinogenesis*. **2020**;41(1):36-43.
170. Valko M, Izakovic M, Mazur M, Rhodes CJ, Telser J. Role of oxygen radicals in DNA damage and cancer incidence. *Mol Cell Biochem*. **2004**;266(1-2):37-56.
171. Kelly FJ, Mudway IS. Protein oxidation at the air-lung interface. *Amino Acids*. **2003**;25(3-4):375-96.
172. Perkins ND. Integrating cell-signalling pathways with NF-kappaB and IKK function. *Nat Rev Mol Cell Bio*l. **2007**;8(1):49-62.
173. Abate C, Patel L, Rauscher FJ 3rd, Curran T. Redox regulation of fos and jun DNA-binding activity in vitro. *Science*. **1990**;249(4973):1157-61.
174. Ameyar M, Wisniewska M, Weitzman JB. A role for AP-1 in apoptosis: the case for and against. *Biochimie*. **2003**;85(8):747-52.
175. Idelchik MDPS, Begley U, Begley TJ, Melendez JA. Mitochondrial ROS control of cancer. *Semin Cancer Biol*. **2017**;47:57-66.
176. Rahman I, MacNee W. Lung glutathione and oxidative stress: implications in cigarette smoke-induced airway disease. *Am J Physiol*. **1999**;277(6):1067-88.
177. Weinberg F, Chandel NS. Mitochondrial metabolism and cancer. *Ann N Y Acad Sci*. **2009**;1177:66-73.
178. Adler V, Yin Z, Tew KD, Ronai Z. Role of redox potential and reactive oxygen species in stress signaling. *Oncogene*. **1999**;18(45):6104-11.
179. Woo SH, Park IC, Park MJ, An S, Lee HC, Jin HO, *et al*. Arsenic trioxide sensitizes CD95/Fas-induced apoptosis through ROS-mediated upregulation of CD95/Fas by NF-kappaB activation. *Int J Cancer*. **2004**;112(4):596-606.
180. Kim S, Lee TJ, Leem J, Choi KS, Park JW, Kwon TK. Sanguinarine-induced apoptosis: generation of ROS, down-regulation of Bcl-2, c-FLIP, and synergy with TRAIL. *J Cell Biochem*. **2008**;104(3):895-907.
181. Devadas S, Zaritskaya L, Rhee SG, Oberley L, Williams MS. Discrete generation of superoxide and hydrogen peroxide by T cell receptor stimulation: selective regulation of mitogen-activated protein kinase activation and fas ligand expression. *J Exp Med*. **2002**;195(1):59-70.
182. Yu CY, Jerry Teng CL, Hung PS, Cheng CC, Hsu SL, Hwang GY, *et al*. Ovatodiolide isolated from Anisomeles indica induces cell cycle G2/M arrest and apoptosis via a ROS-dependent ATM/ATR signaling pathways. *Eur J Pharmacol*. **2018**;819:16-29.
183. Qian, Kumar, Roginskaya, Fouquerel, Opresko PL, Shiva S, *et al*. Chemoptogenetic damage to mitochondria causes rapid telomere dysfunction. *Proc Natl Acad Sci U S A*. **2019**;116(37):18435–44.
184. Waring P. Redox active calcium ion channels and cell death. *Arch Biochem Biophys*. **2005**;434(1):33-42.
185. Wang SJ, Gu W. To be, or not to be: functional dilemma of p53 metabolic regulation. *Curr Opin Oncol*. **2014**;26(1):78-85.
186. Kruiswijk F, Labuschagne CF, Vousden KH. p53 in survival, death and metabolic health: a lifeguard with a licence to kill. *Nat Rev Mol Cell Biol*. **2015**;16(7):393-405.
187. Gao W, Xu K, Li P, Tang B. Functional roles of superoxide and hydrogen peroxide generated by mitochondrial DNA mutation in regulating tumorigenicity of HepG2 cells. *Cell Biochem Funct*. **2011**;29(5):400-7.
188. Bell EL, Emerling BM, Ricoult SJ, Guarente L. SirT3 suppresses hypoxia inducible factor 1α and tumor growth by inhibiting mitochondrial ROS production. *Oncogene*. **2011**;30(26):2986-96.
189. Liu H, Kato Y, Erzinger SA, Kiriakova GM, Qian Y, Palmieri D, *et al*. The role of MMP-1 in breast cancer growth and metastasis to the brain in a xenograft model. *BMC Cancer*. **2012**;12(583);1-11.

190. Nelson KK, Melendez JA. Mitochondrial redox control of matrix metalloproteinases. *Free Radic Biol Med*. **2004**;37(6):768-84.
191. Lee SY, Jeong EK, Ju MK, Jeon HM, Kim MY, Kim CH, *et al*. Induction of metastasis, cancer stem cell phenotype, and oncogenic metabolism in cancer cells by ionizing radiation. *Mol Cancer*. **2017**;16(10):1-25.
192. Nagarajan D, Melo T, Deng Z, Almeida C, Zhao W. ERK/GSK3β/Snail signaling mediates radiation-induced alveolar epithelial-to-mesenchymal transition. *Free Radic Biol Med*. **2012**;52(6):983-92.
193. Wu Y, Deng J, Rychahou PG, Qiu S, Evers BM, Zhou BP. Stabilization of snail by NF-kappaB is required for inflammation-induced cell migration and invasion. *Cancer Cell*. **2009**;15(5):416-28.
194. He E, Pan F, Li G, Li J. Fractionated Ionizing Radiation Promotes Epithelial-Mesenchymal Transition in Human Esophageal Cancer Cells through PTEN Deficiency-Mediated Akt Activation. *PLoS One*. **2015**;10(5):1-14.
195. Mori K, Uchida T, Yoshie T, Mizote Y, Ishikawa F, Katsuyama M, *et al*. mitochondrial ROS pathway controls matrix metalloproteinase 9 levels and invasive properties in RAS-activated cancer cells. *FEBS J*. **2019**;286(3):459-478.
196. Meng Y, Chen CW, Yung MMH, Sun W, Sun J, Li Z, *et al*. DUOXA1-mediated ROS production promotes cisplatin resistance by activating ATR-Chk1 pathway in ovarian cancer. *Cancer Lett*. **2018**;428:104-16.
197. Yang Y, Guo R, Tian X, Zhang Z, Zhang P, Li C, *et al*. Synergistic anti-tumor activity of Nimotuzumab in combination with Trastuzumab in HER2-positive breast cancer. *Biochem Biophys Res Commun.* **2017**;489(4):523-7.
198. Santoro V, Jia R, Thompson H, Nijhuis A, Jeffery R, Kiakos K, *et al*. Role of Reactive Oxygen Species in the Abrogation of Oxaliplatin Activity by Cetuximab in Colorectal Cancer. *J Natl Cancer Inst.* **2015**;108(6):1-11.
199. Cao S, Xia M, Mao Y, Zhang Q, Donkor PO, Qiu F, *et al*. Combined oridonin with cetuximab treatment shows synergistic anticancer effects on laryngeal squamous cell carcinoma: involvement of inhibition of EGFR and activation of reactive oxygen species-mediated JNK pathway. *Int J Oncol.* **2016**;49(5):2075-87.
200. Leone A, Roca MS, Ciardiello C, Terranova-Barberio M, Vitagliano C, Ciliberto G, *et al*. Vorinostat synergizes with EGFR inhibitors in NSCLC cells by increasing ROS via up-regulation of the major mitochondrial porin VDAC1 and modulation of the c-Myc-NRF2-KEAP1 pathway. *Free Radic Biol Med*. **2015**;89:287-99.
201. Oh H, Lee M, Kim E, Kwak A, Seo J, Yoon G, *et al*. Dual inhibition of EGFR and MET by Echinatin retards cell growth and induces apoptosis of lung cancer cells sensitive or resistant to gefitinib. *Phytother Res*. **2020**;34(2):388-400.
202. Hui KF, Lam BH, Ho DN, Tsao SW, Chiang AK. Bortezomib and SAHA synergistically induce ROS-driven caspase-dependent apoptosis of nasopharyngeal carcinoma and block replication of Epstein-Barr virus. *Mol Cancer Ther*. **2013**;12(5):747-58.
203. Hu Y, Zhao C, Zheng H, Lu K, Shi D, Liu Z, *et al*. A novel STAT3 inhibitor HO-3867 induces cell apoptosis by reactive oxygen species-dependent endoplasmic reticulum stress in human pancreatic cancer cells. *Anticancer Drugs*. **2017**;28(4):392-400.
204. Wu S, Xing D. Mechanism of mitochondrial membrane permeabilization during apoptosis under photofrin-mediated photodynamic therapy. *J Xray Sci Technol*. **2012**;20(3):363-72.
205. Gdovin MJ, Kadri N, Rios L, Holliday S, Jordan Z. Focal photodynamic intracellular acidification as a cancer therapeutic. *Semin Cancer Biol*. **2017**;43:147-56.
206. Dayal R, Singh A, Pandey A, Mishra KP. Reactive oxygen species as mediator of tumor radiosensitivity. *Cancer Res Ther*. **2014**;10(4):811-8.
207. Pluchino LA, Choudhary S, Wang HC. Reactive oxygen species-mediated synergistic and preferential induction of cell death and reduction of clonogenic resistance in breast cancer cells by combined cisplatin and FK228. *Cancer Lett*. **2016**;381(1):124-32.
208. Itoh T, Terazawa R, Kojima K, Nakane K, Deguchi T, Ando M, *et al*. Cisplatin induces production of reactive oxygen species via NADPH oxidase activation in human prostate cancer cells. *Free Radic Res*. **2011**;45(9):1033-9.

209. Marullo R, Werner E, Degtyareva N, Moore B, Altavilla G, Ramalingam SS, *et al*. Cisplatin induces a mitochondrial-ROS response that contributes to cytotoxicity depending on mitochondrial redox status and bioenergetic functions. *PLoS One*. **2013**;8(11):1-15.
210. Zhang LH, Yang AJ, Wang M, Liu W, Wang CY, Xie XF, *et al*. Enhanced autophagy reveals vulnerability of P-gp mediated epirubicin resistance in triple negative breast cancer cells. *Apoptosis*. **2016**;21(4):473-88.
211. Ledoux S, Yang R, Friedlander G, Laouari D. Glucose depletion enhances P-glycoprotein expression in hepatoma cells: role of endoplasmic reticulum stress response. *Cancer Res*. **2003**;63(21):7284-90.
212. Terada Y, Ogura J, Tsujimoto T, Kuwayama K, Koizumi T, Sasaki S, *et al*. Intestinal P-glycoprotein expression is multimodally regulated by intestinal ischemia-reperfusion. *J Pharm Pharm Sci*. **2014**;17(2):266-76.
213. Nguyen C, Pandey S. Exploiting Mitochondrial Vulnerabilities to Trigger Apoptosis Selectively in Cancer Cells. *Cancers (Basel)*. **2019**;11(7):916-35.
214. Xu RH, Pelicano H, Zhou Y, Carew JS, Feng L, Bhalla KN, *et al*. Inhibition of glycolysis in cancer cells: a novel strategy to overcome drug resistance associated with mitochondrial respiratory defect and hypoxia. *Cancer Res*. **2005**;65(2):613-21.
215. Gill KS, Fernandes P, O'Donovan TR, McKenna SL, Doddakula KK, Power DG, *et al*. Glycolysis inhibition as a cancer treatment and its role in an anti-tumour immune response. *Biochim Biophys Acta*. **2016**;1866(1):87-105.
216. Wang F, Ogasawara MA, Huang P. Small mitochondria-targeting molecules as anti-cancer agents. *Mol Aspects Med*. **2010**;31(1):75-92.
217. Montero J, Letai A. Why do BCL-2 inhibitors work and where should we use them in the clinic?. *Cell Death Differ*. **2018**;25(1):56-64.
218. Wolvetang EJ, Johnson KL, Krauer K, Ralph SJ, Linnane AW. Mitochondrial respiratory chain inhibitors induce apoptosis. *FEBS Lett*. **1994**;339(1-2):40-4.
219. Pelicano H, Feng L, Zhou Y, Carew JS, Hileman EO, Plunkett W, *et al*. Inhibition of mitochondrial respiration: a novel strategy to enhance drug-induced apoptosis in human leukemia cells by a reactive oxygen species-mediated mechanism. *J Biol Chem*. **2003**;278(39):37832-9.
220. Huang P, Feng L, Oldham EA, Keating MJ, Plunkett W. Superoxide dismutase as a target for the selective killing of cancer cells. *Nature*. **2000**;407(6802):390-5.
221. Matei D, Schilder J, Sutton G, Perkins S, Breen T, Quon C, *et al*. Activity of 2 methoxyestradiol (Panzem NCD) in advanced, platinum-resistant ovarian cancer and primary peritoneal carcinomatosis: a Hoosier Oncology Group trial. *Gynecol Oncol*. **2009**;115(1):90-96.
222. Tevaarwerk AJ, Holen KD, Alberti DB, Sidor C, Arnott J, Quon C, *et al*. Phase I trial of 2-methoxyestradiol Nano Crystal dispersion in advanced solid malignancies. *Clin Cancer Res*. **2009**;15(4):1460-5.
223. Kim SH, Kil IS, Kwon OS, Kang BS, Lee DS, Lee HS, *et al*. Oxalomalate reduces tumor progression in melanoma via ROS-dependent proapoptotic and antiangiogenic effects. *Biochimie*. **2019**;158:165-71.
224. Pastorino JG, Hoek JB. Regulation of hexokinase binding to VDAC. *J Bioenerg Biomembr*. **2008**;40(3):171-82.
225. Haridas V, Li X, Mizumachi T, Higuchi M, Lemeshko VV, Colombini M, *et al*. A novel plant-derived metabolite lowers energy metabolism in tumor cells by targeting the outer mitochondrial membrane. *Mitochondrion*. **2007**;7(3):234-40.
226. Giurgiovich AJ, Diwan BA, Olivero OA, Anderson LM, Rice JM, Poirier MC. Elevated mitochondrial cisplatin-DNA adduct levels in rat tissues after transplacental cisplatin exposure. *Carcinogenesis*. **1997**;18(1):93-6.
227. Segal-Bendirdjian E, Coulaud D, Roques BP, Le Pecq JB. Selective loss of mitochondrial DNA after treatment of cells with ditercalinium (NSC 335153), an antitumor bis-intercalating agent. *Cancer Res*. **1988**;48(17):4982-92.
228. Galanski M. Recent developments in the field of anticancer platinum complexes. *Recent Pat Anticancer Drug Discov*. 2006;1(2):285-95.
229. Dasari S, Tchounwou PB. Cisplatin in cancer therapy: molecular mechanisms of action. *Eur J Pharmacol*. **2014**;740:364-78.

230. Martinho N, Santos TCB, Florindo HF, Silva LC. Cisplatin-Membrane Interactions and Their Influence on Platinum Complexes Activity and Toxicity. *Front Physiol*. **2019**;9:1-15.
231. Pascoe JM, Roberts JJ. Interactions between mammalian cell DNA and inorganic platinum compounds. II. Interstrand cross-linking of isolated and cellular DNA by platinum(IV) compounds. *Biochem Pharmacol*. **1974**;23(9):1345-57.
232. Fichtinger-Schepman AM, van der Veer JL, den Hartog JH, Lohman PH, Reedijk J. Adducts of the antitumor drug cis-diamminedichloroplatinum (II) with DNA: formation, identification, and quantitation. *Biochemistry*. **1985**;24(3):707-13.
233. Robertazzi A, Platts JA. Hydrogen bonding and covalent effects in binding of cisplatin to purine bases: Ab initio and atoms in molecules studies. *Inorg Chem*. **2005**;44(2):267–74.
234. Pinto AL, Lippard SJ. Sequence-dependent termination of in vitro DNA synthesis by cis- and trans-diamminedichloroplatinum (II). *Proc Natl Acad Sci U S A*. **1985**;82(14):4616-9.
235. Ciccarelli RB, Solomon MJ, Varshavsky A, Lippard SJ. In vivo effects of cis- and trans-diamminedichloroplatinum (II) on SV40 chromosomes: differential repair, DNA-protein cross-linking, and inhibition of replication. *Biochemistry*. **1985**;24(26):7533-40.
236. Mello JA, Lippard SJ, Essigmann JM. DNA adducts of cis-diamminedichloroplatinum (II) and its trans isomer inhibit RNA polymerase II differentially in vivo. *Biochemistry*. **1995**;34(45):14783-91.
237. Ormerod MG, Orr RM, Peacock JH. The role of apoptosis in cell killing by cisplatin: a flow cytometric study. *Br J Cancer*. **1994**;69(1):93-100.
238. Dzamitika S, Salerno M, Pereira-Maia E, Le Moyec L, Garnier-Suillerot A. Preferential energy- and potential-dependent accumulation of cisplatin-gutathione complexes in human cancer cell lines (GLC4 and K562): A likely role of mitochondria. *J Bioenerg Biomembr*. **2006**;38(1):11-21.
239. Alborzinia H, Can S, Holenya P, Scholl C, Lederer E, Kitanovic I, *et al*. Real-time monitoring of cisplatin-induced cell death. *PLoS One*. **2011**;6(5):1-9.
240. Choi YM, Kim HK, Shim W, Anwar MA, Kwon JW, Kwon HK, *et al*. Mechanism of Cisplatin-Induced Cytotoxicity Is Correlated to Impaired Metabolism Due to Mitochondrial ROS Generation. *PLoS One*. **2015**;10(8):1-21.
241. Brock PR, Knight KR, Freyer DR, Campbell KC, Steyger PS, Blakley BW, *et al*. Platinum-induced ototoxicity in children: a consensus review on mechanisms, predisposition, and protection, including a new International Society of Pediatric Oncology Boston ototoxicity scale. *J Clin Oncol.* **2012**;30(19):2408-17.
242. McWhinney SR, Goldberg RM, McLeod HL. Platinum neurotoxicity pharmacogenetics. *Mol Cancer Ther.* **2009**;8(1):10-6.
243. Yao X, Panichpisal K, Kurtzman N, Nugent K. Cisplatin nephrotoxicity: a review. *Am J Med Sci*. **2007**;334(2):115-24.
244. Amable L. Cisplatin resistance and opportunities for precision medicine. *Pharmacol Res*. **2016**;106:27-36.
245. Ozols RF. Treatment goals in ovarian cancer. *Int J Gynecol Cancer*. **2005**;15:3-11.
246. Giaccone G. Clinical perspectives on platinum resistance. *Drugs*. **2000**;59:9-17.
247. Köberle B, Tomicic MT, Usanova S, Kaina B. Cisplatin resistance: preclinical findings and clinical implications. *Biochim Biophys Acta*. **2010**;1806(2):172-82.
248. Kartalou M, Essigmann JM. Mechanisms of resistance to cisplatin. *Mutat Res*. **2001**;478(1-2):23-43.
249. Siddik ZH. Cisplatin: mode of cytotoxic action and molecular basis of resistance. *Oncogene*. **2003**;22(47):7265-79.
250. Galluzzi L, Senovilla L, Vitale I, Michels J, Martins I, Kepp O, *et al*. Molecular mechanisms of cisplatin resistance. *Oncogene*. **2012**;31(15):1869-83.
251. Damia G, Broggini M. Platinum Resistance in Ovarian Cancer: Role of DNA Repair. *Cancers*. **2019**;11(1):1-15.
252. Qian W, Nishikawa M, Haque AM, Hirose M, Mashimo M, Sato E, *et al*. Mitochondrial density determines the cellular sensitivity to cisplatin-induced cell death. *Am J Physiol Cell Physiol.* **2005**;289(6):1466-75.
253. Park SY, Chang I, Kim JY, Kang SW, Park SH, Singh K, *et al*. Resistance of mitochondrial DNA-depleted cells against cell death: role of mitochondrial superoxide dismutase. *J Biol Chem*. **2004**;279(9):7512-20.

254. Marrache S, Pathak RK, Dhar S. Detouring of cisplatin to access mitochondrial genome for overcoming resistance. *Proc Natl Acad Sci U S A*. **2014**;111(29):10444-9.
255. Modica-Napolitano JS, Aprille JR. Delocalized lipophilic cations selectively target the mitochondria of carcinoma cells. *Adv Drug Deliv Rev*. **2001**;49(1-2):63-70.
256. Modica-Napolitano JS, Nalbandian R, Kidd ME, Nalbandian A, Nguyen CC. The selective in vitro cytotoxicity of carcinoma cells by AZT is enhanced by concurrent treatment with delocalized lipophilic cations. *Cancer Lett*. **2003**;198(1):59-68.
257. Modica-Napolitano JS, Aprille JR. Basis for the selective cytotoxicity of rhodamine 123. *Cancer Res*. **1987**;47(16):4361-5.
258. Murphy MP, Smith RA. Drug delivery to mitochondria: the key to mitochondrial medicine. *Adv Drug Deliv Rev*. **2000**;41(2):235-50.
259. Baracca A, Sgarbi G, Solaini G, Lenaz G. Rhodamine 123 as a probe of mitochondrial membrane potential: evaluation of proton flux through F(0) during ATP synthesis. *Biochim Biophys Acta*. **2003**;1606(1-3):137-46.
260. Anderson WM, Patheja HS, Delinck DL, Baldwin WW, Smiley ST, Chen LB. Inhibition of bovine heart mitochondrial and Paracoccus denitrificans NADH----ubiquinone reductase by dequalinium chloride and three structurally related quinolinium compounds. *Biochem Int*. **1989**;19(4):673-85.
261. Chunta JL, Vistisen KS, Yazdi Z, Braun RD. Uptake rate of cationic mitochondrial inhibitor MKT-077 determines cellular oxygen consumption change in carcinoma cells. *PLoS One*. **2012**;7(5):1-15.
262. Singh KK, Russell J, Sigala B, Zhang Y, Williams J, Keshav KF. Mitochondrial DNA determines the cellular response to cancer therapeutic agents. *Oncogene*. **1999**;18(48):6641-6.
263. Bernal SD, Lampidis TJ, Summerhayes IC, Chen LB. Rhodamine-123 selectively reduces clonal growth of carcinoma cells in vitro. *Science*. **1982**;218(4577):1117-9.
264. Bernal SD, Lampidis TJ, McIsaac RM, Chen LB. Anticarcinoma activity in vivo of rhodamine 123, a mitochondrial-specific dye. *Science*. **1983**;222(4620):169-72.
265. Bleday R, Weiss MJ, Salem RR, Wilson RE, Chen LB, Steele G Jr. Inhibition of rat colon tumor isograft growth with dequalinium chloride. *Arch Surg*. **1986**;121(11):1272-5.
266. Modica-Napolitano JS, Koya K, Weisberg E, Brunelli BT, Li Y, Chen LB. Selective damage to carcinoma mitochondria by the rhodacyanine MKT-077. *Cancer Res*. **1996**;56(3):544-50.
267. Yang N, Weinfeld M, Lemieux H, Montpetit B, Goping IS. Photo-activation of the delocalized lipophilic cation D112 potentiates cancer selective ROS production and apoptosis. Cell Death Dis. **2017**;8(2):1-13.
268. Weissig V, Lizano C, Torchilin VP. Micellar Delivery System for Dequalinium—A Lipophilic Cationic Drug with Anticarcinoma Activity. *J Liposome Res.* **1998**;8(3);391-400.
269. Schneider Berlin KR, Ammini CV, Rowe TC. Dequalinium induces a selective depletion of mitochondrial DNA from HeLa human cervical carcinoma cells. *Exp Cell Res.* **1998**;245(1):137-45.
270. Sancho P, Galeano E, Nieto E, Delgado MD, García-Pérez AI. Dequalinium induces cell death in human leukemia cells by early mitochondrial alterations which enhance ROS production. *Leuk Res*. **2007**;31(7):969-78.
271. García-Pérez AI, Galeano E, Nieto E, Sancho P. Dequalinium induces human leukemia cell death by affecting the redox balance. *Leuk Res*. **2011**;35(10):1395-401.
272. Makowska K, Estañ MC, Gañán-Gómez I, Boyano-Adánez MC, García-Pérez AI, Sancho P. Changes in Mitochondrial Function Induced by Dequalinium Precede Oxidative Stress and Apoptosis in the Human Prostate-Cancer Cell Line PC-3. *Molecular Biology*. **2014**;48(3);416-28.
273. Goossens N, Nakagawa S, Sun X, Hoshida Y. Cancer biomarker discovery and validation. *Transl Cancer Res*. **2015**;4(3):256-69.
274. Slamon DJ, Leyland-Jones B, Shak S, Fuchs H, Paton V, Bajamonde A, *et al*. Use of chemotherapy plus a monoclonal antibody against HER2 for metastatic breast cancer that overexpresses HER2. *N Engl J Med*. **2001**;344(11):783-92.
275. Piccart-Gebhart MJ, Procter M, Leyland-Jones B, Goldhirsch A, Untch M, Smith I, *et al*. Trastuzumab after adjuvant chemotherapy in HER2-positive breast cancer. *N Engl J Med*. **2005**;353(16):1659-72.
276. Bang YJ, Van Cutsem E, Feyereislova A, Chung HC, Shen L, Sawaki A, *et al*. Trastuzumab in combination with chemotherapy versus chemotherapy alone for treatment of HER2-positive

advanced gastric or gastro-oesophageal junction cancer (ToGA): a phase 3, open-label, randomised controlled trial. *Lancet*. **2010**;376(9742):687-97.
277. Van Cutsem E, Köhne CH, Hitre E, Zaluski J, Chang Chien CR, Makhson A, *et al*. Cetuximab and chemotherapy as initial treatment for metastatic colorectal cancer. *N Engl J Med*. **2009**;360(14):1408-17.
278. Liang C, Shi S, Liu M, Qin Y, Meng Q, Hua J, *et al*. PIN1 maintains redox balance via the c-Myc/Nrf2 axis to counteract KRas-induced mitochondrial respiratory injury in pancreatic cancer cells. *Cancer Res*. **2019**;79(1):133-45.
279. Davies C, Godwin J, Gray R, Clarke M, Cutter D, Darby S, *et al*. Relevance of breast cancer hormone receptors and other factors to the efficacy of adjuvant tamoxifen: patient-level meta-analysis of randomised trials. *Lancet*. **2011**;378(9793):771-84.
280. Jordan VC. Selective estrogen receptor modulation: concept and consequences in cancer. *Cancer Cell*. **2004**;5(3):207-13.
281. Amado RG, Wolf M, Peeters M, Van Cutsem E, Siena S, Freeman DJ, *et al*. Wild-type KRAS is required for panitumumab efficacy in patients with metastatic colorectal cancer. *J Clin Oncol*. **2008**;26(10):1626-34.
282. Dematteo RP, Ballman KV, Antonescu CR, Maki RG, Pisters PW, Demetri GD, *et al*. Adjuvant imatinib mesylate after resection of localised, primary gastrointestinal stromal tumour: a randomised, double-blind, placebo-controlled trial. *Lancet*. **2009**;373(9669):1097-104.
283. Kantarjian H, Sawyers C, Hochhaus A, Guilhot F, Schiffer C, Gambacorti-Passerini C, *et al*. Hematologic and cytogenetic responses to imatinib mesylate in chronic myelogenous leukemia. *N Engl J Med*. **2002**;346(9):645-52.
284. Pao W, Girard N. New driver mutations in non-small-cell lung cancer. *Lancet Oncol*. **2011**;12(2):175-80.
285. Kris MG, Johnson BE, Berry LD, Kwiatkowski DJ, Iafrate AJ, Wistuba II, *et al*. Using multiplexed assays of oncogenic drivers in lung cancers to select targeted drugs. *JAMA*. 2014;311(19):1998-2006.
286. Chapman PB, Hauschild A, Robert C, Haanen JB, Ascierto P, Larkin J, *et al*. Improved survival with vemurafenib in melanoma with BRAF V600E mutation. *N Engl J Med.* **2011**;364(26):2507-16.
287. Berridge MV, Herst PM, Tan AS. Tetrazolium dyes as tools in cell biology: new insights into their cellular reduction. *Biotechnol Annu Rev*. **2005**;11:127-52.
288. Riss TL, Moravec RA, Niles AL, Duellman S, Benink HA, Worzella TJ, *et al*. Cell Viability Assays. *Assay Guid. Man*. **2013**;114:785–96.
289. Chou T. Theoretical basis, experimental design, and computerized simulation of synergism and antagonism in drug combination studies. *Pharmacol Rev*. **2006**;58:621–81.
290. Niles AL, Moravec RA, Eric Hesselberth P, Scurria MA, Daily WJ, Riss TL. A homogeneous assay to measure live and dead cells in the same sample by detecting different protease markers. *Anal Biochem*. **2007**;366(2):197-206.
291. Luo Y, Wang D, Abbruzzese JL, Lu W. Measurement of Reactive Oxygen Species by Fluorescent Probes in Pancreatic Cancer Cells. *Methods Mol Biol*. **2019**;1882:207-19.
292. Yu M, Wan Y, Zou Q. Decreased copy number of mitochondrial DNA in Ewing's sarcoma. *Clin Chim Acta*. **2010**;411(9-10):679-83.
293. Schneider CA, Rasband WS, Eliceiri KW. NIH Image to ImageJ: 25 years of image analysis. *Nat Methods*. **2012**;9(7):671-5.
294. Brandon MC, Lott MT, Nguyen KC, Spolim S, Navathe SB, Baldi P, *et al*. MITOMAP: a human mitochondrial genome database--2004 update. *Nucleic Acids Res*. **2005**;33:611-3.
295. Burley SK, Berman HM, Kleywegt GJ, Markley JL, Nakamura H, Velankar S. Protein Data Bank (PDB): The Single Global Macromolecular Structure Archive. *Methods Mol Biol*. **2017**;1607:627-41.
296. Emsley P, Lohkamp B, Scott WG, Cowtan K. Features and development of Coot. *Acta Crystallogr D Biol Crystallogr*. **2010**;66(4):486-501.
297. Vaseghi H, Houshmand M, Jadali Z. Increased levels of mitochondrial DNA copy number in patients with vitiligo. *Clin Exp Dermatol*. **2017**;42(7):749-54.

298. Ju SM, Pae HO, Kim WS, Kang DG, Lee HS, Jeon BH. Role of reactive oxygen species in p53 activation during cisplatin-induced apoptosis of rat mesangial cells. *Eur Rev Med Pharmacol Sci*. **2014**;18(8):1135-41.
299. Weiss MJ, Wong JR, Ha CS, Bleday R, Salem RR, Steele GD Jr, *et al*. Dequalinium, a topical antimicrobial agent, displays anticarcinoma activity based on selective mitochondrial accumulation. *Proc Natl Acad Sci U S A*. **1987**;84(15):5444-8.
300. Christman JE, Miller DS, Coward P, Smith LH, Teng NN. Study of the selective cytotoxic properties of cationic, lipophilic mitochondrial-specific compounds in gynecologic malignancies. *Gynecol Oncol*. **1990**;39(1):72-9.
301. Park SJ, Kim YT, Jeon YJ. Antioxidant dieckol downregulates the Rac1/ROS signaling pathway and inhibits Wiskott-Aldrich syndrome protein (WASP)-family verprolin-homologous protein 2 (WAVE2)-mediated invasive migration of B16 mouse melanoma cells. *Mol Cells*. **2012**;33(4):363-9.
302. Li P, Wu M, Wang J, Sui Y, Liu S, Shi D. NAC selectively inhibit cancer telomerase activity: A higher redox homeostasis threshold exists in cancer cells. *Redox Biol*. **2016**;8:91-7.
303. Rodic S, Vincent MD. Reactive oxygen species (ROS) are a key determinant of cancer's metabolic phenotype. *Int J Cancer*. **2018**;142(3):440-8.
304. Bae Y, Jung MK, Lee S, Song SJ, Mun JY, Green ES, *et al*. Dequalinium-based functional nanosomes show increased mitochondria targeting and anticancer effect. *Eur J Pharm Biopharm*. **2018**;124:104-115.
305. Barabas K, Milner R, Lurie D, Adin C. Cisplatin: a review of toxicities and therapeutic applications. *Vet Comp Oncol*. **2008**;6(1):1-18.
306. Pelicano H, Carney D, Huang P. ROS stress in cancer cells and therapeutic implications. *Drug Resist Updat*. **2004**;7(2):97-110.
307. Wisnovsky SP, Wilson JJ, Radford RJ, Pereira MP, Chan MR, Laposa RR, *et al*. Targeting mitochondrial DNA with a platinum-based anticancer agent. *Chem Biol*. **2013**;20(11):1323-8.
308. Zhu Z, Wang Z, Zhang C, Wang Y, Zhang H, Gan Z, *et al*. Mitochondrion-targeted platinum complexes suppressing lung cancer through multiple pathways involving energy metabolism. *Chem Sci*. **2019**;10(10):3089-95.
309. Brandes RP, Weissmann N, Schröder K. Nox family NADPH oxidases: Molecular mechanisms of activation. *Free Radic Biol Med*. **2014**;76:208-26.
310. Varanita T, Soriano ME, Romanello V, Zaglia T, Quintana-Cabrera R, Semenzato M, *et al*. The OPA1-dependent mitochondrial cristae remodeling pathway controls atrophic, apoptotic, and ischemic tissue damage. *Cell Metab*. 2015;21(6):834-44.
311. Fang HY, Chen CY, Chiou SH, Wang YT, Lin TY, Chang HW, *et al*. Overexpression of optic atrophy 1 protein increases cisplatin resistance via inactivation of caspase-dependent apoptosis in lung adenocarcinoma cells. *Hum Pathol*. **2012**;43(1):105-14.
312. Santin G, Piccolini VM, Barni S, Veneroni P, Giansanti V, Dal Bo V, *et al*. Mitochondrial fusion: a mechanism of cisplatin-induced resistance in neuroblastoma cells?. *Neurotoxicology*. **2013**;34:51-60.
313. Pickles S, Vigié P, Youle RJ. Mitophagy and Quality Control Mechanisms in Mitochondrial Maintenance. *Curr Biol*. **2018**;28(4):170-85.
314. Ivankovic D, Chau KY, Schapira AH, Gegg ME. Mitochondrial and lysosomal biogenesis are activated following PINK1/parkin-mediated mitophagy. *J Neurochem*. **2016**;136(2):388-402.
315. Narendra DP, Jin SM, Tanaka A, Suen DF, Gautier CA, Shen J, *et al*. PINK1 is selectively stabilized on impaired mitochondria to activate Parkin. *PLoS Biol*. **2010**;8(1):1-15.
316. Lazarou M, Narendra DP, Jin SM, Tekle E, Banerjee S, Youle RJ. PINK1 drives Parkin self-association and HECT-like E3 activity upstream of mitochondrial binding. *J Cell Biol*. **2013** ;200(2):163-72.
317. McLelland GL, Soubannier V, Chen CX, McBride HM, Fon EA. Parkin and PINK1 function in a vesicular trafficking pathway regulating mitochondrial quality control. *EMBO J*. **2014**;33(4):282-95.
318. Su YC, Davuluri GV, Chen CH, Shiau DC, Chen CC, Chen CL, *et al*. Galectin-1-Induced Autophagy Facilitates Cisplatin Resistance of Hepatocellular Carcinoma. PLoS One. 2016 Feb 9;11(2):1.14.

319. MacKeigan JP, Murphy LO, Blenis J. Sensitized RNAi screen of human kinases and phosphatases identifies new regulators of apoptosis and chemoresistance. *Nat Cell Biol*. **2005**;7(6):591-600.
320. Liu J, Chen Z, Guo J, Wang L, Liu X. Ambra1 induces autophagy and desensitizes human prostate cancer cells to cisplatin. *Biosci Rep*. **2019**;39(8):1-10.
321. Datta S, Choudhury D, Das A, Mukherjee D Das, Dasgupta M, Bandopadhyay S, *et al*. Autophagy inhibition with chloroquine reverts paclitaxel resistance and attenuates metastatic potential in human nonsmall lung adenocarcinoma A549 cells via ROS mediated modulation of β-catenin pathway. *Apoptosis*. **2019**;24(5-6):414-33.
322. Green PD, Sharma NK, Santos JH. Telomerase Impinges on the Cellular Response to Oxidative Stress Through Mitochondrial ROS-Mediated Regulation of Autophagy. *Int J Mol Sci*. **2019**;20(6):1509-24.
323. Stordal B, Davey M. Understanding cisplatin resistance using cellular models. *IUBMB Life*. **2007**;59(11):696-9.
324. Jones PM, George AM. A reciprocating twin-channel model for ABC transporters. *Q Rev Biophys*. **2014**;47(3):189-220.
325. Chang G, Roth CB. Structure of MsbA from E. coli: a homolog of the multidrug resistance ATP binding cassette (ABC) transporters. *Science*. **2001**;293(5536):1793-800.
326. Anreddy N, Gupta P, Kathawala RJ, Patel A, Wurpel JN, Chen ZS. Tyrosine kinase inhibitors as reversal agents for ABC transporter mediated drug resistance. *Molecules*. **2014**;19(9):13848-77.
327. Kathawala RJ, Gupta P, Ashby CR Jr, Chen ZS. The modulation of ABC transporter-mediated multidrug resistance in cancer: a review of the past decade. *Drug Resist Updat*. **2015**;18:1-17.
328. Sun Y, Guan Z, Liang L, Cheng Y, Zhou J, Li J, *et al*. HIF-1α/MDR1 pathway confers chemoresistance to cisplatin in bladder cancer. *Oncol Rep*. **2016**;35(3):1549-56.
329. Huang XP, Li X, Situ MY, Huang LY, Wang JY, He TC, *et al*. Entinostat reverses cisplatin resistance in esophageal squamous cell carcinoma via down-regulation of multidrug resistance gene 1. *Cancer Lett*. **2018**;414:294-300.
330. Rocha CRR, Silva MM, Quinet A, Cabral-Neto JB, Menck CFM. DNA repair pathways and cisplatin resistance: an intimate relationship. *Clinics*. **2018**;73(1):1-10.
331. Martin LP, Hamilton TC, Schilder RJ. Platinum resistance: the role of DNA repair pathways. *Clin Cancer Res*. **2008**;14(5):1291-5.
332. Zuliani T, Denis V, Noblesse E, Schnebert S, Andre P, Dumas M, *et al*. Hydrogen peroxide-induced cell death in normal human keratinocytes is differentiation dependent. *Free Radic Biol Med*. **2005**;38(3):307-16.
333. Sancar A, Lindsey-Boltz LA, Unsal-Kaçmaz K, Linn S. Molecular mechanisms of mammalian DNA repair and the DNA damage checkpoints. *Annu Rev Biochem*. **2004**;73:39-85.
334. Camara AK, Bienengraeber M, Stowe DF. Mitochondrial approaches to protect against cardiac ischemia and reperfusion injury. *Front Physiol*. **2011**;2(13):1-34.
335. Martin SJ, Reutelingsperger CP, McGahon AJ, Rader JA, van Schie RC, LaFace DM, *et al*. Early redistribution of plasma membrane phosphatidylserine is a general feature of apoptosis regardless of the initiating stimulus: inhibition by overexpression of Bcl-2 and Abl. *J Exp Med*. **1995**;182(5):1545-56.
336. Cogliati S, Frezza C, Soriano ME, Varanita T, Quintana-Cabrera R, Corrado M, *et al*. Mitochondrial cristae shape determines respiratory chain supercomplexes assembly and respiratory efficiency. *Cell*. **2013**;155(1):160-71.
337. Kuo ML, Sy AJ, Xue L, Chi M, Lee MT, Yen T, *et al*. RRM2B suppresses activation of the oxidative stress pathway and is up-regulated by p53 during senescence. *Sci Rep*. **2012**;2(822):1-9.
338. Vařecha M, Potěšilová M, Matula P, Kozubek M. Endonuclease G interacts with histone H2B and DNA topoisomerase II alpha during apoptosis. *Mol Cell Biochem*. **2012**;363(1-2):301-7.
339. Lee JS, Seo TW, Yi JH, Shin KS, Yoo SJ. CHIP has a protective role against oxidative stress-induced cell death through specific regulation of endonuclease G. *Cell Death Dis*. **2013**;4:1-12.
340. Muir R, Diot A, Poulton J. Mitochondrial content is central to nuclear gene expression: Profound implications for human health. *Bioessays*. **2016**;38(2):150-6.
341. Hahn A, Zuryn S. Mitochondrial Genome (mtDNA) Mutations that Generate Reactive Oxygen Species. *Antioxidants (Basel)*. **2019**;8(9):392.410.

342. Ishikawa K, Takenaga K, Akimoto M, Koshikawa N, Yamaguchi A, Imanishi H, *et al*. ROS-generating mitochondrial DNA mutations can regulate tumor cell metastasis. *Science*. **2008**;320(5876):661-4.
343. Lobo-Jarne T, Ugalde C. Respiratory chain supercomplexes: Structures, function and biogenesis. *Semin Cell Dev Biol*. **2018**;76:179-190.
344. Lee HC, Yin PH, Lu CY, Chi CW, Wei YH. Increase of mitochondria and mitochondrial DNA in response to oxidative stress in human cells. *Biochem J*. **2000**;348(2):425-32.
345. Mizumachi T, Muskhelishvili L, Naito A, Furusawa J, Fan CY, Siegel ER, *et al*. Increased distributional variance of mitochondrial DNA content associated with prostate cancer cells as compared with normal prostate cells. *Prostate*. **2008**;68(4):408-17.
346. Grzybowska-Szatkowska L, Slaska B, Rzymowska J, Brzozowska A, Floriańczyk B. Novel mitochondrial mutations in the ATP6 and ATP8 genes in patients with breast cancer. *Mol Med Rep*. **2014**;10(4):1772-8.
347. Ghaffarpour M, Mahdian R, Fereidooni F, Kamalidehghan B, Moazami N, Houshmand M. The mitochondrial ATPase6 gene is more susceptible to mutation than the ATPase8 gene in breast cancer patients. *Cancer Cell Int*. **201**;14(21):1-9.
348. Li W, Zhang W, Li F, Wang C. Mitochondrial genetic analysis in a Chinese family suffering from both mitochondrial encephalomyopathy with lactic acidosis and stroke-like episodes and diabetes. *Int J Clin Exp Pathol*. **2015**;8(6):7022-7.
349. Tanwar M, Dada T, Sihota R, Dada R. Mitochondrial DNA analysis in primary congenital glaucoma. *Mol Vis*. **2010**;16:518-33.
350. Blein S, Bardel C, Danjean V, McGuffog L, Healey S, Barrowdale D, *et al*. An original phylogenetic approach identified mitochondrial haplogroup T1a1 as inversely associated with breast cancer risk in BRCA2 mutation carriers. *Breast Cancer Res*. **2015**;17(61):1-15.
351. Koshikawa N, Akimoto M, Hayashi JI, Nagase H, Takenaga K. Association of predicted pathogenic mutations in mitochondrial ND genes with distant metastasis in NSCLC and colon cancer. *Sci Rep*. **2017**;7(1):1-11.
352. Ji F, Sharpley MS, Derbeneva O, Alves LS, Qian P, Wang Y, *et al*. Mitochondrial DNA variant associated with Leber hereditary optic neuropathy and high-altitude Tibetans. *Proc Natl Acad Sci U S A*. **2012**;109(19):7391-6.
353. Imanishi H, Hattori K, Wada R, Ishikawa K, Fukuda S, Takenaga K, *et al*. Mitochondrial DNA mutations regulate metastasis of human breast cancer cells. *PLoS One*. **2011**;6(8):1-7.
354. Yadava N, Schneider SS, Jerry DJ, Kim C. Impaired mitochondrial metabolism and mammary carcinogenesis. *J Mammary Gland Biol Neoplasia*. **2013**;18(1):75-87.
355. Petros JA, Baumann AK, Ruiz-Pesini E, Amin MB, Sun CQ, Hall J, *et al*. mtDNA mutations increase tumorigenicity in prostate cancer. *Proc Natl Acad Sci U S A*. **2005**;102(3):719-24.
356. Mohamed Yusoff AA, Zulfakhar FN, Mohd Khair SZN, Wan Abdullah WS, Abdullah JM, Idris Z. Mitochondrial 10398A>G NADH-Dehydrogenase Subunit 3 of Complex I Is Frequently Altered in Intra-Axial Brain Tumors in Malaysia. *Brain Tumor Res Treat*. **2018**;6(1):31-38.
357. Canter JA, Kallianpur AR, Parl FF, Millikan RC. Mitochondrial DNA G10398A polymorphism and invasive breast cancer in African-American women. *Cancer Res*. **2005**;65(17):8028-33.
358. Czarnecka AM, Krawczyk T, Zdrozny M, Lubiński J, Arnold RS, Kukwa W, *et al*. Mitochondrial NADH-dehydrogenase subunit 3 (ND3) polymorphism (A10398G) and sporadic breast cancer in Poland. *Breast Cancer Res Treat*. **2010**;121(2):511-8.
359. Li Y, Li X, Wang Z, Feng Z, Li L, Ke X. Subhaplogroup D4b1 enhances the risk of cervical cancer initiation: A case-control study in southern China. *J Obstet Gynaecol Res*. **2016**;42(3):325-30.
360. Shuwen H, Xi Y, Yuefen P. Can Mitochondria DNA Provide a Novel Biomarker for Evaluating the Risk and Prognosis of Colorectal Cancer?. Dis Markers. 2017;2017:1-10.
361. Guney AI, Ergec DS, Tavukcu HH, Koc G, Kirac D, Ulucan K, *et al*. Detection of mitochondrial DNA mutations in nonmuscle invasive bladder cancer. *Genet Test Mol Biomarkers*. **2012**;16(7):672-8.
362. Zhu W, Qin W, Bradley P, Wessel A, Puckett CL, Sauter ER. Mitochondrial DNA mutations in breast cancer tissue and in matched nipple aspirate fluid. *Carcinogenesis*. **2005**;26(1):145-52.
363. Yu M, Zhou Y, Shi Y, Ning L, Yang Y, Wei X, *et al*. Reduced mitochondrial DNA copy number is correlated with tumor progression and prognosis in Chinese breast cancer patients. *IUBMB Life*. **2007**;59(7):450-7.

364. Shakhssalim N, Houshmand M, Kamalidehghan B, Faraji A, Sarhangnejad R, Dadgar S, *et al*. The mitochondrial C16069T polymorphism, not mitochondrial D310 (D-loop) mononucleotide sequence variations, is associated with bladder cancer. *Cancer Cell Int*. **2013**;13(1):1-9.
365. Yadav N, Chandra D. Mitochondrial DNA mutations and breast tumorigenesis. *Biochim Biophys Acta*. **2013**;1836(2):336-44.
366. Zhou H, Nie K, Qiu R, Xiong J, Shao X, Wang B, *et al*. Generation and Bioenergetic Profiles of Cybrids with East Asian mtDNA Haplogroups. Oxid Med Cell Longev. 2017;2017:1-13.
367. Bussard KM, Siracusa LD. Understanding Mitochondrial Polymorphisms in Cancer. *Cancer Res*. **2017**;77(22):6051-9.
368. Suissa S, Wang Z, Poole J, Wittkopp S, Feder J, Shutt TE, *et al*. Ancient mtDNA genetic variants modulate mtDNA transcription and replication. *PLoS Genet*. **2009**;5(5):1-10.
369. Zaidieh T, Smith JR, Ball KE, An Q. ROS as a novel indicator to predict anticancer drug efficacy. *BMC Cancer*. **2019**;19(1):1-14.

Appendices

Appendix Table 1. List of common mutations identified in the 5 cell lines.

Mutations	PNT-2	Ishikawa	MDA-MB-231	PC-3	Caco-2	Region	Mutation type	Amino acid change
A73G		✓		✓	✓	D-loop	Non-protein coding	
T195C			✓	✓		D-loop	Non-protein coding	
A263G		✓	✓	✓	✓	D-loop	Non-protein coding	
310insC		✓	✓	✓		D-loop	Non-protein coding	
A750G	✓	✓	✓	✓	✓	12S ribosomal RNA	Non-protein coding	
A1438G	✓	✓		✓	✓	12S ribosomal RNA	Non-protein coding	
A2706G		✓	✓	✓	✓	16S ribosomal RNA	Non-protein coding	
2800insA		✓	✓			16S ribosomal RNA	Non-protein coding	
3107delN		✓	✓		✓	16S ribosomal RNA	Non-protein coding	
A4769G	✓	✓	✓	✓	✓	Complex I	Synonymous	
C7028T		✓	✓	✓	✓	Complex IV	Synonymous	
A8860G	✓	✓	✓	✓	✓	Complex V	Non-synonymous	Thr - Ala
G11719A		✓	✓	✓	✓	Complex I	Synonymous	
G12372A		✓		✓		Complex I	Synonymous	
C12705T		✓	✓			Complex I	Synonymous	
G13708A				✓	✓	Complex I	Non-synonymous	Ala -Thr
C14766T		✓	✓	✓	✓	Complex III	Non-synonymous	Thr -Ile
A15326G	✓	✓	✓		✓	Complex III	Non-synonymous	Thr -Ala
T16172C		✓		✓		D-loop	Non-protein coding	
C16261T		✓			✓	D-loop	Non-protein coding	

Appendix Table 2. List of unique mutations identified in the 5 cell lines.

Mutations	PNT-2	Ishikawa	MDA-MB-231	PC-3	Caco-2	Region	Mutation type	Amino acid change
513insCA	✓					D-loop	Non-protein coding	
G16319A	✓					D-loop	Non-protein coding	
T16325C	✓					D-loop	Non-protein coding	
T16519C	✓					D-loop	Non-protein coding	
C150T		✓				D-loop	Non-protein coding	
C338T		✓				D-loop	Non-protein coding	
T961C		✓				12S ribosomal RNA	Non-protein coding	
A1937C		✓				16S ribosomal RNA	Non-protein coding	
T3394C		✓				Complex I	Non-synonymous	Tyr - His
G5231A		✓				Complex I	Synonymous	
G5417A		✓				Complex I	Synonymous	
T14968C		✓				Complex III	Synonymous	
C16223T		✓				D-loop	Non-protein coding	
C16257A		✓				D-loop	Non-protein coding	
T16304C		✓				D-loop	Non-protein coding	
A16497G		✓				D-loop	Non-protein coding	
A153G			✓			D-loop	Non-protein coding	
646insA			✓			tRNA-Phe	Non-protein coding	
653insT			✓			12S ribosomal RNA	Non-protein coding	
G709A			✓			12S ribosomal RNA	Non-protein coding	

Mutations	PNT-2	Ishikawa	MDA-MB-231	PC-3	Caco-2	Region	Mutation type	Amino acid change
G1719A			✓			16S ribosomal RNA	Non-protein coding	
T6221C			✓			Complex IV	Synonymous	
T8506C			✓			Complex V	Synonymous	
C12084T			✓			Complex I	Non-synonymous	Ser - Phe
A13966G			✓			Complex I	Non-synonymous	Thr - Ala
T14470C			✓			Complex I	Synonymous	
T15310C			✓			Complex III	Synonymous	
T11120C				✓		Complex I	Non-synonymous	Phe - Leu
A11467G				✓		Complex I	Synonymous	
A12308G				✓		tRNA-Leu	Non-protein coding	
T13617C				✓		Complex I	Synonymous	
C13802T				✓		Complex I	Non-synonymous	Thr - Met
A14793G				✓		Complex III	Non-synonymous	His - Arg
C16192T				✓		D-loop	Non-protein coding	
C16256T				✓		D-loop	Non-protein coding	
C16270T				✓		D-loop	Non-protein coding	
C16320T				✓		D-loop	Non-protein coding	
A16399G				✓		D-loop	Non-protein coding	
G47A					✓	D-loop	Non-protein coding	

Mutations	PNT-2	Ishikawa	MDA-MB-231	PC-3	Caco-2	Region	Mutation type	Amino acid change
G185A					✔	D-loop	Non-protein coding	
G228A					✔	D-loop	Non-protein coding	
C295T					✔	D-loop	Non-protein coding	
C462T					✔	D-loop	Non-protein coding	
T489C					✔	D-loop	Non-protein coding	
T4216C					✔	Complex I	Non-synonymous	Tyr - His
C6464A					✔	Complex IV	Synonymous	
C6554T					✔	Complex IV	Synonymous	
G7977C					✔	Complex IV	Non-synonymous	Gly - Ala
A10398G					✔	Complex I	Non-synonymous	Thr - Ala
A11251G					✔	Complex I	Synonymous	
G12127A					✔	Complex I	Synonymous	
A12612G					✔	Complex I	Synonymous	
A13681G					✔	Complex I	Non-synonymous	Thr - Ala
T14798C					✔	Complex III	Non-synonymous	Phe - Leu
A14927G					✔	Complex III	Non-synonymous	Thr - Ala
A14959G					✔	Complex III	Synonymous	
C15452A					✔	Complex III	Non-synonymous	Leu - Ile
C16069T					✔	D-loop	Non-protein coding	
T16126C					✔	D-loop	Non-protein coding	

Appendix Table 3. List of disease association of mutations in the 5 cell lines.

Mutations	Disease association search (MitoMap)	Human Mitochondrial DataBase (HmtDB)
G47A	None	Thyroid cancer
A73G	POLG/PEO & control muscle, buccal cell, thyroid & prostate tumours.	Thyroid cancer, Leber Hereditary Optic Neuropathy, Myoclonic Epilepsy and Ragged Red Muscle Fibers, Diabetes type2, Renal oncocytoma, Pituitary adenoma, Prostate cancer, Alzheimer's Disease, Endometrial cancer type I, Cardiomyopathy familial, hypertrophic,Bipolar disorder type I, Glioma, Noonan syndrome, Invasive mammal carcinoma, Dilated Cardiomyopathy, Epilepsy , Neurogenic muscle weakness Ataxia and Retinitis Pigmentosa, Meningococcal disease, Glaucoma, Black Death, Ataxia and Retinitis Pigmentosa/Mills syndrome, Renal cell carcinoma.
C150T	Cervical Carcinoma. lung, thyroid and prostate tumours.	Thyroid cancer, Mitochondrial Encephalomyopathy Lactic Acidosis and Stroke like episodes, Parkinson`s Disease, Leber Hereditary Optic Neuropathy, Pituitary adenoma, Gastric carcinoma, Colorectal cancer, Cardiomyopathy, Prostate cancer, Glioma, Noonan syndrome, Neurogenic muscle weakness Ataxia and Retinitis Pigmentosa, Mental disorder, Meningococcal disease, Glaucoma, Epilepsy, Diabetes type2, Renal cell carcinoma.
A153G	None	Breast cancer, Diabetes type2, Oncocytic pituitary adenoma, Endometrial cancer type I, Schizophrenia, Noonan syndrome, Leber Hereditary Optic Neuropathy.
G185A	POLG/PEO muscle, thyroid tumour, glioblastoma.	Thyroid cancer, Leber Hereditary Optic Neuropathy, Renal oncocytoma, Minor salivary benign neopl, Colorectal cancer, Endometrial cancer type I, Schizophrenia, Noonan syndrome, Invasive mammal carcinoma, Leber Hereditary Optic Neuropathy, Glaucoma, Epilepsy, Diabetes type2.
T195C	Tumours: melanoma, lung, thyroid, ovarian, prostate and glioblastoma.	Breast cancer, Leber Hereditary Optic Neuropathy, Diabetes type2, Pituitary adenoma, Gastric carcinoma, Noonan syndrome, Dilated Cardiomyopathy, Neurogenic muscle weakness Ataxia and Retinitis Pigmentosa, periodic paralyses and neuropathy.
G228A	None	Thyroid cancer, Diabetes type2, Chronic Progressive External Ophthalmoplegia, Trigon carcinoma, Chronic Periodontitis, Prostate cancer, Schizoaffective disorder, Glioma, Noonan syndrome, Invasive mammal carcinoma, Dilated Cardiomyopathy.
A263G	POLG/MNGIE muscle.	Breast cancer, Parkinson`s Disease, Colorectal cancer, Noonan syndrome, Mental disorder, Diabetes type2.
C295T	POLG/MNGIE muscle, glioblastoma.	Thyroid cancer, Leber Hereditary Optic Neuropathy, Pituitary adenoma, Noonan syndrome, Diabetes type2, Renal cell carcinoma.
310insC	Melanoma	None

Mutations	Disease association search (MitoMap)	Human Mitochondrial DataBase (HmtDB)
C338T	None	Diabetes type2.
C462T	thyroid tumour.	Thyroid cancer, Leber Hereditary Optic Neuropathy, Minor salivary benign neopl, Noonan syndrome, Optic atrophy, Epilepsy, Diabetes type2.
T489C	Ovarian carcinoma, prostate tumour.	Thyroid cancer, Leber Hereditary Optic Neuropathy, Parkinson`s Disease, Diabetes type2, Colorectal cancer, Optic atrophy, Mental disorder, Meningococcal disease, Epilepsy.
513insCA	None	None
646insA	None	None
653insT	None	None
G709A	None	Thyroid cancer, Parkinson`s Disease, Oncocytic pituitary adenoma, Chronic Periodontitis, Colorectal cancer, Prostate cancer, Leber Hereditary Optic Neuropathy, Noonan syndrome, Dilated Cardiomyopathy, Invasive primary mammal carcinoma, Mental disorder, Glaucoma, Epilepsy, Diabetes type2.
A750G	None	Glioma, Glaucoma, Neurofibromatosis type 1, Leber Hereditary Optic Neuropathy, Lung cancer, Epilepsy, Diabetes type2.
T961C	DEAF, possibly LVNC-associated	Breast cancer, Parkinson`s Disease, Noonan syndrome, Invasive mammal carcinoma, Leber Hereditary Optic Neuropathy, Diabetes type2.
A1438G	None	Thyroid cancer, Alzheimer's Disease, Gastric carcinoma, Chronic Periodontitis, Leber Hereditary Optic Neuropathy, Optic atrophy, Diabetes type2.
G1719A	None	Thyroid cancer, Oncocytic pituitary adenoma, Chronic Periodontitis, Prostate cancer, Schizoaffective disorder, Noonan syndrome, Leber Hereditary Optic Neuropathy, Diabetes type2.
A1937C	None	None

Mutations	Disease association search (MitoMap)	Human Mitochondrial DataBase (HmtDB)
A2706G	None	Thyroid cancer, Diabetes type2, Renal oncocytoma, Pituitary adenoma, Cardiomyopathy, Prostate cancer, Alzheimer's Disease, Endometrial cancer type I, Noonan syndrome, Invasive mammal carcinoma, Leber Hereditary Optic Neuropathy, Meningococcal disease, Epilepsy, BHD-related renal tumour.
2800insA	None	None
G3010A	Cyclic Vomiting Syndrome with Migraine	Thyroid cancer, Leber Hereditary Optic Neuropathy, Parkinson`s Disease, Oncocytic pituitary adenoma, Prostate cancer, Schizophrenia, Noonan syndrome, Invasive mammal carcinoma, Hypertrophic cardiomyopathy, Optic atrophy, Mental disorder, Glaucoma, Epilepsy, Diabetes type2.
3107delN	None	Thyroid cancer, Parkinson`s Disease, Alzheimer's Disease, Diabetes type2, Pituitary adenoma, Chronic Periodontitis, Colorectal cancer, Prostate cancer, Endometrial cancer type I, Bipolar disorder type I, Noonan syndrome, Breast cancer, Invasive mammal carcinoma, Dilated Cardiomyopathy, Leber Hereditary Optic Neuropathy, Mental disorder, BHD-related renal tumour.
T3197C	None	Thyroid cancer, Mitochondrial Encephalomyopathy Lactic Acidosis and Stroke like episodes, Renal oncocytoma, Pituitary adenoma, Prostate cancer, Noonan syndrome, Epilepsy, Diabetes type2.
T3394C	acute leukemia platelets, leukocytes & bone marrow, various tumours	Thyroid cancer, Prostate cancer, Noonan syndrome, Noonan syndrome.
T4216C	acute leukemia platelets, leukocytes & bone marrow.	Thyroid cancer, Leber Hereditary Optic Neuropathy, Pituitary adenoma, Dilated Cardiomyopathy, Noonan syndrome, Invasive primary mammal carcinoma, Epilepsy, Glaucoma, Neurofibromatosis type 1, BHD-related renal tumour.
A4769G	None	Thyroid cancer, Chronic Periodontitis, Diabetes type2 with coronary artery disease, Invasive mammal carcinoma, Epilepsy.
G5231A	Endometrium control tissue	Thyroid cancer, Parkinson`s Disease, Obesity, Colorectal cancer, Endometrial cancer type I, Leber Hereditary Optic Neuropathy, Diabetes type2
G5417A	None	Thyroid cancer, Parkinson`s Disease, Diabetes type2, Colorectal cancer, Leber Hereditary Optic Neuropathy, Mental disorder.

Mutations	Disease association search (MitoMap)	Human Mitochondrial DataBase (HmtDB)
T6221C	None	Breast cancer, Parkinson`s Disease, Oncocytic pituitary adenoma, Prostate cancer, Endometrial cancer type I, Schizophrenia, Noonan syndrome, Diabetes type2.
C6464A	None	Leber Hereditary Optic Neuropathy, Epilepsy, Diabetes type2, Renal cell carcinoma.
C6554T	None	Leber Hereditary Optic Neuropathy, Optic atrophy, Epilepsy, Diabetes type2, Renal cell carcinoma.
C7028T	None	Thyroid cancer, Leber Hereditary Optic Neuropathy, Myoclonic Epilepsy and Ragged Red Muscle Fibers, Renal oncocytoma, Pituitary adenoma, Prostate cancer, Alzheimer's Disease, Schizophrenia, Noonan syndrome, Hypertrophic cardiomyopathy, periodic paralyses and neuropathy, Epilepsy, Diabetes type2, Bilateral multifocal renal oncocytoma.
G7977C	None	None
T8506C	None	Thyroid cancer.
A8860G	None	Chronic Periodontitis, Neurogenic muscle weakness Ataxia and Retinitis Pigmentosa, Epilepsy, Diabetes type2.
A10398G	Various tumours.	Thyroid cancer, Parkinson`s Disease, High grade renal clear cell carcinoma, Pituitary adenoma, Chronic Periodontitis, Colorectal cancer, Cardiomyopathy, Prostate cancer, Alzheimer's Disease, Endometrial cancer type I, Schizophrenia, Noonan syndrome, Invasive mammal carcinoma, Noonan syndrome, Meningococcal disease, Leber Hereditary Optic Neuropathy, Lung cancer.
T11120C	None	Diabetes type2.
A11251G	None	Thyroid cancer, Pituitary adenoma, Prostate cancer, Noonan syndrome, Leber Hereditary Optic Neuropathy, Invasive primary mammal carcinoma, Optic atrophy, Diabetes type2.

Mutations	Disease association search (MitoMap)	Human Mitochondrial DataBase (HmtDB)
A11467G	Altered brain pH / sCJD patient.	Thyroid cancer, Mitochondrial Encephalomyopathy Lactic Acidosis and Stroke like episodes, Renal oncocytoma, Leber Hereditary Optic Neuropathy, Rhinopharinx oncocytoma, Chronic Periodontitis, Prostate cancer, Endometrial cancer type I, Glioma, Neurofibromatosis type 1.
G11719A	None	Thyroid cancer, Renal oncocytoma, Pituitary adenoma, Chronic Periodontitis, Cardiomyopathy, Prostate cancer, Alzheimer's Disease, Endometrial cancer type I, Diabetes mellitus type2, Noonan syndrome, Invasive mammal carcinoma, Hypertrophic cardiomyopathy, Invasive primary mammal carcinoma, periodic paralyses and neuropathy, Epilepsy, Renal cell carcinoma.
C12084T	None	Parkinson`s Disease.
G12127A	None	Leber Hereditary Optic Neuropathy, Optic atrophy, BHD-related renal tumour.
A12308G	lung tumour, prostate tumour	Thyroid cancer, Mitochondrial Encephalomyopathy Lactic Acidosis and Stroke like episodes, Renal oncocytoma, Pituitary adenoma, Chronic Periodontitis, Prostate cancer, Endometrial cancer type I, Endometrial cancer type I.
G12372A	prostate tumour, Altered brain pH / sCJD patients.	Thyroid cancer, Mitochondrial Encephalomyopathy Lactic Acidosis and Stroke like episodes, Parkinson`s Disease, Rhinopharinx oncocytoma, Chronic Periodontitis, Prostate cancer, Endometrial cancer type I, Schizophrenia, Glioma, Neurofibromatosis type 1, Noonan syndrome, Mental disorder, periodic paralyses and neuropathy, Epilepsy, Diabetes type2, Bilateral multifocal renal oncocytoma.
A12612G	None	Thyroid cancer, Leber Hereditary Optic Neuropathy, Obesity, Minor salivary benign neopl, Noonan syndrome, Dilated Cardiomyopathy, Optic atrophy, Glaucoma, Neurofibromatosis type 1, Diabetes type2.
C12705T	prostate tumour	Thyroid cancer, Parkinson`s Disease, Renal oncocytoma, Pituitary adenoma, Warthin tumour, Chronic Periodontitis, Colorectal cancer, Prostate cancer, Alzheimer's Disease, Endometrial cancer type I, Schizophrenia, Noonan syndrome, Breast cancer, Invasive mammal carcinoma, Hypertrophic cardiomyopathy, Noonan syndrome, Leber Hereditary Optic Neuropathy, Meningococcal disease, Black Death, Lung cancer, Epilepsy, Diabetes type2, BHD-related renal tumour.
T13617C	None	Thyroid cancer, Mitochondrial Encephalomyopathy Lactic Acidosis and Stroke like episodes, Diabetes type2, Renal oncocytoma, Pituitary adenoma, LEOPARD syndrome, periodic paralyses and neuropathy, Epilepsy, Diabetes type2.
A13681G	None	Colorectal cancer, Leber Hereditary Optic Neuropathy, Epilepsy, Renal cell carcinoma.
G13708A	acute leukemia platelets, leukocytes & bone marrow, breast tumour	Thyroid cancer, Parkinson`s Disease, Colorectal cancer, Schizoaffective disorder, Dilated Cardiomyopathy, Leber Hereditary Optic Neuropathy, Epilepsy, Diabetes type2, BHD-related renal tumour.

Mutations	Disease association search (MitoMap)	Human Mitochondrial DataBase (HmtDB)
C13802T	None	Warthin tumour.
A13966G	None	Breast cancer, Oncocytic pituitary adenoma, Prostate cancer, Endometrial cancer type I, Schizophrenia, Noonan syndrome, Diabetes type2.
T14470C	None	Thyroid cancer, Diabetes type2, Oncocytic pituitary adenoma, Colorectal cancer, Leber Hereditary Optic Neuropathy, Schizoaffective disorder, Mental disorder.
C14766T	None	Thyroid cancer, High grade renal clear cell carcinoma, Pituitary adenoma, Chronic Periodontitis, Prostate cancer, Alzheimer's Disease, Endometrial cancer type I, Noonan syndrome, Hypertrophic cardiomyopathy, Neurogenic muscle weakness Ataxia and Retinitis Pigmentosa, periodic paralyses and neuropathy, Epilepsy, Diabetes type2, BHD-related renal tumour.
A14793G	None	Thyroid cancer, Mitochondrial Encephalomyopathy Lactic Acidosis and Stroke like episodes, Alzheimer's Disease, Renal oncocytoma, Pituitary adenoma, Prostate cancer, Lynphoma, Epilepsy.
T14798C	glioblastoma	Thyroid cancer, Oral cavity carcinoma, Prostate cancer, Endometrial cancer type I, Invasive mammal carcinoma, Leber Hereditary Optic Neuropathy, Optic atrophy, Diabetes type2.
A14927G	None	Parkinson`s Disease, Leber Hereditary Optic Neuropathy, Diabetes type2.
A14959G	None	Alzheimer's Disease, Diabetes type2.
T14968C	None	Alzheimer's Disease, Mental disorder, Diabetes type2, Prostate cancer.
T15310C	None	Oncocytic pituitary adenoma, Schizoaffective disorder, Glaucoma, Diabetes type2.
A15326G	None	Neurogenic muscle weakness Ataxia and Retinitis Pigmentosa, Leber Hereditary Optic Neuropathy, Diabetes type2.
C15452A	None	Thyroid cancer, High grade renal clear cell carcinoma, Pituitary adenoma, Prostate cancer, Schizoaffective disorder, Noonan syndrome, Leber Hereditary Optic Neuropathy, Diabetes type2.

Mutations	Disease association search (MitoMap)	Human Mitochondrial DataBase (HmtDB)
C16069T	None	Thyroid cancer, Leber Hereditary Optic Neuropathy, Pituitary adenoma, Noonan syndrome, Diabetes type2.
T16126C	glioblastoma	Thyroid cancer, Diabetes type2, High grade renal clear cell carcinoma, Pituitary adenoma, Parotid oncocytoma, Prostate cancer, Endometrial cancer type I, Noonan syndrome, Invasive mammal carcinoma, Dilated Cardiomyopathy, Leber Hereditary Optic Neuropathy, Mental disorder.
T16172C	MNGIE tissues, head/neck tumour back-mutation	Breast cancer, Parkinson`s Disease, Diabetes type2, Warthin tumour, Colorectal cancer, Schizophrenia, Leber Hereditary Optic Neuropathy.
C16192T	Melanoma	Thyroid cancer, Mitochondrial Encephalomyopathy Lactic Acidosis and Stroke like episodes, Parkinson`s Disease, Chronic Periodontitis, Colorectal cancer, Endometrial cancer type I, Leber Hereditary Optic Neuropathy, Epilepsy.
C16223T	Tumour	Thyroid cancer, Leber Hereditary Optic Neuropathy, Mitochondrial Encephalomyopathy Latic Acidosis and Stroke like episodes, Parkinson`s Disease, High grade renal clear cell carcinoma, Pituitary adenoma, Parotid oncocytoma, Colorectal cancer, Prostate cancer, Alzheimer's Disease, Endometrial cancer type I, Diabetes
C16256T	None	Thyroid cancer, Mitochondrial Encephalomyopathy Lactic Acidosis and Stroke like episodes, Diabetes type2, Oncocytic pituitary adenoma, Gastric carcinoma, Prostate cancer, Noonan syndrome, Dilated Cardiomyopathy.
C16257A	None	Parkinson`s Disease, Obesity, Diabetes type2, Mental disorder.
C16261T	None	Thyroid cancer, Parkinson`s Disease, Pituitary adenoma, Noonan syndrome, Leber Hereditary Optic Neuropathy, Mental disorder, Lung cancer, Diabetes type2.

Mutations	Disease association search (MitoMap)	Human Mitochondrial DataBase (HmtDB)
C16270T	Melanoma	Thyroid cancer, Mitochondrial Encephalomyopathy Lactic Acidosis and Stroke like episodes, Renal oncocytoma, Oncocytic pituitary adenoma, Colorectal cancer, Glioma, Noonan syndrome, Dilated Cardiomyopathy, Epilepsy.
T16304C	esophageal, breast & prostate tumours.	Mental disorder Thyroid cancer, Alzheimer's Disease, Chronic Periodontitis, Colorectal cancer, Alzheimer's Disease, Breast cancer, Noonan syndrome, Epilepsy, Diabetes type2.
G16319A	None	Thyroid cancer, Parkinson`s Disease, Alzheimer's Disease, Diabetes type2, Oncocytic pituitary adenoma, Colorectal cancer, Schizophrenia, Breast cancer, Epilepsy, Leber Hereditary Optic Neuropathy.
C16320T	None	Breast cancer, Diabetes type2, renal clear cell carcinoma, Warthin tumour, Chronic Periodontitis.
T16325C	None	Parkinson`s Disease, Diabetes type2, Chronic Periodontitis, Leber Hereditary Optic Neuropathy.
A16399G	gastric carcinoma	Thyroid cancer, Mitochondrial Encephalomyopathy Lactic Acidosis and Stroke like episodes, Parkinson`s Disease, Renal oncocytoma, Oncocytic pituitary adenoma, Ovarian cancer, Epilepsy.
A16497G	None	Parkinson`s Disease, Diabetes type2, Mental disorder, Non-syndromic Hearing loss.
T16519C	Glioblastoma, gastric, lung, ovarian, prostate tumours	Thyroid cancer, Breast cancer, Parkinson`s Disease, Diabetes type2, Warthin tumour, Gastric carcinoma, Chronic Periodontitis, Colorectal cancer, Prostate cancer, Alzheimer's Disease, Noonan syndrome, Leber Hereditary Optic Neuropathy, Mental disorder.

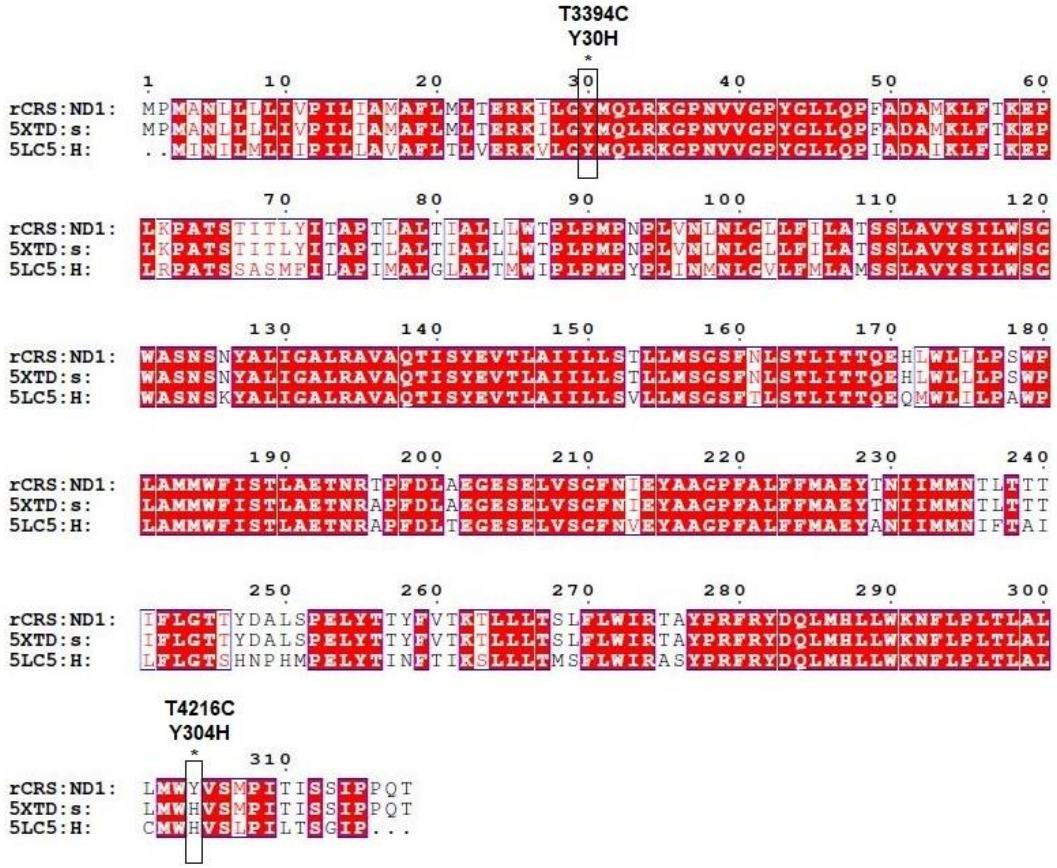

Appendix Figure 1. Alignment of the three reference protein sequences of the ND1 subunit used in the 3D modelling analyses with the identified mutation positions marked. rCRS: NCBI Reference Sequence, 5XTD: *Homo sapiens* homolog, 5LC5: *Bos taurus* homolog.

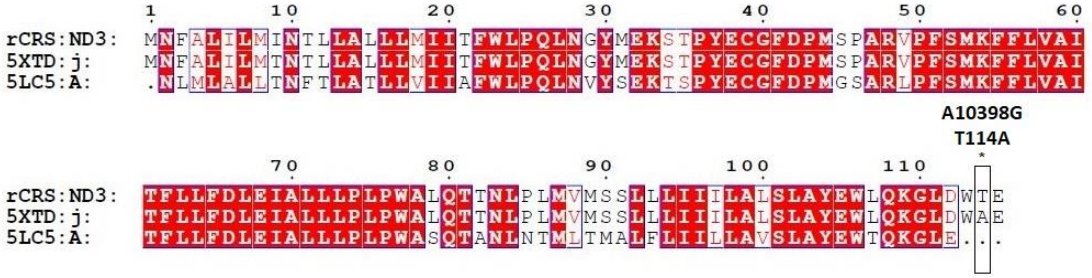

Appendix Figure 2. Alignment of the three reference protein sequences of the ND3 subunit used in the 3D modelling analyses with the identified mutation position marked. rCRS: NCBI Reference Sequence, 5XTD: *Homo sapiens* homolog, 5LC5: *Bos taurus* homolog.

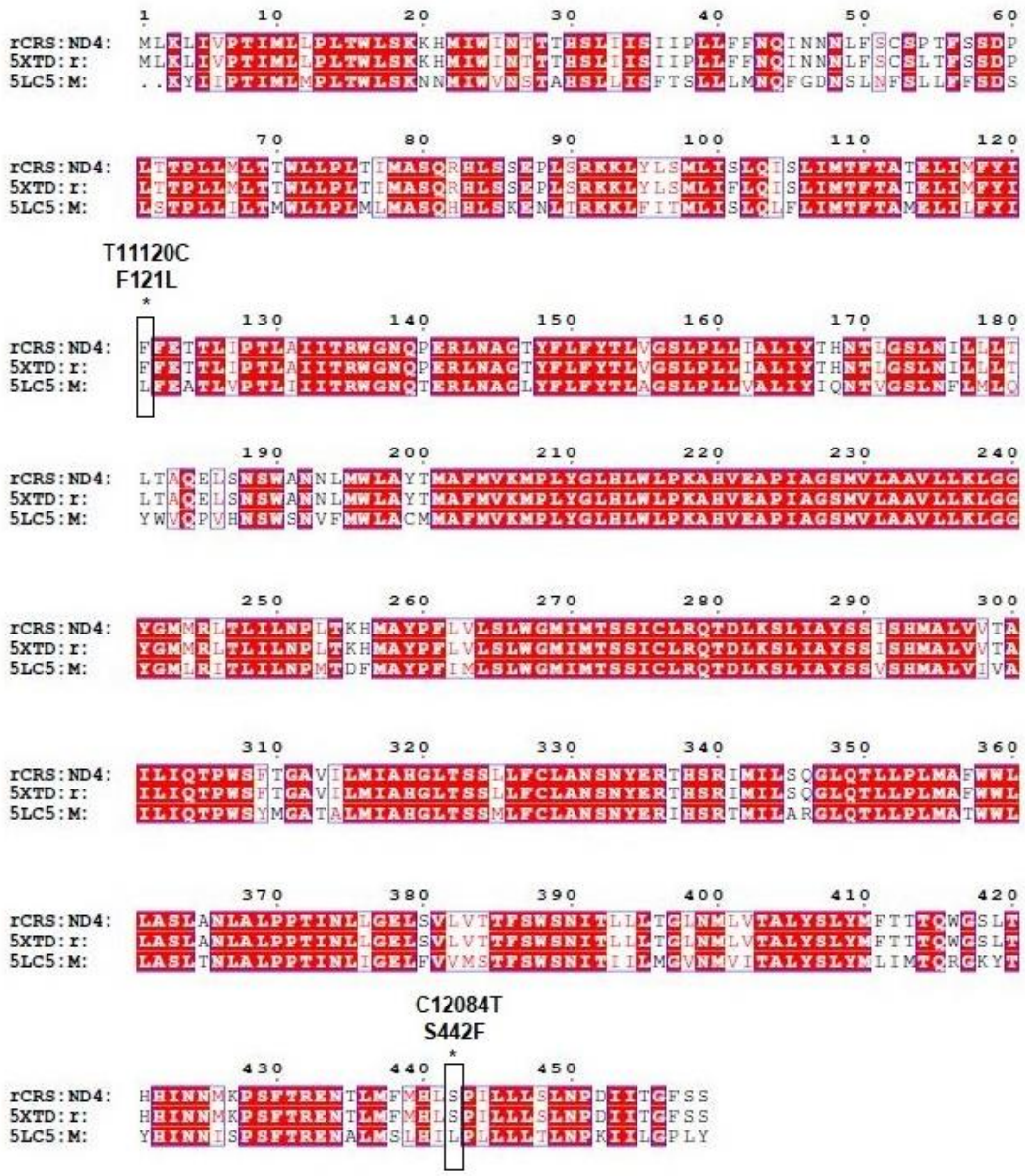

Appendix Figure 3. Alignment of the three reference protein sequences of the ND4 subunit used in the 3D modelling analyses with the identified mutation positions marked. rCRS: NCBI Reference Sequence, 5XTD: *Homo sapiens* homolog, 5LC5: *Bos taurus* homolog.

Appendix Figure 4. Alignment of the three reference protein sequences of the ND5 subunit used in the 3D modelling analyses with the identified mutation positions marked. rCRS: NCBI Reference Sequence, 5XTD: *Homo sapiens* homolog, 5LC5: *Bos taurus* homolog.

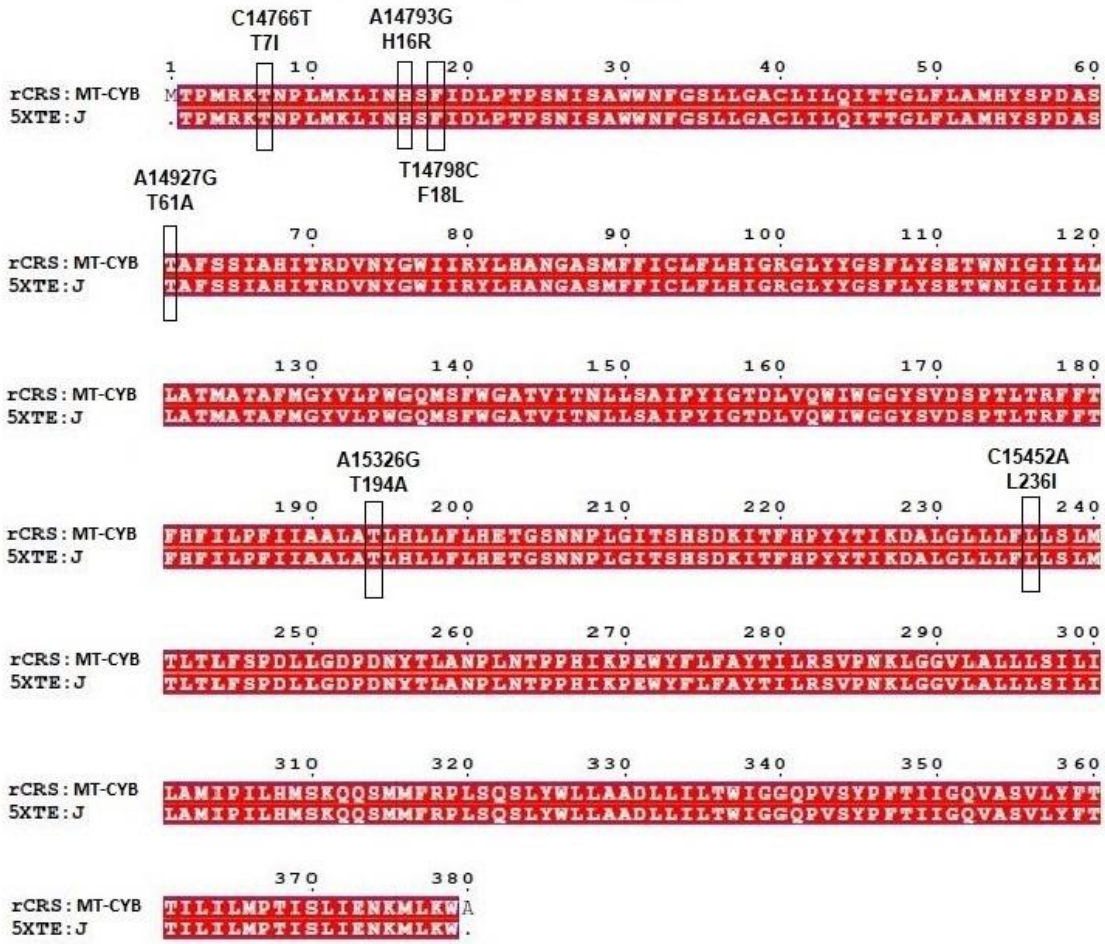

Appendix Figure 5. Alignment of the two reference protein sequences of the MT-CYB subunit used in the 3D modelling analyses with the identified mutation positions marked. rCRS: NCBI Reference Sequence, 5XTE: *Homo sapiens* homolog.

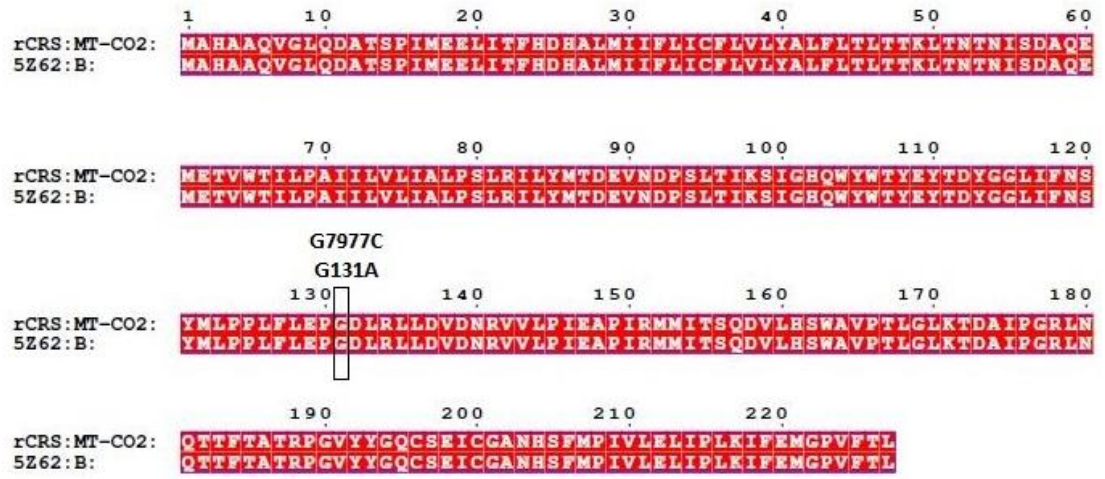

Appendix Figure 6. Alignment of the two reference protein sequences of the MT-CO2 subunit used in the 3D modelling analyses with the identified mutation position marked. rCRS: NCBI Reference Sequence, 5Z6N: *Homo sapiens* homolog.

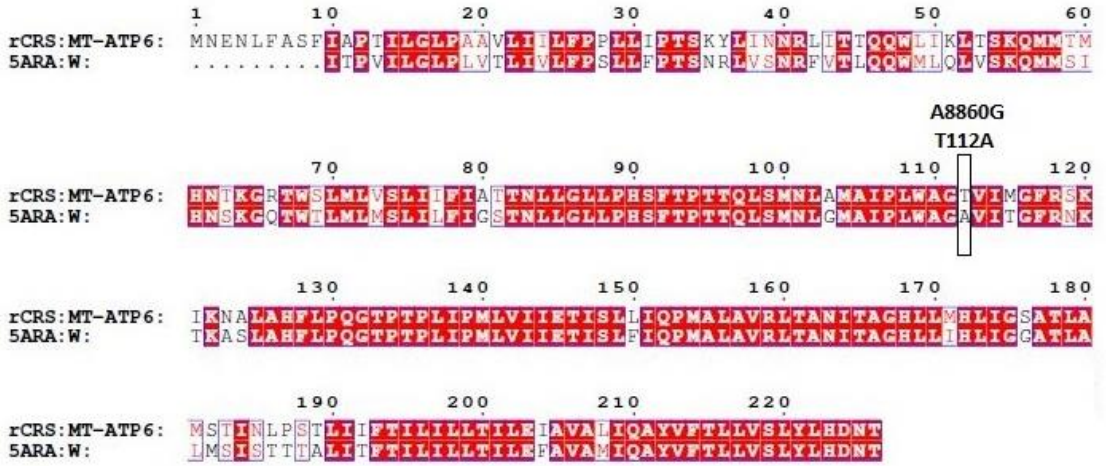

Appendix Figure 7. Alignment of the two reference protein sequences of the MT-ATP6 subunit used in the 3D modelling analyses with the identified mutation position marked. rCRS: NCBI Reference Sequence, 5ARA: *Bos taurus* homolog.

FORM UPR16

Research Ethics Review Checklist

Please include this completed form as an appendix to your thesis (see the Research Degrees Operational Handbook for more information

Postgraduate Research Student (PGRS) Information			**Student ID:**	840355	
PGRS Name:	Tarek Zaidieh				
Department:	PHBM	**First Supervisor:**	Qian An		
Start Date: (or progression date for Prof Doc students)	01/02/2017				
Study Mode and Route:	Part-time ☐		MPhil ☐		MD ☐
	Full-time ☒		PhD ☐		Professional Doctorate ☐

Title of Thesis:	ROS and mitochondrial genetic abnormalities as novel indicators to predict anticancer drug efficacy
Thesis Word Count: (excluding ancillary data)	43320

If you are unsure about any of the following, please contact the local representative on your Faculty Ethics Committee for advice. Please note that it is your responsibility to follow the University's Ethics Policy and any relevant University, academic or professional guidelines in the conduct of your study

Although the Ethics Committee may have given your study a favourable opinion, the final responsibility for the ethical conduct of this work lies with the researcher(s).

UKRIO Finished Research Checklist:
(If you would like to know more about the checklist, please see your Faculty or Departmental Ethics Committee rep or see the online version of the full checklist at: http://www.ukrio.org/what-we-do/code-of-practice-for-research/)

a) Have all of your research and findings been reported accurately, honestly and within a reasonable time frame?	YES ☒ NO ☐
b) Have all contributions to knowledge been acknowledged?	YES ☒ NO ☐
c) Have you complied with all agreements relating to intellectual property, publication and authorship?	YES ☒ NO ☐
d) Has your research data been retained in a secure and accessible form and will it remain so for the required duration?	YES ☒ NO ☐
e) Does your research comply with all legal, ethical, and contractual requirements?	YES ☒ NO ☐

Candidate Statement:

I have considered the ethical dimensions of the above named research project, and have successfully obtained the necessary ethical approval(s)

Ethical review number(s) from Faculty Ethics Committee (or from NRES/SCREC):	ETHIC-2019-109

If you have *not* submitted your work for ethical review, and/or you have answered 'No' to one or more of questions a) to e), please explain below why this is so:

Signed *(PGRS)*:		**Date:** 10/04/2020

UPR16 – April 2018